



University of HUDDERSFIELD

University of Huddersfield Repository

Fisher, Olivia

Towards Understanding Cellular Stress Responses and Signalling Pathways Impacted by klo-1/ KL and klo-2/ KL Deletion in *Caenorhabditis elegans*

Original Citation

Fisher, Olivia (2021) Towards Understanding Cellular Stress Responses and Signalling Pathways Impacted by klo-1/ KL and klo-2/ KL Deletion in *Caenorhabditis elegans*. Doctoral thesis, University of Huddersfield.

This version is available at <http://eprints.hud.ac.uk/id/eprint/35722/>

The University Repository is a digital collection of the research output of the University, available on Open Access. Copyright and Moral Rights for the items on this site are retained by the individual author and/or other copyright owners. Users may access full items free of charge; copies of full text items generally can be reproduced, displayed or performed and given to third parties in any format or medium for personal research or study, educational or not-for-profit purposes without prior permission or charge, provided:

- The authors, title and full bibliographic details is credited in any copy;
- A hyperlink and/or URL is included for the original metadata page; and
- The content is not changed in any way.

For more information, including our policy and submission procedure, please contact the Repository Team at: E.mailbox@hud.ac.uk.

<http://eprints.hud.ac.uk/>

Towards Understanding Cellular Stress
Responses and Signalling Pathways
Impacted by *klo-1/ KL* and *klo-2/ KL*
Deletion in *Caenorhabditis elegans*

OLIVIA FISHER

A thesis submitted to the University of Huddersfield in partial
fulfilment of the requirements for the degree of Doctor of
Philosophy

The University of Huddersfield

Department of Biological and Geographical Sciences

School of Applied Sciences

19th July 2021

Abstract

Background: Klotho (KL) and its paralog β -klotho (KLB) are transmembrane proteins that function as co-factors to aid binding of endocrine fibroblast growth factors (eFGFs) to their respective fibroblast growth factor receptors (FGFR). Klotho has been found to have protective effects at cellular and organismal levels, although the signalling pathways governing these are yet to be determined.

Methods: *C. elegans* strains with genetic deletions in *klo-1/ KL* and *klo-2/ KL* were subject to health and stress resistance analyses. To determine signalling pathways governed by klotho, *C. elegans* strains with null *klo-1/ KL* and *klo-2/ KL* alleles were crossed into mutants for intracellular signalling components then subject to health and stress analyses.

Due to reported impacts of Klotho function in oxidative stress responses, staining for reactive oxygen species was performed in wild-type and *klo-2 (ok1862); klo-1 (ok2925)* double mutant *C. elegans* to determine ROS levels in these strains prior to and following stress exposure. Fluorescent reporters for *klo-1* and *klo-2* gene expression were analysed in wild-type and *klo-2; klo-1* double mutant genetic backgrounds before and after pharmacological intervention using reported AMPK activators and TOR pathway inhibitors to elucidate whether AMPK or TOR signalling pathways are impacted by *klo-1* and *klo-2* deletion.

Results: *C. elegans* with deletion of *klo-1/ KL*, *klo-2/ KL*, or both, have increased survival upon exposure to acute oxidative stress, and show reduced levels of reactive oxygen species (ROS) compared to wild-type counterparts in untreated (control) conditions. Interestingly, in heat stress responses while there is some survival advantage displayed by *klo-1/ KL* or *klo-2/ KL* single mutants compared to wild-type counterparts at the 8 hour time point, deletion of both genes does not increase survival in *C. elegans*. The survival advantages demonstrated by *klotho* mutant nematodes is dependent on functional AAK-2/ AMPK.

Conclusions: In contrast to literature, which suggests removal of *klotho* would diminish stress responses, *C. elegans* strains with *klo-1/ KL* or *klo-2/ KL* deletion backgrounds have a survival advantage upon acute stress exposure. This survival advantage is characterised by lowered ROS levels in these animals. The current working theory is that *klo-2; klo-1* double mutant mutants could have increased AAK-2/AMPK activity compared to wild-type animals however further research is needed to support this hypothesis.

Table of Contents

Abstract.....	2
List of Abbreviations	9
List of Figures	13
List of Tables	16
Acknowledgements.....	19
Chapter 1: Introduction	20
1.1. Implications of an ageing population.....	20
1.2. Oxidative stress and health.....	22
1.2.1. What is oxidative stress?	22
1.2.2. Types of reactive oxygen species (ROS)	22
1.2.3. Endogenous sources of ROS.....	24
1.2.4. Exogenous sources of ROS.....	26
1.2.5. Intracellular responses to ROS.....	27
1.2.6. Implications of oxidative stress on health	31
1.2.7. The oxidative damage theory of ageing.....	31
1.2.8. Criticisms of the oxidative damage theory of ageing	32
1.3. <i>Klotho</i> and β - <i>klotho</i>	33
1.3.1. An introduction to <i>klotho</i>	33
1.3.2. <i>Klotho</i> and β - <i>klotho</i>	34
1.3.3. Typical Fibroblast Growth Factor (FGF) signalling	36
1.3.4. Endocrine fibroblast growth factor (eFGF) signalling	36
1.3.4.1.1. <i>Klotho</i> as a pro-longevity regulator	38
1.3.5. <i>Klotho</i> and metabolic disease	40
1.3.6. Intracellular pathways associated with eFGF- <i>klotho</i> -FGFR function.....	42
1.4. <i>Caenorhabditis elegans</i> as a model of study	44
1.4.1. A brief introduction to <i>Caenorhabditis elegans</i>	44
1.4.2. The <i>C. elegans</i> genome	45
1.4.3. Endocrine signalling in <i>C. elegans</i> stress responses.....	48
1.4.4. Fibroblast growth factor (FGF)- <i>klotho</i> signalling in <i>C. elegans</i>	48
1.5. Aims of research	50
Chapter 2: Materials and Methods	52
2.1. <i>Caenorhabditis elegans</i> strains	52
2.2. Media	53
2.2.1. Nematode growth media	53

2.2.2. Bacterial growth solutions	53
2.2.3. Nematode freezing solution	53
2.2.4. M9 medium.....	53
2.2.5. Complete K-medium	54
2.2.6. S basal medium	54
2.3. Bacterial cultures	54
2.3.1. <i>Escherichia coli</i> OP50	54
2.3.2. <i>Escherichia coli</i> HB101	54
2.4. Preparation of <i>C. elegans</i> strains	55
2.4.1. General maintenance.....	55
2.4.2. Liquid nematode cultures	55
2.4.3. Freezing nematode cultures	55
2.4.4. Age synchronization.....	56
2.5. Genetic crosses	57
2.5.1. Crossing <i>klo-1</i> and <i>klo-2</i> genetic mutants with mutants for intracellular signalling components	57
2.5.2. Crossing transgenic reporters into <i>klo-1</i> and <i>klo-2</i> mutants	57
2.6. Genotyping.....	58
2.6.1. Nematode lysis.....	58
2.6.2. Genotyping polymerase chain reaction (PCR)	58
2.6.3. Gel electrophoresis	60
2.7. <i>C. elegans</i> Health Analysis	60
2.7.1. Lifespan assays.....	60
2.7.2. Viable progeny analysis.....	61
2.8. Stress Response assays	61
2.8.1. Oxidative stress assays.....	61
2.8.2. Acute heat stress.....	63
2.8.3. Chronic starvation.....	63
2.9. Interpretation of survival assays: epistatic analysis.....	63
2.10. Analysis of <i>klo-1</i> and <i>klo-2</i> reporter expression in <i>C. elegans</i>	64
2.10.1. Treatment with 100 μ M forskolin.....	64
2.10.2. Treatment with 50 mM metformin	64
2.10.3. Treatment with 100 μ M rapamycin.....	64
2.11. Analysis of excretory canal morphology	65
2.12. Detection of <i>lgg-1::GFP</i> reporter expression in <i>C. elegans</i>	65
2.13. Microscopy.....	65

2.13.1. Fluorescence microscopy and imaging	65
2.14. Western blotting of <i>C. elegans</i> extracts.....	66
2.14.1. Preparation of buffers.....	66
2.14.2. Preparation of <i>C. elegans</i> protein extracts	66
2.14.3. SDS-PAGE	66
2.14.4. Transfer of proteins to PVDF membrane	67
2.14.5. Blocking PVDF membrane.....	67
2.14.6. Antibody incubation.....	68
2.14.7. Detection of antibody	68
2.15. Quantification of hexokinase activity	68
2.15.1. Hexokinase activity assay buffers	68
2.15.2. Homogenisation of <i>C. elegans</i> samples	68
2.15.3. Hexokinase assay plate set up	69
2.15.4. BCA protein quantification assay.....	69
2.15.5. Calculating enzyme activity.....	69
Chapter 3: Effects of <i>klo-1/ KL</i> and <i>klo-2/ KL</i> deletion on health and stress responses in <i>C. elegans</i>	70
3.1. Introduction and key hypotheses	70
3.2. Lifespan analysis of <i>C. elegans</i> strains	71
3.2.1. <i>klo-1/ KL</i> and <i>klo-2/ KL</i> deletion mutations do not impact lifespan in <i>C. elegans</i>	71
3.2.2. Lifespan analysis of <i>C. elegans</i> strains with altered FGF- <i>klotho</i> -FGFR signalling.....	73
3.2.2.1. Effects of diminished FGF-FGFR signalling on the lifespan of <i>klo-1</i> and <i>klo-2</i> mutants... 73	
3.3. <i>klo-1/ KL</i> and <i>klo-2/ KL</i> single mutants exhibit trend for increased survival upon exposure to acute heat stress at 37 °C	82
3.4. Survival of wild-type vs <i>klo-1/ KL</i> and <i>klo-2/ KL</i> deletion mutants exposed to chronic starvation	85
3.5. <i>klo-1/ KL</i> single mutants exhibit fewer viable progeny than wild-type, <i>klo-2</i> and <i>klo-2; klo-1</i> counterparts	89
3.6. Effects of <i>klo-1</i> and <i>klo-2</i> deletion on autophagy reporter expression	91
3.7. Discussion: The roles of KLO-1 and KLO-2 in longevity and stress resistance in <i>C. elegans</i>	95
3.7.1. The roles of KLO-1/ KL and KLO-2/ KL in ageing.....	95
3.7.2. <i>klo-1/ kl</i> deletion reduces viable progeny in <i>C. elegans</i> in line with effects on nematode lifespan.....	98
3.7.3. KLO-1/ KL and KLO-2/ KL in chronic starvation responses.....	99
3.7.4. Further investigation into the roles of KLO-1 and KLO-2 in autophagic process is required	100
3.7.5. Chapter three conclusions	101

Chapter 4: The effects of <i>klo-1</i> and <i>klo-2</i> deletion on oxidative stress responses in <i>C. elegans</i>.....	102
4.1. Chapter four: hypotheses to be tested.....	102
4.2. Deletion of <i>klo-1/ KL</i> or <i>klo-2/ KL</i> leads to increased resistance to oxidative stress	102
4.2.1. <i>C. elegans</i> strains containing either <i>klo-1/ KL</i> or <i>klo-2/ KL</i> deletion mutations exhibit increased survival upon acute exposure to oxidative stress over 9 hours	102
4.2.2. Increased survival of <i>klo-1</i> and <i>klo-2</i> deletion mutants upon exposure to oxidative stress is dependent on functional FGF/ FGFR signalling in <i>C. elegans</i>	105
4.2.3. KLO-1/ KL and KLO-2/ KL function in parallel with AGE-1/ PI3K in oxidative stress resistance	109
4.2.4. <i>C. elegans</i> containing <i>klo-1/ KL</i> or <i>klo-2/ KL</i> deletion mutations display trend for increased resistance to oxidative agent following prolonged exposure.....	112
4.2.5. Wild-type <i>C. elegans</i> display more intensive staining for ROS compared to <i>C. elegans</i> strains with <i>klo-1/ KL</i> or <i>klo-2/ KL</i> genetic backgrounds.....	114
4.2.5.1. Acute exposure to oxidative agent decreases staining for ROS in <i>C. elegans</i>	114
4.2.5.2. Prolonged exposure to oxidative agent increases staining for ROS in wild-type <i>C. elegans</i>	121
4.2.5.3. <i>C. elegans</i> strains with <i>klo-1/ KL</i> or <i>klo-2/ KL</i> genetic backgrounds exhibit trend for lowered staining of ROS upon prolonged exposure to oxidative agent	124
4.2.5.4. <i>klo-1/ KL</i> and <i>klo-2/ KL</i> mutants display resistance to oxidative agent sodium arsenite	127
4.2.6. <i>klo-1/ KL</i> and <i>klo-2/ KL</i> genetic background does not confer increased resistance upon chronic exposure to oxidative agent.....	130
4.3. Discussion: <i>C. elegans</i> strains with <i>klotho</i> mutant backgrounds exhibit resistance to acute but not chronic stress.....	134
4.3.1. <i>klo-1/ KL</i> and <i>klo-2/ KL</i> mutants have lower overall ROS than wild-type <i>C. elegans</i>	134
4.3.2. Deletion of <i>klo-1/ KL</i> and <i>klo-2/ KL</i> promotes acute oxidative stress resistance in <i>C. elegans</i>	134
4.3.3. There is no survival advantage of <i>klo-1/ KL</i> or <i>klo-2/ KL</i> deletion mutants upon chronic oxidative stress exposure.....	136
4.3.4. Chapter four conclusions	137
Chapter 5: The effects of <i>aak-2/ AMPK</i> knockdown in <i>klo-1</i> and <i>klo-2</i> mutants	139
5.1. Introduction: overview of AAK-2/ AMPK	139
5.1.1. Introduction to AMPK	139
5.1.2. AMPK: structure and activation.....	139
5.1.3. Downstream targets of AMPK	140
5.1.4. AMPK in health and disease.....	140
5.1.5. AMPK and <i>klotho</i>	141
5.1.6. AAK-2 – the <i>C. elegans</i> orthologue for mammalian AMPK α	143
5.1.6. Chapter five: hypotheses to be tested.....	144

5.2. Survival advantage of <i>klo-1/ KL</i> and <i>klo-2/ KL</i> deletion mutants requires <i>aak-2/ AMPK</i>	146
5.3. Thermotolerance of <i>klo-1/ KL</i> and <i>klo-2/ KL</i> deletion mutants is diminished in combination with <i>aak-2/ AMPK</i> loss-of-function alleles	150
5.4. <i>aak-2/ AMPK</i> loss-of-function diminishes lifespan in <i>C. elegans</i>	156
5.5. Viable progeny is reduced in <i>C. elegans</i> with <i>aak-2/ AMPK</i> loss-of-function backgrounds	160
5.6. Treatment with AMPK-activators increases expression of <i>klotho</i> reporters in <i>C. elegans</i>	163
5.6.1. Forskolin activation of <i>aak-2/ AMPK</i> increases expression of <i>pklo-2::GFP</i> reporter in wild-type and <i>klo-2; klo-1 C. elegans</i>	163
5.6.3. Forskolin activation of AAK-2/ AMPK could lead to osmotic stress in <i>C. elegans</i>	169
5.7. Effects of metformin on <i>klo-1/ KL</i> and <i>klo-2/ KL</i> reporter expression.....	171
5.7.1. Metformin treatment increases the expression of <i>pklo-1::mCherry</i> reporter in <i>C. elegans</i>	171
5.7.2. Metformin treatment increases <i>pklo-2::GFP</i> reporter expression in <i>C. elegans</i>	174
5.8. Effects of mTOR signalling manipulation on <i>klo-1/ KL</i> and <i>klo-2/ KL</i> reporter expression.....	177
5.8.1. Rapamycin treatment increases expression of <i>pklo-1::mCherry</i> reporter in wild-type <i>C. elegans</i> but has little effect on <i>C. elegans</i> with <i>klo-2; klo-1</i> deletion background.....	177
5.8.2. Rapamycin treatment shows no effect on <i>pklo-2::GFP</i> reporter expression in <i>C. elegans</i>	181
5.9. Western blotting for <i>aak-2/ AMPK</i>	184
5.9.1. Western blotting for total AMPK in wild-type vs <i>klo-1; klo-1</i> double mutants	184
5.9.2. Western blotting for phosphorylated AMPK in wild-type vs <i>klo-2; klo-1</i> mutants.....	187
5.10. Discussion: survival advantages of <i>klo-1/ KL</i> and <i>klo-2/ KL</i> deletion mutants is dependent on functional AAK-2/ AMPK.....	190
5.10.1. <i>klo-1</i> mutants require <i>aak-2/ AMPK</i> in heat stress responses	190
5.10.2. AAK-2/ AMPK is required for oxidative stress resistance in <i>klo-1/ KL</i> and <i>klo-2/ KL</i> deletion mutants.....	190
5.10.3. AAK-2/ AMPK could function upstream of KLO-1 and KLO-2	192
5.11. Discussion: a role for TOR signalling in <i>klotho</i> -governed responses	192
5.11.1. Chapter five conclusions	193
Chapter 6: Stress responses in <i>C. elegans</i> with altered <i>klotho</i> function could be linked to the antagonistic pathways of AMPK and mTOR.....	194
6.1. <i>klo-1/ KL</i> and <i>klo-2/ KL</i> mutants display similar longevity phenotypes to strains with diminished mTOR activity	194
6.2. KLO-1/ KL and KLO-2/ KL have demonstrable links to increased AAK-2/ AMPK activity, and decreased mTOR activity in <i>C. elegans</i>	196
6.3. Oxidative stress responses in <i>klo-1/ KL</i> and <i>klo-2/ KL</i> mutants are characterized by increased AAK-2/ AMPK function.....	198
6.4. The theory that <i>klotho</i> inhibits IIS pathway in stress responses could be attributed to AMPK-TOR-IIS crosstalk	203

Chapter 7: Limitations and future directions	206
7.1. Limitations: impact of COVID-19 on research output.....	206
7.2. Improvements and future work.....	206
7.2.1. Investigating the impact of KLO-1 and KLO-2 in autophagic responses	206
7.2.2. Further work using <i>pklo-1::mCherry</i> and <i>pklo-2::GFP</i> reporters	207
7.2.3. Hexokinase activity of <i>C. elegans</i> homogenates.....	208
7.2.4. Consolidation of the role of AAK-2/ AMPK in <i>klo-1/ KL</i> and <i>klo-2/ KL</i> deletion mutants .	208
7.2.5. Further insights into other pathways mediated by KLO-1/ KL and KLO-2/ KL.....	209
Chapter 8: Conclusions	210
Appendix 1	234
Appendix 2	239
Appendix 3	240
Appendix 4	242
Appendix 5	247

List of Abbreviations

$\bullet\text{O}_2^-$	Superoxide radical
$\bullet\text{OH}$	Hydroxyl radical
1,25(OH) ₂ D	1,25 hydroxyvitamin D
$^1\text{O}_2$	Singlet oxygen
8-Oxo-dG	8-Oxo-2'-deoxyguanosine
ADAM	A disintegrin and metalloprotease proteases
AFT2	Activating transcription factor 2
AICAR	5'-aminoimidazole-4-carboxamide ribonucleotide
AMPK	AMP-activated protein kinase
AOPP	Advanced oxidation protein products
ARE	Antioxidant response element
BAT	Brown adipose tissue
BCA	Bicinchoninic acid
CAMKK β	Ca ²⁺ / calmodulin-dependent protein kinase β
CAT	Catalase
CGC	<i>Caenorhabditis</i> Genetics Centre
CKD	Chronic kidney disease
CREBPH	cAMP-responsive element binding protein H
CVD	Cardiovascular disease
CYP	Cytochrome P450
Cyp24	25-hydroxyvitamin D3-24-hydroxylase
Cyp27b1	Cytochrome P450 family 27 subfamily B member 1
dCAPS	Derived cleaved amplified polymorphic sequences

eFGF	Endocrine fibroblast growth factor
esRAGE	Endogenous secretory receptor for advanced glycation end products
ETC	Electron transport chain
FGF	Fibroblast growth factor
FGFR	Fibroblast growth factor receptor
FoxO	Forkhead box transcription factor
FUDR	Fluorodeoxyuridine
FXR	Farnesoid X-activated receptor
G6PDH	Glucose-6-phosphate dehydrogenase
GADD45	Growth arrest and DNA damage-inducible 45 protein
GLUT1	Glucose transporter 1
GR	Glucocorticoid receptor
GST	Glutathione S-transferase
H ₂ O ₂	Hydrogen peroxide
HFD	High fat diet
HO ₂	Hydroperoxyl radical
HOCl	Hypochlorous acid
hsCRP	High-sensitivity C-reactive protein
HSPG	Heparan sulphate proteoglycan
IGF-1	Insulin-like growth factor 1
IGFR	Insulin-like growth factor 1 receptor
IIS	Insulin/ Insulin-like growth factor-1 signalling
IRS-1	Insulin receptor substrate 1

IκK	IκB kinase
JNK	c-Jun N-terminal kinase
Keap1	Kelch-like ECH-associated protein 1
KL	Klotho (human/ murine)
KLB	β-klotho
KLG	γ-klotho
LC3	Microtubule-associated protein 1A/ 1B-light chain 3 protein
LKB1	Liver kinase B1
MAPK	Mitogen-activated protein kinase
MDA	Malonaldehydes
MEK	Mitogen-activated protein kinase
mTOR	Mammalian target of rapamycin
mTORC1	Mammalian target of rapamycin complex 1
NaAsO ₂	Sodium arsenite
NAFLD	Non-alcoholic fatty liver disease
NF-κB	Nuclear factor kappa-light-chain-enhancer of activated B cells
NGM	Nematode growth media
NO [•]	Nitric oxide radical
NQO1	NADPF quinone dehydrogenase 1
Nrf2	Nuclear factor erythroid 2-related factor
O ₃	Ozone
ONO ₂ ⁻	Peroxynitrite
PC	Protein carbonyls

PI3K	Phosphoinositide 3-kinase
PIP ₃	Phosphatidylinositol (3,4,5)-triphosphate
PKB/ AKT	Protein kinase B
PPAR α	Peroxisome proliferator-activated receptor alpha
PPAR γ	Peroxisome proliferator-activated receptor gamma
PQ	Paraquat
PTEN	Phosphate and tensin homolog
RBA	Receptor binding arm
ROS	Reactive oxygen species
SIRT1	Sirtuin 1
SOD	Superoxide dismutase
T2DM	Type 2 diabetes mellitus
TK	Tyrosine kinase
TSC	Tuberous sclerosis proteins
ULK1	Unc-51 like autophagy activating kinase
WAT	White adipose tissue

List of Figures

Figure 1.1. Schematic representation of the electron transport chain (ETC) in mitochondrion.....	25
Figure 1.2. Schematic diagram of pathways influenced by reactive oxygen species (ROS)	29
Figure 1.3. Schematic diagram of human klotho proteins.....	35
Figure 1.4. Schematic representation of an eFGF-klotho-FGFR complex.	37
Figure 1.5. Schematic diagram of <i>Caenorhabditis elegans</i> model organism.....	44
Figure 1.6. Schematic diagram of speculated mechanisms of klotho-mediated activation of DAF-16/ FOXO.	50
Figure 3.1. Lifespan of N2 (wild-type), <i>klo-1</i> , <i>klo-2</i> and <i>klo-2; klo-1</i> animals	72
Figure 3.2. Lifespan analysis of <i>egl-15</i> , <i>egl-17</i> , <i>klo-1</i> and <i>klo-2</i> compound mutants.	75
Figure 3.3. Lifespan analysis of <i>egl-15</i> , <i>egl-17</i> , <i>klo-1</i> and <i>klo-2</i> compound strains assayed on NGM agar plates supplemented with 100 μ M FUDR.	79
Figure 3.4. Survival of N2 (wild-type), <i>klo-1</i> , <i>klo-2</i> and <i>klo-2; klo-1</i> exposed to heat stress (37°C).....	83
Figure 3.5. Survival of <i>C. elegans</i> strains subject to chronic starvation.....	87
Figure 3.6. Viable progeny analysis of wild-type, <i>klo-1</i> , <i>klo-2</i> and <i>klo-2; klo-1</i> strains.	90
Figure 3.7. <i>lgg-1::GFP</i> reporter expression in wild-type, <i>klo-1</i> and <i>klo-2</i> <i>C. elegans</i> strains.....	93
Figure 4.1. Survival of wild-type, <i>klo-1</i> , <i>klo-2</i> and <i>klo-2; klo-1</i> strains over 9 hours when exposed to 300 mM Paraquat.	104
Figure 4.2. Survival of <i>egl-15</i> , <i>egl-17</i> , <i>klo-1</i> and <i>klo-2</i> compound mutants upon exposure to acute oxidative stress.	106
Figure 4.3. Survival of <i>age-1</i> , <i>klo-1</i> and <i>klo-2</i> compound mutants upon exposure to acute oxidative stress (300 mM paraquat) over 9 hours.	110

Figure 4.4. Survival of wild-type, <i>klo-1</i> , <i>klo-2</i> and <i>klo-2; klo-1</i> <i>C. elegans</i> strains over 20 hours when exposed to 100 mM paraquat.....	112
Figure 4.5. ROS levels in wild-type (N2), <i>klo-1</i> , <i>klo-2</i> and <i>klo-2; klo-1</i> strains.....	115
Figure 4.6. ROS levels in <i>klo-1</i> and <i>klo-2</i> deletion mutants.....	118
Figure 4.7. ROS levels of wild-type animals exposed to varying concentrations of paraquat (PQ) for 20 hours.....	122
Figure 4.8. ROS levels (mean pixel intensity) in wild-type, <i>klo-1</i> , <i>klo-2</i> and <i>klo-2; klo-1</i> strains before and after treatment with 100 mM paraquat (PQ) for 20 hours.....	125
Figure 4.9. ROS levels in wild-type, <i>klo-1</i> , <i>klo-2</i> and <i>klo-2; klo-1</i> strains before and after treatment with 100 μ M sodium arsenite (NaAsO ₂).....	128
Figure 4.10. Survival of N2 (wild-type), <i>klo-1</i> , <i>klo-2</i> and <i>klo-2; klo-1</i> strains upon chronic paraquat exposure.....	132
Figure 5.1. Survival of wild-type, <i>aak-2</i> , <i>klo-1</i> and <i>klo-2</i> compound strains over 9 hours when exposed to acute oxidative stress.....	147
Figure 5.2. Survival of wild-type, <i>klo-1; klo-1</i> , <i>aak-2 (gt33)</i> , <i>aak-2 (ok524)</i> and compound mutants upon exposure to 37°C heat stress over 9 hours.....	152
Figure 5.3. Proportion of living animals (%) at 8- and 9-hour time points following exposure to heat stress at 37°C.....	154
Figure 5.4. Lifespan analysis of wild-type, <i>klo-1</i> , <i>klo-2</i> and <i>aak-2</i> compound mutants.....	157
Figure 5.5. Viable progeny analysis for wild-type, <i>aak-2</i> , <i>klo-1</i> and <i>klo-2</i> compound mutants.....	160
Figure 5.6. <i>pklo-2 reporter</i> expression in wild-type and <i>klo-2; klo-1</i> double mutants before and after forskolin treatment.....	164
Figure 5.7. <i>pklo-1 reporter</i> expression in wild-type and <i>klo-2; klo-1</i> double mutants, before and after forskolin treatment.....	167

Figure 5.8. Morphology of the excretory canals of wild-type and *klo-2; klo-1* double mutants.
.....170

Figure 5.9. Expression of *pklo-1::mCherry* reporter expression in wild-type vs *klo-2; klo-1* strains.....172

Figure 5.10. Relative expression of *pklo-2::GFP* reporter expression in wild-type and *klo-2; klo-1* strains upon exposure to 50 mM metformin.....175

Figure 5.11. Expression of *pklo-1::mCherry* reporter expression in wild-type vs *klo-2; klo-1* strains prior to and following treatment with 100 μ M rapamycin.....179

Figure 5.12. Expression of *pklo-2::GFP* reporter expression in wild-type vs *klo-2; klo-1* strains.....182

Figure 5.13. Western blotting for AAK-2/ AMPK in *C. elegans*.....185

Figure 5.14. Detection of AAK-2 phosphorylation in *C. elegans* strains prior to and following paraquat (PQ) or forskolin (F) treatment.189

Figure 6.1. Schematic diagram representing effects of AAK-2/ AMPK activators and TOR inhibitors on *klo-1/ KL* expression in *C. elegans*.....196

Figure 6.2. Schematic depiction of proposed hypothesis for acute and prolonged oxidative stress responses in wild -type, *klo-1/ KL* and *klo-2/ KL C. elegans*.....200

Figure 6.3. Schematic diagram of proposed crosstalk of klotho, AMPK, mTOR and IIS
.....204

List of Tables

Table 1.1. Summary of several <i>C. elegans</i> genes required for stress response and longevity pathways, and details of their human orthologues.....	46
Table 2.1. Primer sets used for genotyping.	59
Table 2.2. Details of Western blotting conditions for total- and phospho-AMPK α on <i>C. elegans</i> and HCT116 cell extracts.	67
Table 3.1. Means comparison for the lifespan of N2 (wild-type), <i>klo-1</i> , <i>klo-2</i> and <i>klo-2; klo-1</i> strains.....	72
Table 3.2. Mean lifespan of <i>egl-15</i> , <i>egl-17</i> , <i>klo-1</i> and <i>klo-2</i> compound strains	77
Table 3.3. Mean lifespan of <i>egl-15</i> , <i>egl-17</i> , <i>klo-1</i> and <i>klo-2</i> compound strains grown on NGM plates supplemented with 100 μ M FUDR.	81
Table 3.4. Survival of N2 (wild-type), <i>klo-1</i> , <i>klo-2</i> and <i>klo-2; klo-1</i> strains exposed to 37°C heat stress over 9 hours.....	84
Table 3.5. Mean viable progeny values for wild-type, <i>klo-1</i> , <i>klo-2</i> and <i>klo-2; klo-1</i> strains.....	90
Table 3.6. Relative puncta frequency of <i>lgg-1::GFP</i> reporter in wild-type, <i>klo-1</i> and <i>klo-2</i> <i>C. elegans</i> strains.....	94
Table 4.1. Mean survival times of wild-type, <i>klo-1</i> , <i>klo-2</i> and <i>klo-2; klo-1</i> strains upon exposure to 300 mM paraquat.....	104
Table 4.2. Mean survival of <i>egl-15</i> , <i>egl-17</i> , <i>klo-1</i> and <i>klo-2</i> compound strains upon exposure to acute oxidative stress (300 mM paraquat over 9 hours).....	108
Table 4.3. Survival of <i>age-1</i> , <i>klo-1</i> and <i>klo-2</i> strains upon exposure to acute oxidative stress (300 mM paraquat over 9 hours).....	111
Table 4.4. Survival of wild-type, <i>klo-1</i> , <i>klo-2</i> and <i>klo-2; klo-1 double</i> mutants at 15- and 20-hour time points when exposed to 100 mM paraquat.....	113

Table 4.5. CellROX staining to determine ROS levels (mean pixel intensity) of wild-type, <i>klo-1</i> , <i>klo-2</i> and <i>klo-2; klo-1</i> before and after treatment with 300 mM paraquat (PQ) for one hour.....	116
Table 4.6. CellROX staining to determine ROS levels (mean pixel intensity) of wild-type, <i>klo-1</i> , <i>klo-2</i> and <i>klo-2; klo-1</i> before and after treatment with 200 mM paraquat (PQ) for one hour.....	119
Table 4.7. CellROX staining to determine ROS levels (mean pixel intensity) of wild-type, <i>klo-1</i> , <i>klo-2</i> and <i>klo-2; klo-1</i> before and after treatment with 100 mM paraquat (PQ) for two hours.....	120
Table 4.8. ROS levels (mean pixel intensity) of wild-type animals exposed to 0 mM, 20 mM, 40 mM, 60 mM, 80 mM and 100 mM paraquat (PQ) for 20 hours.....	123
Table 4.9. ROS levels (mean pixel intensity) of N2 (wild-type), <i>klo-1</i> , <i>klo-2</i> and <i>klo-2; klo-1</i> strains before and after exposure to 100 mM paraquat (PQ) for 20 hours.....	126
Table 4.10. ROS levels (mean pixel intensity) of N2 (wild-type), <i>klo-1</i> , <i>klo-2</i> , and <i>klo-2; klo-1</i> strains before and after treatment with 100 μ M sodium arsenite (NaAsO ₂).....	129
Table 4.11. Survival of N2 (wild-type), <i>klo-1</i> , <i>klo-2</i> and <i>klo-2; klo-1</i> strains exposed to chronic oxidative stress (0 mM, 2 mM, 4 mM or 6 mM paraquat).....	133
Table 5.1. Mean survival of wild-type, <i>klo-1</i> , <i>klo-2</i> and <i>aak-2</i> single and compound mutants upon exposure to acute oxidative stress (300 mM paraquat over 9 hours).....	149
Table 5.2. Survival of wild-type, <i>klo-1</i> , <i>klo-2</i> and <i>aak-2</i> compound mutants upon exposure to heat stress at 37°C over 9 hours.....	155
Table 5.3. Comparison of mean lifespan of wild-type (N2), <i>klo-1</i> , <i>klo-2</i> and <i>aak-2</i> compound strains.....	159
Table 5.4. Mean viable progeny values for wild-type, <i>aak-2</i> , <i>klo-1</i> and <i>klo-2</i> compound strains.....	162
Table 5.5. Relative expression (mean pixel intensity) of <i>pklo-2::GFP</i> reporter in <i>klo-2; klo-1</i> double mutants compared to wild-type controls (where wild-type controls equal 1).....	165

Table 5.6. Mean expression of <i>pklo-1::mCherry</i> (relative pixel intensity) in wild-type (N2) vs <i>klo-2; klo-1</i> double mutants.....	168
Table 5.7. Relative expression of <i>pklo::mCherry</i> reporter in wild-type vs <i>klo-2; klo-1</i> strains exposed to 50 mM metformin.....	173
Table 5.8. Relative expression of <i>pklo-2::GFP</i> reporter in wild-type vs <i>klo-2; klo-1</i> strains exposed to 50 mM metformin.....	176
Table 5.9. Relative expression of <i>pklo-1::mCherry</i> expression in wild-type vs <i>klo-2; klo-1</i> upon treatment with 100 μ M rapamycin.....	180
Table 5.10. Relative expression of <i>pklo-2::GFP</i> reporter expression in wild-type vs <i>klo-2; klo-1</i> upon treatment with 100 μ M rapamycin.....	183

Acknowledgements

I'd like to extend my appreciation to the numerous individuals who have facilitated, supported and encouraged my endeavours throughout the past four years. Thank you to family, friends and colleagues who have provided a stable network throughout the peaks and troughs the journey has brought.

I'd like to give special thanks to the friends I have made during the course for offering perspective, a shoulder to cry on or comedic relief, and to the technicians who continue to be an indispensable asset to the staff and students at the University of Huddersfield.

Finally, I would like to express my utmost gratitude to Dr. Tarja Kinnunen, whose tutelage has been invaluable.

Dedicated to Richard Anthony Fisher.

Chapter 1: Introduction

1.1. Implications of an ageing population

Globally, since the 1980s, the number of people aged >60 years has more than doubled (United Nations Population Division, 2017). It is predicted that by 2030 individuals aged 60 or over will outnumber children under the age of 10, and by 2050 older persons will outnumber children and adolescents aged between 10-24 years (United Nations Population Division, 2017). In the UK, it was reported that current life expectancies are 79.3 and 82.9 years for males and females, respectively, and historical trends imply these values are expected to continue to rise over the next 50 years (Office for National Statistics, 2019). However, the impact of the current COVID-19 pandemic could negatively impact these predictions (Marois et al., 2020).

Some recent studies have suggested there may be a maximum limit for human lifespan due to natural constraints (Dong et al., 2016, Pyrkov et al., 2021). Dong et al (2016) estimates that it would be unlikely for human lifespan to exceed 125 years old with a second study (Pyrkov et al, 2021), estimating human lifespan to be capped between 120 to 150 years (Dong et al., 2016, Pyrkov et al., 2021). These studies provide commentary that the reason for these maximum lifespan estimates is that after ~100 years, the human body loses its ability to recover from stressors such as injury, and that it is this lack of resilience to stressors in old age that may ultimately lead to death (Dong et al., 2016, Pyrkov et al., 2021). Researchers suggest that it would require therapies focussed on improved health resilience to speed up recovery, healthspan and ultimately, maximum human lifespan (Dong et al., 2016, Pyrkov et al., 2021).

The Office for National Statistics (ONS) also reported that healthy life expectancy (or “healthspan”) for UK individuals is currently 63.1 years for males and 63.6 years for females (Office for National Statistics, 2019). However, whilst life expectancy has increased in the past decade, there has been little change in healthspan, meaning that as life expectancy increases the amount of time spent in poor health also increases (Office for National Statistics, 2019). Furthermore, recent analysis has revealed that individuals in the UK may experience their first major chronic health condition at an earlier age than previously thought indicating we could experience an even greater period of ill health in the latter stages of life (Green et al., 2021).

There are several theories of ageing that generally fall into one of two categories; programmed or damage theories (Jin, 2010). Programmed theories suggest ageing is pre-determined based on genetics and regulated by gene expression e.g., the up- or downregulation of genes over time that affect a system's repair and defence mechanisms (da Costa et al., 2016, Jin, 2010). Alternatively, damage or error theories attribute ageing to environmental factors i.e., external stressors that lead to cumulative damage to cells and tissues leading to dysfunction (da Costa et al., 2016, Jin, 2010). While there is conflict between theories of the root causes of ageing, it is predicted from twin studies that 20-30% of variation in human lifespan can be linked to genetics, with the remainder down to environmental factors and behaviour (van Hjelmborg et al., 2006). It is likely that the cause of ageing is a combination of both programmed and environmental factors. For example, chimpanzees and humans share 98.6% of their DNA, but their maximum lifespan is ~60 years, versus the predicted 120 to 150 years for humans (Dong et al., 2016, Guevara et al., 2020, Pyrkov et al., 2021). While there is a high degree of conservation for human and chimpanzee epigenetic ageing, there are huge variabilities in the rate of ageing between species characterized by increased DNA methylation in chimpanzees (Guevara et al., 2020).

There are some theories to suggest that as we age, an accumulation of damage leads to the onset of multiple morbidities including arthritis, cancer, cardiovascular disease (CVD) and neurological disorders such as dementia (Krisiko and Radman, 2019, Maynard et al., 2015). It should be noted that this theory is not without dispute, and several other theories of ageing and cause of associated morbidities has been discussed in several reviews (Borrás, 2021, da Costa et al., 2016, Jin, 2010).

The Health Survey for England (2016) found that of those aged 60-64 years, 29% had two or more chronic illnesses, and in those aged >75 years this rises to almost half of the population, partly due to the prevalence of disease increasing with age (Office for National Statistics, 2019). A greater understanding of the genetic basis for senescence, and the pathways governing this could provide clues to how to promote healthy ageing with the goal of improving healthspan.

1.2. Oxidative stress and health

1.2.1. What is oxidative stress?

Oxidative stress arises as the result of an excess production of reactive oxygen species (ROS), that overrides the antioxidant responses that function to neutralise these molecules (Pizzino et al., 2017). Prolonged exposure to oxidative stress may have detrimental effects on health due to damage caused to cellular components which leads to their dysfunction (Younus, 2018). To understand the basis of oxidative stress, it is important to understand the function and impact of ROS, and the events which may lead to a disruption in the equilibrium between production and neutralisation of these molecules.

1.2.2. Types of reactive oxygen species (ROS)

Reactive oxygen species (ROS) are reactive chemical species or free radicals derived from molecular oxygen e.g., superoxide (O_2^-), hydrogen peroxide (H_2O_2) and hydroxyl radicals (OH^\bullet). These highly reactive molecules are produced endogenously as by-products of oxidative metabolism, mainly produced by the mitochondria (Pizzino et al., 2017, Younus, 2018).

ROS are important signalling molecules that initiate intracellular signalling cascades leading to the up- and down-regulation of an array of genes involved in cell differentiation and stress responses. However, they can have detrimental effects on health upon imbalance of their generation and detoxification leading to oxidative stress. A defence system of antioxidant enzymes neutralise these ROS to ensure they do not reach harmful levels (Younus, 2018).

Superoxide (O_2^-)

Superoxide is the reduced form of molecular oxygen (O_2) and is considered to be one of the major forms of widespread ROS. Two forms are known, O_2^- , and its protonated form, hydroperoxyl (HO_2). HO_2 can enter the phospholipid bi-layer more readily than charged O_2^- and can induce fatty acid peroxidation (Phaniendra et al., 2015). However, under physiological conditions, HO_2 accounts for just 0.3% of total superoxide found in cytosol (De Grey, 2002).

Mitochondria are considered to be one of the major sources of $\cdot\text{O}_2^-$. Due to its charged state, $\cdot\text{O}_2^-$ cannot typically cross biological membranes, so $\cdot\text{O}_2^-$ generated by complexes I and III of the electron transport chain are usually retained in the matrix and intermembrane space, respectively, where superoxide dismutase (SOD) enzymes are able to dismutate $\cdot\text{O}_2^-$ radicals to form hydrogen peroxide H_2O_2 (Loschen et al., 1974). It has also been reported that $\cdot\text{O}_2^-$ can utilize voltage-dependent anion channels and accumulate in the cytosol (Han et al., 2003).

Hydrogen Peroxide (H_2O_2)

Hydrogen peroxide is formed from the dismutation of superoxide by superoxide dismutase (SOD) (Loschen et al., 1974). Although technically not a free radical, H_2O_2 can be toxic to cells and is a precursor of more reactive oxygen species such as the $\cdot\text{OH}$ radical which subsequently causes damage to organic and inorganic molecules including DNA, proteins and lipids (Phaniendra et al., 2015).

Hydroxyl radical ($\cdot\text{OH}$)

The $\cdot\text{OH}$ radical is highly reactive and can be generated *in vivo* as a result of the Haber-Weiss reaction (Haber et al., 1934). In the first step of the reaction, ferric (Fe^{3+}) ions are reduced to ferrous (Fe^{2+}) ions by superoxide. These ferrous ions are subsequently oxidized by H_2O_2 in the Fenton reaction generating the $\cdot\text{OH}$ radical (Fenton, 1894, Phaniendra et al., 2015). The high reactivity of $\cdot\text{OH}$ means it can be particularly damaging to a vast array of cellular components including DNA, RNA, lipids, and proteins if not kept tightly under control (Balasubramanian et al., 1998, Halliwell and Gutteridge, 1995). The hydroxyl radical is typically formed *in vivo* under hypoxic conditions due to the impacts of hypoxia on cytochrome chain activity ultimately driving increased generation of ROS such as $\cdot\text{O}_2^-$, which may be converted to the highly reactive hydroxyl radical as a result of the Haber-Weiss reaction (Coimbra-Costa et al., 2017, Michiels, 2004).

Other notable ROS

Nitric oxide (NO^\bullet) or nitrogen monoxide is a reactive oxygen and nitrogen species (RONS) formed by various nitric oxide synthases. It is aqueous and lipid soluble and can readily diffuse across biological membranes (Chiueh, 1999). NO^\bullet is an important intracellular messenger in vascular homeostasis and is involved in immune defence (Félétou et al., 2012, Tripathi, 2007).

If nitric oxide reacts with superoxide it can form peroxynitrite (ONO_2^-), a powerful oxidant that is highly toxic and can react with carbon dioxide (CO_2) to form other highly reactive nitrogen species that can lead to cellular damage (Pacher et al., 2007).

Hypochlorous acid (HOCl) can be generated from H_2O_2 reacting with chlorine, a reaction catalysed by myeloperoxidase (Klebanoff, 2005). It is produced *in vivo* by neutrophils during immune responses and inflammation (Ulfig and Leichert, 2020).

Singlet oxygen ($^1\text{O}_2$) is a highly reactive and toxic ROS generated by neutrophils and eosinophils in immune responses. It is a highly potent oxidizing radical with the capabilities of causing DNA and tissue damage. Singlet oxygen can also be converted to ozone (O_3) - another highly reactive radical utilized by white blood cells to neutralize invading pathogens (Wentworth, 2002).

1.2.3. Endogenous sources of ROS

After the discovery that mitochondria generate hydrogen peroxide in the 1960s, and the subsequent findings that hydrogen peroxide arose as a result of the dismutation of mitochondrial $^{\bullet}\text{O}_2^-$, these organelles have been considered a major source of endogenous ROS (Jensen, 1966, Loschen et al., 1974). However, it is pertinent to note that while these early studies gave rise to the ROS theory of ageing, it has since been demonstrated that the use of isolated mitochondria in initial studies lead to overinterpretation of the levels of ROS *in vivo* that has subsequently been de-bunked by several studies and reviews (Gems and Doonan, 2009, Gladyshev, 2014, Harman, 2006, Salmon et al., 2010).

Typically, mitochondrial ROS is generated as a by-product of oxidative phosphorylation. To generate ATP, hydrogen ions are sequestered into the matrix space to create a concentration gradient (Jastroch et al., 2010). This concentration gradient drives the passing of hydrogen ions through ATP synthase, phosphorylating molecules of ADP to ATP. The generation of this concentration gradient is dependent on the electron transport chain, which is composed of four complexes that undergo a series of redox reactions, passing electrons from one component to the next (Figure 1.1).

The electron transport chain can sometimes “leak” electrons as they pass from one complex to the next (Jastroch et al., 2010). Complexes I (NADH-dehydrogenase) and III (cytochrome c-oxidoreductase) are the main sources of these “leaky” electrons which react with molecular oxygen to form superoxide ions (Zorov et al., 2014). In typical conditions, SOD converts these superoxide anions into hydrogen peroxide, which is subsequently converted to molecular oxygen and water by catalase (CAT) (Younus, 2018).

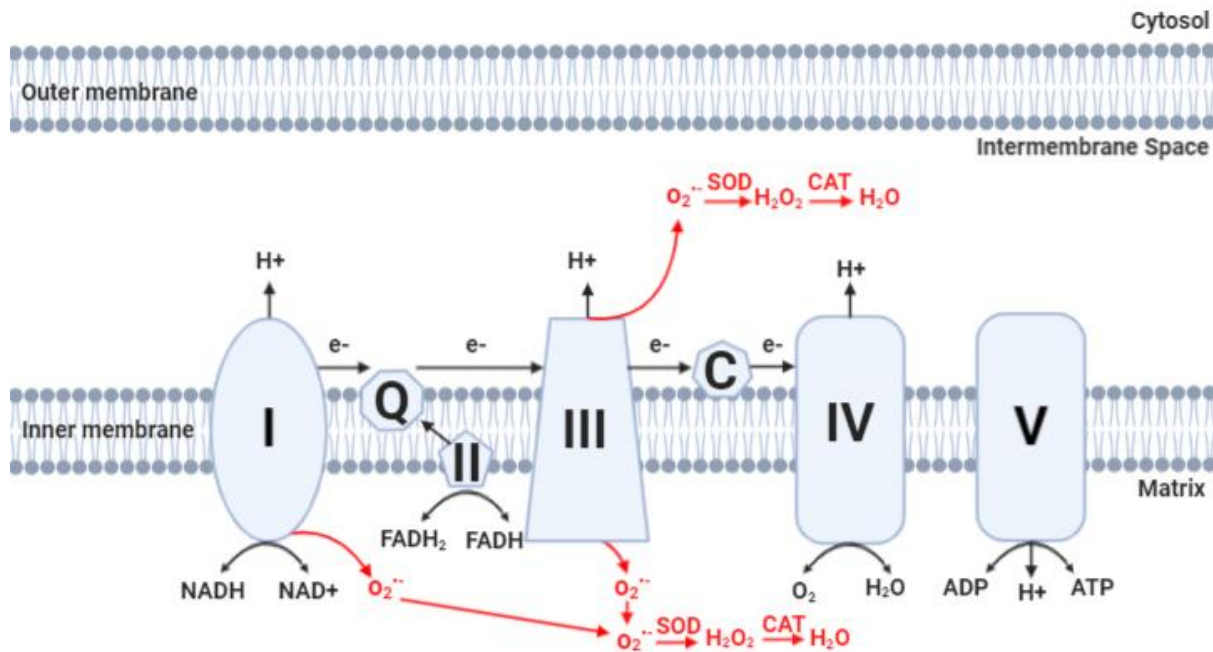


Figure 1.1. Schematic representation of the electron transport chain (ETC) in mitochondrion. Electrons sourced from NADH and FADH₂ are passed through the ECT from one complex to the next but can sometimes “leak” from complexes I and III where they react with molecular oxygen generating superoxide anions (O₂^{•-}). O₂^{•-} radicals are then converted to hydrogen peroxide (H₂O₂) by superoxide dismutase (SOD). H₂O₂ is subsequently converted to water and oxygen by catalase (CAT). Image created using BioRender.

Another source of endogenous ROS is the endoplasmic reticulum, which contains cytochrome P450 (CYP) enzymes that may contribute to the formation of ROS. CYPs are primarily expressed in the liver, and the main function of these enzymes is relevant to the synthesis and metabolism of lipids, and metabolism of xenobiotic compounds (Palrasu and Siddavaram, 2018). Several steps in the CYP reaction mechanism produce ROS including [•]O₂, H₂O₂ and [•]OH, which, if not tightly controlled, may lead to cellular damage (Hrycay and Bandiera, 2012).

Other endogenous sources of ROS include NADPH oxidases (Meitzler et al., 2014), lipoxygenases (Thornber et al., 2009) and peroxidases (Parker and Winterbourn, 2013). The former generates superoxide radicals to be utilized by phagosomes to inactivate invading pathogens in immune responses, whereas the latter two produce ROS during lipid metabolism (Meitzler et al., 2014, Parker and Winterbourn, 2013).

1.2.4. Exogenous sources of ROS

External stressors may contribute to an imbalance in the generation and neutralization of ROS, thus causing oxidative stress leading to cellular damage and dysfunction. These stressors include pollutants, xenobiotics, ultraviolet (UV) or other types of radiation, and lifestyle factors such as alcohol consumption (Azzam et al., 2012b, Barzilai and Yamamoto, 2004).

Several studies have linked a rise in air pollution with increased ROS levels, and the resulting oxidative stress has been shown to exacerbate adverse health effects of patients suffering from respiratory diseases (Lakey, 2016). This is thought to be due to highly redox active molecules found in fine particulate matter, including transition metals and quinones.

Radiation can cause both direct and indirect cellular damage. Ionizing radiation is capable of causing direct damage to DNA molecules, or can indirectly cause damage through the radiolysis of water to generate hydroxyl and hydrogen radicals (Azzam et al., 2012a). UV radiation catalyses a range of molecular changes in dermal cells. UV photons may directly cause DNA lesions by promoting the formation of thymine dimers (Beukers et al.). UV radiation also promotes the generation of ROS (including H₂O₂, •OH and singlet oxygen), and the release of pro-inflammatory cytokines such as IL-1 and TNF-α (Pillai et al.).

Xenobiotics include drugs, food additives and some pollutants, which are metabolised by CYP enzymes. As previously mentioned, (see '1.2.3. Endogenous sources of ROS'), several steps of the CYP pathway generate ROS (Hrycay and Bandiera, 2012).

Dietary factors may also play a role in the generation of ROS. High-carbohydrate and high-fat diets can increase cellular respiration, thus increase the amount of •O₂ generated from mitochondria (Tan et al., 2018, Teodoro et al., 2013). High glucose levels has been demonstrated to induce toll-like receptor expression in human monocytes via stimulation of

NADPH oxidase, this, in turn, leads to ROS production and inflammation via a nuclear factor kappa-light-chain-enhancer of B cells (NF- κ B) mediated pathway (Dasu et al., 2008, Jia et al., 2013). The cooking of uncured red meat releases Fe²⁺ which can subsequently react with hydrogen peroxide in a Fenton reaction to produce hydroxyl radicals (Tan et al., 2018, Van Hecke et al., 2015). The study by Van Hecke et al (2015) noted that nitrite-cured meat from the same batch of red meat contained significantly less Fe²⁺ than corresponding uncured meats, hence reduced levels of hydroxyl radicals produced. It is also thought that the process of cooking meat depletes levels of antioxidant enzymes such as glutathione peroxidase that would normally combat the ROS produced (Hoac et al., 2006, Serpen et al., 2012).

Alcohol metabolism provides a variety of avenues by which ROS may be generated. Alcohol causes heightened cellular respiration, initiates change in the production of cytokines therefore influencing immune responses, activates CYP enzymes, affects the activity of antioxidants such as glutathione, and in some cases leads to alcohol-induced oxygen deficiency i.e., hypoxia (Cunningham and Horn, 2003, Wu and Cederbaum, 2003).

1.2.5. Intracellular responses to ROS

The generation of ROS prompts stress response signalling cascades to mediate cellular repair and adaptation mechanisms, autophagy, and in some cases, cell death.

Signalling pathways that are either directly, or indirectly, influenced by ROS include; mitogen-activated protein kinase (MAPK) pathways including c-Jun terminal kinases (JNK) and p38 kinase (p38) (Son et al., 2013), phosphoinositide 3-kinase (PI3K) pathways such as the insulin/IGF-1 signalling (IIS) pathway (Kim et al., 2018, Wen et al., 2019), activation of nuclear factor erythroid-2-related factor 2 (Nrf2) (Taguchi et al., 2011), 5' AMPK-activated protein kinase (AMPK) (Hinchy et al., 2018), and mediators upstream of NF- κ B, including I κ B kinase (I κ K) or PI3K pathway mediators (Gloire et al., 2006). These pathways are summarised in Figure 1.2.

Pro-apoptotic genes are transcribed following the activation of c-Jun and activating transcription factor 2 (ATF2) by JNK and p38 pathways (Fan and Chambers, 2001, Walton et al., 1998). Activation of the transcription factor NF- κ B leads to the transcription of cytokines and proteins required for inflammatory responses, cellular proliferation and cell cycle regulators (Gloire et al., 2006). Following its dissociation from Kelch-like ECH-associated

protein 1 (Keap1), Nrf2 translocates to the nucleus where it binds to an enhancer known as the antioxidant response element (ARE) (Venugopal and Jaiswal, 1996), triggering the transcription of antioxidant genes including glutathione-S-transferase (GST) and NADPH quinone oxidoreductase (NQO1) (Lewis et al., 2015). Forkhead box O transcription factors (FoxO) activation either by AMPK or through inhibition of the PI3K pathway promotes the transcription of antioxidant genes including superoxide dismutase (SOD) and catalase (CAT) (Greer and Brunet, 2005, Kops et al., 2002), and DNA repair enzymes such as growth arrest and DNA damage-inducible 45 family members (GADD45) (Fornace et al., 1988, Tran et al., 2002).

The initiation of these signalling cascades by ROS may have short-term protective effects. For example, it has been demonstrated that increased ROS generation from regular exercise leads to the upregulation of antioxidant and stress responses, which have protective effects over time (Simioni et al., 2018). Also, as previously mentioned (see '1.2.3. Endogenous sources of ROS'), ROS can be utilized in immune responses to protect the host organisms from invading pathogens (Féléto et al., 2012, Tripathi, 2007).

However, repeated or prolonged exposure to stressors that increase ROS levels may override these protective stress responses, causing cellular damage and thus cellular dysfunction, which may lead to deterioration of health (Pizzino et al., 2017).

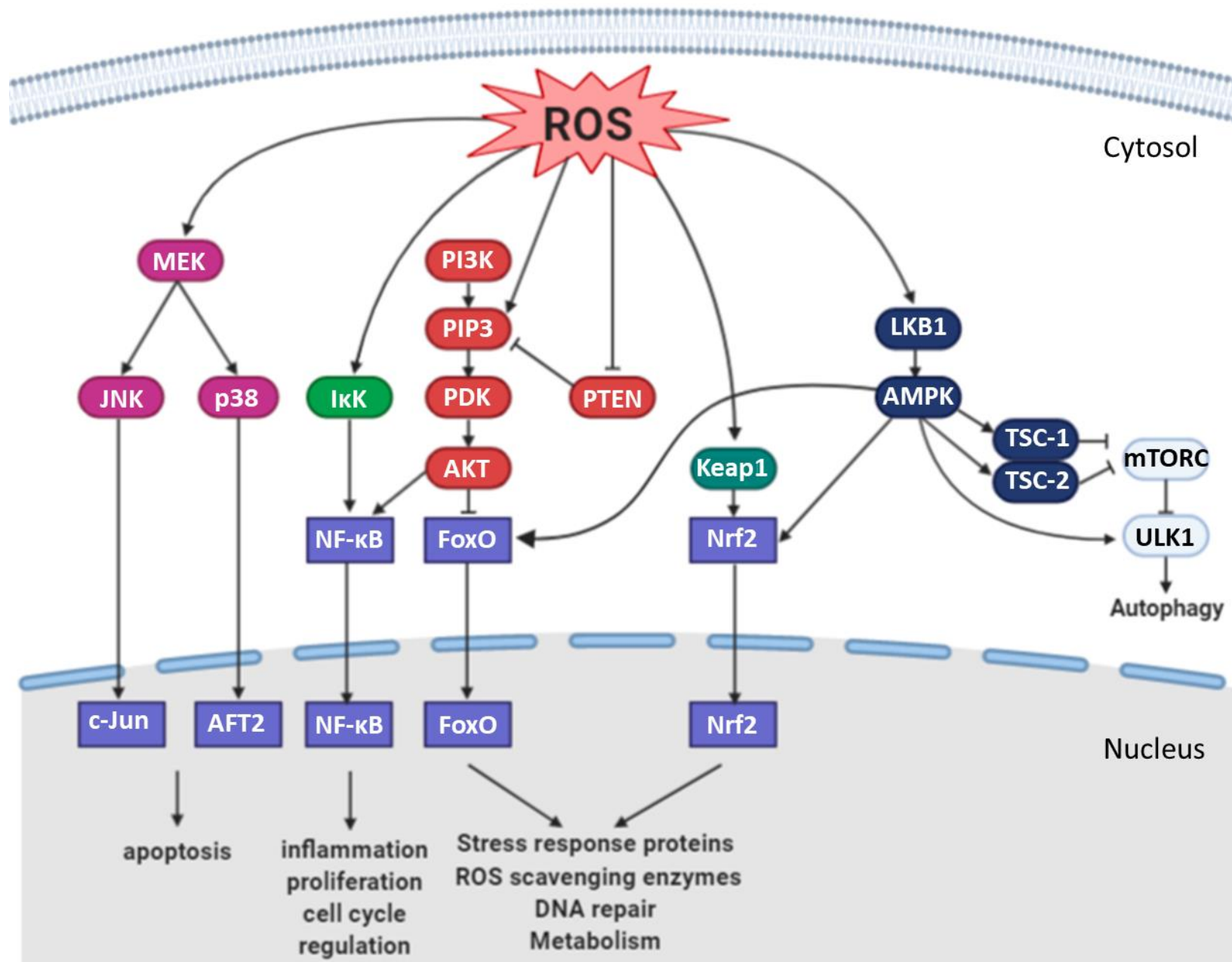


Figure 1.2. Schematic diagram of pathways influenced by reactive oxygen species (ROS). ROS can activate MAPK pathways, indicated in purple, via mitogen-activated protein kinase (MEK). MEK activates c-Jun terminal kinase (JNK) and p38 kinase (p38) activating transcription factors including c-Jun and activating transcription factor 2 (ATF2), indicated in blue, which promote the transcription of pro-apoptotic genes. The transcription factor nuclear factor kappa-light-chain-enhancer of B cells (NF- κ B) can be activated either through ROS-induced activation of the I κ B kinase (IKK), or through the phosphoinositide 3-kinase (PI3K) pathway (indicated in red) via protein kinase B (PKB), also known as Akt. ROS can activate the PI3K pathway either through direct activation of phosphatidylinositol (3,4,5)-trisphosphate (PIP₃), or through inhibition of the PIP₃ inhibitor phosphatase and tensin homolog (PTEN). Activation of Akt phosphorylates Forkhead box O transcription factors (FoxO), preventing their translocation to the nucleus where they promote the transcription of genes linked to stress responses, DNA repair and metabolism. Kelch-like ECH-associated protein 1 (Keap1), indicated in teal, associates with the nuclear factor erythroid-2-related factor 2 (Nrf2) under non-stressed conditions, but ROS causes Keap1 to dissociate from Nrf2 allowing it to translocate to the nucleus, where it activates the transcription of antioxidant response genes. The 5' AMP-activated protein kinase (AMPK) pathway, indicated in navy, is activated through the upstream messenger liver kinase B1 (LKB1). AMPK can activate transcription factors including FoxOs and Nrf2 to promote transcription of stress response genes or is able to inhibit the mTORC pathway via tuberous sclerosis proteins (TSC). AMPK can directly and indirectly activate autophagy either by inhibition of the mTORC pathway or direct activation of unc-51 like autophagy activating kinase 1 (ULK1). *Image created using BioRender.*

1.2.6. Implications of oxidative stress on health

While short-term, or mild exposure to ROS has been demonstrated to be beneficial for the upregulation of antioxidant and stress responses, prolonged exposure to oxidative stress may lead to lasting cellular damage which results in tissue dysfunction (Barzilai and Yamamoto, 2004, Rahman et al., 2012, Stadtman, 1997). This tissue dysfunction, in turn, may lead to the onset of, and symptoms of the many conditions including; cardiovascular disease (CVD), respiratory and kidney disease, arthritis, neurological disorders and cancer (Belenguer-Varea et al., 2020, Pizzino et al., 2017, Rahman et al., 2012). For example, in the instance of CVD, increased ROS may lead to decreased nitric oxide availability and vasoconstriction promoting hypertension – one cause of CVD (Senoner and Dichtl, 2019).

Many of these conditions are characterized by an increase in levels of biomarkers indicative of oxidative stress. Some examples include protein carbonyls (PC), malondialdehydes (MDA) and 8-oxo-2'-deoxyguanosine (8-oxo-dG), used to detect protein, lipid and DNA damage, respectively. There are, of course, many more biomarkers for oxidative stress, which have been summarised in numerous reviews (Bernstein et al., 2008, Dalle-Donne et al., 2003, Del Rio et al., 2005).

1.2.7. The oxidative damage theory of ageing

The oxidative damage theory of ageing was first proposed in the 1950s (Harman, 1956), and has since been extended and adapted in subsequent decades (Alexander, 1967, Harman, 2006). The current theory proposes that while there are complex processes governing the ageing process, a factor in this is the accumulation of oxidative damage to cellular components (i.e., lipids, proteins, and DNA), leading to cellular dysfunction, age-related disease and ultimately, death.

Numerous studies have implicated increased ROS levels to ageing (Cui et al., 2012, Salmon et al., 2010). It has been demonstrated that levels of biomarkers indicative of oxidative damage, such as 8-Oxo-dG, increase with age in mice, rats, and humans (Bernstein et al., 2008). While there seems to be limited evidence to suggest oxidative stress plays a role in determining the lifespan of an animal, murine models deficient in antioxidant enzymes are prone to earlier onset of ageing-related disease, while overexpression of antioxidant enzymes correlates with

increased healthspan (Hamilton et al., 2012). Further to this, an extension of lifespan in organisms such as yeast and *Drosophila melanogaster* has been demonstrated through the reduction of oxidative damage (Fontana et al, 2010), adding to the plausibility of this theory.

Although this evidence highlights the detrimental effects of oxidative damage in senescence, the theory does not come without dispute. Overexpression of the antioxidant enzyme SOD (see '1.2.1. Types of Reactive Oxygen Species (ROS)') has no effect on lifespan in mice (Pérez et al., 2009), and deletion of these enzymes in *C. elegans* has no impact on lifespan (Van Raamsdonk and Hekimi, 2012). In fact, one study showed that treatment with antioxidant supplements shortened lifespan in voles (Selman et al., 2013), and a review by Gems and Doonan (2009) failed to find convincing evidence to support the oxidative damage theory. In addition, it has been demonstrated that exogenous sources of ROS may have a mitohormetic effect. For example, low dosage of ROS-producing arsenite can promote the growth of mammalian cell cultures as well as promote stress resistance and longevity in *C. elegans* (Schmeisser et al., 2013). Taken together, the data emphasises the complex relationship between oxidative stress, health, and lifespan.

1.2.8. Criticisms of the oxidative damage theory of ageing

The main criticism of the oxidative damage theories of ageing is that there are a myriad of other factors which contribute to ageing that fail to be considered, and as alluded to previously (see "1.1. Implications of an ageing population") there are many varied theories as to the root cause of ageing (Borrás, 2021, da Costa et al., 2016, Jin, 2010).

One main criticism of the theory is that early studies may have grossly overestimated the amount of free radicals generated by oxidative phosphorylation. Early studies to assess ROS production were performed using isolated mitochondria which are known endogenous sources of ROS (see "1.2.3. Endogenous sources of ROS"). However, if oxidative stress occurs in localised areas of the cell, such as in mitochondria, these analyses of oxidative stress may not be representative of true damage caused by ROS (Gladyshev, 2014). In line with this, several papers have been published to de-bunk the initial overinterpretation of *in vivo* ROS levels from early studies (Gems and Doonan, 2009, Salmon et al., 2010).

In addition, it is hard to ignore that the oxidative damage theory of ageing only considers one type of cellular damage as a contributor to ageing, when in fact there are several types of damage that are associated with ageing processes, such as oxidative stress, glycation, telomere shortening, DNA damage, mutations and protein aggregation (Gladyshev, 2014, Liochev, 2015). Further to this, the genetic basis for longevity cannot be ignored (see “1.1. Implications of an ageing population”) (da Costa et al., 2016, Jin, 2010, van Hjelmborg et al., 2006).

Gladyshev (2014) proposes that the true cause of ageing may lie in “biological imperfectness” whereby “all biomolecules and biological processes are imperfect resulting in unintended activities and functions”. The theory takes in to consideration the fact that biological processes all produce unwanted by-products that can lead to damage accumulation, and that while natural selection may enhance an organisms ability to neutralise damage and promote repair, ultimately the damage accumulation will compromise cellular function leading to death (Gladyshev, 2014).

1.3. *Klotho* and β -*klotho*

1.3.1. An introduction to *klotho*

The *klotho* gene, named after one of three Fates in Greek Mythology, was first dubbed an “anti-ageing” gene after its discovery in the late 1990s (Kuro-o et al., 1997). It was found that mice with hypomorphic *klotho* alleles displayed phenotypes resembling human accelerated ageing, including early onset of; arteriosclerosis, osteoporosis, emphysema, infertility and diminished lifespan (Kuro-o et al., 1997). A later study found extended lifespan of up to 20.0-30.8% in male and 18.8-19.0% in female murine models overexpressing *klotho*, emphasising the importance of this gene in senescence and longevity (Kurosu et al., 2005). In addition, injection of soluble recombinant *klotho* protein into *kl/kl* mice extended lifespan and suppressed the accelerated senescence of these models (Chen et al., 2013b). Furthermore, in human populations, genetic variants of *klotho* have been demonstrated as indicators of health and longevity (Arking et al., 2005, Majumdar and Christopher, 2011).

So far, the only known function of *klotho* and paralogous β -*klotho* proteins is as co-factors for endocrine fibroblast growth factor (FGF) signalling, enabling the binding of FGFs -19, -21 and

-23 to their cognate fibroblast growth factor receptors (FGFRs) (Kurosu et al., 2006). These endocrine FGFs have broad roles in metabolism, which will be discussed below (see '1.3.4. Endocrine Fibroblast Growth Factor (eFGF) Signalling').

1.3.2. Klotho and β -klotho

The human genome encodes three genes within the klotho family; *klotho*/*KL* (also referred to as α -*klotho*), β -*klotho*/*KLB* and γ -*klotho*/*KLG* (Ito et al., 2000, Matsumura et al., 1998). While *klotho* and β -*klotho* have reported functions in FGF signalling (Kurosu et al., 2006, Razzaque, 2009, Shi et al., 2018, Tomiyama et al., 2010), this is not the case for γ -*klotho*, and little is known for the function of this isoform, though it is noted γ -*klotho* could serve as a novel cell survival biomarker (Trošt et al., 2016). This review will focus on α -*klotho* and β -*klotho*.

The human *KL* gene is located on chromosome 13q13.1 and is composed of five exons ranging over 50kb in length (Matsumura et al., 1998). The *KLB* gene is located on chromosome 4p14 and shares 41.2% homology to α -*klotho* (Ito et al., 2000). These genes encode single pass type 1 transmembrane glycoproteins composed of just over 1000 amino acids and are expressed primarily in plasma membranes and Golgi apparatus (Matsumura et al., 1998, Olejnik et al., 2018). The klotho proteins are composed of a short intracellular domain and two extracellular KL1 and KL2 domains, which share amino-acid homology to family 1 β -glycosidases and to each other (Figure 1.3) (Kim et al., 2015, Kuro-o et al., 1997, Matsumura et al., 1998, Shiraki-lida et al., 1998).

While β -*klotho* exist only as a membrane protein, α -*klotho* is able to enter circulation following cleavage by A Disintegrin and Metalloproteinases ADAM10 and ADAM17 (see Figure 1.3.) (van Loon et al., 2015). These ADAM proteases are able to cleave α -*klotho* at the plasma membrane to generate full-length soluble α -*klotho* consisting of both the KL1 and KL2 extracellular domain, or in between the KL1 and KL2 domains to generate soluble klotho fragments (Chen et al., 2007, van Loon et al., 2015). In addition, another form of circulating α -*klotho* is generated from alternate splicing of mRNA producing a secreted protein consisting mainly of the KL1 domain (Matsumura et al., 1998, Shiraki-lida et al., 1998). Alongside the established roles as scaffold proteins for FGF signalling, it was thought the cleaved forms of

klotho could have glycosidase activity (Chang et al., 2005), however recent structural evidence is incompatible with this theory (Chen et al., 2018).

Transcripts of *klotho* and *β-klotho* are primarily expressed in metabolic tissues. *Klotho* is expressed in the kidney, placenta, and small intestine tissues, whereas *β-klotho* is mainly expressed in brown and white adipose tissues, liver, and pancreas (Ito et al., 2000, Lim et al., 2015, Matsumura et al., 1998). Currently, the only known functions of *klotho* and *β-klotho* are as co-factors for endocrine FGF signalling, as discussed below.

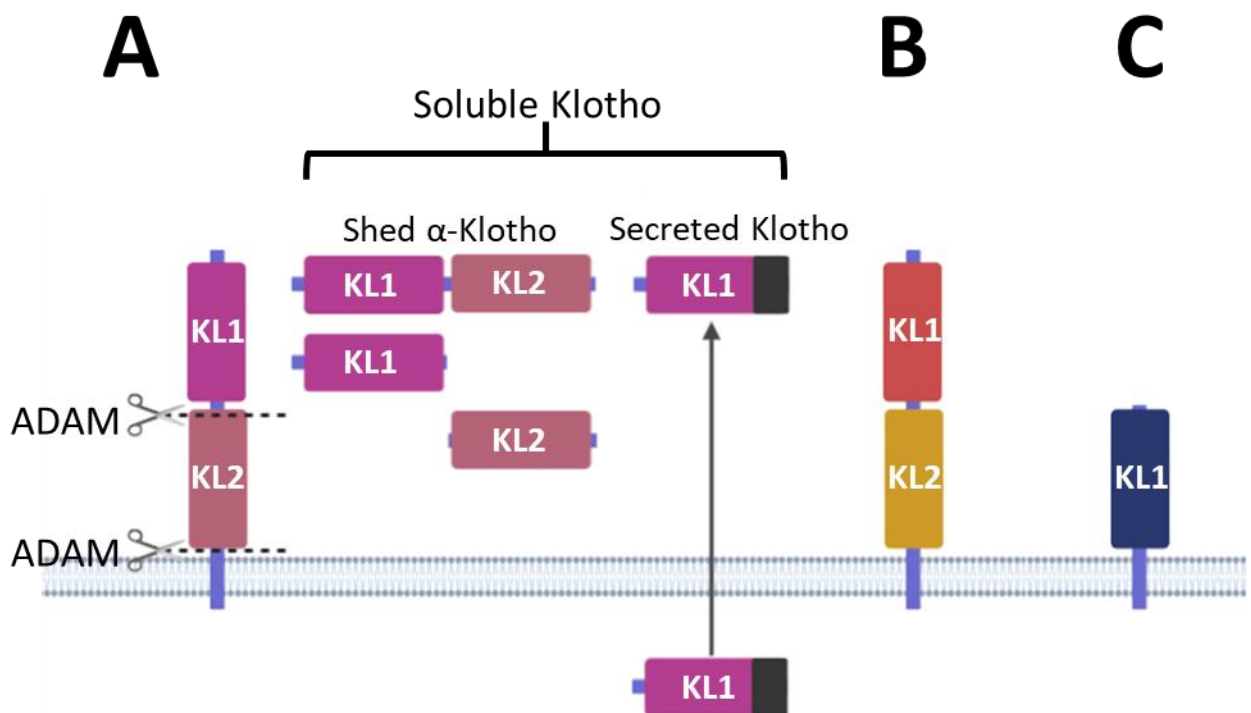


Figure 1.3. Schematic diagram of human klotho proteins. (A) α -klotho can exist tethered to the membrane of the cell or may be cleaved by A Disintegrin Metalloproteases (ADAM) to form several forms of shed α -klotho proteins that may enter circulation. Alternate splicing of α -klotho mRNA also generates a secreted form of the protein consisting of the KL1 domain only. (B) β -klotho protein consisting of KL and K2 domains. (C) γ -klotho protein consisting of one KL1 domain and a short transmembrane domain. Image adapted from Olejnik et al. (2018), created in BioRender.

1.3.3. Typical Fibroblast Growth Factor (FGF) signalling

Fibroblast growth factors (FGFs) are cell signalling proteins with crucial roles in paracrine and endocrine signalling from embryonic development through to adulthood (Kinnunen, 2019, Ornitz and Itoh, 2015). In humans, 22 growth factors fall under the FGF family umbrella, identified as such due to their structural similarities (Ornitz and Itoh, 2015).

There are four FGF receptors (FGFR) encoded for by the human genome. Of these, there are several variants of FGFRs -1, -2 and -3 (due to alternate mRNA slicing), meaning up to seven sub-types of FGFR may be expressed at the surface of the cell (Gong, 2014). These FGFRs consist of three extracellular immunoglobulin-like domains (D1-3), a single span transmembrane domain and an intracellular tyrosine kinase domain (Ornitz and Itoh, 2015).

FGFs interact with the D2 and D3 domains of FGFRs (Ornitz and Itoh, 2015). In typical FGF signalling, heparan sulphate proteoglycans (HSPG) are required for the binding of FGF ligands to their respective receptor (Lin, 2004). Due to the ubiquitous nature of HSPG expression the majority of FGF ligands have paracrine functions physiologically (Lin, 2004). However, a subset of FGF ligands, endocrine FGFs, have low affinity for heparan sulphate meaning they do not act locally from the tissue of secretion and instead enter circulation (Itoh et al., 2015).

1.3.4. Endocrine fibroblast growth factor (eFGF) signalling

Endocrine FGFs -19 (FGF15 in rodents), -21 and -23 have roles in bile acid synthesis, glucose and lipid metabolism, and vitamin D metabolism, respectively (Inagaki et al., 2005, Micanovic et al., 2009, White et al., 2000). These eFGFs form 1:1:1 ternary complexes with either klotho or β -klotho via their C-terminus, and the respective FGFR via the N-terminus (Figure 1.4) (Chen et al., 2018, Kurosu et al., 2006, Lee et al., 2018b, Micanovic et al., 2009, Wu et al., 2007, Yie et al., 2009) FGF21 requires β -klotho as a co-factor and FGF23 requires α -klotho, whereas FGF19 is reported to have no preference over α - or β -klotho (Kurosu et al., 2006, Micanovic et al., 2009, Shi et al., 2018, Wu et al., 2007). Kurosu et al. (2006) found that klotho bound to all isoforms of FGFR, with a preference for “c” isoforms of each receptor, but with a lower affinity for variants of FGFR2 (Kurosu et al., 2006). A later study also found that β -klotho engaged a conserved site in the Ig-like D3 domain of FGFR1c (Goetz et al., 2012). Due to the broad expression of FGFRs, it is the select expression of membrane-bound klotho and

β -klotho in metabolic tissues that governs the specificity of these circulating FGFs (Ito et al., 2000, Lim et al., 2015).

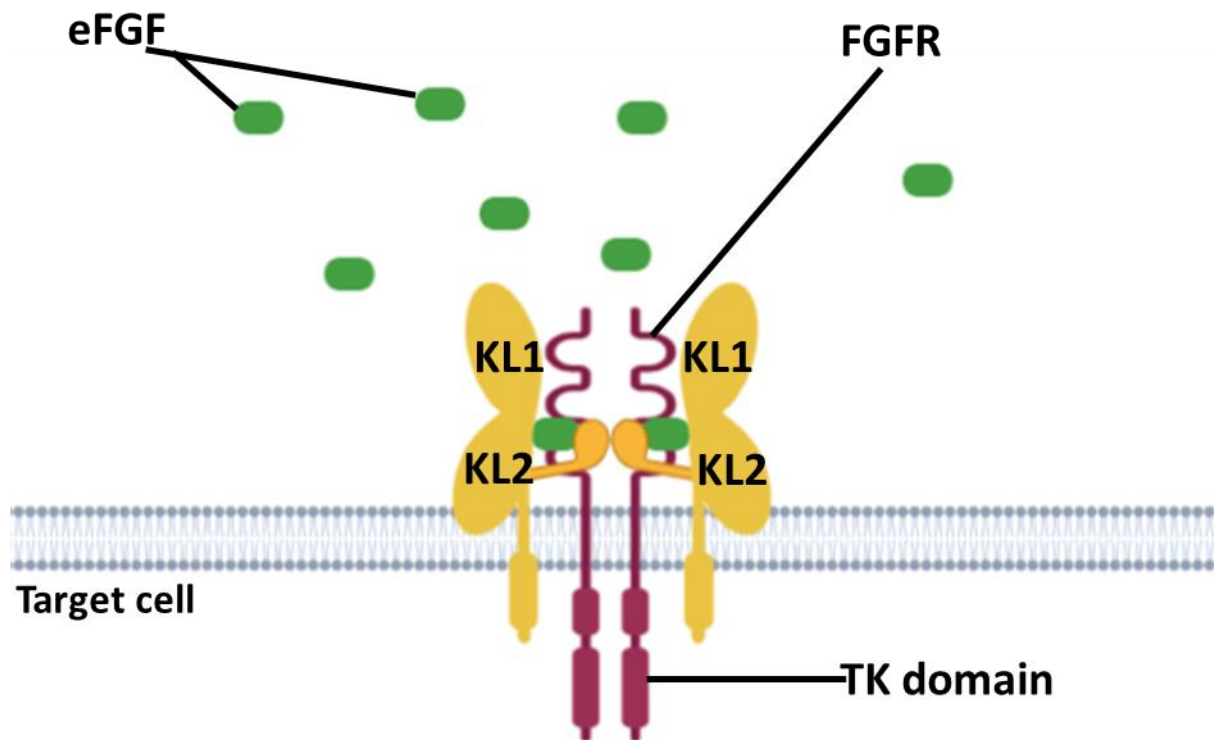


Figure 1.4. Schematic representation of an eFGF-klotho-FGFR complex. Klotho proteins (yellow) consist of KL1 and KL2 extracellular domains as well as a short intracellular domain. The KL2 domain of α -klotho has a “receptor binding arm” (RBA) for the purpose of tethering eFGFs to their respective receptor. Fibroblast Growth Factor Receptor (FGFR) (purple) has 3 extracellular domains and one intracellular tyrosine kinase (TK) domain. Endocrine fibroblast growth factors (eFGFs) (green) are secreted from produce cells and bind to the eFGF-klotho-FGFR complex between the D2 and D3 extracellular domains of the respective FGFR. Image adapted from (Kuro-o, 2019), created in BioRender.

1.3.4.1. Roles of FGF23 in vitamin D metabolism

FGF23 is predominantly expressed in osteoblasts and osteocytes in response to calcitriol (1,25(OH)₂D) as part of a bone-kidney feedback loop (Quarles, 2012). Upon entering circulation, FGF23 targets FGFRs and α -klotho expressed in the kidneys, and upon binding to

the receptor complex promotes a signalling cascade that downregulates sodium (Na)-dependent co-transporters along the distal tubules leading to decreased phosphate reabsorption (Farrow et al., 2009). FGF23 also decreases the amount of 1,25(OH)₂D generated in the kidneys through deactivation of cytochrome P450 family 27 subfamily B member 1 (Cyp27b1) and activation of cytochrome P450 family 24 subfamily A (Cyp24) (Bai et al., 2016, Bai et al., 2003).

The importance of orderly FGF23 function for calcium and phosphate homeostasis is emphasised by mutations that cause an increase or decrease in its activity. Mutations that increase FGF23 levels have been shown to cause autosomal dominant hypophosphatemic rickets characterized by the excessive loss of phosphate through urine (White et al., 2000). Conversely, *Fgf23*^{-/-} murine models displayed hyperphosphatemia and abnormal bone phenotypes (Shimada et al., 2004). This hyperphosphatemic phenotype is consistent with progeria phenotypes caused by *Klotho* mutations (Shiels et al., 2017).

1.3.4.1.1. *Klotho* as a pro-longevity regulator

Soluble α -klotho has been demonstrated to modulate a number of evolutionarily conserved longevity pathways including; IIS, TOR, cAMP, PKC and Wnt (Imai et al., 2004, Liu et al., 2007, Rakugi et al., 2007, Yamamoto et al., 2005, Zhao et al., 2015). The precise mechanisms governing the effects of α -klotho on these longevity pathways remain to be elucidated.

However, it can be argued that the effects of α -klotho on ageing can be attributed to the roles of this protein in vitamin and mineral homeostasis. For example, there are some paradoxical findings that both α -klotho-deficient and overexpressing mice demonstrate premature ageing-like phenotypes, and that this can be attributed to increased serum levels of FGF23 (Cheikhi et al., 2019, Razzaque, 2009). In addition, the ageing-related phenotypes described in the Kuro-o (1997) paper which first lead α -klotho to be referred to as an “anti-ageing” gene, such as atherosclerosis, osteoporosis and emphysema, have been demonstrated to be associated with impaired calcium and phosphate metabolism characterised by α -klotho and FGF23 dysfunction (Bi et al., 2020, Cheikhi et al., 2019, Donate-Correa et al., 2015, Kraen et al., 2021, Lanzani et al., 2020). Furthermore, the premature ageing-like phenotypes exhibited by FGF23 or klotho knockout mice is diminished in combination with vitamin D receptor (VDR) knockout (Andrukhova et al., 2017), further cementing the theory that the impacts of klotho on healthspan and lifespan may be the result of the key roles for which the protein plays in vitamin and mineral homeostasis.

1.3.4.2. *Roles of FGF21 in lipid and glucose metabolism*

The role of FGF21 was unclear until the discovery that injection of FGF21 into diabetic mice lowers circulating glucose and lipids, highlighting the importance of this signalling protein in glucose and lipid homeostasis (Kharitonov et al., 2005). FGF21 is expressed in several tissues including liver, adipocytes, pancreas, and the brain (Hsueh et al., 2007, Johnson et al., 2009, Nishimura et al., 2000, Tezze et al., 2019, Zhang et al., 2008).

The liver is considered the main site of FGF21 synthesis, with a cross-talk between FGF21 and peroxisome proliferator-activated receptor α (PPAR α) during fasted states (Inagaki et al., 2007). Regulation of FGF21 in the liver is complex with reports of regulation by glucocorticoid receptor (GR), cAMP-responsive element binding protein H (CREBPH), peroxisome proliferator-activated receptor γ (PPAR γ) and farnesoid X receptor (FXR) (Cyphert et al., 2012, Lee et al., 2017, Moyers et al., 2007, Patel et al., 2015, Tezze et al., 2019, Wang et al., 2008). In white adipose tissue (WAT) and brown adipose tissue (BAT), FGF21 is reported to be regulated by PPAR γ (Dutchak et al., 2012) and activating transcription factor 2 (ATF2) (Hondares et al., 2011), respectively. It has also been found that FGF21 in skeletal muscle tissues is regulated by activating transcription factor 4 (ATF4) and the phosphoinositide 3-kinase (PI3K)/ protein kinase B (AKT) pathways (Izumiya et al., 2008, Kim et al., 2013).

FGF21 has been dubbed a “stress-responsive hormone” due to elevated levels in response to oxidative stress, starvation, ER stress, mitochondrial dysfunction and more (Fazeli et al., 2015, Inagaki et al., 2007, Izumiya et al., 2008, Kim et al., 2015, Lin et al., 2011, Morovat et al., 2017, Schaap et al., 2013). This stress-induced protein is elevated in patients with chronic diseases characterized by oxidative stress, and has demonstrable therapeutic effects in instances of obesity, type 2 diabetes, chronic kidney disease (CKD), cardiovascular disease (CVD) and non-alcoholic fatty liver disease (NAFLD) (Lin et al., 2011, Mottillo et al., 2017, Nygaard et al., 2012, Planavila et al., 2015, Schaap et al., 2013).

FGF21 requires β -klotho as a co-factor to form a complex with its respective FGFRs and exert its downstream effects (Yie et al., 2009). Reported pathways regulated by FGF21 include MAPK/ ERK, IIS and mTOR (Ge et al., 2011, Inagaki et al., 2007, Moyers et al., 2007, Muise et al., 2013). There are also noted cross-talks with AMPK signalling with studies indicating mechanisms both dependent and independent of AMPK (Mottillo et al., 2017, Salminen et al., 2016, Sunaga et al., 2019).

1.3.4.3. Role of FGF19/ FGF15 in bile acid synthesis

FGF19 (and its murine orthologue, FGF15) is produced in the ileum in response to bile acid absorption (Inagaki et al., 2005). Upon entering circulation, FGF19 acts on hepatocytes to repress *Cyp7a1* gene expression, thus inhibiting bile acid synthesis (Inagaki et al., 2005). The role of FGF19 in bile acid homeostasis is highlighted in conditions such as bile acid malabsorption, frequently characterized by chronic diarrhoea, which has been linked to low serum levels of FGF19 (Walters et al., 2009).

Overexpression of FGF19 in transgenic mice skeletal muscle increases metabolic rate and reverses obesity-related concerns including hepatic lipid accumulation and insulin resistance (Tomlinson et al., 2002). FGF19 treatment applied to *ob/ob* mice, (which have a genetic mutation in *leptin* causing them to become obese) or mice given a high-fat-diet (HFD), led to weight loss and improvements on glucose regulation and insulin sensitivity due to its effects on metabolic rate (Fu et al., 2004, Kir et al., 2011). These metabolic effects are similar to FGF21 function suggesting there could be some overlap in common pathways (Inagaki et al., 2005, Kharitonov et al., 2005, Wu et al., 2011).

FGF19 activation is reported to stimulate several pathways including ERK1/2, mTOR and c-Jun N kinase pathways (see review: Somm and Jornayvaz (2018)). There are also reported roles in antioxidant responses showing that FGF19 stimulates Nrf2 and reduces ROS production via an AMPK pathway (Li et al., 2018).

1.3.5. Klotho and metabolic disease

Impaired *klotho* and *β-klotho* expression is implicated in many conditions associated with metabolic dysfunction such as chronic kidney disease (CKD), cardiovascular disease (CVD), metabolic syndrome, diabetes mellitus and several cancers (Donate-Correa et al., 2015, Kim et al., 2019, Majumdar and Christopher, 2011, Sachdeva et al., 2020, Zou et al., 2018).

Metabolic Syndrome

Metabolic syndrome is a combination of several risk factors for disease including obesity, insulin resistance and hypertension (Rochlani et al., 2017). The condition is becoming increasingly common, often attributed to the consumption of a Western diet (Kopp, 2019). In

addition to lifestyle choice, it has been predicted that genetic factors could play a part in an individual's predisposition to the disease, with genetic variants of *klotho* being linked to increased risk of the condition (Majumdar and Christopher, 2011). In accordance with other evidence, *klotho* has a protective effect on the prevention of metabolic syndrome, and serum levels of *klotho* are inversely linked to metabolic syndrome in patients with CKD (Kim et al., 2019).

Diabetes

Several studies have linked *klotho* physiology to type 2 diabetes (T2DM) (Lee et al., 2014a, Nie et al., 2017). Levels of both α -*klotho* and β -*klotho* were downregulated in patients with T2DM linking serum levels of these proteins to the development of the disease (Zhang and Liu, 2018). In addition to reduced *klotho* in circulation, serum levels of FGF19 and FGF21 are lowered and raised, respectively, in T2DM patients with metabolic syndrome (Barutcuoglu et al., 2011, Zhang et al., 2008). In fact, FGF19 and -21 have been proposed as therapeutics for treatment of T2DM (DePaoli et al., 2019, Martinez de la Escalera et al., 2017, Mottillo et al., 2017).

Chronic Kidney Disease (CKD)

The two main causes of CKD are diabetes and hypertension (Webster et al., 2017). Early stages of CKD can be characterized by a decrease in serum and urinary *klotho* as well as a rise in serum FGF23 levels (Lu and Hu, 2017). These levels of FGF23 correlate to oxidative stress and inflammation markers in haemodialysis patients (Nasrallah et al., 2013). In addition, *kl/kl* mice were found to have similar phenotypes to CKD demonstrating the notion that *klotho* is tightly associated with the pathogenesis of the disease (Hu et al., 2011). One proposed mechanism of renoprotective drug Sulodexide is the upregulation of *klotho* expression to prevent disease progression, further highlighting the protective effects of *klotho* (Liu et al., 2017).

Cardiovascular Disease (CVD)

The leading cause of death in CKD patients is complications as a result of CVD (Donate-Correa et al., 2015, Stenvinkel, 2010). Both reduced *klotho* levels and increased serum FGF23 have

been associated with the increased risk and onset of CVD for CKD patients (Arnlov et al., 2013, Hu et al., 2011).

Cancer

A number of studies summarized by Sachdeva et al. (2020) have demonstrated decreased klotho expression in a variety of cancers. These include malignancies of the following tissues: breast, cervical, colorectal, oesophageal and gastric, ovarian, pancreatic, renal, and thyroid (Dai et al., 2015, Fakhar et al., 2018, Gigante et al., 2015, Lee et al., 2010, Pan et al., 2011, Tang et al., 2016, Wolf et al., 2008, Yan et al., 2017). It has been suggested that klotho may function as a potential tumour suppressor and inhibitor of the IIS pathway in cancer demonstrating the protective role of this protein (Wolf et al., 2008).

1.3.6. Intracellular pathways associated with eFGF-klotho-FGFR function

The mechanisms governing the effects of klotho on stress responses and longevity remain ambiguous. It was speculated that the anti-ageing effects of klotho were due to the inhibition of the Insulin/ Insulin-like growth factor signalling (IIS) pathway (Kurosu et al., 2006). The IIS pathway is reported to inhibit FOXO transcription factors from translocating from the cytoplasm to the nucleus where they would typically promote the transcription of stress response and repair genes that may promote longevity (Carter and Brunet, 2007). Klotho has been shown to upregulate antioxidant enzyme expression via a FoxO3-mediated mechanism that negatively regulates the PI3K pathway associated with IIS (Lim et al., 2017, Yamamoto et al., 2005). Moreover, it was noted that *kl/kl* mice were extremely sensitive to insulin (Utsugi et al., 2000), and secreted klotho was shown to inhibit the IIS pathway *in vitro* indicating a potential mechanism of klotho function (Wolf et al., 2008). However, Lorenzi et al. (2010) found no direct inhibition of Insulin-like growth factor 1 (IGF-1) by klotho in several cell lines opposing the argument for a direct role of klotho in IIS. In addition, data from *C. elegans* models suggest that *klotho* could function in parallel to IIS in longevity and stress responses (Château et al., 2010).

Several pathways have been linked to longevity and oxidative stress (see '1.2.7. The Oxidative Damage Theory of Ageing'), many of which have also been associated with the protective effects of klotho. For example, the expression of FGFs -19, -21 and -23 have been

demonstrated to be regulated by AMPK-dependent pathways in conditions characterised by oxidative stress (Glosse et al., 2018, Guo et al., 2020, Li et al., 2018, Nygaard et al., 2012). In addition, treatments with AMPK-activating pharmaceuticals (e.g., metformin), have been shown to increase the expression of α -klotho and β -klotho (Cheng et al., 2017, Videla et al., 2018). Klotho deficiency has also been linked to decreases in AMPK and SIRT1 activity (Gao et al., 2016). Other reported links to klotho function include; RAS/RAF/MEK/ERK (Ho and Bergwitz, 2020), mTOR (Lin et al., 2013), and JNK pathways (Lee et al., 2018a). Therefore, it could be that the protective effects of Klotho are mediated by pathways associated with oxidative stress, which have been previously discussed (see '1.2.5. Intracellular responses to ROS'). This thesis will explore the impact of genetic deletion of klotho on oxidative stress responses in *C. elegans* and aim to work towards understanding of the relationship between klotho and some of the key pathways associated with control of ROS.

1.4. *Caenorhabditis elegans* as a model of study

1.4.1. A brief introduction to *Caenorhabditis elegans*

Since the 1960s *Caenorhabditis elegans* (*C. elegans*) has been used as a model to study organism development and behaviour (Brenner, 1974). These nematodes have many traits desirable of a genetic model organism including; small size, short life cycle, large brood size, inexpensive culture methods and a relatively short lifespan (Meneely et al., 2019). Benefits of a short life cycle in combination with the production of many progeny (on average an adult hermaphrodite produces almost 300 offspring) are that large scale cultures of these organisms is possible (Meneely et al., 2019).

C. elegans populations consist primarily of hermaphrodites that have the ability to self-fertilize meaning the maintenance of homozygous stocks is straightforward. Male animals account for just 0.2% of *C. elegans* populations under laboratory conditions and typically arise as the result of spontaneous loss of an X chromosome, which occurs at a rate of approximately 1 in 600 animals (Corsi, 2006, Meneely et al., 2019). Despite the rarity of males, it is possible to utilize them to introduce genetic variation into a strain by cross-fertilization with hermaphrodites (Meneely et al., 2019).

C. elegans provides an established model for examining biological processes including; signal transduction, immune responses, stress responses and longevity, to name a few, and because many *C. elegans* genes are conserved across mammalian organisms, these animals provide a tractable, *in vivo* model for mapping molecular and genetic pathways (Harrington et al., 2010).

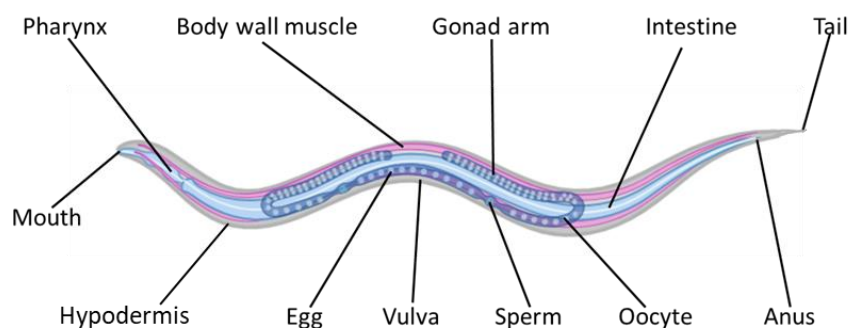


Figure 1.5. Schematic diagram of *Caenorhabditis elegans* model organism. From left to right; mouth, pharynx, hypodermis (grey), body wall muscle (pink), egg, vulva, gonad arm, sperm, oocyte, intestine (blue) anus and tail. Image created using BioRender.

1.4.2. The *C. elegans* genome

The *C. elegans* genome consists of 5 pairs of autosomes and sex chromosomes (XX in hermaphrodites and just one X chromosome in males), and is reported to contain ~20,000 protein-coding genes (Hillier et al., 2004). It is predicted that these genes share homology with up to 80% of human protein-coding genes (Kuwabara and O'Neil, 2001). For example, signalling components of pathways established in stress responses and longevity have been shown to be evolutionarily conserved across species including; IIS pathway components (Guarente and Kenyon, 2000, Hashmi et al., 2013, Kenyon et al., 1993), FOXO-mediated pathways (Lehtinen et al., 2006), AMPK (Apfeld et al., 2004), Nrf2 (An and Blackwell, 2003), and mTOR pathway components (Vellai et al., 2003). Details of several *C. elegans* genes orthologous to human signalling pathway components discussed in this thesis can be found in Table 1.1.

The conserved nature of signal transduction pathways between the *C. elegans* and mammalian models has led to the *C. elegans* model being key in early research for unravelling the genetic and molecular basis for many cellular processes (Meneely et al., 2019).

Table 1.1. Summary of several *C. elegans* genes required for stress response and longevity pathways, and details of their human orthologues.

<i>C. elegans</i> gene	Origin of gene name	Human Orthologue(s)	Reference
<i>aak-1</i>	AMP-Activated Kinase	PKAA1 (AMP-Activated Kinase alpha subunit 1), PRKAA2 (AMPK-Activated Kinase alpha subunit 2)	Apfeld et al. (2004)
<i>aak-2</i>	AMP-Activated Kinase	PKAA1 (AMP-Activated Kinase alpha subunit 1), PRKAA2 (AMPK-Activated Kinase alpha subunit 2)	Apfeld et al. (2004)
<i>age-1</i>	Ageing Alteration	PI3KCA (p110 alpha protein), PI3KCB (Phosphatidylinositol-4,5-Bisphosphate 3-Kinase), PI3KCD (Phosphatidylinositol 3-Kinase Catalytic, Delta)	Johnson (1988)
<i>daf-2</i>	Abnormal Dauer Formation	IGF1R (Insulin like Growth Factor 1 Receptor), INSR (Insulin Receptor), INSRR (Insulin Receptor Related Receptor)	Kimura et al. (1997)
<i>daf-16</i>	Abnormal Dauer Formation	Forkhead Box O1 (FOXO1), Forkhead Box O3 (FOXO3), Forkhead Box O4 (FOXO4)	Kenyon et al. (1993)
<i>egl-15</i>	Egg Laying defective	FGFR (Fibroblast Growth Factor Receptor)	Goodman (2003)
<i>egl-17</i>	Egg Laying defective	FGF17 (Fibroblast Growth Factor 17), FGF18 (Fibroblast Growth Factor 18), FGF8 (Fibroblast Growth Factor 8)	Burdine R. D. (1996)

<i>klo-1</i>	Klotho (mammalian ageing-associated protein) homolog	γ -klotho	Polanska et al. (2011)
<i>klo-2</i>	Klotho (mammalian ageing-associated protein) homolog	γ -klotho	Polanska et al. (2011)
<i>let-756</i>	Lethal	FGF16 (Fibroblast Growth Factor 16), FGF20 (Fibroblast Growth Factor 20), FGF9 (Fibroblast Growth Factor 9)	Roubin et al. (1999)

1.4.3. Endocrine signalling in *C. elegans* stress responses

In humans, activation of the Insulin/ Insulin-like growth factor-1 receptor (IGFR), a PI3K-mediated pathway is activated, resulting in the phosphorylation of FOXO transcription factors in the cytoplasm, preventing translocation to the nucleus, ultimately preventing the transcription of FoxO targets (Murphy and Hu, 2013). In *C. elegans*, the orthologue for insulin/IGF receptor is encoded for by the *daf-2* gene (Kenyon et al., 1993, Kimura et al., 1997). Mammalian genomes encode four FoxO genes, FoxO1, FoxO3, FoxO4 and FoxO6, whereas *C. elegans* has just one orthologue for these, encoded for by *daf-16* (Albert et al., 1981).

Reduced IIS in *C. elegans*, caused by hypomorphic *daf-2* alleles, causes nematodes to age more slowly and live twice as long as their wild-type counterparts, and this lifespan extension is dependent on DAF-16/ FOXO activity (Kenyon et al., 1993, Lin et al., 1997). *daf-2* mutants are also resistant to heat stress, oxidative stress, and hypoxia, most of which is dependent on DAF-16/ FOXO targets (Honda and Honda, 1999, Hsu et al., 2003, Scott et al., 2002).

Evidence in mammalian models suggest that *klotho* could function to inhibit IIS (Lim et al., 2017, Yamamoto et al., 2005). However, it is not clear whether this inhibition of IIS is due to direct inhibition of pathway components, or alternative mechanisms which in turn downregulate IIS (Château et al., 2010, Lorenzi et al., 2010).

1.4.4. Fibroblast growth factor (FGF)-*klotho* signalling in *C. elegans*

The *C. elegans* model provides a simplified model for studying FGF pathways. The *C. elegans* genome encodes two genes orthologous to the 22 mammalian FGFs, *egl-17* and *let-756*, and only one orthologue for the four mammalian FGFRs, *egl-15* (Polanska et al., 2009). So far, it has been reported that *egl-17/ FGF* is orthologous to human genes encoding FGFs -8, -17 and -18 (Burdine R. D., 1996), whereas *let-756/ FGF* is orthologous to human FGFs -9, -16 and -20 (see table 1.1.) (Roubin et al., 1999). EGL-15/ FGFR, EGL-17/ FGF and LET-756/ FGF are reported to have roles in cell proliferation, differentiation and migration, and EGL-15/ FGFR has also demonstrated a novel function in protein degradation in differentiated muscle (Goodman, 2003, Szewczyk and Jacobson, 2003).

There are two genes in *C. elegans* orthologous to human *klotho* and β -*klotho*, *klo-1* and *klo-2* (Polanska et al., 2011). These genes are predominantly expressed in the hypodermis,

intestinal and excretory canal tissues, which are responsible for many of *C. elegans* metabolic processes (Polanska et al., 2011). It is predicted that *C. elegans* KLO-1 and KLO-2 consist of 479 amino acids and 479 amino acids, respectively, share between 33-35% homology to vertebrate klothos, and 29-30% and 33-34% homology to vertebrate β -klothos (Polanska et al., 2011).

KLO-1/ KL is found to associate with EGL-15/ FGFR *in vitro*, and *pklo-1::GFP* reporter expression is absent in *C. elegans* with *egl-15/fgfr* loss of function and *let-756/fgf* partial loss of function alleles, suggesting *klo-1* expression is dependent on functional FGF signalling in the nematode, and highlighting the conserved nature of FGF-klotho signalling (Polanska et al., 2011).

As mentioned previously (see '1.3.6. Intracellular pathways associated with eFGF-klotho-FGFR function'), several links have been made to suggest that the protective effects of klotho could be due to inhibition of IIS (Lim et al., 2017, Yamamoto et al., 2005). However, lifespan analysis of *C. elegans* mutants indicates that *klotho* could in fact function in a pathway parallel to IIS to extend lifespan (Buj and Kinnunen, manuscript in preparation). Here it was found that the prolonged lifespan of *daf-2/INR* mutants was further extended in combination with *klo-2/ KL* and *klo-1/ KL* indicating klotho could function via a pathway alternate to IIS to promote longevity (Buj and Kinnunen, manuscript in preparation). In addition, it has been reported that klotho functions in a DAF-2/ INR-independent, DAF-16/ FOXO-dependent manner to mediate stress responses in *C. elegans*, further supporting the notion that klotho functions via an alternative pathway to mediate these responses (Château et al., 2010). Currently, the potential mechanisms governing this remain ambiguous.

1.5. Aims of research

Literature suggests that klothos could function via a pathway parallel to IIS to promote resistance to environmental stress and promote longevity (Château et al., 2010, Lim et al., 2017, Lorenzi et al., 2010, Yamamoto et al., 2005). Unravelling of the mechanisms governing these protective effects could provide clues as to how to promote healthy ageing and the extension of lifespan in *C. elegans* and could have broader implications for other organisms.

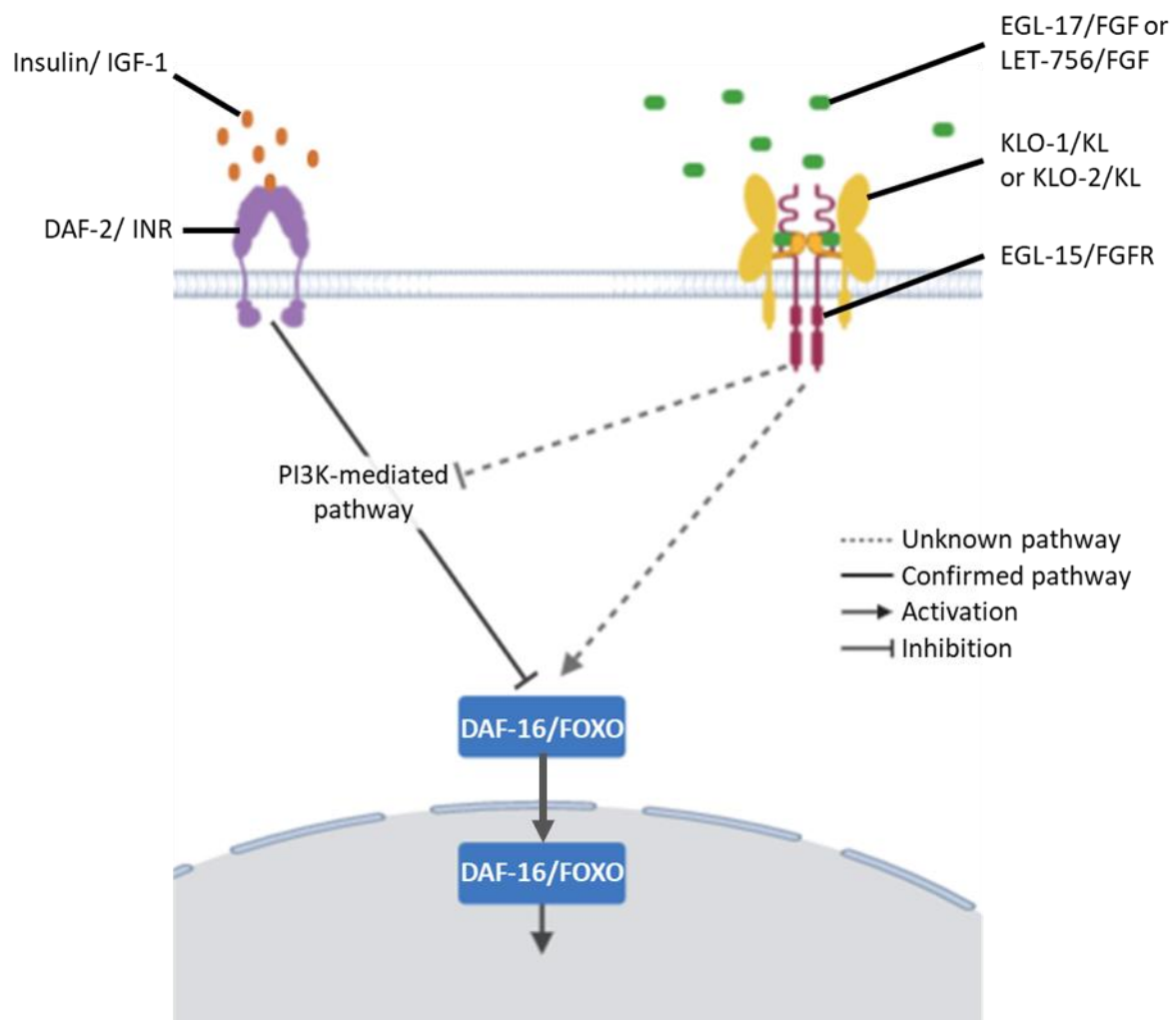


Figure 1.6. Schematic diagram of speculated mechanisms of Klotho-mediated activation of DAF-16/ FOXO. Overall aims of research are to shed light on the signalling pathways governed by KLO-1/ KL and KLO-2/ KL. Enhanced stress responses in mutants with reduced DAF-2/ INR function is dependent on functional DAF-16/ FOXO, as are stress responses governed by mammalian klothos. Evidence links klotho function to IIS inhibition, though more research into whether this is via direct inhibition of IIS pathways, or the result of manipulation of alternate pathways, remains ambiguous. Image created using BioRender.

The overall aim of this research is to explore the pathways that function in a linear manner to *klo-1/ KL* and *klo-2/ KL* in the *C. elegans* model. Strains for null or loss of function alleles for intracellular signalling components in combination with *klo-1* and *klo-2* genetic deletion will be subject to a variety of health and behavioural analyses to elucidate on potential mechanisms of klotho action. Pharmacological manipulation of intracellular signalling on the effects of *klotho* reporter expression will also be examined.

This research will continue to elaborate on previous results into the effects of *klo-1* and *klo-2* deletion mutations on health and in stress responses *in vivo*, with an emphasis on the roles of klotho in oxidative stress responses. In addition, as current understanding is that klotho functions as a co-factor for eFGF-FGFR signalling, another aim of research is to consolidate evidence for the roles of FGF-klotho-FGFR signalling in health and stress responses.

Chapter 2: Materials and Methods

2.1. *Caenorhabditis elegans* strains

Wild-type reference strain was N2 Bristol (Brenner, 1977). The following genetic mutant *C. elegans* strains were used; NH2038 *clr-1* (*e2530*) II; *egl-15* (*n1477*) X, RB754 *aak-2* (*ok524*) X, TC127 *egl-17* (*n1377*) *hst-2* (*ok595*) X, TC380 *klo-2* (*ok1862*) III, TC462 *klo-1* (*ok2925*) IV, TC446 *klo-2* (*ok1862*) III; *klo-1* (*ok2925*) IV, TC531 *klo-1* (*ok2925*) IV; *egl-15* (*n1477*) X, TC532 *klo-2* (*ok1862*) III; *egl-15* (*n1477*) X, TC533 *klo-2* (*ok1862*) III; *klo-1* (*ok2925*) IV; *egl-15* (*n1477*) X, TC534 *klo-2* (*ok1862*) III; *klo-1* (*ok2925*) IV; *egl-17* (*n1377*) *hst-2* (*ok595*) X, TC535 *klo-1* (*ok2925*) IV; *egl-17* (*n1377*) X *hst-2* (*ok595*) X, TC536 *klo-2* (*ok1862*) III; *klo-1* (*ok2925*) IV; *egl-17* (*n1377*) X, TG38 *aak-2* (*gt33*) X and TJ1052 *age-1* (*hx546*) II.

The following strains were generated following using genetic crossing methods; *klo-1* (*ok2925*) IV; *aak-2* (*gt33*) X, *klo-2* (*ok1862*) III; *aak-2* (*gt33*) X, *klo-2* (*ok1862*) III; *klo-1* (*ok2925*) IV; *aak-2* (*gt33*) X, *klo-1* (*ok2925*) IV; *aak-2* (*ok524*) X, *klo-2* (*ok1862*) III; *aak-2* (*ok524*) X and *klo-2* (*ok1862*) III; *klo-1* (*ok2925*) IV; *aak-2* (*ok524*) X.

Transgenic strains containing fluorescent reporters were; DA2123 *adls2122*, TC391 N2 (Bristol); *jtEx129*, TC474 N2; *jtEx179* and TC475 *klo-2(ok1862)*; *klo-1(ok2925)*; *jtEx179.adls2122 [lgg-1p::GFP::lgg-1+rol-6 (su1006)]* is a transgene used as a GFP reporter for *lgg-1* expression with a *rol-6 (su1006)* co-injection marker used to identify transgenic nematodes (Kang et al., 2007). *jtEx129 [pklo-2::GFP; ptph-1::mCherry]* is an extrachromosomal array used as a GFP reporter for *klo-2* expression with *tph-1* promoter reporter used as a co-injection marker to identify transgenic animals (Polanska et al., 2011). *jtEx179 [pklo-1::mCherry; pmyo-3::GFP]* is an extrachromosomal array used as an mCherry reporter for *klo-1* expression in the nematode with a *myo-3* promoter reporter used as a co-injection marker to identify transgenic animals.

Some strains were provided by the *Caenorhabditis* Genetics Centre (CGC) which is funded by the NIH Office of Research Infrastructure Programs (P40 OD010440).

2.2. Media

2.2.1. Nematode growth media

Nematode growth media (NGM) contained 17.1g bacteriological agar (OXOID), 3g NaCl (Fisher) and 2.5g tryptone (Fisher) per 1L of ddH₂O. Once autoclaved, 1 mL cholesterol (5mg/mL in EtOH; Sigma), 1 mL of 1M CaCl₂, 1 mL of MgSO₄ and 25 mL of 1M KPO₄ buffer (pH 6.0) were added per 1L of media. The NGM plates were left to dry overnight before seeding with a lawn of *Escherichia coli* (*E. coli*) OP50.

2.2.2. Bacterial growth solutions

LB agar consisted of 10g tryptone, 5g yeast Extract (Fisher), 10g NaCl and 15g bacteriological agar per 1 L ddH₂O. pH was adjusted to 7.5 using 1 M NaOH and the media was autoclaved to sterilize.

B broth consisted of 10g tryptone and 5g NaCl per 1 L ddH₂O. pH was adjusted to 7.0 using 1 M NaOH then the solution was autoclaved to sterilize.

TY media (2 X) was composed of 16g tryptone (Fisher), 10g yeast extract (Fisher), 5g NaCl per 1 L in ddH₂O. Media was sterilised by autoclaving.

2.2.3. Nematode freezing solution

Freezing solution contained 5.85g of NaCl, 6.8g of Na₂HPO₄, 300g glycerol (Sigma) and 5.6 mL of 1 M NaOH per 1 L. The solution was autoclaved to sterilize.

2.2.4. M9 medium

M9 buffer was made to a composition of 400 mM Na₂HPO₄, 2 mM KH₂PO₄, 8.6 mM NaCl (Fisher), 18.7 mM NH₄Cl and autoclaved to sterilize. Following sterilization, 1mM MgSO₄ was added to buffer solution.

2.2.5. Complete K-medium

Complete K medium was made to a composition of 51 mM NaCl, 32 mM KCl, 1 mM CaCl₂, 1 mM MgSO₄, 13 µM cholesterol and autoclaved to sterilize.

2.2.6. S basal medium

S basal medium contained 5.85g NaCl, 1.0g K₂HPO₄, 6.0g KH₂PO₄. Media was autoclaved to sterilize. 1 mL cholesterol (stock at 5 mg/ mL in EtOH) per 1 L was added to buffer following sterilization.

2.3. Bacterial cultures

2.3.1. *Escherichia coli* OP50

E. coli OP50 grows slower than other strains of *E. coli*, and this slower growth forms a thin lawn on NGM agarose plates allowing for easier observation of nematodes (Stiernagle, 2006). OP50 colonies were grown on LB agar plates containing no antibiotic, incubated overnight at 37°C, then stored at 4°C for about four weeks. Overnight cultures were prepared by inoculating one colony of OP50 in 5-10 mL B Broth, then incubated overnight at 37°C. This OP50 slurry was then used to seed NGM agar plates. For more concentrated OP50 slurries, the bacteria were centrifuged at 4000 rpm for 15 minutes, the supernatant removed then resuspended in sterile B broth to a higher bacterial density.

2.3.2. *Escherichia coli* HB101

E. coli HB101 is the recommended strain for growth of nematodes in liquid culture, due to its promotion of rapid development and increased culture yields (MacNeil et al., 2013). Colonies of HB101 were grown on LB agar containing 35 µg/ mL streptomycin. Overnight cultures were prepared by inoculating one colony of HB101 in 5 mL LB broth containing 35 µg/ mL streptomycin then incubated overnight at 37°C. The following day, 1 L of 2 X TY media containing 35 µg/ mL streptomycin was seeded with the HB101 overnight culture then again incubated overnight at 37°C in a rotating incubator (180 rpm). Following incubation, the HB101 cultures were centrifuged for 15 minutes at 4000 rpm, the supernatant was removed

then resuspended in sterile M9 solution (see '2.2.5. M9 medium'). This bacterial suspension was centrifuged again for 15 minutes at 4000 rpm. The bacteria were stored in a 50% slurry in M9 buffer supplemented with 35 µg/ mL streptomycin at 4°C until required.

2.4. Preparation of *C. elegans* strains

2.4.1. General maintenance

C. elegans stocks were generally maintained on NGM agarose plates seeded with *E. coli* OP50, as described by Brenner (1974). 10-20 gravid hermaphrodites were picked onto fresh NGM plates as and when required to ensure strains were not starved. Nematodes were maintained at 20° C, unless specified otherwise.

2.4.2. Liquid nematode cultures

Where large volumes of *C. elegans* were required for analysis, nematodes were cultured using liquid culture techniques. 4-6 starter plates containing mixed stage animals were washed with M9 three times then transferred to 25 X 25 cm plates with a glass Pasteur pipette. Nematodes were grown in a solution of 10 mL of 50% *E. coli* HB101 slurry (see '2.3.2. *Escherichia coli* HB101'), 100 µL of 25 mg/ mL cholesterol in ethanol, 50 µL of 35 mg/ mL streptomycin and M9 buffer to 50 mL. Nematodes were grown at 20°C in a shaking incubator set to 70 rpm.

C. elegans were checked daily under a dissection microscope to confirm there was *E. coli* present and so would not be starved. Once the nematodes were at the desired stage/ density, they were collected from plates, centrifuged at 400 rpm for 2 minutes to collect the nematodes, washed three times in M9 buffer then prepared as needed (see '2.4.3.2. Snap freezing of liquid nematode cultures' and '2.4.4. Age synchronization').

2.4.3. Freezing nematode cultures

2.4.3.1. Freezing and recovery of nematode stocks

Methods were adapted from Stiernagle (Stiernagle, 2006). Plates that had no fungal or bacterial contamination, containing plenty of L1 and L2 stage nematodes were selected for freezing. Nematodes were washed off plates using M9 buffer into 1.5 mL cryotubes or Eppendorf tubes. An equal volume of freezing solution (see '2.2.4. Freezing solution') was

added. The nematodes were then placed in a Styrofoam rack for slow freezing and subsequently stored at -80°C.

To recover, stocks were thawed at room temperature then placed onto fresh NGM plates. Animals were left to recover for 24 hours, then if successful, recovered nematodes were transferred to fresh plates.

2.4.3.2. Snap freezing of liquid nematode cultures

C. elegans that were to be used for subsequent enzyme assays or Western blotting, were aliquoted into 1.5 mL Eppendorf tubes, dropped into liquid nitrogen to snap freeze and stored at -80°C for subsequent use.

2.4.4. Age synchronization

Methods were adapted from Stiernagle (2006). For typical age synchronization on NGM plates, between 20-30 gravid hermaphrodites were transferred to fresh plates and left to lay eggs for 2-4 hours. After this time, mothers were removed from the plates and the eggs were left at 20°C until desired stage was reached. Larvae were grown for approximately 48 hours to reach L4 stage, or for 72 hours for day one adults. Age synchronisation was performed in this way to enable larger cultures of worms to be available for analysis where picking L4s from mixed-stage cultures would have been a laborious process.

To age synchronize liquid media cultures, mixed stage nematodes grown in liquid media were washed off 25 X 25 cm plates into falcon tubes and spun down at 200-400 rpm for 1 minute to allow animals to settle at the bottom of the tube. These animals were washed three times in M9 buffer to remove as much bacteria as possible. After washing, as much M9 buffer was removed then nematodes were suspended in approximately 5 X volume of 0.5 M NaOH -1% bleach in water. The animals were agitated in this mixture for a couple of minutes to lyse all mothers. Once lysed, the embryos were washed quickly in M9 buffer three times, then either dispensed onto NGM plates or returned to liquid media and grown at 20°C until the desired stage was reached.

2.5. Genetic crosses

2.5.1. Crossing *klo-1* and *klo-2* genetic mutants with mutants for intracellular signalling components

To generate double and triple mutants for *klo-1* and *klo-2* mutant alleles in combination with mutants for intracellular signalling components, homozygous double *klo-2;klo-1* mutant males containing the *jtEx179 [klo-1::mCherry]* reporter were crossed with homozygous hermaphrodites containing presumed null mutations for intracellular signalling components such as *aak-2 ok524* or *gt33*. The F₁ cross progeny generation was selected based on the presence of the *klo-1::mCherry* reporter as all of the F₁ generation progeny containing this reporter would be heterozygous for all three alleles.

F₁ mothers were picked on to fresh plates (1 animal per plate) and left to lay progeny. Following this, F₂ hermaphrodites were picked onto fresh plates (1 animal per plate) and left to lay progeny for 1-2 days. F₂ mothers were then lysed and genotyped (see '2.6. Genotyping') for each allele. Based off genotyping, F₃ animals were selected based on whether the F₂ mother was heterozygous or homozygous for the desired mutant allele. F₃ animals were picked and left to lay progeny. As above, F₃ mothers were then genotyped for desired alleles and progeny selected based on genotyping results. This process was repeated for each generation until the desired mutant strains were generated.

2.5.2. Crossing transgenic reporters into *klo-1* and *klo-2* mutants

Male wild-type animals carrying the *jtEx129 [pklo-2::GFP, ptp-1::mCherry]* reporter were crossed with TC446 *klo-2 (ok1862); klo-1 (ok2925)* double mutant hermaphrodites. Hermaphrodite F₁ progeny positive for *jtEx129* were cloned at L4 stage by placing a single hermaphrodite into a plate and allowed to lay eggs for 1-2 days. F₂ progeny positive for the co-injection marker were cloned and allowed to lay progeny. F₂ mothers were genotyped for *klo-1 (ok2925)* and *klo-2 (ok1862)* by PCR. All clones and resultant strains were picked and maintained based on the positive expression of *jtEx129*. The primer sets used for genotyping can be found in table 2.1.

To cross the *adIs2122 [lgg-1p::GFP::lgg-1+rol-6 (su1006)]* into animals with *klo-1* and *klo-2* mutant backgrounds, *adIs2122* positive hermaphrodites were crossed with males carrying the

jtEx179 [pklo-1::mCherry; pmyo-3::GFP] reporter. Hermaphrodite F₁ progeny positive for both *adIs2122* and *jtEx179* reporters were cloned at the L4 stage as above. F₂ progeny were selected based on the presence of the *adIs2122* reporter, as were subsequent generations, and animals were genotyped for *klo-1 (ok2925)* and *klo-2 (ok1862)*. The strains generated from the cross were maintained by picking “roller” nematodes which were positive for the *adIs2122* transgene.

2.6. Genotyping

2.6.1. Nematode lysis

To genotype, single hermaphrodite mothers were picked into 10 µL of nematode lysis buffer composed of 50 mM KCl, 10 mM Tris (pH 8.2), 2.5 mM MgCl₂, 0.45% Tween 20 (Sigma), 0.45% NP-40 (Sigma), 0.01% gelatine and 10 µL of 10 mg/mL proteinase K per 1 mL of lysis buffer. Animals were lysed by incubation at 60°C for 45 minutes followed by 95°C for 15 minutes to inactivate proteinase K. 2.5 µL of nematode lysate was used as PCR template for genotyping.

2.6.2. Genotyping polymerase chain reaction (PCR)

Primer sequences can be found in table 2.1.

BioTaq PCR genotyping mix was composed of a final concentration of 2 mM MgCl₂, 0.2 mM of each dNTP (Bioline), 200 nM of each primer and 1 U of BioTaq polymerase (Bioline). For PCR using MyTaq (Bioline), the composition of genotyping mixture was 1 X MyTaq reaction buffer (1 mM dNTPs, 3 mM MgCl₂, stabilizers and enhancers; Bioline), 0.1 µL MyTaq polymerase and a final primer concentration of 0.4 mM of each primer.

All MyTaq PCR reactions excluding *klo-1 (ok2925)* were carried out at 95°C for 3 minutes, followed by 35 cycles of 95°C for 15 seconds, annealing for 15 seconds (see table 2.1. for annealing temperatures), and extension at 72°C for 30 seconds. For *klo-1 (ok2925)* PCR, initial denaturation was 95°C for 3 minutes followed by 35 cycles of 95°C for 30 seconds, 60°C for 30 seconds and extension at 72°C for 1 minute. BioTaq PCR reactions were carried out at 94°C for 2-3 minutes, followed by 35 cycles of 94°C for 20 seconds, annealing for 20 seconds, and extension at 72°C for 5 minutes. All PCR reactions had a final extension at 72°C for 5 minutes.

Derived cleaved amplified polymorphic sequence (dCAPS) genotyping involves a the design of a primer which introduces a restriction enzyme (RE) digestion site to either wild-type or mutant DNA product to allow for the discrimination between alleles when genotyping (Hrubá, 2007).

To genotype for *age-1 (hx546)*, a forward dCAPS primer was designed to contain a single mismatch that would introduce a BseRI restriction site 5'GAGGAG(N)₁₀▼3' into the wild-type PCR product. To digest, 10 X CutSmart Buffer (New England Biolabs) was added directly to PCR product to an overall concentration of 1 X CutSmart Buffer. 0.5 µL BseRI (New England Biolabs) was added to each reaction. Following digestion, bands of 197bp and 30bp are formed for the wild-type product and a single band of 227bp is visible for the *age-1 (hx546)* mutants. Due to the small size difference between the digested and undigested products, gel electrophoresis was run using a 1% agarose gel for 90 minutes at 60 V.

Table 2.1. Primer sets used for genotyping. Those indicated with an asterisk (*) are PCR products following digestion with BseRI

Allele	Primer	5'→3'	Annealing temperature (°C)	Wild-type product (bp)	Mutant product (bp)
ok524	F	GATAGCACAGACAACAGTTCG	58	557	882
	R1	CGTCCGTGCTTAACAATGTAG			
	R2	CGCCAAAACATAGTAATAGTGCC			
gt33	F	GATAGCACAGACAACAGTTCG	58	557	624
	R1	CGTCCGTGCTTAACAATGTAG			
	R2	CGCCAAAACATAGTAATAGTGCC			
hx546	F	CAGTTTGTACACAGGATCCAGAG	60	197 and 30*	227*
	R1	GTGAAGAATATCGCCGTATCTCAC			
ok1862	F	GACCTTTCTTGTGATGGTCTC	59	500	640
	R1	TCACAGTTCTCCCTGTTAAGC			

	R2	TCAATGTCTTCCTGCGAATCG			
ok2925	F	GTTCAAACCTTCTGGTATTCCATTTTC	60	462	645
	R1	ACCGATTTTTGAGAGAAGAGCAAC			
	R2	GGTAATTTTTCTCTCATTGAGGCTG			

2.6.3. Gel electrophoresis

For gel electrophoresis, 2% agarose (Bioline) gels in TAE buffer (40 mM Tris Base, 20 mM Acetic acid, 1mM EDTA) were used unless otherwise specified.

2.7. *C. elegans* Health Analysis

2.7.1. Lifespan assays

2.7.1.1. Standard lifespan analysis

Animals for each strain were counted daily from larval stage 4 (L4; counted as day 0) until death. Dead nematodes were identified if they did not respond to gentle prodding and showed no pumping of the pharyngeal muscles. Animals that had crawled off the plate or had an “exploded” phenotype were censored from analysis on the day of that event. Data was analysed by Kaplan-Meier survival test using IBM SPSS Statistics 24 software.

2.7.1.2. Lifespan analysis of *egl-* mutants

Methods were adapted from Senchuk et al (Senchuk et al., 2017). For some *egl-* mutant strains, the egg laying defective phenotype causes increased instances of internal hatching of progeny, resulting in early death of the hermaphrodites. Therefore, NGM plates were supplemented with 25 µg/ mL 5’fluoro-2’-deoxyuridine (FUDR) (final concentration of 100 µM) to limit the production and development of progeny in treated animals (Van Raamsdonk and Hekimi, 2011). Lifespan analysis was then carried out as previously described. Wild-type *C. elegans* controls were grown similarly on FUDR-containing plates for these experiments.

2.7.2. Viable progeny analysis

Age synchronized L4 *C. elegans* were picked onto fresh plates (1 animal per plate, 5 plates per strain). Each day, plates were counted for the number of eggs (including dead and unfertilised) and larvae, and the hermaphrodite mothers were transferred to fresh plates. This was repeated daily for all plates until progeny had reached adulthood.

2.8. Stress Response assays

2.8.1. Oxidative stress assays

2.8.1.1. Acute oxidative stress assays

Oxidative stress survival over 9 hours

Paraquat (Methyl viologen dichloride hydrate, Sigma CAS 75365-73-0) solution was prepared to a concentration of 300 mM in M9 buffer. 15 μ L of the paraquat solution was dispensed into 200 μ L tubes. Age synchronized L4 larvae were transferred to the solution. Eight nematodes of each strain were used per assay (2 animals per tube, 4 tubes per strain). Nematodes were incubated at 20°C and dead animals were counted each hour for 9 hours. Control animals were transferred to 15 μ L M9 buffer and were counted similarly for 9 hours. Assays were repeated at least three times. Data was analysed using Kaplan-Meier survival test in IBM SPSS Statistics 24.

Oxidative stress survival over 20 hours

Method was adapted from Lee et al. (2008). Paraquat solution was prepared as above to a concentration of 100 mM. L4 hermaphrodites were transferred to 15 μ L of the paraquat solution and dead animals were counted every 5 hours for 20 hours. The animals were incubated at 20°C and control *C. elegans* were submerged in M9 solution and counted similarly. 50 animals per strain were analysed per assay and the assay was repeated four times.

2.8.1.2. Detection of reactive oxygen species

Treatment with oxidants: *C. elegans* were age synchronized depending on oxidant treatment. For 20-hour incubation in 100 μ M sodium arsenite (NaAsO₂) (Sigma Aldrich S7400) or 100 mM

paraquat, the hermaphrodites were harvested at the L4 stage. For 1–2-hour incubation in 100 mM, 200 mM or 300 mM paraquat solution, the animals were harvested as day one old adults.

Age synchronized *C. elegans* were washed off plates into 1.5 mL Eppendorf tubes using S-Basal medium (see '2.2.7. S Basal medium'). The animals were pelleted by centrifuging at 400rpm for 2 minutes and washed in S-Basal three times. Following the third wash as much S-Basal was removed as possible.

150 µL of oxidant solution was added to each strain. The animals were incubated at 20°C for specified duration. Acute exposure was for 1 hour for 200 mM and 300 mM paraquat concentrations, and 2 hours for 100 mM paraquat solution. For longer term exposure to 100 µM NaAsO₂ or 100 mM paraquat, nematodes were incubated for 20 hours, and these experiments were supplemented with *E. coli* OP50 to ensure the animals would not starve.

The oxidizing agent was washed off the animals using complete K-medium (see '2.2.6. Complete K-medium') three times before proceeding to CellROX Deep Red staining.

CellROX deep red staining: CellROX deep red is a cell permeable stain that upon oxidation, leads to fluorescence of the compound with an absorption maxima of 644/ 655 nm. 50 µL of complete K-medium containing 20 µM CellROX Deep Red Reagent (Invitrogen, Carlsbad, CA, USA) was added to each strain then incubated for 30 minutes. *C. elegans* were washed three times with K-medium as above then mounted onto microscope slides for imaging using 1 mM levamisole (Sigma Aldrich) in M9 as an anaesthetic.

2.8.1.3. Chronic oxidative stress exposure

Methods were adapted from Senchuk et al (Senchuk et al., 2017). Age synchronised L4 hermaphrodites were placed on NGM plates supplemented with either 0 mM, 2 mM, 4 mM or 6 mM paraquat. Paraquat exposure increases the likelihood of internal hatching of progeny, therefore NGM plates supplemented with Paraquat were also supplemented with 100 µg/ mL FUDR (Senchuk et al., 2017, Van Raamsdonk and Hekimi, 2011). Lifespan analysis was then carried out as previously described (see '2.7.1. Lifespan assays').

2.8.2. Acute heat stress

Age synchronized L4 larvae were incubated at 37°C and counted every hour for 9 hours for dead animals. 30 animals per strain were analysed and the experiment was repeated three times. Statistical significance was determined using Tukey's test.

2.8.3. Chronic starvation

C. elegans were age synchronised as per '2.4.4. Age synchronization' for liquid media nematodes. Once bleached, the embryos were transferred to 10 cm NGM plates and grown at 20°C until they reached early L4 stage. The animals were washed off plates into 15 mL falcon tubes with M9 buffer and washed thoroughly three to four times to ensure all traces of bacteria were removed. Nematodes were resuspended in M9 buffer to a density of approximately 5-6 nematodes/ 10 µL. The tubes were kept at 20°C in a shaking incubator on a gentle setting (70 rpm) for the duration of the assay (Malik, 2019).

An aliquot of the nematode suspension was taken daily and dispensed onto OP50-seeded plates. After 2-3 hours live and dead animals were scored. Nematodes that had crawled off the plates, exploded or displayed internal hatching were censored. Statistical significance was determined using Tukey's test.

2.9. Interpretation of survival assays: epistatic analysis

The general rule for epistatic analysis of strains containing multiple alleles is that in instances where an allele has an additive effect on a phenotype, this is taken to indicate that the intervening alleles function via separate mechanisms. In instances of non-additive effect, this is taken to indicate that the intervening alleles may function in the same process or pathway. Further depth regarding these rules may be found in a journal article written by David Gems and team (David Gems, 2002).

These traditional rules for epistatic analysis have been applied to interpret data presented in this thesis.

2.10. Analysis of *klo-1* and *klo-2* reporter expression in *C. elegans*

2.10.1. Treatment with 100 μ M forskolin

N2 and *klo-1*, *klo-2* and *klo-2 ;klo-1* double mutants positive for either *jtEx129* [*pklo-2::GFP*; *ptph-1::mCherry*] or *jtEx179* [*pklo-1::mCherry*; *pmyo-3::GFP*] reporters were washed off plates into 1.5 mL Eppendorf tubes using M9 buffer. The animals were washed three times with M9 buffer. Strains were incubated in 100 μ M Forskolin (Sigma Aldrich) solution (stock solution dissolved in DMSO, then subsequent dilutions in M9 buffer to a final DMSO concentration of 0.1%) for 1 hour. Following incubation, the animals were washed a further three times in M9 buffer then mounted onto slides for microscopy. For analysis, mean pixel intensity of reporters was analysed in the first two intestinal cells of the nematode.

2.10.2. Treatment with 50 mM metformin

Methods for metformin treatment were adapted from (Cabreiro et al., 2013). *E. coli* OP50 was grown on NGM plates containing a metformin (SigmaAldrich, CAS N^o 1115-70-4) at concentration of 50 mM. Day one age synchronised *C. elegans* strains positive for either *jtEx129* [*pklo-2::GFP*; *ptph-1::mCherry*] or *jtEx179* [*pklo-1::mCherry*; *pmyo-3::GFP*] reporters were washed three times using M9 buffer before being fed on metformin-supplemented plates for 4 hours to see the effects on transcription of these promoters. Plates were incubated at 20°C. Following incubation, nematodes were washed three times using M9 buffer before being transferred to slides for microscopy. For analysis, measurements for mean pixel intensity were taken from the first two intestinal cells.

2.10.3. Treatment with 100 μ M rapamycin

Methods for rapamycin treatment were adapted from Robida-Stubbs et al. (2012). Rapamycin (Melfords, R64500-0.005) was dissolved in DMSO to a concentration of 54.7 mM. To make rapamycin plates, rapamycin solution was added to NGM agar (see '2.2.1. Nematode Growth Media') to a concentration of 100 μ M and poured onto 12-well plates. Control plates were supplemented with a DMSO concentration identical to the amount added to rapamycin plates. Plates were left to dry a minimum of overnight before seeding with concentrated *E. coli* OP50 (see "2.3.1. *Escherichia coli* OP50").

Day one age synchronised wild-type (N2) and *klo-2* (*ok1862*); *klo-1* (*ok2925*) strains positive for either *jtEx129* [*pklo-2::GFP*; *ptph-1::mCherry*] or *jtEx179* [*pklo-1::mCherry*; *pmyo-3::GFP*] reporters, were washed off plates three times using M9 buffer before being transferred to rapamycin-supplemented plates. Animals were left to incubate at 20°C for four hours, before again being washed three times using M9 buffer prior to microscopy. Following microscopy, mean pixel intensity of each reporter was measured from the first two intestinal cells of the animals before subsequent analysis.

2.11. Analysis of excretory canal morphology

Forskolin treated *C. elegans* were analysed for excretory canal morphology using the *pklo-1::mCherry* reporter, which allows visualisation of the canals. Images were taken using Zeiss Axiomager Z1 and Zeiss Zen software (see '2.12.1. Fluorescence microscopy and imaging').

2.12. Detection of *lgg-1::GFP* reporter expression in *C. elegans*

Methods were adapted from Palmisano and Meléndez (2016). L1 and L2 larvae were washed of NGM plates three times using M9 buffer then mounted onto microscopy slides using 0.2% levamisole. Following microscopy, fluorescent *lgg-1::GFP* puncta found in the intestine were quantified for each strain using ImageJ software. Statistical analysis carried out using Microsoft Office Excel Software.

2.13. Microscopy

2.13.1. Fluorescence microscopy and imaging

Fluorescent and DIC images were taken using either a Zeiss Axiomager Z1 or Zeiss Axio Observer 488 each equipped with Zeiss AxioCam MRm camera and Zeiss Zen software. Images were analysed using ImageJ and statistical analysis was carried out using Microsoft Office Excel software.

The microscope suite is located in a dark room, and for assays images were taken using the same parameters and exposures to limit the effects of invasive or ambient light.

2.14. Western blotting of *C. elegans* extracts

2.14.1. Preparation of buffers

5 X SDS-PAGE running buffer consisted of 15.15g Tris base, 72.05g glycine and 25 mL of 20% sodium dodecyl sulphate (SDS) per 1 L. pH was adjusted to 8.8 using 2 M HCl. Before use, the buffer was diluted 1:5 in ddH₂O. Transfer buffer consisted of 3.8g Tris, 18.8g glycine, 0.5 mL of 20% SDS and 100 mL methanol (MetOH) in 1 L.

5 X Tris buffered saline (TBS) contained 100 mL of 1 M Tris-HCl (pH 7.4), and 146.1g NaCl in 1 L. This was diluted 1:5 before use. TBS plus Tween 20 (TBST) consisted of 200 mL of 5 X TBS and 0.5 mL of Tween 20 diluted to 1L using ddH₂O .

2.14.2. Preparation of *C. elegans* protein extracts

Preparation of *C. elegans* protein extracts was adapted from Hyman lab protocols (Hyman lab, n.d.). 1.5 mL Eppendorf tubes were marked at 25 μ L. 100-200 μ L of M9 buffer was added to each tube. For each strain, 50 animals were picked into the M9 buffer and the animals were washed three times to remove any trace of bacteria. After the third wash as much M9 was removed as possible.

For drug treatment, *C. elegans* were incubated in 100-200 μ L of 100 mM paraquat solution, 100 μ M Forskolin or M9 buffer (controls) for two hours at 20°C. After incubation, *C. elegans* were washed three times in M9 buffer. The M9 buffer was pipetted off leaving the animals in 25 μ L M9, then frozen in liquid nitrogen and stored at -80°C until required.

Prior to SDS-PAGE, *C. elegans* samples were thawed at room temperature and 25 μ L sample buffer (0.2 M Tris-HCl pH 6.8, 8% sodium dodecyl sulphate (SDS), 40% glycerol, 0.08% bromophenol blue, 10% β -mercaptoethanol) was added. *C. elegans* were sonicated in a water bath for 2 minutes then placed at 95°C immediately for 5 minutes to inhibit proteases and to break disulphide bonds of the proteins before loading onto SDS-PAGE gels.

2.14.3. SDS-PAGE

Proteins were separated in 10% SDS-PAGE. For 10 mL of separating gels 2.5 mL of 40% acrylamide (Bio-Rad), 2.5 mL of separating gel buffer (1.5 M Tris-HCl, pH 8.8), 0.1 mL of 10%

APS (SigmaAldrich), 4.9 mL ddH₂O and 7 µL TEMED (SigmaAldrich) was used. 4.5% acrylamide stacking gel (4 mL) contained 0.45 mL of 40% acrylamide, 1.0 mL of stacking buffer (0.5 M Tris-HCl, pH 6.8), 40 µL of 10% APS, 2.49 mL ddH₂O and 1.5 µL TEMED.

15 µL of samples were loaded per well, along with 10 µL of Precision Plus All-Blue (BioRad #1610373) pre-stained molecular weight marker. SDS-PAGE was carried out in 1 X SDS-PAGE running buffer for 35-40 minutes at 200V.

2.14.4. Transfer of proteins to PVDF membrane

Immobilon FL polyvinylidene fluoride (PVDF) membranes (MerckMillipore) were cut to the size of the SDS-PAGE gel, and wet in MeOH, ddH₂O, then finally 1 X transfer buffer. Proteins were transferred for approximately 80 minutes at 100V.

2.14.5. Blocking PVDF membrane

To prevent non-specific binding of primary and secondary antibodies, membranes were blocked with either 2% solution of dried skimmed milk or a 1:1 solution of blocking buffer (Li-Cor) with TBS, overnight at 4°C. Details of which blocking buffer and antibody dilutions used per blot can be found in table 2.2.

Table 2.2. Details of Western blotting conditions for total- and phospho-AMPKα on *C. elegans* and HCT116 cell extracts.

Figures	Blocking Solution	Secondary Antibody Dilution
5.13A & 5.14A	2% dried skimmed milk solution	1:1000
5.13B & 5.14B	2% dried skimmed milk solution	1:1000
5.13C & 5.14C	1:1 blocking buffer (Li-Cor): TBS	1:500
5.13D & 5.14D	1:1 blocking buffer (Li-Cor): TBS	1:500
5.13E & 5.14E	1:1 blocking buffer (Li-Cor): TBS	1:500
5.13F & 5.14F	1:1 blocking buffer (Li-Cor): TBS	1:300

2.14.6. Antibody incubation

After blocking, membranes were washed three times in 1 X TBST and incubated with primary antibodies. Primary antibodies used were anti-phospho-AMPK (Thr172) rabbit antibody (Cell Signalling technologies #2531S), and total AMPK (23A3) rabbit mAb (Cell Signalling Technologies #2603S) diluted to either 1:1,000 or 1:500 in 5% BSA in 1 X TBST. Membranes were incubated in primary antibody for three hours, washed three times 10 minutes in 1 X TBST before secondary antibody was added.

Secondary antibody was Anti Rabbit IgG DyLight 800 (Tebu-Bio #611-145-122) diluted to 1:10,000. Membranes were incubated in secondary antibody for 40 minutes, then washed three times in 1 X TBST as above, then stored in 1 X TBS (no Tween) until ready for detection.

2.14.7. Detection of antibody

Luminescence was detected using Li-Cor Odyssey imaging system.

2.15. Quantification of hexokinase activity

2.15.1. Hexokinase activity assay buffers

Three buffers were used for hexokinase activity assays; Buffer A (an ATP buffer composed of 50 mM sodium HEPES, 100 mM potassium chloride, 7.5 mM magnesium chloride, 1 mM NAD, 2.5 mM Dithioerythritol (DTE) and excess glucose-6-phosphate dehydrogenase (G6PDH), and 5 mM ATP), buffer B (a no phosphate donor buffer composed of 50 mM sodium HEPES, 100 mM potassium chloride, 7.5 mM magnesium chloride, 1 mM NAD, 2.5 mM DTE and excess G6PDH), and buffer C (homogenisation buffer; 50 mM sodium HEPES, 100 mM potassium chloride, 7.5 mM magnesium chloride, 1 mM NAD and 2.5 mM DTE) (Davidson and Arion, 1987).

2.15.2. Homogenisation of *C. elegans* samples

For homogenisation, 1 g of frozen nematode culture (see '2.4.2. Liquid nematode cultures') was ground using a pestle and mortar precooled with liquid nitrogen. Nematodes were pulverised for five minutes to create a fine powder. 1 mL homogenisation buffer (see buffer

C, above) was added to the nematode powder to form homogenised nematode solution. This homogenate was then centrifuged at 17,000 g to clarify solution.

2.15.3. Hexokinase assay plate set up

For assay set up, 96-well plates were used. First, 15 μL of 10 X glucose solution was added to each well (to a final concentration of 100 mM glucose), for controls this was replaced with 15 μL ddH₂O. Following this, 95 μL of buffer A was added to each well followed by 50 μL of nematode homogenate. As a second control parameter, some wells substituted buffer A (ATP buffer) for buffer B (a no phosphate donor buffer). The total volume of components added to each well was 160 μL . Upon addition of nematode homogenate, the plates were then quickly transferred to the plate reader (SPECTROstar Nano, BMG Labtech), as to avoid missing the read outs for enzyme activity. Activity was recorded by measuring absorption at 340 nm to detect NADH production.

2.15.4. BCA protein quantification assay

To quantify total protein in each nematode sample, and to correct enzyme activity values based on this, a bicinchoninic acid (BCA) assay, adapted from Smith et al. (1985), was conducted on each of the *C. elegans* homogenates.

Assay mixture contained 50:1 parts BCA solution to copper (II) sulphate pentahydrate. 300 μL of this mixture was loaded into each well (using a 96-well plate) with 15 μL of *C. elegans* homogenate. The samples were incubated at 37 °C for 30 minutes then absorption of each sample was measured at 562 nm (SPECTROstar Nano, BMG Labtech). A bovine serum albumin (BSA) standard was made up to calibrate the assay at concentrations of 0, 0.2, 0.4, 0.6, 0.8 and 1 (mg/ mL).

2.15.5. Calculating enzyme activity

Hexokinase activity was determined based on micromoles of G6P produced per milligram of protein (mM of G6P/ mg of protein).

Chapter 3: Effects of *klo-1/KL* and *klo-2/KL* deletion on Health and Stress Responses in *C. elegans*

3.1. Introduction and key hypotheses

Following generation of strains containing *klo-1/kl* and *klo-2/kl* deletion mutation alleles, a variety of assays were performed to examine general health and stress responses in these nematodes in comparison to their wild-type counterparts. Results presented in this chapter include; lifespan analysis, viable progeny analysis, starvation responses and analysis of autophagy markers in *klotho* mutants compared to wild-type *C. elegans*.

As *klotho* has previously attracted the moniker of being an “anti-ageing gene” (Kuro-o et al., 1997, Kurosu et al., 2005), lifespan was performed on single and double mutants for *klo-1/kl* or *klo-2/kl* and in *klotho* mutants with an FGF mutant background. *Klotho* knockout murine models exhibit diminished lifespan compared to their wild-type counterparts, which initially gave cause for this gene to be given “anti-ageing”-status (Kuro-o et al., 1997, Kurosu et al., 2005). Therefore deletion mutations presumed to be null in *C. elegans* may be expected to lead to diminished lifespan of the animal.

Some reports suggest that extended lifespan may come at the cost of fertility in some species (Chen et al., 2013a, Rollins et al., 2017), therefore viable progeny analysis was also performed on wild-type and *klotho* mutant strains to assess this. If *klotho* mutants were to exhibit any differences in longevity compared to wild-type strains, it is useful to analyse whether fertility of the animal is reflective of this.

In addition, *C. elegans* strains were exposed to heat and starvation stressors, and analysed for expression of autophagic markers. The purpose of these experiments were to potentially identify any indicators of altered metabolism or resistance in *klotho* mutants that may form the basis for more elaborate hypotheses for the impact of impaired *klotho* signalling in the *C. elegans* model which may be explored as part of future research.

3.2. Lifespan analysis of *C. elegans* strains

3.2.1. *klo-1*/*KL* and *klo-2*/*KL* deletion mutations do not impact lifespan in *C. elegans*

There are several lifespan-regulating genes identified in *C. elegans* such as *daf-2*/*InR*, *daf-16*/*FoxO*, TOR signalling components, *sir-2.1*/*SIR* and *aak-2*/*AMPK* (Apfeld et al., 2004, Greer et al., 2007, Guarente and Kenyon, 2000, Johnson, 1990, Kenyon et al., 1993, Lin et al., 1997, Uno and Nishida, 2016, Vellai et al., 2003). The mammalian orthologues of many of these genes have demonstrable links to klotho (Cheng et al., 2017, Lim et al., 2017, Lin et al., 2013, Videla et al., 2018, Yamamoto et al., 2005, Zhao et al., 2015). Given the anti-aging and effects of klotho in vertebrate models (Arking et al., 2005, Chen et al., 2013b, Kuro-o et al., 1997, Kurosu et al., 2005, Majumdar and Christopher, 2011), lifespan analysis was conducted in wild-type vs *klo-1* and *klo-2* deletion mutant strains to determine whether deletion of *C. elegans klo-1* and *klo-2* genes would impact longevity of the nematode.

Wild-type animals had an average lifespan of 18.06 ± 0.74 days compared to 19.38 ± 1.02 , 18.38 ± 1.05 and 17.21 ± 0.78 days for *klo-1* (*ok2925*), *klo-2* (*ok1862*) and *klo-2; klo-1* animals, respectively. There was no significant difference between the lifespan of wild-type animals to that of mutants containing either *klo-1* and/or *klo-2* deletion alleles (Figure 3.1a; table 3.1).

Although no immediate significance in data was identified, it was noted that *klo-1* mutants appeared to show greater survival compared to the wild-type strain in later stages of *C. elegans* lifespan. Therefore, data was re-examined for *klo-1* vs wild-type strain from day 20 of lifespan onwards. Mantel-Cox log rank analysis of strain survival from day 20 onwards ($n = 32$ wild-type nematodes, 36 *klo-1* mutants) revealed significantly greater survival of the *klo-1* strain (Figure 3.2b, $P = 0.009$). This therefore identifies some role for *klo-1* in longevity in *C. elegans* but further research is necessary to explore this.

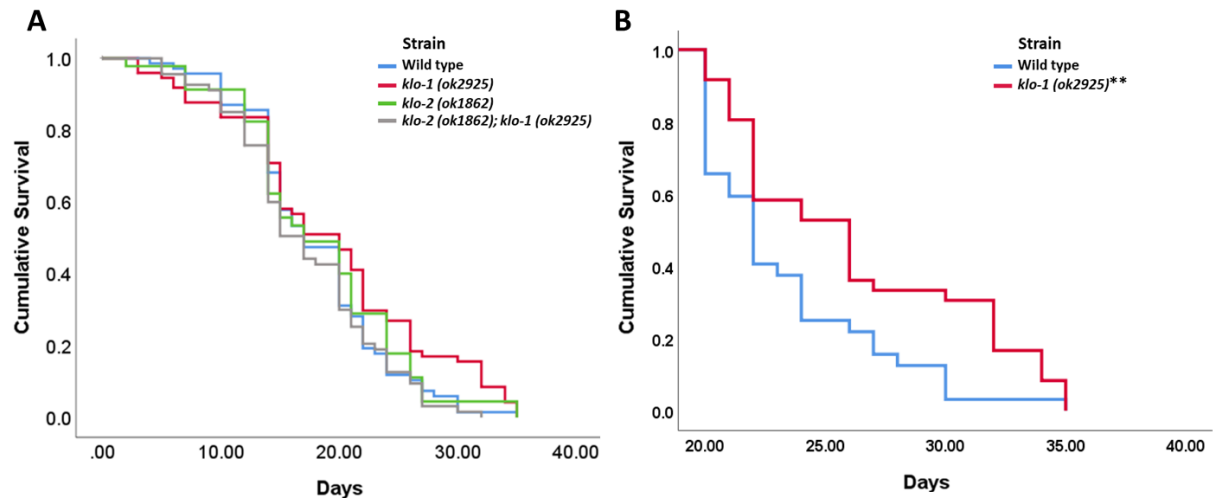


Figure 3.1. (A) Lifespan of N2 (wild-type), *klo-1*, *klo-2* and *klo-2; klo-1* animals. Wild-type ($n = 80$), *klo-1* ($n = 80$), *klo-2* ($n = 50$) and *klo-2; klo-1* ($n = 80$). There were no significant differences between the lifespan of each strain ($P > 0.05$). **(B) Lifespan of N2 (wild-type) and *klo-1* animals from day 20 to death.** Wild-type ($n = 32$), *klo-1* ($n = 36$). Mantel-cox analysis suggested significant increase in survival demonstrated in *klo-1* mutants (* $P < 0.05$, ** $P < 0.01$, *** $P < 0.001$).

Table 3.1. Means comparison for the lifespan of N2 (wild-type), *klo-1*, *klo-2* and *klo-2; klo-1* strains. Lifespan analysed using Kaplan-Meier survival statistics. Statistical significance determined using Tukey's test.

Strain	n	Censored (%)	Mean Lifespan \pm SEM (days)	P values			
				Wild-type	<i>klo-1</i>	<i>klo-2</i>	<i>klo-2; klo-1</i>
N2 (wild-type)	80	15.0	18.06 \pm 0.78	-	0.586	0.914	0.683
<i>klo-1</i> (ok2925)	80	11.3	19.38 \pm 1.02	0.586	-	0.969	0.084
<i>klo-2</i> (ok1862)	50	10.0	18.38 \pm 1.05	0.914	0.969	-	0.364
<i>klo-2</i> (ok1862); <i>klo-1</i> (ok2925)	80	14.5	17.218 \pm 0.78	0.683	0.084	0.364	-

3.2.2. Lifespan analysis of *C. elegans* strains with altered FGF-*klotho*-FGFR signalling

3.2.2.1. Effects of diminished FGF-FGFR signalling on the lifespan of *klo-1* and *klo-2* mutants

Given that currently, the only known roles of klothos are as co-factors for eFGF/ FGFR signalling, the impacts of *klo-1/ KL* and *klo-2/ KL* deletion were examined in combination with components of the *C. elegans* FGF signalling network, *egl-15/ fgfr* and *egl-17/ fgf*. It would be expected that in line with existing literature that klotho functions as a factor for endocrine FGF signalling, the FGF signalling components in *C. elegans* would be required for the effects (if any) that *klo-1/ KL* and *klo-2/ KL* deletion may have on nematode lifespan. It should be noted that the parental strains containing *egl-15* (*n1477*) and *egl-17* (*n1377*) alleles are as follows; *clr-1* (*e2530*) II; *egl-15* (*n1477*) and *hst-2* (*ok595*); *egl-17* (*n1477*) X. *clr-1* encodes receptor tyrosine phosphatases reported to negatively regulate the FGFR signalling pathway (Kokel et al., 1998) and *hst-2* encodes a heparan-2-*O*-sulphotransferase reported as essential for normal cell migration in *C. elegans* (Kinnunen et al., 2005). Both *clr-1*; *egl-15* and *hst-2*; *egl-17* strains were previously generated by our research lab and these were subsequently utilised for the crossing of *egl-15/ FGFR* and *egl-17/ FGF* mutant alleles into *C. elegans* with *Klotho* mutant backgrounds. During crossing, nematodes were selected based on the presence of Egl- phenotype and were genotyped for *klo-1*, *klo-2*, *clr-1* and *hst-2* where required.

The lifespan of *klo-1* and *klo-2*; *klo-1* double mutants were significantly diminished from 19.38 ± 1.02 and 17.22 ± 0.78 days, respectively, to 3.70 ± 0.49 days in *klo-1*; *egl-15* double mutants and 1.47 ± 0.21 days in *klo-2*; *klo-1*; *egl-15* triple mutants (Figure 3.2; Table 3.2). This can be attributed to the Egl-phenotype as the *clr-1*; *egl-15* parent strain had a mean lifespan of just 3.80 ± 0.73 days.

Interestingly, in combination with *klo-2* allele alone, the lifespan of *klo-2*; *egl-15* double mutants is no different to that of wild-type (18.06 ± 0.78 days, $n = 80$) and *klo-2* single mutants (18.38 ± 1.05 days, $n = 50$) (Figure 3.2; Table 3.2). However, given that the *clr-1*; *egl-15* parent strain had significantly diminished lifespan compared to wild-type coupled with *klo-2*; *klo-1*; *egl-15* triple mutants displaying significantly diminished lifespan it is likely that there is an error in the data for the *klo-2*; *egl-15* strain. It is thought that the *egl-15* allele had been lost or crossed out by mistake in this strain meaning they would be wild-type for *egl-15/ FGFR* explaining why these nematodes display a similar lifespan to that of *klo-2* single mutants.

During crossing, *egl-15/ FGF* mutants were identified via phenotype only and not using genotyping techniques. The *egl-15* allele would therefore need to be crossed into the *klo-2* strain again and lifespan analysis to be repeated.

egl-17; hst-2 parent strains have a slightly diminished lifespan compared to their wild-type, *klo-1, klo-2* and *klo-2; klo-1* counterparts with an average lifespan of 16.7 ± 1.41 days, though this was not found to be significant (Table 3.2). In combination with *klo-1*, the survival of these animals is diminished to an average of 10.95 ± 1.60 days ($n = 25$, $P = 0.004$ compared to wild-type) (Figure 3.2; Table 3.2). Similarly, the lifespan of *klo-2; klo-1; egl-17; hst-2* was diminished to 10.55 ± 0.87 days ($n = 25$, $P = 0.005$ compared to wild-type). Interestingly, while *klo-2; klo-1; egl-17* do show slightly diminished lifespan compared to their wild-type, *klo-1, klo-2* and *klo-2; klo-1* counterparts ($n = 25$, lifespan of 14.42 ± 1.84 days), this is only significant when compared to *klo-1* single mutants ($P = 0.024$). This suggests that the diminished lifespan of these mutants could be the result of the *hst-2* allele present in these strains. *klo-2* in combination with *egl-15* was shown to rescue the lifespan of *egl-15* mutants so it could be that *klo-2* mutation rescues the lifespan of *klo-1* and *egl-15/-17*-deficient strains. Unfortunately, the crosses did not generate both *klo-2; egl-17* double mutants or strains lacking the *hst-2* so it is not possible in this instance to determine this.

Due to the egg-laying defective phenotypes of *egl-15/ FGFR* and *egl-17/ FGF* mutant strains, these mutants have significantly decreased lifespan compared to wild-type animals as mothers tend to become “bags of worms” whereby their progeny hatch inside them and mothers burst to release these larvae, killing them in the process. Therefore, no conclusions can reliably be drawn from the data as it stands, and the lifespan analysis needs to be repeated using plates supplemented with Floxuridine (FUDR), an anti-cancer drug that stops the production of eggs in *C. elegans* (Van Raamsdonk and Hekimi, 2011).

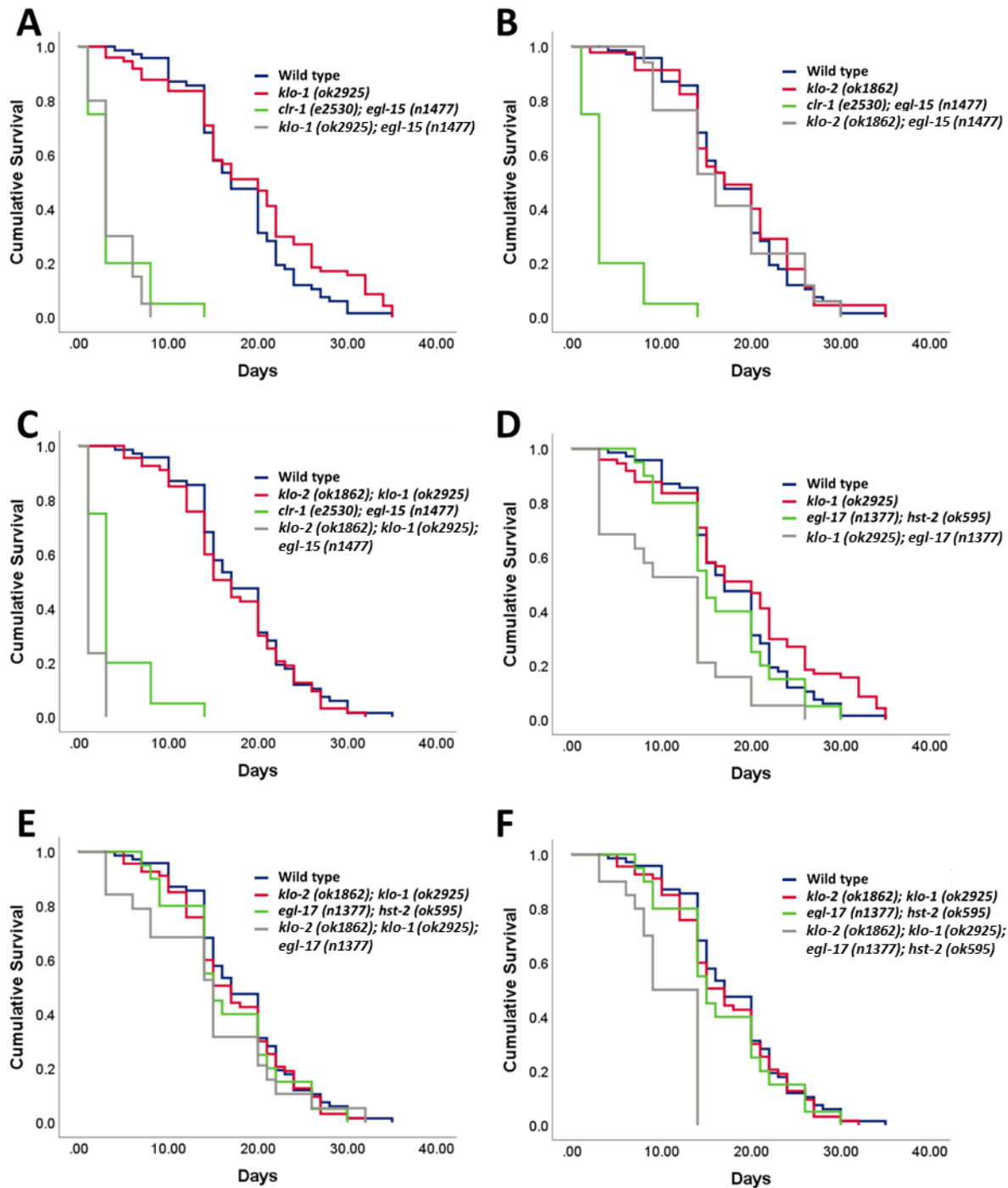


Figure 3.2. Lifespan analysis of *egl-15*, *egl-17*, *klo-1* and *klo-2* compound mutants. A. Wild-type (blue, n = 80), *klo-1* (red, n = 80), *clr-1*; *egl-15* (green, n = 25) and *klo-1*; *egl-15* double mutants (grey, n = 25). B. Wild-type (blue), *klo-2* single mutants (red, n = 50), *clr-1*; *egl-15* (green) and *klo-2*; *egl-15* double mutants (grey, n = 25). C. Wild-type (blue), *klo-2*; *klo-1* (red, n = 80), *clr-1*; *egl-15* (green) and *klo-2*; *klo-1*; *egl-15* triple mutants (grey, n = 25). D. Wild-type (blue), *klo-1* (red), *egl-17*; *hst-2* (green, n = 25) and *klo-1*; *egl-17*; *hst-2* mutants (grey, n = 25). E. Wild-type (blue), *klo-2*; *klo-1* (red), *egl-17*; *hst-2* (green, n = 25) and *klo-2*; *klo-1*; *egl-17* mutants (grey, n = 25). F. Wild-type (blue), *klo-2*; *klo-1* (red), *egl-17*; *hst-2* (green, n = 25) and *klo-2*; *klo-1*; *egl-17*; *hst-2* mutants (grey, n = 25).

E. Wild-type (blue), *klo-2; klo-1* (red), *egl-17; hst-2* (green) and *klo-2; klo-1; egl-17* triple mutants (grey, n =25). F. Wild-type (blue), *klo-2; klo-1* (red), *egl-17; hst-2* (green) and *klo-2; klo-1; egl-17; hst-2* quadruple mutants (grey, n = 25). Asterisks indicate statistical significance compared to wild-type controls as determined using Tukey's test (* P < 0.05, ** P < 0.01, *** P < 0.001).

Table 3.2. Mean lifespan of *egl-15*, *egl-17*, *klo-1* and *klo-2* compound strains. Statistical significance determined using Tukey's test. Asterisks indicate significant values (* P < 0.05, ** P < 0.01, *** P < 0.001).

Strain	n	Censored (%)	Mean Lifespan ±SEM (days)	P values			
				Wild-type	<i>klo-1</i>	<i>klo-2</i>	<i>klo-2</i> ; <i>klo-1</i>
N2 (wild-type) ^a	80	15.0	18.06±0.78	-	0.586	0.914	0.683
<i>klo-1</i> (<i>ok2925</i>) ^a	80	11.3	19.38±1.02	0.586	-	0.969	0.084
<i>klo-2</i> (<i>ok1862</i>) ^a	50	10.0	18.38±1.05	0.914	0.969	-	0.364
<i>klo-2</i> (<i>ok1862</i>); <i>klo-1</i> (<i>ok2925</i>) ^a	80	14.5	17.22±0.78	0.683	0.084	0.364	-
<i>clr-1</i> (<i>e2530</i>); <i>egl-15</i> (<i>n1477</i>)	25	20.0	3.80±0.73	<0.001***	<0.001***	<0.001***	<0.001***
<i>klo-1</i> (<i>ok2925</i>); <i>egl-15</i> (<i>n1477</i>)	25	20.0	3.70±0.49	<0.001***	<0.001***	<0.001***	<0.001***
<i>klo-2</i> (<i>ok1862</i>); <i>egl-15</i> (<i>n1477</i>)	25	32.0	17.18±1.68	0.567	0.079	0.305	0.973
<i>klo-2</i> (<i>ok1862</i>); <i>klo-1</i> (<i>ok2925</i>); <i>egl-15</i> (<i>n1477</i>)	25	32.0	1.47±0.21	<0.001***	<0.001***	<0.001***	<0.001***
<i>hst-2</i> (<i>ok595</i>); <i>egl-17</i> (<i>n1377</i>)	25	20.0	16.7±1.41	0.983	0.539	0.864	1.000
<i>hst-2</i> (<i>ok595</i>); <i>klo-1</i> (<i>ok2925</i>); <i>egl-17</i> (<i>n1377</i>)	25	24.0	10.95±1.60	0.004**	<0.001***	<0.001**	0.071
<i>klo-2</i> (<i>ok1862</i>); <i>klo-1</i> (<i>ok2925</i>); <i>egl-17</i> (<i>n1377</i>)	25	24.0	14.42±1.84	0.301	0.024*	0.135	0.852
<i>klo-2</i> (<i>ok1862</i>); <i>klo-1</i> (<i>ok2925</i>); <i>egl-17</i> (<i>n1377</i>); <i>hst-2</i> (<i>ok595</i>)	25	20.0	10.55±0.87	0.005**	<0.001***	0.002**	0.085

^aData as shown in **Table 3.1.** (see'3.1.1. Lifespan analysis of *klo-1*/ *KL* and *klo-2*/ *KL* mutants).

3.2.2.2. Loss-of-function of *egl-15/fgfr* or *egl-17/fgf* leads to diminished lifespan in *C. elegans*

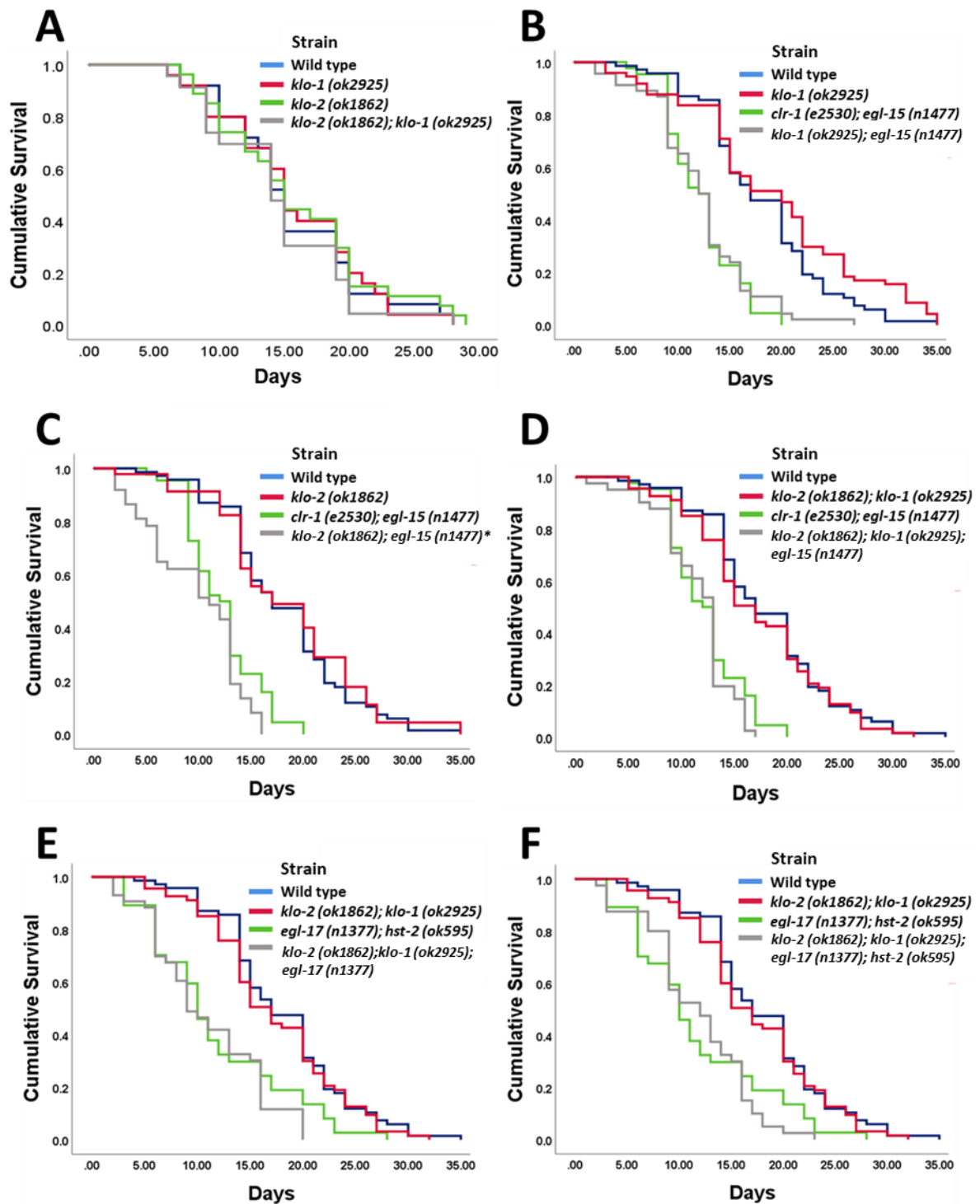
Due to the egg-laying-defective phenotype of *egl-15* and *egl-17* mutant strains, it was unclear whether the above effects on lifespan (see '3.2.2.1. Effects of diminished FGF-FGFR signalling on the lifespan of *klo-1* and *klo-2* mutants') were due to mothers becoming sick as a result of over-crowding of eggs or internal hatching of progeny leaving the mothers to display a "bag of worms" phenotype. To prevent this, NGM agar plates were supplemented with 100 μ M FUDR, which prevents the development of progeny (Van Raamsdonk and Hekimi, 2011).

Control animals kept on plates supplemented with 100 μ M FUDR showed a trend for slightly diminished lifespan compared to those cultured on typical NGM agar plates. Mean lifespan for wild-type animals on FUDR supplemented plates was 15.68 ± 1.09 days ($n = 30$) compared to 18.06 ± 0.78 days for untreated nematodes. Similarly, lifespan of *klo-1*, *klo-2* and *klo-2; klo-1* double mutants were 15.76 ± 1.12 days ($n = 30$), 16.04 ± 1.19 days ($n = 30$) and 14.52 ± 1.09 days ($n = 30$), down from 19.38 ± 1.02 , 18.38 ± 1.05 and 17.22 ± 0.78 days, respectively (see tables 3.3 & 3.3). Despite a trend for lowered lifespan in FUDR supplemented assays, there were no statistically significant differences between the lifespan of treated vs untreated animals.

Presence of either *egl-15* or *egl-17* mutations in combination with *klo-1* or *klo-2* mutations showed a trend for reduced lifespan compared to controls with *clr-1; egl-15* and *egl-17; hst-2* parental strains showing a mean lifespan of 12.25 ± 0.52 days and 11.68 ± 1.08 days, respectively (Figure 3.3, Table 3.3). However, these values were not found to be significant compared to wild-type, *klo-1*, *klo-2* or *klo-2; klo-1* mutant strains (Table 3.3).

The lifespan of *egl-15* and *egl-17* mutants is not impacted in combination with *klo-1* and/ or *klo-2* deletion (Figure 3.3; Table 3.3). There is a trend for *klo-2; egl-15* mutants to have diminished lifespan ($n = 30$, 9.37 ± 0.75 days of mean lifespan) compared to the parental strain *clr-1; egl-15* (12.25 ± 0.52 days), though again, these values are not statistically significant ($p = 0.091$).

Overall, findings suggest Klotho-FGF signalling is required for longevity in *C. elegans*, in line with previous literature findings that comment the protective effects of KL1 are likely the result of cross-talk between both FGF and IIS pathways (Château et al., 2010).



How

Figure 3.3. Lifespan analysis of *egl-15*, *egl-17*, *klo-1* and *klo-2* compound strains assayed on NGM agar plates supplemented with 100 μ M FUDR. A. Wild-type (blue, n = 30), *klo-1* (red, n = 30), *klo-2* (green, n = 30), *klo-2; klo-1* (grey, n = 30). B. Wild-type (blue), *klo-1* (red), *clr-1; egl-15* (green, n = 45) and *klo-1; egl-15* (grey, n = 46). C. Wild-type (blue), *klo-2* (red), *clr-1; egl-15* (green) and *klo-2; egl-15* (grey, n = 45). D. Wild-type (blue), *klo-2; klo-1* (red), *clr-1; egl-15*

(green) and *klo-2; klo-1; egl-15* (grey, n = 44). E. Wild-type (blue), *klo-2* (red), *egl-17; hst-2* (green, n = 45) and *klo-2; klo-1; egl-17* (grey, n = 45). F. Wild-type (blue), *klo-2; klo-1* (red), *egl-17; hst-2* (green) and *klo-2; klo-1; egl-17; hst-2 (ok595)* (grey, n = 45). Asterisks indicate statistical significance compared to wild-type controls as determined using Tukey's test (* P < 0.05, ** P < 0.01, *** P < 0.001).

Table 3.3. Mean lifespan of *egl-15*, *egl-17*, *klo-1* and *klo-2* compound strains grown on NGM plates supplemented with 100 μ M FUDR. Statistical significance determined using Tukey's test. Asterisks indicate significant values (* P < 0.05, ** P < 0.01, * P < 0.001).**

Strain	n	Censored (%)	Mean Lifespan \pm SEM (days)	P values			
				Wild-type	<i>klo-1</i>	<i>klo-2</i>	<i>klo-2</i> ; <i>klo-1</i>
N2 (wild-type)	30	16.7	15.68 \pm 1.09	-	1.000	0.999	0.982
<i>klo-1</i> (<i>ok2925</i>)	30	16.7	15.76 \pm 1.12	1.000	-	0.999	0.977
<i>klo-2</i> (<i>ok1862</i>)	30	10.0	16.04 \pm 1.19	0.999	0.999	-	0.614
<i>klo-2</i> (<i>ok1862</i>); <i>klo-1</i> (<i>ok2925</i>)	30	23.3	14.52 \pm 1.09	0.982	0.977	0.614	-
<i>clr-1</i> (<i>e2530</i>); <i>egl-15</i> (<i>n1477</i>)	45	2.2	12.25 \pm 0.52	1.000	0.999	0.850	1.000
<i>klo-1</i> (<i>ok2925</i>); <i>egl-15</i> (<i>n1477</i>)	46	0.0	12.23 \pm 0.73	1.000	1.000	0.919	1.000
<i>klo-2</i> (<i>ok1862</i>); <i>egl-15</i> (<i>n1477</i>)	45	17.8	9.37 \pm 0.75	0.026*	0.022*	0.001**	0.555
<i>klo-2</i> (<i>ok1862</i>); <i>klo-1</i> (<i>ok2925</i>); <i>egl-15</i> (<i>n1477</i>)	44	6.8	11.53 \pm 0.56	0.894	0.876	0.310	1.000
<i>egl-17</i> (<i>n1377</i>); <i>hst-2</i> (<i>ok595</i>)	45	17.8	11.68 \pm 1.08	0.396	0.366	0.043*	0.994
<i>klo-2</i> (<i>ok1862</i>); <i>klo-1</i> (<i>ok2925</i>); <i>egl-17</i> (<i>n1377</i>)	45	4.4	10.81 \pm 0.83	0.743	0.714	0.165	1.000
<i>klo-2</i> (<i>ok1862</i>); <i>klo-1</i> (<i>ok2925</i>); <i>egl-17</i> (<i>n1377</i>); <i>hst-2</i> (<i>ok595</i>)	45	11.1	11.60 \pm 0.80	0.733	0.704	0.160	1.000

3.3. *klo-1/KL* and *klo-2/KL* single mutants exhibit trend for increased survival upon exposure to acute heat stress at 37 °C

The natural habitat of *C. elegans* is temperate and in the lab conditions they are normally maintained in range between 15°C to 22°C (Zhang et al., 2015). Excessive heat exposure leads to sterility and ultimately death (McMullen et al., 2012). To test the effects of heat exposure on wild-type vs *klo-1*, *klo-2* and *klo-2; klo-1* mutants, nematodes were exposed to 37°C heat and monitored hourly for viability for 9 hours. It would be expected that if *klotho* promotes thermotolerance in *C. elegans*, then deletion of *klo-1/KL* or *klo-2/KL* would result in diminished survival of these strains upon increased heat exposure.

At the 7-hour time point, there were an increased proportion of live *klo-2* (86.67%, 78 of 90 animals) and *klo-1* (83.33%, 75 of 90 animals) *C. elegans*, compared to wild-type (71.43%, 65 of 91 animals) and *klo-2; klo-1* (68.89%, 62 of 90 animals) *C. elegans*, however these differences were not found to be significant ($P > 0.05$).

At the 8-hour time point, both *klo-1* and *klo-2* single mutants had a significantly greater percentage of living animals compared to wild-type (61.54%, 56 of 91 animals, $P = 0.033$ and $P = 0.051$ compared to *klo-1* and *klo-2*, respectively). *klo-1* single mutants also had a significantly higher percentage of living animals compared to *klo-2; klo-1* double mutants (66.67%, 60 of 90 animals, $P = 0.005$), however there was no difference in the proportion of *klo-2; klo-1* double mutants and *klo-2* single mutants at this time point ($P = 0.106$).

At the 9-hour time point, 54.95% of wild-type animals (50 of 91) were still alive compared to 61.11% *klo-1* animals (55 of 90), 62.22% of *klo-2* animals (56 of 90), and 60% of *klo-2; klo-1* double mutants (54 of 90) (Figure 3.4; table 3.4). There was no significant difference between the proportion of nematodes alive between strains at this time point.

Single mutants *klo-1* and *klo-2* seem to have a survival advantage at 7- and 8-hour timepoints compared to wild-type and *klo-2; klo-1* double mutants when exposed to 37°C heat stress. However, this increased survival is acute, and after 9 hours of heat stress exposure, there is no difference in survival between wild-type, *klo-1*, *klo-2* and *klo-2; klo-1* strains. It would be interesting to prolong this heat stress exposure to examine the effects of chronic heat exposure in wild-type vs *C. elegans* strains with *klo-1* or *klo-2* deletion mutations.

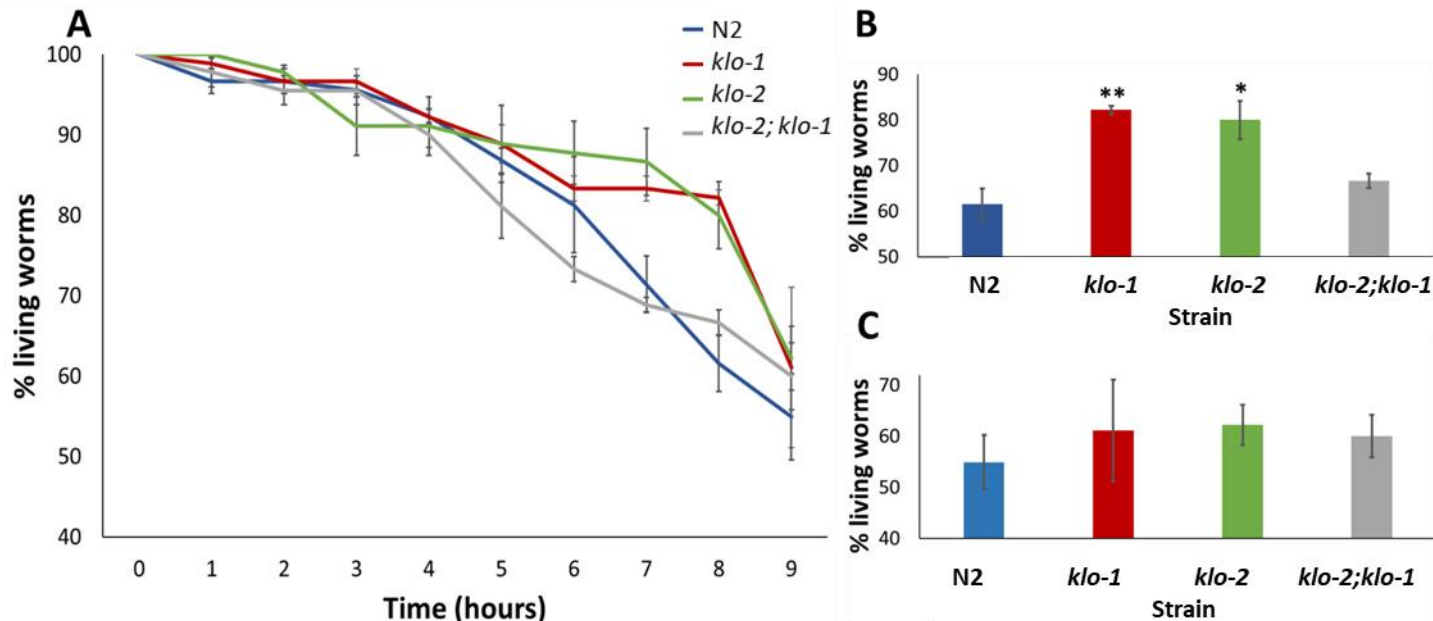


Figure 3.4. Survival of wild-type, *klo-1*, *klo-2* and *klo-2; klo-1* exposed to heat stress (37°C). **A. Survival of strains exposed to heat stress over 9 hours.** Strains; N2 (wild-type) (blue), *klo-1* (red), *klo-2* (green) and *klo-2; klo-1* (grey). Error bars represent standard error of the mean (SEM). No significant difference between strains at any given time point. **B. Percentage of living animals at the 8-hour time point.** At 8 hours, 61.54±3.48% wild-type animals (blue, n = 91) were living compared to; 82.22±0.91% for *klo-1* animals (red, n = 90), 80.00±4.16% for *klo-2* (green, n = 90) and 66.67±1.57% *klo-2; klo-1* double mutants (grey, n = 90). Error bars represent SEM. **C. Percentage of living animals at the 9-hour time point.** At 8 hours, 54.95±5.34% wild-type animals (blue, n = 91) were living compared to; 61.11±9.98% for *klo-1* animals (red, n = 90), 62.22±3.95% for *klo-2* (green, n = 90) and 60.00±4.156% *klo-2; klo-1* double mutants (grey, n = 90). Error bars represent SEM.

Table 3.4. Survival of wild-type, *klo-1*, *klo-2* and *klo-2; klo-1* strains exposed to 37°C heat stress over 9 hours. Survival shown (%) for 7-, 8- and 9-hour time points. Asterisks indicate significance against wild-type animals (*P < 0.05, **P < 0.01, ***P < 0.001). P values determined using Tukey's test.

Strain	<i>n</i>	% Living 7 hours ±SEM	% Living 8 hours ±SEM	% Living 9 hours ±SEM	P value vs N2		
					7 hours	8 hours	9 hours
Wild-type (N2)	91	71.43±3.49	61.54±3.48	54.95±5.34	-	-	-
<i>klo-1</i> (<i>ok2925</i>)	90	83.33±1.57	82.22±0.91	61.11±9.98	0.065	0.009**	0.673
<i>klo-2</i> (<i>ok1862</i>)	90	86.67±4.16	80.00±4.16	62.22±3.95	0.084	0.049*	0.414
<i>klo-2</i> (<i>ok1862</i>); <i>klo-1</i> (<i>ok2925</i>)	90	68.89±0.91	66.67±1.57	60.00±4.15	0.591	0.329	0.565

3.4. Survival of wild-type vs *klo-1*/KL and *klo-2*/KL deletion mutants exposed to chronic starvation

Klotho has been reported to have roles in energy metabolism (Kurosu et al., 2005), and FGF21 (which utilizes *klotho* as a co-factor for binding to its respective receptor), has been described as a starvation hormone shown to extend lifespan in murine models (Zhang et al., 2012). If functional KLO-1/ KL and KLO-2/ KL are required for longevity in states of starvation in *C. elegans* it would be expected that deletion of *klo-1*/KL and *klo-2*/KL would lead to diminished survival upon chronic oxidative stress in these animals.

To examine the effects of *klo-1* and *klo-2* deletion mutations in response to chronic starvation, large quantities of L4 stage wild-type, *klo-1*, *klo-2* and *klo-2; klo-1* *C. elegans* were suspended in M9 buffer only (without *E. coli* to feed on), and aliquots were taken daily, left for a few hours to revive on *E. coli* OP50 NGM plates, then counted for living animals. Aliquots were taken daily until there were no living animals.

Due to setbacks with regards to harvesting of nematodes from liquid media for age synchronization, wild-type and *klo-2* strains were analysed together, then a subsequent assay for *klo-1* and *klo-2; klo-1* strains was conducted. Restrictions enforced as a result of the global Covid19 pandemic which obstructed weekend laboratory access meant there were differences in data collection time points for data collected in the subsequent assay.

Wild-type animals consistently and daily showed a larger proportion of living animals compared to *klo-2* until day 18. For example, on day one, 71.76% *klo-2* ($n = 754$) animals were alive compared to 91.22% wild-type animals ($n = 516$, $P = 0.003$). N2 consistently showed this increased proportion of live animals until day 18 (see figure 3.5; appendix 1 for significant values). Interestingly, despite the larger proportion of live animals found in wild-type aliquots, all wild-type animals had died by day 22 ($n = 104$), whereas there were still some *klo-2* nematodes alive on day 24 (0.69%, 1 of 118 animals).

Conversely, there was no significant difference in the proportion of live animals when comparing wild-type vs *klo-1* or *klo-2; klo-1* strains (at time points where all data was available) until day 10. At the day 10 time point, *klo-1* ($n = 196$) and *klo-2; klo-1* ($n = 312$) strains had a significantly lower proportion of live animals compared to wild-type counterparts ($n = 129$) with values of 0.599 ± 0.01 ($P = 0.034$) and 0.523 ± 0.01 ($P = 0.001$) for

proportion of live animals, respectively, compared to wild-type (where mean proportion of living animals was 0.675 ± 0.01). Similarly, *klo-1* and *klo-2*; *klo-1* strains also had significantly lower proportions of live animals compared to wild-type on days 11 and 15 (P values for these time points can be found in appendix 1). Interestingly, from day 18 onwards, there is a trend for increased proportions of live animals in *klo-1* and *klo-2*; *klo-1* strains in comparison to wild-type, though these differences are not statistically significant (see appendix 1).

Comparison of *klo-1*, *klo-2* and *klo-2*; *klo-1* mutants showed that there was a trend for an increased mean proportion of live animals of *klo-1* genetic background in comparison to *klo-2* single mutants, with these differences being statistically significant at the following time points; day one (P < 0.001), day two (P < 0.001), day three (P = 0.015), day eight (P = 0.037) and day fifteen (P = 0.001). There was no significant difference between the proportion of live animals for *klo-2*; *klo-1* double mutants in comparison to *klo-2* single mutants at any time point excluding day fifteen where there was an increased proportion of *klo-2*; *klo-1* double mutants alive compared to *klo-2* animals (P = 0.007).

Additionally, *klo-1* single mutants showed significantly increased proportions of live animals in comparison to *klo-2*; *klo-1* double mutants at the following time points; day three (P = 0.049), day six (P = 0.046), day seven (P = 0.007), day eight (P = 0.020), day 10 (P = 0.011), day 11 (P = 0.015), day 15 (P = 0.016), and day 20 (P = 0.020).

Taken together, these results could indicate a role for *klo-2*/*KL* in chronic starvation responses given the trend for lower survival compared to wild-type and *klo-1* strains. However, this assay could benefit from technical repeats of data collection for all strains, and for this data to be collected at consistent time points before any conclusions could be drawn.

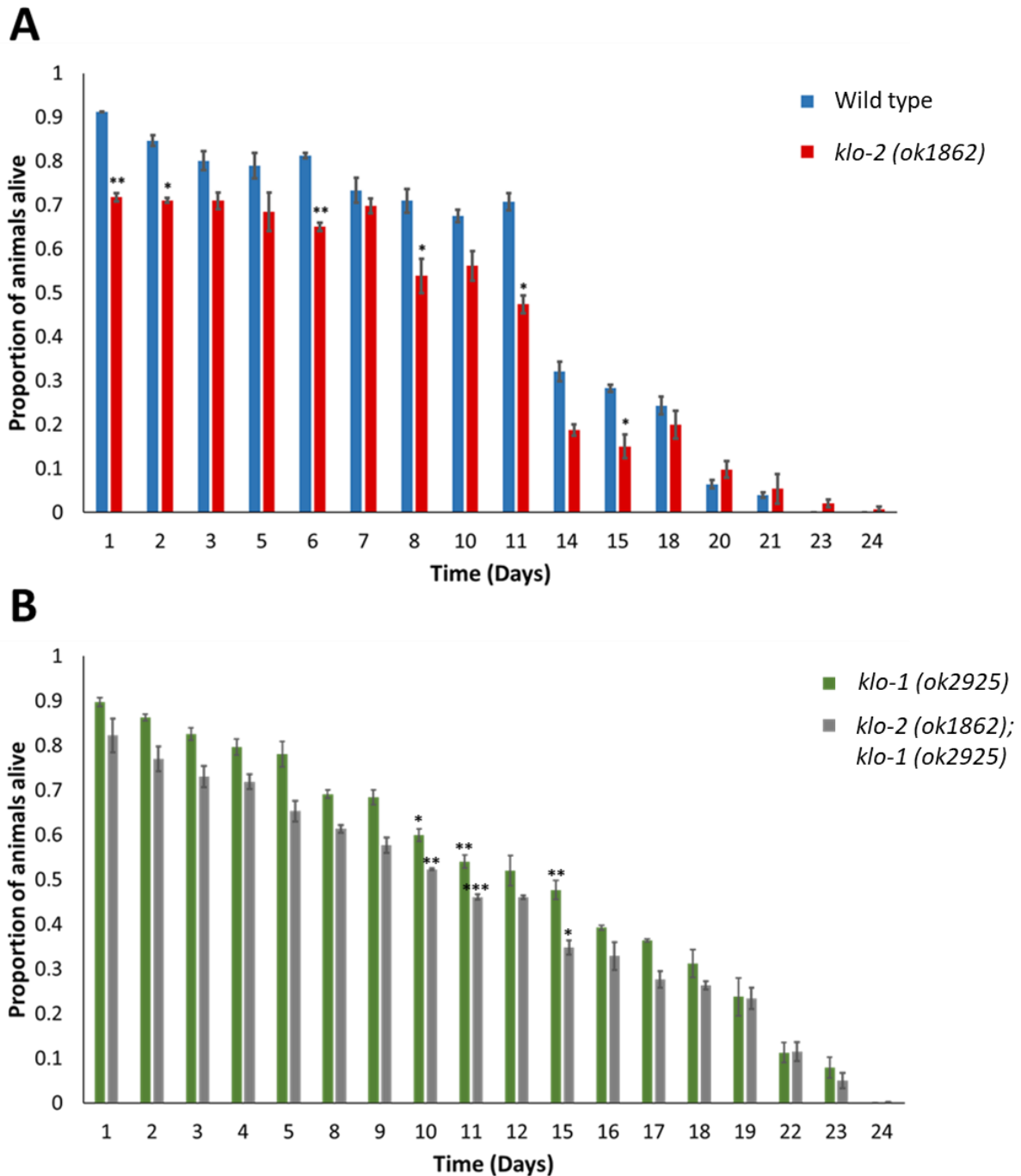


Figure 3.5. Survival of *C. elegans* strains subject to chronic starvation. A. Proportion of living wild-type (N2) vs *klo-2* strains exposed to chronic starvation over time. Wild-type (blue) have an increased proportion of living animals at any given time point until day 19. *klo-2* (red) animals have decreased survival compared to wild-type animals at any given time point but show longer survival overall. Maximum lifespan of wild-type animals exposed to chronic starvation was 20 days whereas *klo-2* still had animals alive up until day 23. **B. Proportion of living *klo-1* and *klo-2*; *klo-1* animals exposed to chronic starvation over time.** *klo-1* (green) and *klo-2*; *klo-1* (grey) mutants show a trend for increased survival compared to *klo-2* single

mutants (see figure 3.5A), but no significant difference between wild-type animals unless otherwise indicated. Error bars represent standard error of the mean (SEM). Asterisks indicate where wild-type had significantly increased proportion of living animals compared to *klo-1*, *klo-2* and *klo-2; klo-1* strains (*P < 0.05, **P < 0.01, ***P < 0.001). Statistical significance determined using Tukey's test.

3.5. *klo-1*/*KL* single mutants exhibit fewer viable progeny than wild-type, *klo-2* and *klo-2*; *klo-1* counterparts

There are reports that resistance to stress in *C. elegans* could come at the cost of reproduction (Chen et al., 2013b, Rollins et al., 2017). Therefore, progeny analysis was carried out in wild-type vs *klo-1*, *klo-2* and *klo-2*; *klo-1* strains. To assess the fitness of mutant strains, the number of eggs laid and successful progression from eggs to adults via the four larval stages was monitored.

Viable progeny analyses of nematodes showed that *klo-2* single mutants produced the most viable progeny with a mean of 296.8 ± 10.95 viable progeny, which was significantly greater compared to wild-type (244.2 ± 5.57 viable progeny, $P = 0.008$), *klo-1* single mutants (176.4 ± 7.67 viable progeny, $P < 0.001$) and *klo-2*; *klo-1* double mutants (242.25 ± 13.76 viable progeny, $P = 0.026$).

klo-1 single mutants also produced significantly fewer viable progeny than wild-type ($P < 0.001$) and *klo-2*; *klo-1* double mutants ($P = 0.009$). *klo-2*; *klo-1* double mutants showed no difference in viable progeny to that of wild-type animals (see figure 3.6 table 3.5).

It should be noted that the average brood size of wild-type *C. elegans* should be ~ 300 progeny (Hodgkin and Barnes, 1991), with the findings here seemingly lowered. It is unclear for the reason of this, however it should be noted that the sample size here is relatively low ($n = 5$ animals) and would benefit from trial repetition to determine reliability of findings.

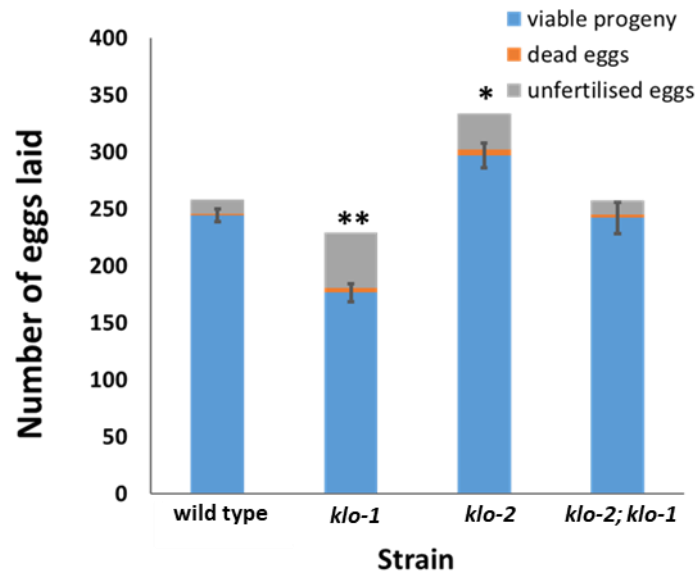


Figure 3.6. Viable progeny analysis of wild-type, *klo-1*, *klo-2* and *klo-2; klo-1* strains. Average viable progeny (indicated in blue) per strain as follows (L-R); Wild-type 244.2±5.57, *klo-1* 176.4±7.67, *klo-2* 296.8±10.95 and *klo-2; klo-1* 242.25±13.76. Unfertilized eggs indicated in grey; dead eggs indicated in orange. Error bars represent SEM. Asterisks indicate statistical significance compared to wild-type, as determined using Tukey’s test (*P < 0.05, **P < 0.01, ***P < 0.001).

Table 3.5. Mean viable progeny values for wild-type, *klo-1*, *klo-2* and *klo-2; klo-1* strains. Progeny of 4-5 nematodes per strain were analysed. Statistical significance determined by Tukey’s test, asterisks indicate significant values (*P < 0.05, **P < 0.01, ***P < 0.001). Mean values and statistical analysis for unfertilised and dead eggs can be found in appendix 2.

Strain	n	Mean Viable Progeny ±SEM	P values				
			N2	<i>klo-1</i>	<i>klo-2</i>	<i>klo-2; klo-1</i>	<i>aak-2</i>
N2 (wild-type)	5	244.2±5.57	-	<0.001***	0.008**	0.905	0.046*
<i>klo-1 (ok2925)</i>	5	176.4±7.67	<0.001***	-	<0.001***	<0.001***	0.637
<i>klo-2 (ok1862)</i>	5	296.8±10.95	0.008**	<0.001***	-	0.026*	0.007**
<i>klo-2 (ok1862); klo-1 (ok2925)</i>	4	242.25±13.76	0.905	0.009**	0.026*	-	0.079

3.6. Effects of *klo-1* and *klo-2* deletion on autophagy reporter expression

Autophagy is an essential process required for the removal of damaged cells and/ or cellular components to maintain organismal health (Kohli and Roth, 2010) In *C. elegans*, autophagic processes in intestinal tissues can be indicative of healthspan and longevity in these animals, dietary restriction driven lifespan extension being dependent on functional autophagy regulation (Gelino et al., 2016). Autophagic responses in *C. elegans* may be upregulated in response to several types of stressors including oxidative and heat stress, therefore monitoring of autophagy in these animals could provide a readout for animal health (Megalou and Tavernarakis, 2009).

Autophagy can be monitored in *C. elegans* using fluorescent reporters such as *lgg-1::GFP*. LGG-1 encodes a protein orthologous to mammalian microtubule-associated protein 1A/ 1B-light chain 3 (LC3) and has previously been used as a marker for the detection of autophagosomes (Mizushima et al., 2004, Palmisano and Meléndez, 2016). Under conditions that induce autophagy, *lgg-1::GFP* reporter forms distinct puncta indicative of autophagy that can subsequently be quantified.

Transgenic hermaphrodites between the life stages of L1-L2 positive for *adIs2122 [lgg-1p::GFP::lgg-1 + rol-6 (su1006)]* were crossed with *klo-2; klo-1* double mutants to generate *klo-1, klo-2* and *klo-2; klo-1* strains positive for the *adIs2122* transgene in preparation for subsequent analysis. Due to the national lockdown as a result of the Covid19 pandemic, a *klo-2; klo-1* strain positive for the *lgg-1::GFP* reporter was lost and we were unable to recover this strain following return to the lab. Therefore, analysis of *lgg-1::GFP* expression was done using wild-type, *klo-1* and *klo-2* animals positive for this reporter.

There is a trend for fewer *lgg-1::GFP* puncta frequency in the intestinal cells of *klo-1* ($n = 20$ animals, relative puncta frequency of 0.866 ± 0.16 , $P = 0.510$) and *klo-2* ($n = 20$ animals, relative puncta frequency of 0.709 ± 0.09 , $P = 0.065$) relative to wild-type strain ($n = 20$ animals), although this data is not statistically significant. Due to low sample size and need for technical repeats, it is difficult to draw conclusions from this data. It should be noted that LGG-1 functions in the early stages of autophagy, acting upstream of LGG-2 which is responsible for the maturation of autophagosomes (Chen et al., 2017). It is not clear from this assay whether the increased instance of these puncta is the cause of increased autophagy, or whether this

could signal blocked autophagy if there is an inability to proceed to later stages of autophagosome maturation. It is discussed under the “7.2.1. Investigating the impact of KLO-1 and KLO-2 in autophagic responses” section of this theses more options for exploration of autophagic responses in *C. elegans* which may provide more robust methods to determine whether autophagy is up- or down-regulated in *C. elegans* strains.

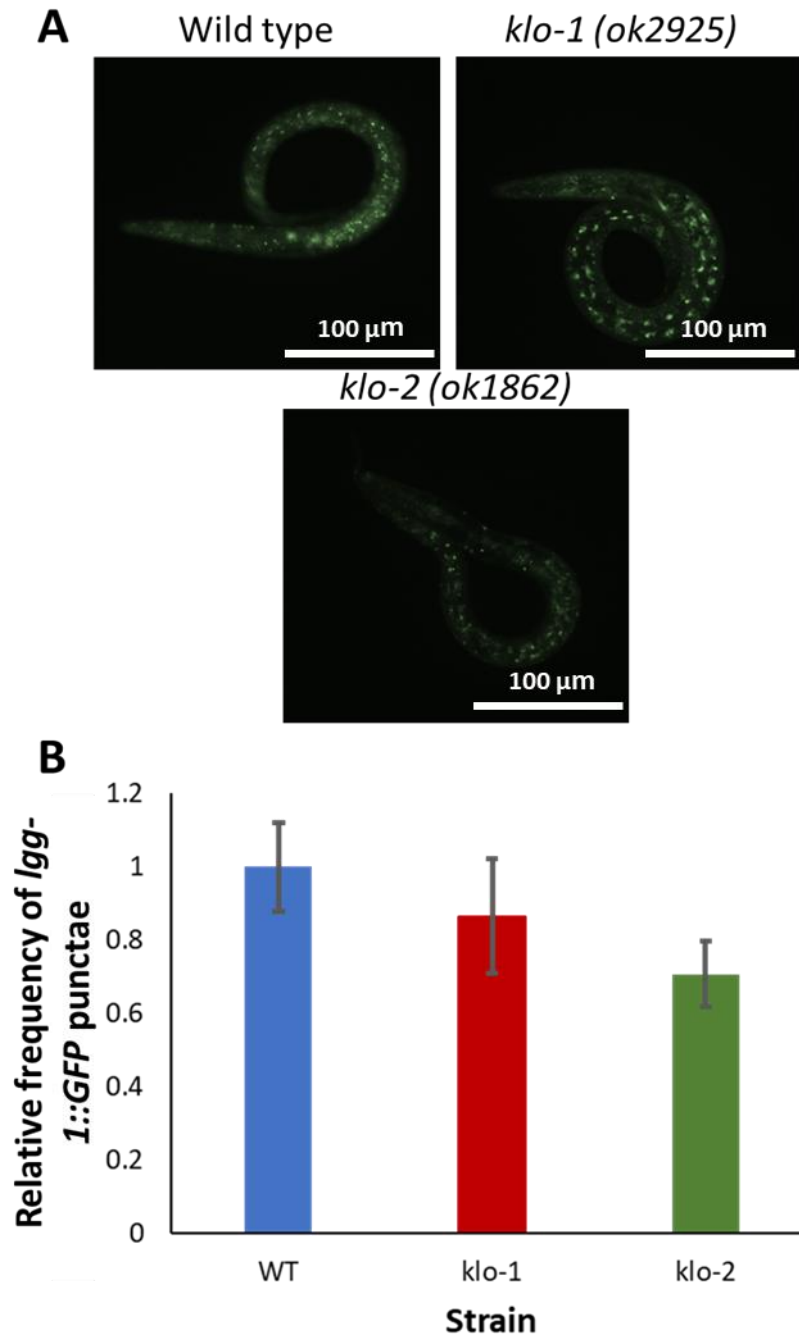


Figure 3.7. *Igg-1::GFP* reporter expression in stage L1-L2 wild-type, *klo-1* and *klo-2* *C. elegans* strains. A. Expression of *Igg-1::GFP* in DA2123 (wild-type, top left), *klo-1* (top right) and *klo-2* (green) strains. B. Relative frequency of *Igg-1::GFP* puncta frequency in *klo-1* (red, n = 20 animals) and *klo-2* (green, n = 20 animals) compared to wild-type (blue, n = 20). Error bars represent SEM.

Table 3.6. Relative puncta frequency of *lgg-1::GFP* reporter in wild-type, *klo-1* and *klo-2* *C. elegans* strains. Values are relative to wild-type (equal to 1.000). 10 animals per strain were analysed per assay. Assay repeated once.

Strain	<i>n</i>	Relative expression to wild-type	P values		
			Wild-type	<i>klo-1 (ok2925)</i>	<i>klo-2 (ok1862)</i>
Wild-type	20	1.000±	-	0.510	0.065
<i>klo-1 (ok2925)</i>	20	0.866±0.16	0.510	-	0.401
<i>klo-2 (ok1862)</i>	20	0.709±0.09	0.065	0.401	-

3.7. Discussion: The roles of KLO-1 and KLO-2 in longevity and stress resistance in *C. elegans*

3.7.1. The roles of KLO-1/ KL and KLO-2/ KL in ageing

3.7.1.1. Lifespan in *C. elegans* of *klo-1/ KL* and *klo-2/ KL* genetic backgrounds

Although several studies suggest a role for klothos in lifespan in vertebrate models (Arking et al., 2005, Chen et al., 2013b, Kuro-o et al., 1997, Kurosu et al., 2005, Majumdar and Christopher, 2011), deletion of *klo-2/ KL* alone does not impact lifespan in *C. elegans* (see '3.1.1. Lifespan analysis of *klo-1/ KL* and *klo-2/ KL* mutants'). This is interesting as the deletions of *klo-2/ KL* are predicted to be loss-of-function mutations (Polanska et al., 2011). Data from previous studies show that overexpression of *klo-1/ KL* leads to lifespan extension (Polanska et al., 2011), while RNAi knockdown of *klo-1* in *C. elegans* has been demonstrated to shorten lifespan (Château et al., 2010), so it could be expected that *klo-1* or *klo-2* deletion in *C. elegans* may have reduce longevity of the animal. However, it should also be noted that the extension of lifespan phenotype due to overexpression of *klo-1/ kl* may be a neomorphic effect of the mutation, and there is an abundance of evidence demonstrating high rates of off-target effects from use of RNAi which may impact interpretation of data (Ui-Tei, 2013).

While *klo-1/ KL* deletion did not significantly impact overall lifespan of *C. elegans* compared to wild-type, analysis of survival of *C. elegans* from day 20 revealed that *klo-1/ KL* deletion background strains have increased survival compared to their wild-type counter parts. This was not explored further during this research but would be something to consider for future projects.

It could be that KLO-1/ KL and KLO-2/ KL function in a pathway that impacts lifespan only when in combination with alterations to other longevity-linked pathways. For example, previous lab data shows that *klo-1/ KL* and *klo-2/ KL* deletion mutations in combination with alleles which reduce IIS in *C. elegans* (Buj & Kinnunen, manuscript in preparation). Nematodes with hypomorphic *daf-2/ InsR* alleles live twice as long as wild-type animals (Kenyon et al., 1993), and in combination with *klo-1/ KL* and/ or *klo-2/ KL* deletion mutations, this lifespan is further extended (Buj & Kinnunen, manuscript in preparation). This suggests that KLO-1/ KL and KLO-2/ KL could have effects on longevity in *C. elegans* in a pathway parallel to IIS, highlighted by the additive effects of lifespan extension in Buj's data (Buj & Kinnunen, manuscript in preparation). It should be noted that the lifespan extending effects of *klo-1/ KL* and *klo-2/ KL* deletion in combination with hypomorphic *daf-2* alleles was a surprising finding

given the roles of Klotho in longevity per existing literature as these alleles are presumed null and it has been reported that knockdown of klotho results in diminished lifespan in murine models (Kuro-o et al., 1997).

This theory is not without basis, as it has been demonstrated in other studies that the deletion of pathway components independent of IIS further augments lifespan of *C. elegans* with hypomorphic *daf-2/InsR* genetic backgrounds (Chen et al., 2013a). This study demonstrates that deletion alleles of *rsks-1*, which encodes the orthologue for mammalian S6 kinase (S6K), a key TOR pathway signalling component, augments the lifespan of hypomorphic *daf-2* strains up to 5-fold that of wild type animals, but deletion of *rsks-1/S6K* alone is not enough to affect lifespan in *C. elegans* (Chen et al., 2013a).

Given the similarities between the effects of *klo-1/KL*, *klo-2/KL* and *rsks-1* mutations on the lifespan of *C. elegans* strains with diminished IIS signalling, it would be worth examining the relationship between *klo-1/KL* and *klo-2/KL* deletions in combination with *rsks-1* genetic background. Using rules for epistatic analysis (see “2.9. Interpretation of survival assays: epistatic analysis”), should these genes function in a linear pathway there should be no additive effects of *rsks-1* on longevity in strains with *klo-2; klo-1; daf-2* backgrounds. Alternatively, if *rsks-1* functions independently of *klo-1* or *klo-2* in longevity responses in *C. elegans*, we may expect that presence of this mutation in nematodes with a *daf-2; klo-2; klo-1* mutant background may have an additive effect on maximum lifespan.

3.7.1.2. Role of FGF-FGFR signalling in longevity

As the current only confirmed functions of *klo-1/ KL* and *klo-2/ KL* are as co-factors for FGF-FGFR signalling, compound mutants of *klo-1/ KL*, *klo-2/ KL* and either FGFR orthologue *egl-15*, or FGF orthologue *egl-17*, were subject to lifespan analysis.

Lifespan analysis revealed that *egl-17; hst-2* mutants had slightly diminished lifespan compared to wild-type, *klo-1*, *klo-2* and *klo-2; klo-1* strains (see '3.1.1. Lifespan analysis of *klo-1/ KL* and *klo-2/ KL* mutants'). However, these findings were not statistically significant. Interestingly, the lifespan of *klo-1* and *klo-2; klo-1* strains were diminished in combination with *egl-17* and *hst-2* alleles (see '3.1.2. Lifespan analysis of *C. elegans* strains with altered FGF-*klotho*-FGFR Signalling'). However, it is unclear whether this could be due to the presence of *egl-17*, *hst-2*, or both. It is likely that this could be the impact of *hst-2 (ok595)* allele, at least for *C. elegans* with a *klo-2; klo-1* genetic backgrounds, as triple mutants for *klo-2; klo-1; egl-17*, excluding *hst-2 (ok595)*, do have a diminished lifespan, though this reduced lifespan was not as diminished as for strains with a *hst-2 (ok595)* genetic background.

Due to the egg-laying-defective phenotype caused by the *egl-15 (n1477)* allele, strains containing this allele had a tendency for internal hatching of progeny which led to early death of these animals (see '3.1.2. Lifespan analysis of *C. elegans* strains with altered FGF-*klotho*-FGFR Signalling'). Therefore, lifespan analysis was repeated on NGM plates supplemented with FUDR to inhibit progeny production in the animals (Van Raamsdonk and Hekimi, 2011).

Upon repetition of lifespan analysis using FUDR supplemented NGM agar plates, lifespan was unexpectedly reduced in wild-type, *klo-1*, *klo-2* and *klo-2; klo-1* strains (see '3.1.2.1. Effects of diminished FGF-FGFR signalling on the lifespan of *klo-1* and *klo-2* mutants'). Typically, FUDR is reported to augment the lifespan of *C. elegans* with certain genetic backgrounds (Kato et al., 2017), whereas this data is inconsistent with these findings. It has also been suggested that FUDR could induce DNA base damage in *C. elegans*, which would ultimately reduce lifespan (Kato et al., 2017), perhaps offering an explanation to the data collected here. Upon examiner review, it was noted that a lower concentration of FUDR may be more appropriate to use to prevent egg laying in *C. elegans*. Therefore the assay should be repeated following methodology adjustments to assess reliability of the findings presented here. This could either confirm or refute the unexpected findings here that wild-type *C. elegans* display diminished lifespan in the presence of FUDR.

Mutants with *egl-15* (n1477) or *egl-17* (n1377) genetic backgrounds showed a trend for diminished lifespan between 3.79 to 6.67 days compared to wild-type, *klo-1* and *klo-2* single mutants, as well as *klo-2; klo-1* double mutants, however statistically these findings were not significant for any strains excluding *klo-2; egl-15* and *egl-17; hst-2*.

Taken together, the data could imply EGL-15/ FGFR and EGL-17/ FGF that there may be a role for these FGF signalling components in wild-type longevity, however this research lacks sufficient evidence to confirm this. In addition, no differences were found between wild-type and *C. elegans* strains with genetic backgrounds featuring deletion mutations for *klo-1* and/ or *klo-2*, it is difficult to draw conclusions based on the data presented here.

A growing body of data does suggest roles for KLO-1/ KL and KLO-2 in *C. elegans* longevity (Buj, unpublished, Château et al., 2010, Polanska et al., 2011), perhaps linking back to the previously mentioned hypothesis that *klo-1/ KL* and *klo-2/ KL* could function in longevity pathways that are not immediately clear unless in combination with the knockdown of other signalling transduction pathways that could have cross-talk with klotho-mediated functions.

3.7.2. *klo-1/ kl* deletion reduces viable progeny in *C. elegans* in line with effects on nematode lifespan

As previously mentioned (see '3.5. Viable progeny analysis'), fertility in many organisms including *C. elegans* has been linked to longevity in some genetic backgrounds (Chen et al., 2014, Rollins et al., 2017). Upon viable progeny analysis, it was found that *klo-2* single mutants had increased progeny production compared to wild-type animals, whereas *klo-1* single mutants showed significantly lower viable progeny production (see '3.5. Viable progeny analysis'). In addition, *klo-2; klo-1* mutants showed no significant difference in progeny production compared to wild-type counterparts.

This is in line with the theory that there is some trade-off between longevity and fertility in several species, where animals with longer lifespans tend to demonstrate reduced fertility and vice versa (Chen et al., 2014, Rollins et al., 2017). For example, *klo-1/ KL* mutants display fewer viable progeny than their wild type counterparts (see sub-section 3.5. "*klo-1/ KL* single mutants exhibit fewer viable progeny than wild-type, *klo-2* and *klo-2; klo-1* counterparts")

and analysis of data from day 20 of *C. elegans* survival data shows that there is improved survival of *klo-1/ KL* mutants compared to wild-type.

However, the causes for differences in viable progeny for *klo-2* single mutants and *klo-2; klo-1* double mutants still remain to be elucidated. It seems that KLO-1/ KL and KLO-2/ KL may have opposing impacts on fertility in *C. elegans* with *klo-2* single mutants having significantly increased viable progeny compared to their wild-type counterparts, while *klo-1* single mutants demonstrate significantly reduced viable progeny. Further to this, *klo-2; klo-1* double mutants show viable progeny similar to that of wild-type, seemingly due to the effects of the *klo-1* and *klo-2* mutations negating one another. Overall, sample size for this assay was low and would benefit from repetition to determine whether the effects observed here are consistent in these strains.

3.7.3. KLO-1/ KL and KLO-2/ KL in chronic starvation responses

Initially, chronic starvation assays were attempted on NGM agar plates. However, this led to *C. elegans* burrowing into the agar, or crawling off plates in search of food, therefore an alternative method was developed adapted from (Malik, 2019). Nematodes were first grown up in liquid media and age synchronised. Due to differences in the quantity of *C. elegans* in starter cultures for liquid media, nematodes for each strain reached desired population density at slightly different rates. Initially, wild-type and *klo-2* strains reached the desired population density for age synchronisation, therefore these strains were assayed first.

Unfortunately, due to the national lockdown enforced as a result of the COVID-19 pandemic, data was not collected for *klo-1* and *klo-2; klo-1* strains until return to the lab, at which point restrictions prohibited weekend lab access, thus impacting the ability to collect data for these strains at identical time points as for wild-type and *klo-2* strains. This meant there were discrepancies in time points for *klo-1* and *klo-2; klo-1* compared to wild-type strains and limited comparisons could be drawn from this data.

Comparisons between wild-type and *klo-2* reveal a trend for lowered survival of *klo-2* single mutants upon chronic starvation until the day 18 timepoint. Interestingly, following day 18, there is a trend for increased survival of *klo-2* mutants compared to wild-type, and while wild-

type had a maximum survival of 21 days, there were still *klo-2* single mutants alive at the day 24 time point.

This trend for lowered survival in *klo-2* single mutants suggests deletion of this gene interferes with stress responses in relation to chronic starvation for these animals. Indeed, possible roles for *klo-1/ KL* and *klo-2/ KL* in response to starvation have been demonstrated, with data collected by Buj (unpublished) demonstrating that short term, 4 hours starvation of wild-type animals increases the expression of *pklo-1::mCherry* and *pklo-2::GFP* reporters. This suggests that during starvation, *KLO-2/ KL* could be upregulated, meaning *klo-2* single mutants, which is predicted to be loss-of-function allele (Polanska et al., 2011), cannot upregulate starvation response pathways leading to the reduced survival of these strains demonstrated in the data collected here (see figure 3.5). However, this does not explain why *klo-2* single mutants have a greater maximum survival to that of their wild-type counterparts. Murine studies demonstrate that β -klotho functions as a co-factor for FGF21 to bind to its cognate FGFR to facilitate glucose and lipid metabolism (Micanovic et al., 2009, Shi et al., 2018) and previous lab results are also indicative of roles of *KLO-1/ KL* and *KLO-2/ KL* roles in starvation responses (Buj, unpublished). Taken together, this highlights the opportunity for further exploration into the roles of *klo-2/ KL* in starvation responses.

In addition, it would be useful to have comparable data for *klo-1* and *klo-2*; *klo-1* strains against their wild-type counterparts for chronic starvation responses in *C. elegans*, so it would be useful to conduct technical repeats of this data to confirm the above findings and elucidate the roles of *klo-1/ KL* and *klo-2/ KL* in starvation.

3.7.4. Further investigation into the roles of KLO-1 and KLO-2 in autophagic process is required

A recent study by Kosztelnik et al. (2019) found that reduced SKN-1/ Nrf2 function leads to constant activation of AAK-2/ AMPK under chronic stress, ultimately leading to hyper-activation of autophagy, which over time leads to poor health in *C. elegans*. In addition, AMPK functions antagonistically to TOR signalling pathways, which also regulates autophagy (Jung et al., 2010), providing another lead for further research into the pathways governing stress responses in *klo-1/ KL* and *klo-2/ KL* *C. elegans* backgrounds. Unfortunately, as the data currently stands, due to low sample size when examining LGG-1::GFP reporter expression

(which can act as a readout for autophagy in *C. elegans*, (Palmisano and Meléndez, 2016)), no conclusions could be drawn regarding the impact of *klo-1/ KL* and *klo-2/ KL* deletion on autophagic processes in *C. elegans*. However, combined with more specific investigation of the impacts of *klo-1/ KL* and *klo-2/ KL* on SKN-1/ Nrf2 and TOR signalling pathways, this could provide interesting leads for further research that could elucidate these mechanisms further.

3.7.5. Chapter three conclusions

The following conclusions may be drawn from the results presented in this chapter;

- Deletion of *klo-2/ kl* does not immediately impact lifespan in *C. elegans*.
- Deletion of *klo-1/ kl* may unexpectedly lead to an increase in lifespan in *C. elegans*. This is in contrast to previous literature which suggests impaired klotho function leads to diminished lifespan (Kuro-o et al., 1997).
- Reduced egg-laying of *klo-1/ kl* mutant strains may be reflective of lifespan phenotypes in these mutants, consistent with literature suggesting a trade-off between longevity and fertility (Chen et al., 2013a, Rollins et al., 2017).
- Improvements are required to assays for autophagic markers and chronic starvation before reasonable conclusions may be drawn.

Chapter 4: The effects of *klo-1* and *klo-2* deletion on oxidative stress responses in *C. elegans*

4.1. Chapter four: hypotheses to be tested

As discussed previously (see Chapter 1 '1.3.6. Intracellular pathways associated with eFGF-*klotho*-FGFR function'), there are numerous reports suggesting Klotho exhibits protective effects against oxidative stress in murine models. Therefore, the aims of this Chapter are to investigate the impact that genetic deletion of *klo-1/ KL* and *klo-2/ KL* has on responses to oxidative agents in the nematode.

It would be expected that should *C. elegans* KLO-1/ KL and KLO-2/ KL function to have protective effects in response to oxidative stress, that deletion alleles for the related genes would lead to diminished resistance to oxidative stress in the nematode.

This will be explored by subjecting *C. elegans* strains to acute and chronic oxidative stress to analyse stress resistance and ROS profiles in selected strains.

4.2. Deletion of *klo-1/ KL* or *klo-2/ KL* leads to increased resistance to oxidative stress

4.2.1. *C. elegans* strains containing either *klo-1/ KL* or *klo-2/ KL* deletion mutations exhibit increased survival upon acute exposure to oxidative stress over 9 hours

Paraquat is a common herbicide known to induce mitochondrial oxidative stress, by inducing the production of superoxide and other potent ROS such as hydrogen peroxide or hydroxyl radicals (Lascano et al., 2012). Nematodes were exposed to 300 mM paraquat to determine whether there was an effect of *klo-1* and/ or *klo-2* deletion mutations on survival upon exposure to oxidative stress. Nematodes were monitored every hour for nine hours for their survival. Given the reported protective effects of Klotho in oxidative stress responses (Lim et al., 2017, Yamamoto et al., 2005), it would be expected that deletion of *klo-1/ KL* and *klo-2/ KL* should lead to diminished survival of *C. elegans* upon exposure to an oxidative agent.

At the 7-hour time point, all wild-type animals ($n = 103$) were deceased, with an average survival time of 2.81 ± 0.20 hours (figure 4.1; table 4.1). Some *klo-1* (2 of 99; 2%), *klo-2* (7 of 78; 9%), and *klo-2; klo-1* double mutant animals (7 of 99; 7%), were alive at the 9-hour time point, with average survival times of 4.19 ± 0.25 hours, 4.61 ± 0.32 hours and 4.06 ± 0.27 hours,

respectively. All *klo-1* and *klo-2* mutants showed significantly increased survival over wild-type animals ($P = 0.002$ for *klo-1*, $P < 0.001$ for *klo-2* and $P = 0.009$ for *klo-2; klo-1*). There was no significant difference in survival between *klo-1*, *klo-2* and *klo-2; klo-1* double mutants (see table 4.1).

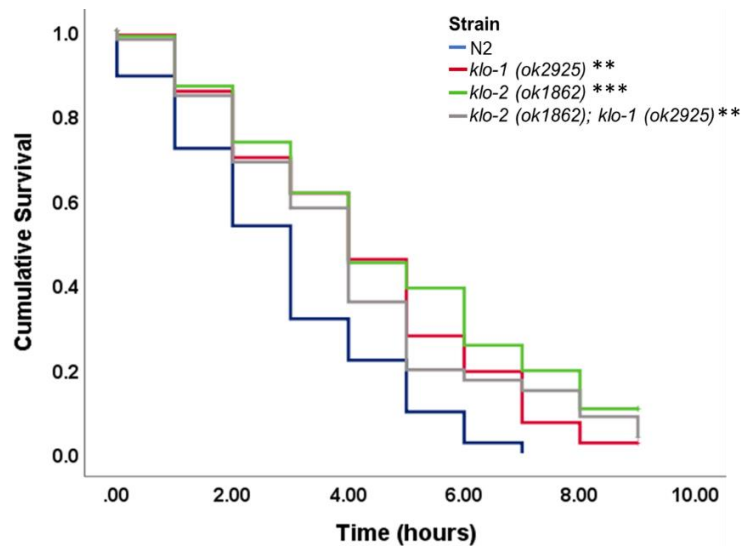


Figure 4.1. Survival of wild-type, *klo-1*, *klo-2* and *klo-2; klo-1* strains over 9 hours when exposed to 300 mM Paraquat. N2 (wild-type) (blue, n = 103), *klo-1* (red, n = 99), *klo-2* (green, n = 78), *klo-2; klo-1* (grey, n = 99). Asterisk indicates a statistical difference compared to wild-type, as determined by Tukey’s test (*P < 0.05, **P < 0.01, ***P < 0.001).

Table 4.1. Mean survival times of wild-type, *klo-1*, *klo-2* and *klo-2; klo-1* strains upon exposure to 300 mM paraquat. Statistical significance given as P values determined by Tukey’s test. Asterisk indicates significant difference (*P < 0.05, **P < 0.01, ***P < 0.001).

Strain	n	Censored (%)	Mean Survival ±SEM (hours)	P values			
				N2	<i>klo-1</i>	<i>klo-2</i>	<i>klo-2; klo-1</i>
N2 (wild-type)	103	18.4	2.81±0.20	-	0.002**	<0.001***	0.009**
<i>klo-1 (ok2925)</i>	99	18.2	4.19±0.25	0.002**	-	0.634	0.980
<i>klo-2 (ok1862)</i>	78	23.1	4.61±0.32	<0.001***	0.634	-	0.405
<i>klo-2 (ok1862); klo-1 (ok2925)</i>	99	20.2	4.06±0.27	0.009**	0.980	0.405	-

4.2.2. Increased survival of *klo-1* and *klo-2* deletion mutants upon exposure to oxidative stress is dependent on functional FGF/ FGFR signalling in *C. elegans*

To determine whether the survival advantage of *klo-1/ KL* and *klo-2/ KL* mutant strains is dependent on functional FGF-FGFR signalling, *C. elegans* with *klo-1 (ok2925)* and/ or *klo-2 (ok1862)* deletion alleles, in combination with either *egl-15 (n1477)* or *egl-17 (n1377)* were exposed to 300 mM paraquat to induce oxidative stress and counted hourly for dead nematodes for 9 hours.

It was found that *clr-1; egl-15* mutants ($n = 28$) have slightly decreased survival of 2.14 ± 1.46 hours compared to wild-type (2.81 ± 0.20 , $n = 103$), though this was not found to be significant (Figure 4.2; table 4.2). *klo-1* in combination with *egl-15* diminished the survival of animals to that of the *egl-15* parent strain, with *klo-1; egl-15* double mutants ($n = 28$) surviving on average 2.00 ± 0.36 hours compared to 4.19 ± 0.25 hours for *klo-1* single mutants ($n = 99$), however this diminished survival was not found to be significant ($P = 0.094$), presumably due to variation within the sample. *klo-2; klo-1; egl-15* triple mutants also displayed a trend for reduced survival upon oxidative stress exposure (2.29 ± 0.29 hours, $n = 30$) in comparison to *klo-2; klo-1* double mutants (4.06 ± 0.27 , $n = 99$) (Figure 4.2; table 4.2). Interestingly, *klo-2; egl-15* double mutants had elevated survival compared to the *egl-15* parent strain and wild-type animals, with a mean survival of 3.69 ± 0.29 hours ($n = 32$), which could indicate a pathway independent of FGF-FGFR signalling governing oxidative stress responses in *klo-2/ KL*-deficient animals.

Similarly, in combination with *egl-17*, the survival of *klo-1/ KL* and *klo-2/ KL* deletion mutants upon oxidative stress exposure was diminished to that of the *egl-17; hst-2* parent strain which had a mean survival of 2.48 ± 0.41 hours ($n = 26$) compared to 2.70 ± 0.41 hours for *klo-1; egl-17; hst-2* mutants ($n = 20$), 2.00 ± 0.29 hours for *klo-2; klo-1; egl-17* triple mutants ($n = 32$) and 2.75 ± 0.36 hours for *klo-2; klo-1; egl-17; hst-2* quadruple mutants ($n = 28$) (Figure 4.2; Table 4.2). Unfortunately, the cross did not generate *klo-2; egl-17* double mutants to determine whether the survival of *klo-2* mutants could have parallel roles to FGF-FGFR signalling in longevity.

Taken together, these results suggest that the enhanced survival of *klo-1/ KL* and *klo-2/ KL* deletion mutants upon exposure to acute oxidative stress is dependent on functional FGF-

FGFR signalling in *C. elegans*, fitting with previous literature in mammalian models that the function of klotho primarily is as a co-factor for FGF-FGFR signalling.

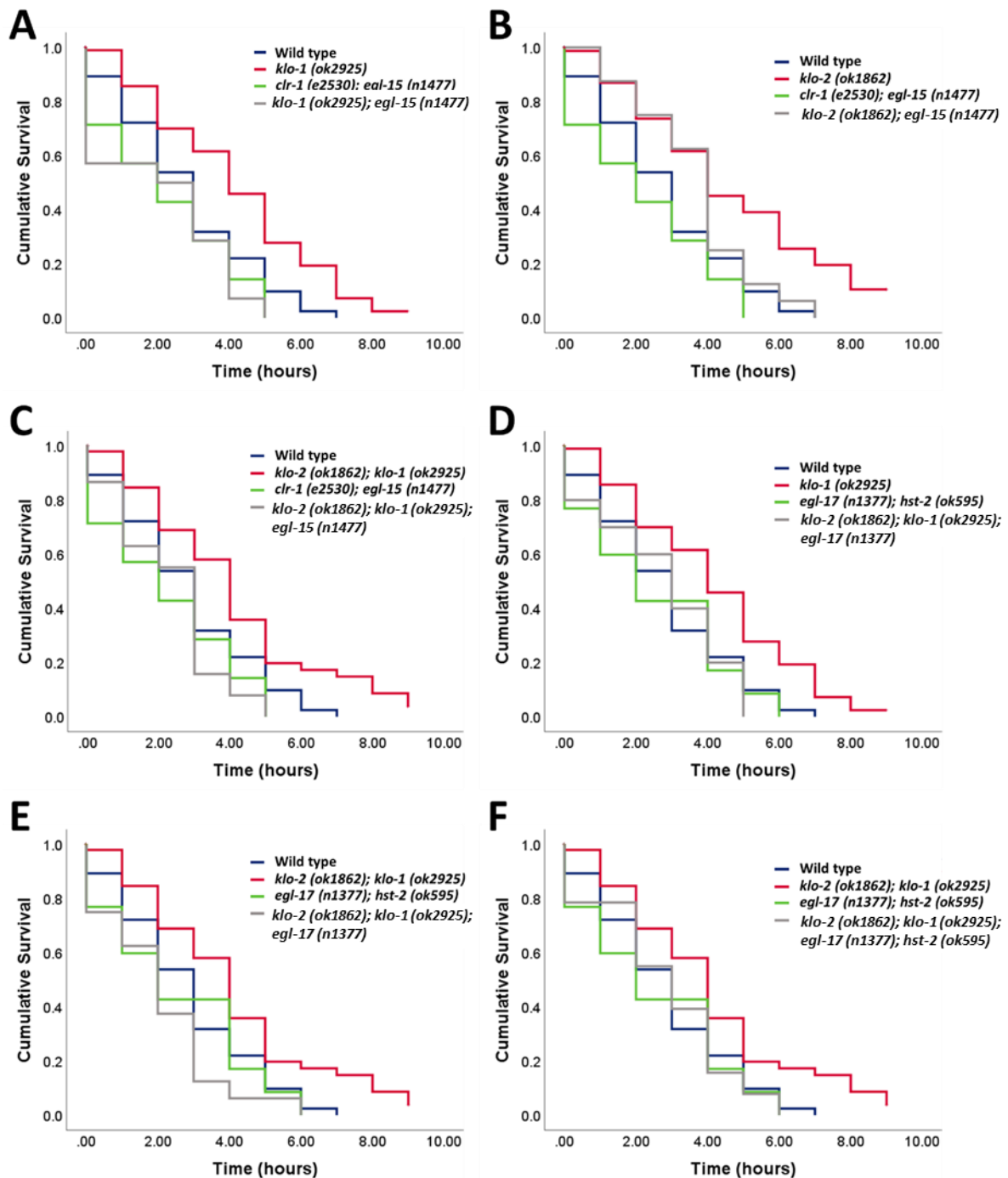


Figure 4.2. Survival of *egl-15*, *egl-17*, *klo-1* and *klo-2* compound mutants upon exposure to acute oxidative stress. A. N2 (wild-type) (blue, n = 103), *klo-1* (red, n = 99), *clr-1*; *egl-15* (green, n = 28) and *klo-1*; *egl-15* double mutants (grey, n = 28). B. Wild-type (blue), *klo-2* single

mutants (red, n = 78), *clr-1; egl-15* (green) and *klo-2; egl-15* double mutants (grey, n = 32). C. Wild-type (blue), *klo-2; klo-1* (red, n = 99), *clr-1; egl-15* (green) and *klo-2; klo-1; egl-15* triple mutants (grey, n = 30). D. Wild-type (blue), *klo-1* (red), *egl-17; hst-2* (green, n = 26) and *klo-1; egl-17; hst-2* mutants (grey, n = 20). E. Wild-type (blue), *klo-2; klo-1* (red), *egl-17; hst-2* (green) and *klo-2; klo-1; egl-17* triple mutants (grey, n = 32). F. Wild-type (blue), *klo-2; klo-1* (red), *egl-17; hst-2* (green) and *klo-2; klo-1; egl-17; hst-2* quadruple mutants (grey, n = 28). Asterisks indicate statistical significance compared to wild-type controls as determined using Tukey's test (* P < 0.05, ** P < 0.01, *** P < 0.001).

Table 4.2. Mean survival of *egl-15*, *egl-17*, *klo-1* and *klo-2* compound strains upon exposure to acute oxidative stress (300 mM paraquat over 9 hours). Statistical significance determined using Tukey's test. Asterisks indicate significant values (* P < 0.05, ** P < 0.01, *** P < 0.001).

Strain	n	Censored (%)	Mean Survival \pm SEM (hours)	P values			
				Wild-type	<i>klo-1</i>	<i>klo-2</i>	<i>klo-2</i> ; <i>klo-1</i>
N2 (wild-type) ^a	103	18.4	2.81 \pm 0.20	-	0.002**	<0.001***	0.009
<i>klo-1</i> (<i>ok2925</i>) ^a	99	18.2	4.19 \pm 0.25	0.002**	-	0.634	0.980
<i>klo-2</i> (<i>ok1862</i>) ^a	78	23.1	4.61 \pm 0.32	<0.001***	0.634	-	0.405
<i>klo-2</i> (<i>ok1862</i>); <i>klo-1</i> (<i>ok2925</i>) ^a	99	20.2	4.06 \pm 0.27	0.009	0.980	0.405	-
<i>clr-1</i> (<i>e2530</i>); <i>egl-15</i> (<i>n1477</i>)	28	0.0	2.14 \pm 1.46	1.000	0.195	0.018*	0.352
<i>klo-1</i> (<i>ok2925</i>); <i>egl-15</i> (<i>n1477</i>)	28	0.0	2.00 \pm 0.36	1.000	0.094	0.007**	0.194
<i>klo-2</i> (<i>ok1862</i>); <i>egl-15</i> (<i>n1477</i>)	32	0.0	3.69 \pm 0.29	0.078	1.000	1.000	1.000
<i>klo-2</i> (<i>ok1862</i>); <i>klo-1</i> (<i>ok2925</i>); <i>egl-15</i> (<i>n1477</i>)	30	13.3	2.29 \pm 0.29	1.000	0.050	0.003**	0.115
<i>hst-2</i> (<i>ok595</i>); <i>egl-17</i> (<i>n1377</i>)	26	7.7	2.48 \pm 0.41	1.000	0.331	0.043*	0.522
<i>hst-2</i> (<i>ok595</i>); <i>klo-1</i> (<i>ok2925</i>); <i>egl-17</i> (<i>n1377</i>)	20	0.0	2.70 \pm 0.41	1.000	0.957	0.556	0.990
<i>klo-2</i> (<i>ok1862</i>); <i>klo-1</i> (<i>ok2925</i>); <i>egl-17</i> (<i>n1377</i>)	32	0.0	2.00 \pm 0.29	1.000	0.060	0.003**	0.137
<i>klo-2</i> (<i>ok1862</i>); <i>klo-1</i> (<i>ok2925</i>); <i>egl-17</i> (<i>n1377</i>); <i>hst-2</i> (<i>ok595</i>)	28	7.1	2.75 \pm 0.36	1.000	0.662	0.148	0.840

^aData as shown in Table 4.1 (see '4.1.1. Survival over 9 hours upon exposure to oxidative stress').

4.2.3. KLO-1/ KL and KLO-2/ KL function in parallel with AGE-1/ PI3K in oxidative stress resistance

Previous expectations were that genetic deletion of *klo-1/ KL* and/ or *klo-2/ KL* in *C. elegans* would diminish survival of these strains upon exposure to oxidative agent. Unexpectedly, it was found that deletion of *klo-1/ KL* or *klo-2/ KL* resulted in increased survival of the strains to the oxidative agent paraquat upon acute exposure (see '4.1.1. *C. elegans* strains containing either *klo-1/ KL* or *klo-2/ KL* deletion mutations exhibit increased survival upon acute exposure to oxidative stress over 9 hours'). It is suggested that mammalian klotho inhibits the insulin/IGF-1-like signalling (IIS) pathway to promote oxidative stress resistance (Yamamoto et al., 2005). To determine whether the augmented survival of *C. elegans klo-1/ KL* and *klo-2/ KL* deletion mutants upon exposure to acute oxidative stress is dependent on its effects on PI3K (an important component in the IIS pathway), mutants for *klo-1/ KL* and/ or *klo-2/ KL* in combination with *age-1/ PI3K* mutation were exposed to 300 mM paraquat over 9 hours, as previously described.

age-1 (hx546) partial loss-of-function mutants have increased survival to oxidative stress (3.73 ± 0.45 hours, $n = 31$) compared to wild-type animals (2.81 ± 0.20 hours, $n = 103$), which fits with previous literature (Vanfleteren, 1993). The survival advantage of *age-1* mutants was unaffected in combination with either *klo-1* and/ or *klo-2* deletion alleles. *klo-2* ($n = 78$) and *klo-1* ($n = 99$) single mutants have the greatest survival advantage upon acute oxidative stress exposure, with mean survival times of 4.61 ± 0.32 hours and 4.19 ± 0.25 hours, respectively (Figure 4.3; Table 4.3), followed by *klo-2; klo-1* double mutants ($n = 99$, mean survival of 4.06 ± 0.27 hours). *age-1* single mutants had similar survival to *C. elegans* strains with mutations to *klo-1/ KL* or *klo-2/ KL*, surviving on average 3.73 ± 0.45 hours, compared to 3.69 ± 0.51 , 3.68 ± 0.41 and 3.60 ± 0.54 hours for *age-1; klo-1*, *age-1; klo-2*, and *age-1; klo-2; klo-1* triple mutants, respectively (Figure 4.3; Table 4.3).

Although strains containing *age-1* did display increased survival compared to their wild-type counterparts, these findings were not significant, presumably due to low sample size and variation within. There was no significant difference between the survival of mutants in combination with *age-1* to the *klo-1/ KL* and *klo-2/ KL* parental strains. Applying traditional rules of epistatic analyses (see Chapter 2 '2.9. Interpretation of survival assays: epistatic

analysis') this could be taken to suggest *age-1/PI3K* and *klo-1/-2/kl* function in the same pathway.

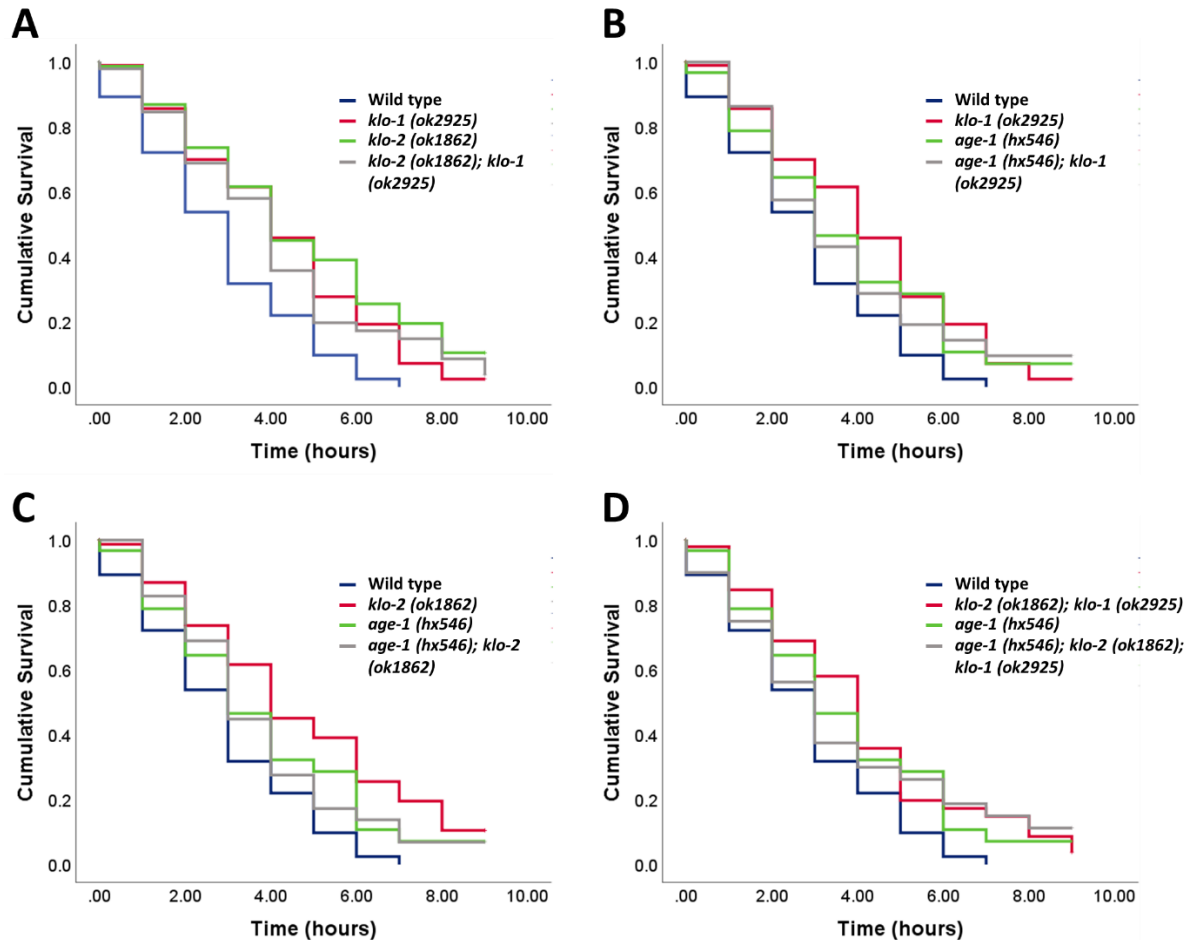


Figure 4.3. Survival of *age-1*, *klo-1* and *klo-2* compound mutants upon exposure to acute oxidative stress (300 mM paraquat) over 9 hours. A. N2 (wild-type) (blue, n = 103), *klo-1* (red, n = 99), *klo-2* (green) and *klo-2*; *klo-1* double mutants (grey, n = 99) as shown in figure 4.1 (see '4.1.1. Survival over 9 hours upon oxidative stress exposure'). B. Wild-type (blue), *klo-1*, *age-1* (green, n = 31) and *age-1*; *klo-1* double mutants (grey, n = 20). C. Wild-type (blue), *klo-2* (red), *age-1* (green) and *age-1*; *klo-2* double mutants (grey, n = 30). D. Wild-type (blue), *klo-2*; *klo-1* double mutants (red), *age-1* (green) and *age-1*; *klo-2*; *klo-1* triple mutants (grey, n = 30). Asterisks indicate significant values compared to wild-type as determined by Tukey's test (* P < 0.05, ** P < 0.01, *** P < 0.001).

Table 4.3. Survival of *age-1*, *klo-1* and *klo-2* strains upon exposure to acute oxidative stress (300 mM paraquat over 9 hours). Asterisks indicate significance compared to wild-type as determined using Tukey's test * P < 0.05, ** P < 0.01, *** P < 0.001).

Strain	n	Censored (%)	Mean Survival \pm SEM (hours)	P values			
				Wild-type	<i>klo-1</i>	<i>klo-2</i>	<i>klo-2</i> ; <i>klo-1</i>
N2 (wild-type) ^a	103	18.4	2.81 \pm 0.20	-	0.002**	<0.001***	0.009**
<i>klo-1</i> (<i>ok2925</i>) a	99	18.2	4.19 \pm 0.25	0.002**	-	0.634	0.980
<i>klo-2</i> (<i>ok1862</i>) a	78	23.1	4.61 \pm 0.32	<0.001***	0.634	-	0.405
<i>klo-2</i> (<i>ok1862</i>); <i>klo-1</i> (<i>ok2925</i>) a	99	20.2	4.06 \pm 0.27	0.009**	0.980	0.405	-
<i>age-1</i> (<i>hx546</i>)	31	16.1	3.73 \pm 0.45	0.384	1.000	0.952	1.000
<i>age-1</i> (<i>hx546</i>); <i>klo-1</i> (<i>ok2925</i>)	23	17.4	3.69 \pm 0.51	0.502	1.000	0.982	1.000
<i>age-1</i> (<i>hx546</i>); <i>klo-2</i> (<i>ok1862</i>)	30	10.0	3.69 \pm 0.41	0.188	1.000	0.996	1.000
<i>age-1</i> (<i>hx546</i>); <i>klo-2</i> (<i>ok1862</i>); <i>klo-1</i> (<i>ok2925</i>)	30	20.0	3.60 \pm 0.54	0.600	0.999	0.861	1.000

^aData as shown in Figure 4.1 (see '4.1.1. Survival over 9 hours upon exposure to oxidative stress').

4.2.4. *C. elegans* containing *klo-1/ KL* or *klo-2/ KL* deletion mutations display trend for increased resistance to oxidative agent following prolonged exposure.

The data from the 9-hour survival assay suggests there could be a survival advantage of *klo-1/ KL* and *klo-2/ KL* deletion mutants upon exposure to acute oxidative stress. To determine whether there was a survival advantage upon prolonged exposure to oxidative stress, nematodes were exposed to 100 mM paraquat solution over 20 hours as per Lee et al. (2008).

After 20 hours, $15.79 \pm 3.90\%$ of wild-type animals (39 of 247 animals) were still alive compared to $37.67 \pm 7.12\%$ (81 of 215) *klo-1* animals, $33.66 \pm 8.52\%$ (68 of 202) of *klo-2* animals and $24.29 \pm 3.93\%$ (43 of 177) of *klo-2; klo-1* double mutants (Figure 4.4; table 4.4). Although statistical analyses showed no significant difference between the strains at the 20-hour time point (Table 4.4), the data still indicates a trend for increased survival of *klo-1/ KL* and *klo-2/ KL* deletion mutants over wild-type animals when exposed to oxidative stress for prolonged periods of time. The lack of significance in these findings is thought to be due to the broad variation within the data.

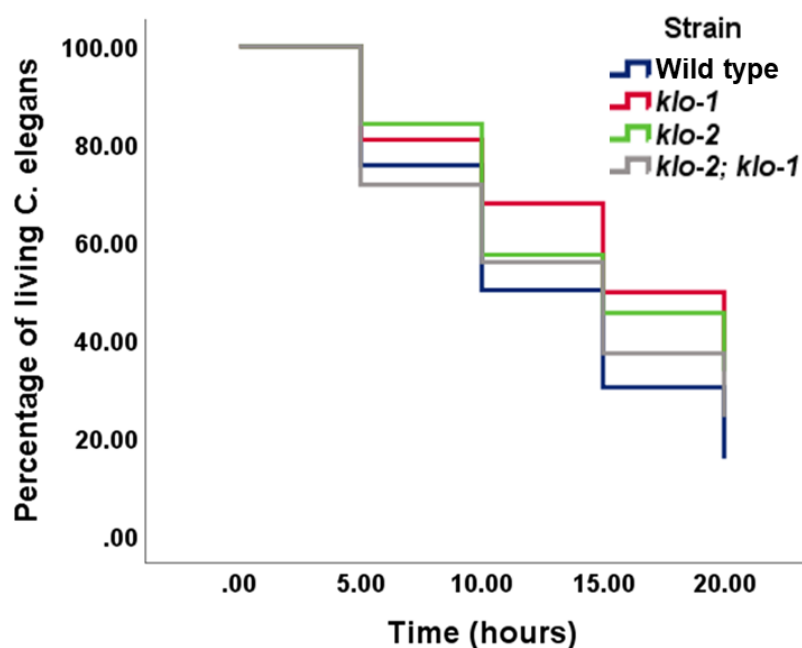


Figure 4.4. Survival of wild-type, *klo-1*, *klo-2* and *klo-2; klo-1* *C. elegans* strains over 20 hours when exposed to 100 mM paraquat. Wild-type (blue, n = 247), *klo-1* (red, n = 215), *klo-2* (green, n = 202) and *klo-2; klo-1* double mutants (grey, n = 177).

Table 4.4. Survival of wild-type, *klo-1*, *klo-2* and *klo-2; klo-1* double mutants at 15- and 20-hour time points when exposed to 100 mM paraquat. Asterisk indicates significant difference (*P < 0.05, **P < 0.01, *P < 0.001). P values determined using Tukey's test.**

Strain	<i>n</i>	Live animals (%±SEM)		P values							
				Wild-type		<i>klo-1</i>		<i>klo-2</i>		<i>klo-2; klo-1</i>	
				15 H	20 H	15 H	20 H	15 H	20 H	15 H	20 H
N2 (wild-type)	247	30.36 ±5.70	15.79 ±3.90	-	-	0.287	0.110	0.202	0.225	0.330	0.151
<i>klo-1</i> (<i>ok2925</i>)	215	49.77 ±8.92	37.67 ±7.12	0.287	0.110	-	-	0.901	0.785	0.563	0.448
<i>klo-2</i> (<i>ok1862</i>)	202	45.55 ±5.06	33.66 ±8.52	0.202	0.225	0.901	0.785	-	-	0.479	0.721
<i>klo-2</i> (<i>ok1862</i>); <i>klo-1</i> (<i>ok2925</i>)	177	37.29 ±2.88	24.29 ±3.93	0.330	0.151	0.563	0.448	0.479	0.721	-	-

4.2.5. Wild-type *C. elegans* display more intensive staining for ROS compared to *C. elegans* strains with *klo-1/ KL* or *klo-2/ KL* genetic backgrounds

4.1.5.1. Acute exposure to oxidative agent decreases staining for ROS in *C. elegans*

Oxidative stress is characterized by cellular damage caused by the overproduction of ROS, that overwhelms the organism's antioxidant responses (Hrycay and Bandiera, 2012, Pacher et al., 2007, Phaniendra et al., 2015, Younus, 2018). Therefore, it would be expected that mutants exhibiting increased resistance to ROS generators compared to their wild-type counterparts, may have reduced levels of ROS. To determine ROS levels, nematodes were exposed to acute oxidative stress (300 mM paraquat for one hour) and stained with CellROX deep red prior to microscopy. CellROX deep red is a stain that exhibits bright fluorescence with an absorption/ emission of ~664/665 nm upon oxidation by ROS (Yu and Liao, 2014).

In control conditions, wild-type animals showed increased staining for ROS compared to *klo-1* and *klo-2* deletion mutants, with a mean pixel intensity of 30.46 ± 0.65 , compared to 23.81 ± 0.72 , 23.80 ± 0.55 and 23.39 ± 0.71 for *klo-1* ($n = 27$, $P < 0.001$), *klo-2* ($n = 44$, $P < 0.001$) and *klo-2; klo-1* double mutant controls ($n = 41$, $P < 0.001$), respectively. There was no significant difference between ROS levels for *klo-1*, *klo-2* and *klo-2; klo-1* double mutants in control conditions.

Upon treatment with 300 mM paraquat for one hour, staining for ROS significantly decreased ($P < 0.001$) for all strains excluding *klo-1* ($n = 42$, $P = 0.445$) which had a mean pixel intensity of 23.13 ± 0.48 compared to 20.35 ± 0.56 for wild-type animals ($n = 46$), 20.56 ± 0.37 for *klo-2* ($n = 31$) mutants and 19.12 ± 0.37 for *klo-2; klo-1* ($n = 39$) double mutants.

This decrease in ROS levels upon paraquat exposure was somewhat unexpected given that it has been frequently cited in literature that paraquat induces ROS production in various organisms (Hosamani and Muralidhara, 2013, Jadavji et al., 2019, Lascano et al., 2012, Truong et al., 2015, Yang and Hekimi, 2010).

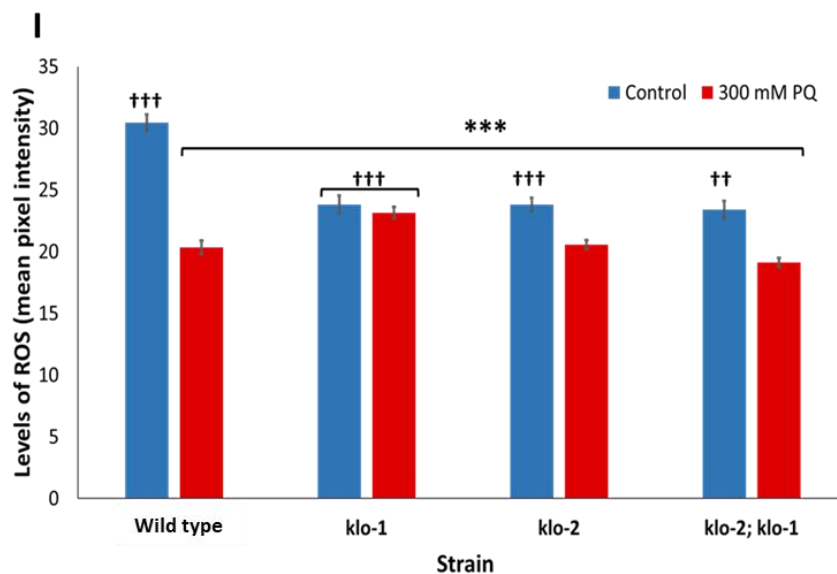
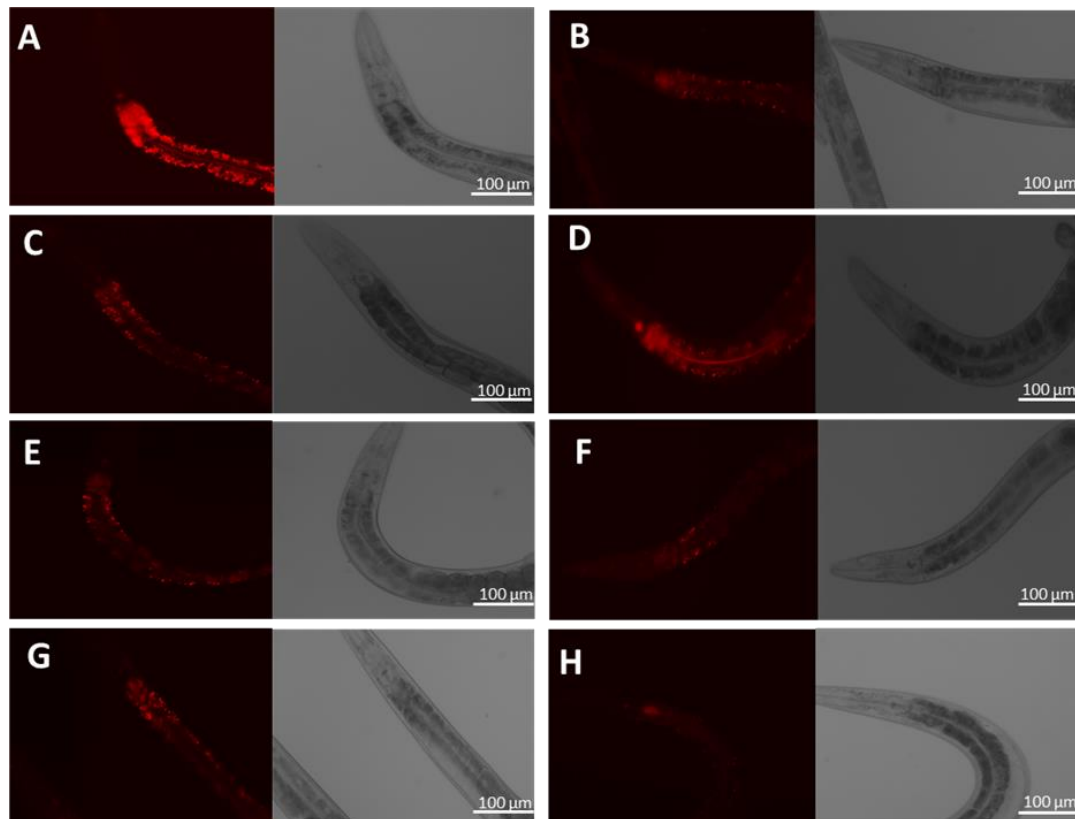


Figure 4.5. ROS levels in wild-type (N2), *klo-1*, *klo-2* and *klo-2; klo-1* strains. Images A-H: fluorescence staining of ROS (A-H) and brightfield (A'-H') images of *C. elegans*. A. Wild-type controls. B. Wild-type animals treated with 300 mM paraquat. C. *klo-1* controls. D. *klo-1* animals treated with 300 mM paraquat. E. *klo-2* controls. F. *klo-2* strain treated with 300 mM paraquat. G. *klo-2; klo-1* controls. H. *klo-2; klo-1* strain treated with 300 mM paraquat. I: ROS levels in wild-type, *klo-1*, *klo-2* and *klo-2; klo-1* strains. Untreated controls (blue) indicate that *klo-1*, *klo-2*, and *klo-2; klo-1* double mutants naturally have lower ROS levels compared to

wild-type. Asterisks indicate significance against wild-type controls (*P < 0.05, **P < 0.01, ***P < 0.001). Obelisk indicates significance against wild-type treated with 300 mM paraquat for 1 hour (+P < 0.05, ++P < 0.01, +++P < 0.001). Error bars represent SEM.

Table 4.5. CellROX staining to determine ROS levels (mean pixel intensity) of wild-type, *klo-1*, *klo-2* and *klo-2; klo-1* before and after treatment with 300 mM paraquat (PQ) for 1 hour. Mean pixel intensity was measured using ImageJ software. Asterisk indicates significant difference (*P < 0.05, **P < 0.01, ***P < 0.001). Statistical significance determined using Tukey's test.

Strain	Condition	n	Mean pixel intensity ±SEM	P values	
				N2 control	N2 + 300 mM PQ
N2 (wild-type)	Control	54	30.46±0.65	-	<0.001***
	+ 300 mM PQ	46	20.35±0.56	<0.001***	-
<i>klo-1</i> (<i>ok2925</i>)	Control	27	23.81±0.72	<0.001***	<0.001***
	+ 300 mM PQ	42	23.13±0.48	<0.001***	<0.001***
<i>klo-2</i> (<i>ok1862</i>)	Control	44	23.80±0.55	<0.001***	<0.001***
	+ 300 mM PQ	31	20.56±0.37	<0.001***	0.757
<i>klo-2</i> (<i>ok1862</i>); <i>klo-1</i> (<i>ok2925</i>)	Control	41	23.39±0.71	<0.001***	0.001**
	+ 300 mM PQ	39	19.12±0.37	<0.001***	0.074

To confirm that acute incubation with paraquat decreases ROS levels, nematodes were exposed to 200 mM and 100 mM concentrations of paraquat solution for one or two hours, respectively.

In control conditions, there was a consistent trend for increased ROS levels in wild-type animals compared to *klo-1*, *klo-2* and *klo-2; klo-1* strains and this was statistically significant in all scenarios (Figure 4.6; table 4.6).

Upon exposure to 200 mM paraquat, there was a decrease in ROS levels for wild-type animals from 36.78 ± 4.16 to 28.25 ± 0.86 (although this was found to not be significant ($P = 0.139$)). *klo-1*, *klo-2*, and *klo-2; klo-1* mutants showed no significant difference in ROS levels between control and treated conditions (Figure 4.6; table 4.6).

Upon exposure to 100 mM paraquat for 2 hours, treated wild-type animals showed no significant difference in ROS levels compared to controls, with mean pixel intensity values of 24.05 ± 0.78 and 21.12 ± 0.74 , respectively. ROS levels did increase upon treatment for *klo-1/ KL* and *klo-2/ KL* strains, from 18.38 ± 0.72 to 21.97 ± 0.77 for *klo-1* animals, 17.59 ± 0.52 to 18.01 ± 0.60 for *klo-2* animals and from 19.45 ± 1.03 to 21.99 ± 1.40 for *klo-2; klo-1* double mutant strains. These increases in ROS levels in 100 mM paraquat treated *klo-1/ KL* and *klo-2/ KL* strains were found to be significant ($P = 0.020$, $P = 0.026$ and $P = 0.048$, respectively). For *klo-2* single mutants, the increased ROS levels were still significantly lower than that of wild-type controls, and wild-type, *klo-1* and *klo-2; klo-1* treated animals (Figure 4.6; table 4.7).

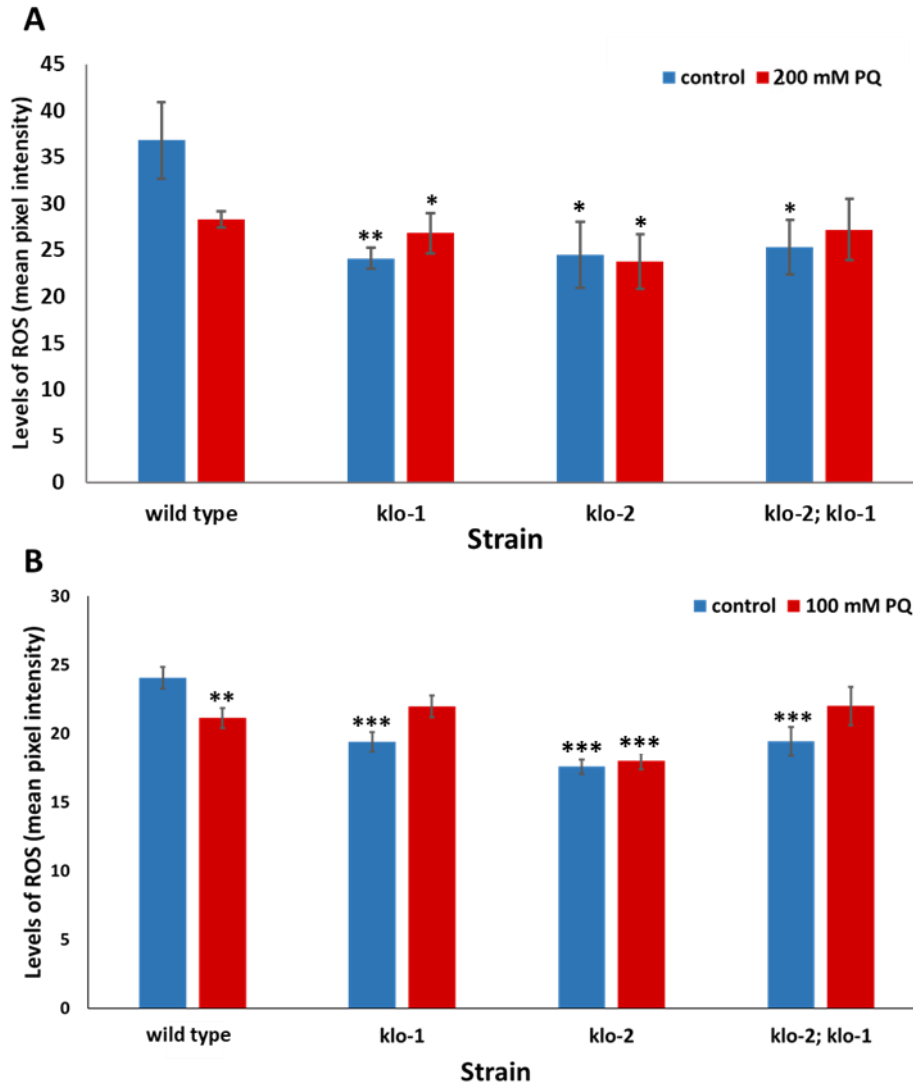


Figure 4.6. ROS levels in *klo-1* and *klo-2* deletion mutants. A. Exposure to 200 mM paraquat for 1 hour. Untreated controls indicated in blue; 200 mM treated animals indicated in red. *klo-2*, *klo-1* and *klo-2; klo-1* double mutant controls have significantly lower ROS levels than wild-type controls ($p < 0.05$). Upon treatment with 200 mM paraquat, wild-type ROS levels decrease from 36.78 ± 4.15 to 28.25 ± 0.86 (though this is not significant, $P = 0.139$). There is no difference between *klo-1*, *klo-2* and *klo-2; klo-1* controls and those treated with 200 mM PQ ($P > 0.05$). B. Exposure to 100 mM paraquat for 2 hours. Untreated controls indicated in blue, 100 mM paraquat treated animals indicated in red. All *klo-1* and *klo-2* deletion mutant controls have significantly decreased ROS levels compared to wild-type controls. ROS levels increase in all strains excluding wild-type when exposed to oxidising agent. Asterisks indicate statistical significance compared to wild-type controls (* $P < 0.05$, ** $P < 0.01$, *** $P < 0.001$). P values determined using Tukey's test.

Table 4.6. CellROX staining to determine ROS levels (mean pixel intensity) of wild-type, *klo-1*, *klo-2* and *klo-2; klo-1* before and after treatment with 200 mM paraquat (PQ) for 1 hour. Mean pixel intensity measured using ImageJ software. Asterisk indicates significant difference (*P < 0.05, **P < 0.01, ***P < 0.001). Statistical significance determined using Tukey's test.

Strain	Condition	n	ROS levels (Mean pixel intensity±SEM)	P values	
				Wild-type control	N2 + 100 mM PQ
N2 (wild-type)	Control	34	36.78±4.15	-	0.139
	+ 200 mM PQ	20	28.25±0.86	0.139	-
<i>klo-2 (ok1862)</i>	Control	22	24.52±3.55	0.029*	0.481
	+ 200 mM PQ	24	23.78±2.94	0.014*	0.363
<i>klo-1 (ok2925)</i>	Control	22	24.11±1.10	0.005**	0.314
	+ 200 mM PQ	21	26.815±2.19	0.040*	0.750
<i>klo-2 (ok1862); klo-1 (ok2925)</i>	Control	37	25.33±2.95	< 0.001***	0.551
	+ 200 mM PQ	25	27.20±3.31	0.077	0.838

Table 4.7. CellROX staining to determine ROS levels (mean pixel intensity) of wild-type, *klo-1*, *klo-2* and *klo-2; klo-1* before and after treatment with 100 mM paraquat (PQ) for 2 hours. Mean pixel intensity measured using ImageJ software. Asterisk indicates significant difference (*P < 0.05, **P < 0.01, ***P < 0.001). Statistical significance determined using Tukey's test.

Strain	Condition	n	ROS levels (Mean pixel intensity±SEM)	P values	
				N2 control	N2 + 100 mM PQ
N2 (wild-type)	Control	53	24.05±0.78	-	0.007**
	+ 100 mM PQ	60	21.12±0.74	0.007**	-
<i>klo-1</i> (<i>ok2925</i>)	Control	62	19.38±0.72	< 0.001***	0.096
	+ 100 mM PQ	64	21.97±0.77	0.063	0.434
<i>klo-2</i> (<i>ok1862</i>)	Control	60	17.59±0.52	< 0.001***	< 0.001***
	+ 100 mM PQ	60	18.01±0.60	< 0.001***	0.001**
<i>klo-2</i> (<i>ok1862</i>); <i>klo-1</i> (<i>ok2925</i>)	Control	59	19.45±1.03	< 0.001***	0.194
	+ 100 mM PQ	57	21.99±1.40	0.207	0.586

4.2.5.2. Prolonged exposure to oxidative agent increases staining for ROS in wild-type *C. elegans*

Paraquat has been extensively shown in literature to induce oxidative stress in a variety of organisms (Hosamani and Muralidhara, 2013, Jadavji et al., 2019, Truong et al., 2015) however, the above data indicates acute exposure of wild-type animals to paraquat decreases ROS levels. It was thought that this could be due to the length of time that animals were incubated in paraquat prior to staining for ROS. To test this, wild-type nematodes were exposed to varying concentrations of paraquat (0 mM, 20 mM, 40 mM, 60 mM, 80 mM or 100 mM) for an extended period of time (20 hours). Previous findings indicate that a low proportion of wild type worms are living at the 20 hour time point (see '4.1.4. *C. elegans* containing klo-1/ KL or klo-2/ KL deletion mutations display trend for increased resistance to oxidative agent following prolonged exposure') therefore when during microscopy, only living nematodes were imaged identified by active pumping of the pharynx.

There was no significant difference ($P > 0.05$) between control animals (0 mM paraquat) and those incubated in 20 mM, 40 mM and 60 mM concentrations of paraquat at the 20 hour time point (Figure 4.7; Table 4.8). At higher paraquat concentrations, mean pixel intensity significantly increased from 17.05 ± 1.51 in controls, to 25.38 ± 2.51 for animals incubated in 80 mM paraquat ($P = 0.011$), and to 27.00 ± 1.29 for animals treated with 100 mM paraquat ($P < 0.001$) (Table 4.8). At the 9-hour time point, up to 86% of wild-type animals were deceased (see '3.1.2. Survival over 20 hours upon exposure to oxidative stress') which is why the majority of oxidative stress exposure experiments were carried out for shorter periods of time.

These findings indicate that after prolonged exposure to oxidative stress at paraquat concentrations of 80 mM or above, ROS levels are increased in wild-type animals, supporting literature indicating paraquat induces ROS production.

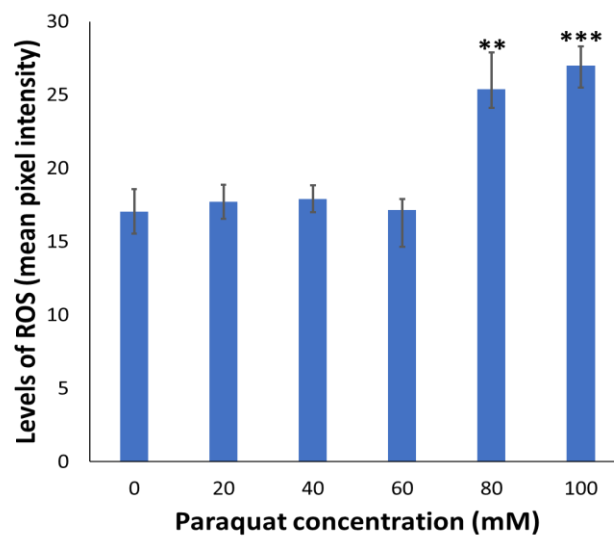
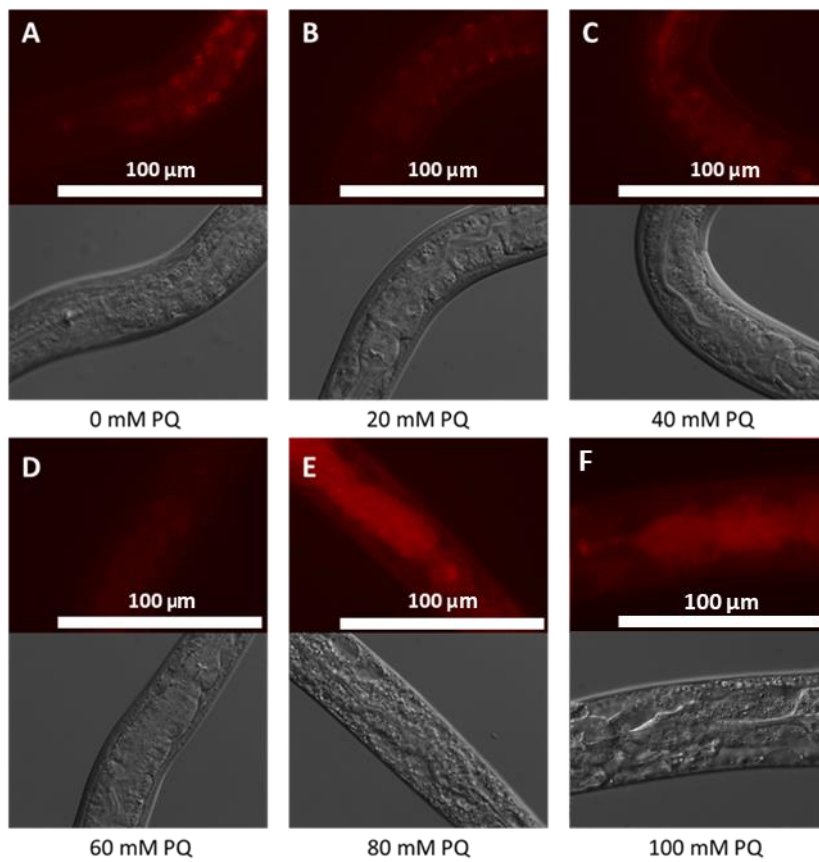


Figure 4.7. ROS levels of wild-type animals exposed to varying concentrations of paraquat (PQ) for 20 hours. Images A-F: Fluorescence staining of ROS (top) and brightfield images of wild-type animals exposed A) 0 mM, B) 20 mM, C) 40 mM, D) 60 mM, E) 80 mM and F) 100

mM PQ. G. Mean pixel intensity of CellROX staining in wild-type *C. elegans* exposed to varying concentrations of paraquat. Asterisks indicate significance compared to controls (0 mM PQ) (*P < 0.05, **P < 0.01, ***P < 0.001). P values determined using Tukey's test.

Table 4.8. ROS levels (mean pixel intensity) of wild-type animals exposed to 0 mM, 20 mM, 40 mM, 60 mM, 80 mM and 100 mM paraquat (PQ) for 20 hours. Mean pixel intensity measured using ImageJ software. Statistical significance determined using Tukey's test, asterisks indicate statistical difference compared to wild-type controls (0 mM PQ) (*P < 0.05, **P < 0.01, ***P < 0.001).

Condition	ROS levels (mean pixel intensity ± SEM)		P value against N2 control
	<i>n</i>		
0 mM PQ (control)	13	17.05±1.51	-
20 mM PQ	14	17.73±1.16	0.735
40 mM PQ	16	17.91±0.91	0.613
60 mM PQ	19	17.14±2.52	0.961
80 mM PQ	16	25.38±2.51	0.011**
100 mM PQ	13	26.03±0.95	< 0.001***

4.2.5.3. *C. elegans* strains with *klo-1/ KL* or *klo-2/ KL* genetic backgrounds exhibit trend for lowered staining of ROS upon prolonged exposure to oxidative agent

To determine whether ROS levels were altered in *klo-1/ KL* and *klo-2/ KL* deletion mutants upon prolonged paraquat exposure, wild-type, *klo-1*, *klo-2* and *klo-2; klo-1* nematodes were incubated in 100 mM paraquat solution as above for 20 hours before staining with CellROX Deep Red.

As with previous data, in control conditions, wild-type animals had significantly higher ROS levels than *klo-1* ($P = 0.002$), *klo-2* ($P = 0.020$) and *klo-2; klo-1* ($P = 0.006$) animals. There was no significant difference in ROS levels between strains containing either *klo-1* or *klo-2* mutants in control conditions.

Upon exposure to 100 mM paraquat for 20 hours, ROS levels significantly increased in all strains (Figure 4.8; Table 4.9). Treated wild-type animals had significantly increased ROS compared to treated *klo-2* mutants (68.37 ± 2.70 , $P = 0.035$). Although there was no significant difference between treated wild-type animals (78.91 ± 3.99 mean pixel intensity) and treated *klo-1* (67.71 ± 4.59 , $P = 0.237$), and *klo-2; klo-1* double mutants (72.39 ± 2.86 , $P = 0.195$), there was a trend for these strains to have lower ROS than their wild-type counterparts. There was no difference between ROS levels in *klo-2* treated animals compared to *klo-1* and *klo-2; klo-1* treated animals.

Overall, while it is expected that paraquat treatment should increase ROS staining in *C. elegans* following exposure, this is variable to previous research findings that *klo-1/ KL* and *klo-2/ KL* deletion *C. elegans* strains have increased survival upon oxidative stress exposure compared to wild type worms. Therefore, this suggests that the protective phenotype demonstrated by *klo-1/ KL* and *klo-2/ KL* deletion for oxidative stress responses may only be operative upon acute exposure to oxidative agents, and that prolonged exposure may override these initially protective effects. This is explored further in this chapter (see '4.1.6. *klo-1/ KL* and *klo-2/ KL* genetic background does not confer increased resistance upon chronic exposure to oxidative agent').

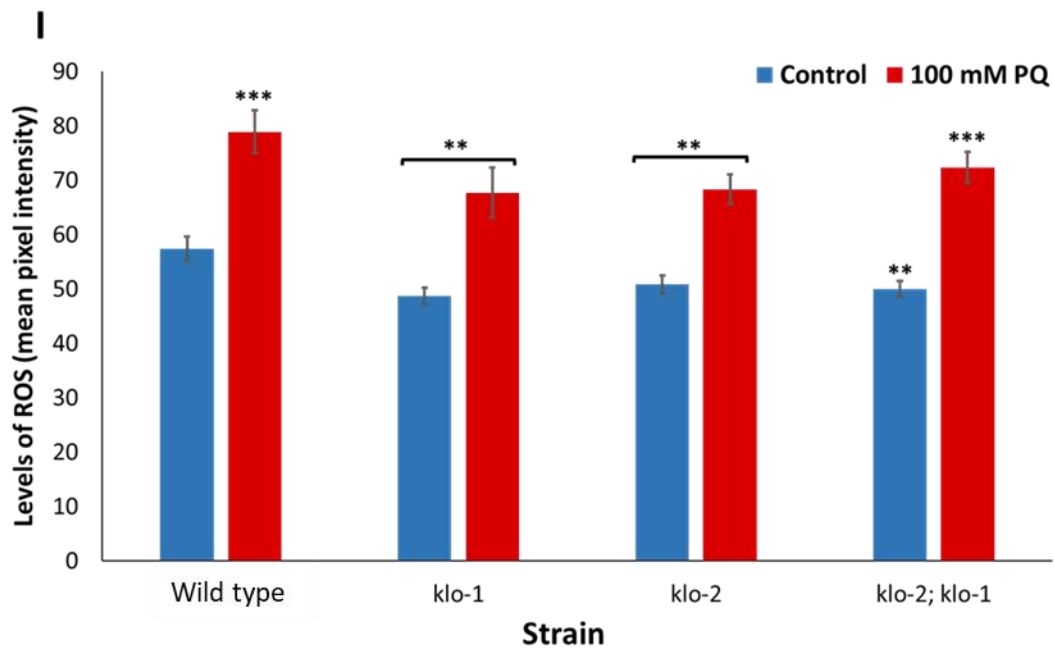
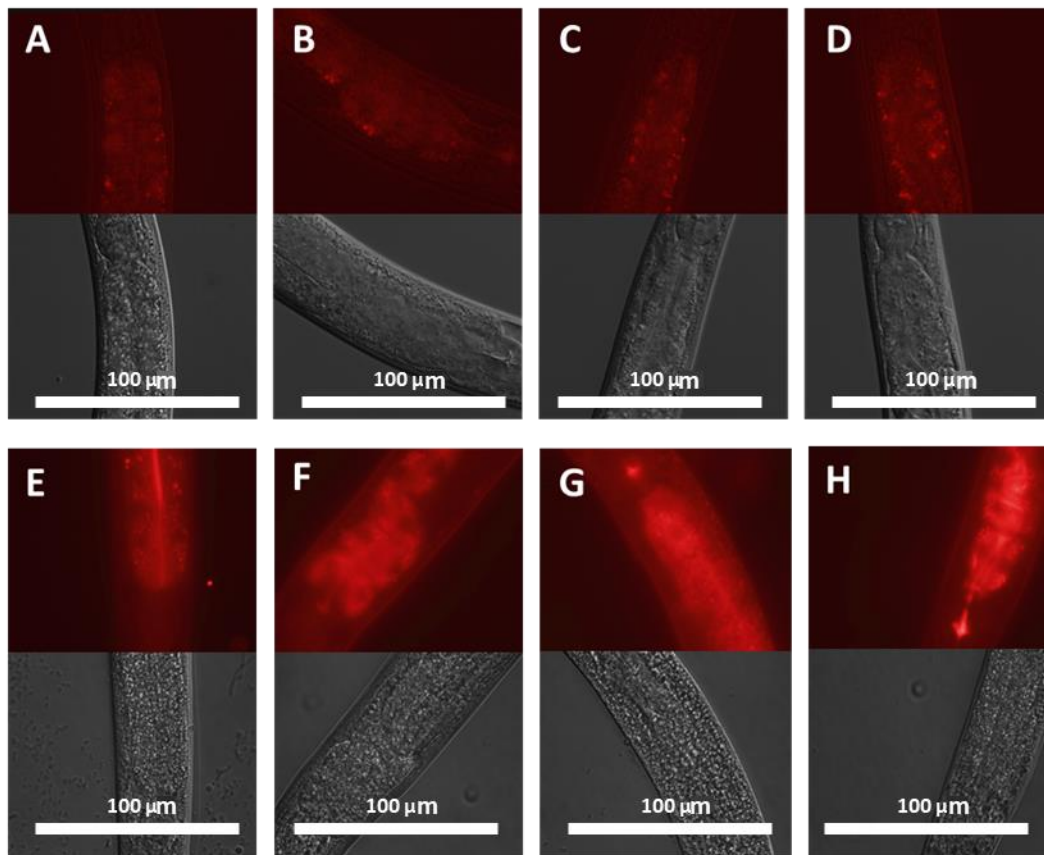


Figure 4.8. ROS levels (mean pixel intensity) in wild-type, *klo-1*, *klo-2* and *klo-2; klo-1* strains before and after treatment with 100 mM paraquat (PQ) for 20 hours. A-D: fluorescence staining of ROS (top) and brightfield images of (L-R); N2 control (untreated), *klo-1* control, *klo-2* control and *klo-2; klo-1* control. E-H: fluorescence staining of ROS (top) and brightfield (bottom) images of (L-R); N2 + 100 mM PQ, *klo-1* + 100 mM PQ, *klo-2* + 100 mM PQ and *klo-*

2; *klo-1* + 100 mM PQ. I. Mean pixel intensity of CellROX staining. Untreated controls indicated in blue; 100 mM PQ treatment indicated in red. In normal conditions wild-type animals have lower ROS levels than *klo-1*, *klo-2* and *klo-2; klo-1* animals. Following incubation in 100 mM paraquat for 20 hours, ROS levels are increased in wild-type animals, *klo-1*, *klo-2* and *klo-2; klo-1* double mutants. Asterisks indicate statistical significance compared to wild-type controls (*P < 0.05, **P < 0.01, ***P < 0.001). P values determined using Tukey's test.

Table 4.9. ROS levels (mean pixel intensity) of wild-type, *klo-1*, *klo-2* and *klo-2; klo-1* strains before and after exposure to 100 mM paraquat (PQ) for 20 hours. Statistical significance determined using Tukey's test. Asterisks indicate statistical significance (*P < 0.05, **P < 0.01, ***P < 0.001).

Strain	Condition	n	ROS levels (mean pixel intensity ± SEM)	P values	
				N2 control	N2 + 100 mM PQ
N2 (wild-type)	Control	39	57.44±2.16	-	< 0.001***
	+ 100 mM PQ	34	78.91±3.99	< 0.001***	-
<i>klo-1</i> (<i>ok2925</i>)	Control	52	48.69±1.55	0.002**	< 0.001***
	+ 100 mM PQ	34	67.71±4.59	0.009**	0.237
<i>klo-2</i> (<i>ok1862</i>)	Control	39	50.92±1.62	0.020**	< 0.001***
	+ 100 mM PQ	41	68.37±2.70	0.003**	0.035*
<i>klo-2</i> (<i>ok1862</i>); <i>klo-1</i> (<i>ok2925</i>)	Control	45	50.02±1.44	0.006**	< 0.001***
	+ 100 mM PQ	45	72.39±2.86	< 0.001***	0.195

4.2.5.4. *klo-1/ KL* and *klo-2/ KL* mutants display resistance to oxidative agent sodium arsenite
Sodium arsenite (NaAsO_2) is another compound frequently used to induce oxidative stress (Wang et al., 2012). To confirm findings that *klo-1/ KL* and *klo-2/ KL* deletion mutant animals could show signs of less ROS accumulation upon oxidative stress compared to their wild-type counterparts, nematodes were exposed to 100 μM sodium arsenite for 24 hours, as per Yu and Liao (2014) then stained with CellROX to determine ROS levels.

Upon treatment with 100 μM NaAsO_2 , CellROX staining for ROS significantly increased from a mean pixel intensity of 67.77 ± 2.11 to 91.54 ± 4.61 ($P < 0.001$) in wild-type animals (Figure 4.9; table 4.10). In treated conditions, and consistent with the paraquat induced oxidative stress, wild-type animals also had significantly greater ROS levels than *klo-1* (68.97 ± 2.49 , $n = 68$, $P < 0.001$), *klo-2* (61.31 ± 1.83 , $n = 68$, $P < 0.001$), and *klo-2; klo-1* animals (72.03 ± 2.93 , $n = 68$, $P < 0.001$).

There was no significant difference in ROS levels between NaAsO_2 treated animals compared to controls in *klo-1* ($P = 0.096$), *klo-1* ($P = 0.251$) and *klo-2; klo-1* mutants ($P = 0.299$) (Figure 4.9; table 4.10). In treated conditions, there was no difference in ROS between *klo-1* and *klo-2; klo-1* double mutants (0.430), however *klo-2* single mutants did have significantly lower ROS levels compared to its *klo-1/ KL* and *klo-2/ KL* counterparts ($P = 0.013$ and $P = 0.002$ compared to *klo-1* and *klo-2; klo-1* double mutants, respectively).

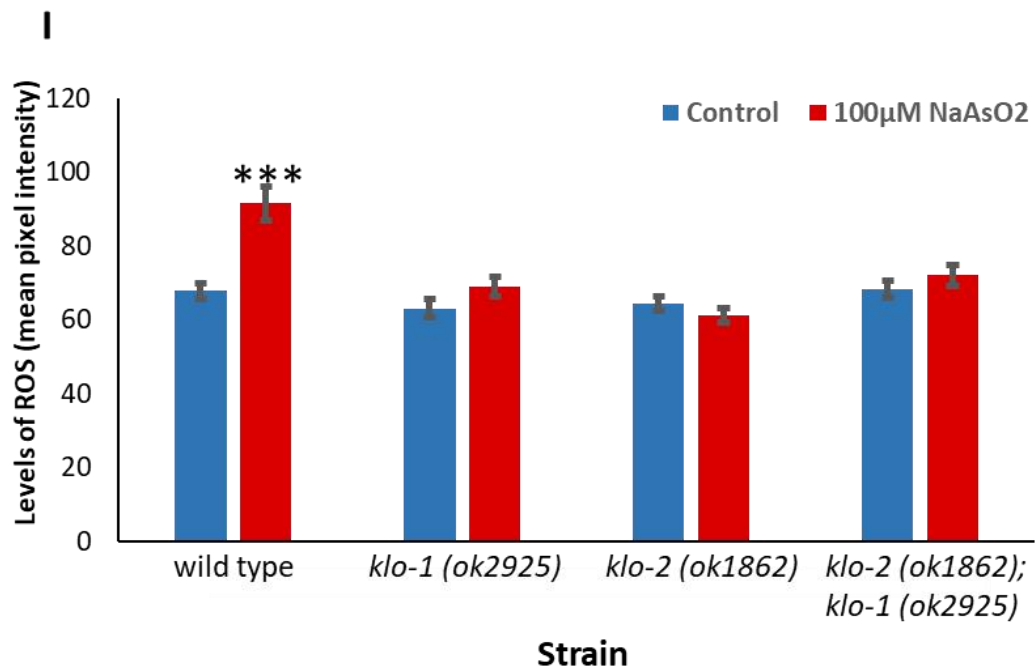
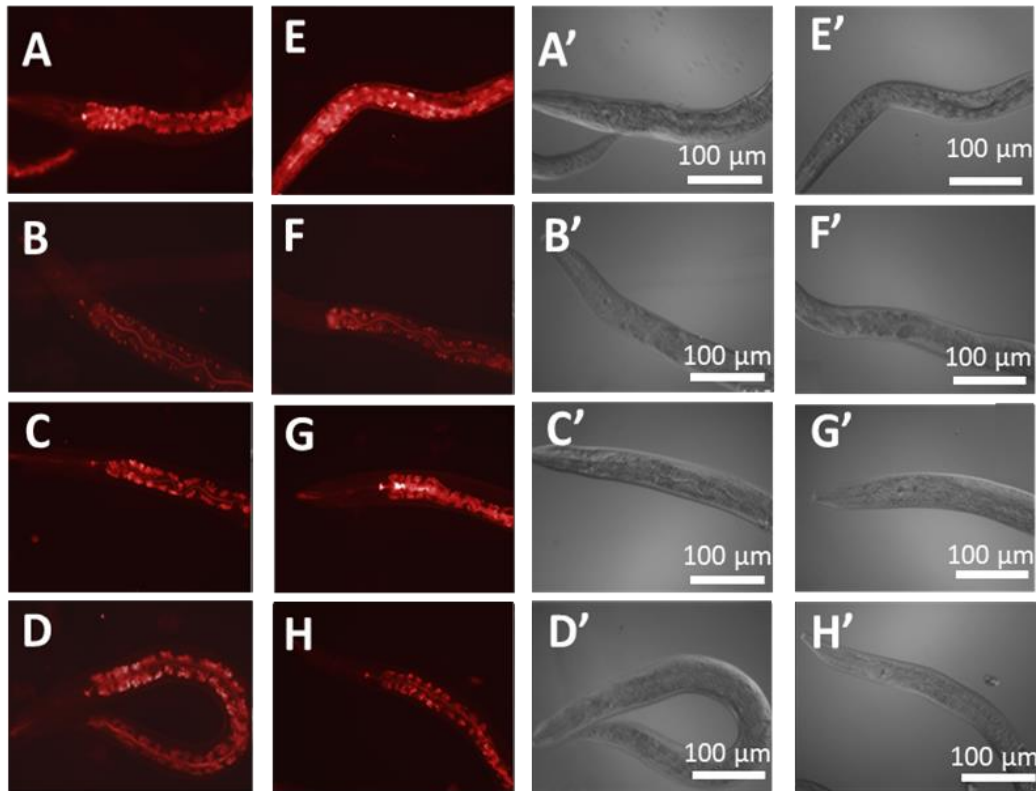


Figure 4.9. ROS levels in wild-type, *klo-1*, *klo-2* and *klo-2; klo-1* strains before and after treatment with 100 μM sodium arsenite (NaAsO₂). Images A-H: Fluorescence staining of ROS (left) and brightfield (right) images; A-D; wild-type, *klo-1*, *klo-2* and *klo-2; klo-1* untreated animals, respectively. E-H; wild-type, *klo-1*, *klo-2* and *klo-2; klo-1* animals treated with 100 μM NaAsO₂, respectively. I. ROS levels (Mean pixel intensity). Untreated controls indicated in

blue; animals treated with NaAsO₂ indicated in red. Upon exposure to NaAsO₂, mean pixel intensity in wild-type animals increased. ROS levels in wild-type animals treated with NaAsO₂ was significantly greater than treated *klo-1* (n = 68), *klo-2* (n = 68), and *klo-2; klo-1* (n = 68). Error bars represent SEM. Asterisks indicate significant difference been wild-type controls (*P < 0.05, **P < 0.01, ***P < 0.001). P values determined using Tukey's test.

Table 4.10. ROS levels (mean pixel intensity) of N2 (wild-type), *klo-1*, *klo-2*, and *klo-2; klo-1* strains before and after treatment with 100 μM sodium arsenite (NaAsO₂). Statistical significance determined using Tukey's test. Asterisks indicate statistical significance (*P < 0.05, **P < 0.01, *P < 0.001).**

Strain	Condition	n	ROS levels (mean pixel intensity ± SEM)	P values				
				N2	N2 + NaAsO ₂	<i>klo-1</i>	<i>klo-2</i>	<i>klo-2; klo-1</i>
N2 (wild-type)	Control	73	67.77±2.11	-	<0.001***	0.152	0.251	0.915
	+ NaAsO ₂	74	91.54±4.61	<0.001* **	-	<0.001***	<0.001***	<0.001***
<i>klo-1</i> (<i>ok2925</i>)	Control	67	63.06±2.46	0.152	<0.001***	-	0.695	0.141
	+ NaAsO ₂	68	68.96±2.49	0.716	<0.001***	0.096	0.158	0.801
<i>klo-2</i> (<i>ok1862</i>)	Control	77	64.34±2.01	0.251	<0.001***	0.695	-	0.230
	+ NaAsO ₂	68	61.31±1.83	0.020	<0.001***	0.533	0.251	0.020*
<i>klo-2</i> (<i>ok1862</i>); <i>klo-1</i> (<i>ok2925</i>)	Control	72	68.10±2.31	0.915	<0.001***	0.141	0.230	-
	+ NaAsO ₂	68	72.03±2.93	0.244	<0.001***	0.022*	0.035*	0.299

4.2.6. *klo-1/ KL* and *klo-2/ KL* genetic background does not confer increased resistance upon chronic exposure to oxidative agent

The data gathered suggests that upon exposure to paraquat, deletion of *klo-1* or *klo-2* may, at least in acute stress responses, have a survival advantage over their wild-type counterparts. To determine whether *klo-1* and/ or *klo-2* loss-of-function affect the survival of nematodes exposed to chronic oxidative stress, nematodes were exposed to low concentrations of paraquat (0-6 mM concentrations), and animals were counted daily until death. Paraquat is known to increase the incidence of internal hatching of progeny in *C. elegans*, thus harming the mothers leading to poor health and ultimately death (Senchuk et al., 2017). To prevent this, plates were supplemented with FUDR, which has been shown to alter lifespan in *C. elegans* (Kato et al., 2017, Van Raamsdonk and Hekimi, 2011). Controls were therefore exposed to the same concentration of FUDR.

In each condition, it was found there was no significant difference between strains for survival. When exposed to 0 mM PQ, the average survival was 15.68 ± 1.09 day, 15.76 ± 1.12 , 16.04 ± 1.19 days and 14.52 ± 1.09 days for N2 (wild-type) ($n = 30$), *klo-1* ($n = 30$), *klo-2* ($n = 30$), and *klo-2; klo-1* animals ($n = 30$), respectively.

Upon exposure to 2 mM PQ, survival increased to 19.07 ± 1.34 days, 18.93 ± 1.49 , 20.22 ± 1.31 , and 17.72 ± 1.49 days for wild-type ($n = 30$), *klo-1* ($n = 30$), *klo-2*, and *klo-2; klo-1* animals ($n = 30$), respectively. Although there seems to be an extension of lifespan for nematodes exposed to mild oxidative stress, these results were only found to be significant for the wild-type strain ($P = 0.015$. See table 4.11). Initially, it was thought these findings were unusual given previous studies suggesting exposure to the same concentration of paraquat diminished lifespan in *C. elegans* (Keaney et al., 2004), however further reading presented a study which found chronic paraquat exposure to increase longevity of *C. elegans* populations (Bora et al., 2021).

Exposure to 4 mM PQ diminished the lifespan of *C. elegans* strains to a mean survival of 11.81 ± 1.12 days, 11.87 ± 1.23 days, 13.59 ± 1.21 days and 12.93 ± 1.07 days for wild-type, *klo-1; klo-2*, and *klo-2; klo-1* strains though again, this was not found to be significant against the 0 mM paraquat condition.

There was also a trend for diminished survival in all strains upon exposure to 6 mM paraquat, although compared to untreated (0 mM paraquat) controls this was only significant for wild-type ($P = 0.035$) and *klo-2* ($P = 0.017$) strains.

Given that previous longevity data suggests no significant impacts of *klo-1/ KL* or *klo-2/ KL* deletion in *C. elegans* it is not surprising there is no differences found between strains despite the increased survival of *klotho* strains upon acute oxidant exposure. This suggests that longevity in the nematode is not intrinsically linked to oxidative stress responses.

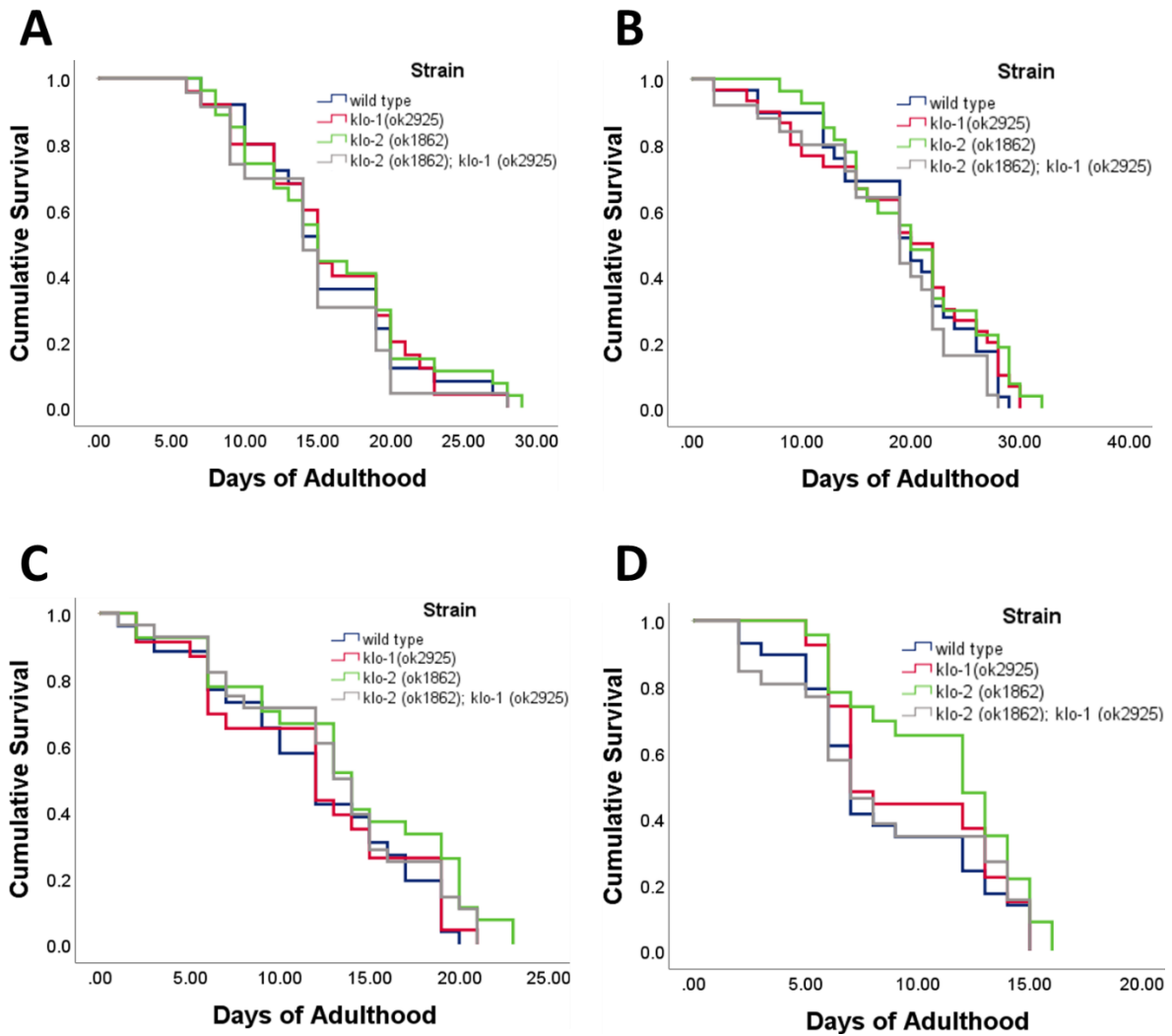


Figure 4.10. Survival of N2 (wild-type), *klo-1*, *klo-2* and *klo-2; klo-1* strains upon chronic paraquat exposure. A. Survival of *C. elegans* strains exposed to 0 mM paraquat (PQ). Average survival of wild-type animals (blue, n = 30), *klo-1* (n = 30), *klo-2* (n = 30) and *klo-2; klo-1* mutants (n = 30). B. Survival of animals exposed to 2 mM PQ. Wild-type (blue, n = 30), *klo-1* (n = 31), *klo-2* (n = 30) and *klo-2; klo-1* (n = 30). C. Survival of animals exposed to 4 mM PQ. Wild-type animals (blue, n = 30), *klo-1* (n = 30), *klo-2* (n = 30) and *klo-2; klo-1* mutants (n = 30). D. Survival of animals exposed to 6 mM PQ. Wild-type animals (blue, n = 30), *klo-1* (n = 30), *klo-2* (n = 30) and *klo-2; klo-1* mutants (n = 30).

Table 4.11. Survival of wild-type, *klo-1*, *klo-2* and *klo-2; klo-1* strains exposed to chronic oxidative stress (0 mM, 2 mM, 4 mM or 6 mM paraquat). Statistical significance determined using Tukey's test. Asterisks indicate statistical significance (*P < 0.05, **P < 0.01, *P < 0.001).**

Strain	Condition	n	Mean survival (days) ±SEM	P values			
				0 mM N2	0 mM <i>klo-1</i>	0 mM <i>klo-2</i>	0 mM <i>klo-2; klo-1</i>
Wild-type (N2)	0 mM PQ	30	15.68 ±1.09	-	1.000	0.903	0.768
	2 mM PQ	30	19.07±1.34	0.015*	-	-	-
	4 mM PQ	30	11.81±1.12	0.377	-	-	-
	6 mM PQ	30	8.52±0.76	0.035*	-	-	-
<i>klo-1 (ok2925)</i>	0 mM PQ	30	15.76±1.12	1.000	-	0.915	0.749
	2 mM PQ	31	18.93±1.49	-	0.032*	-	-
	4 mM PQ	30	11.87±1.23	-	0.146	-	-
	6 mM PQ	30	9.67±0.73	-	0.091	-	-
<i>klo-2 (ok1862)</i>	0 mM PQ	30	16.04±1.19	0.903	0.915	-	0.354
	2 mM PQ	30	20.22±1.31	-	-	0.0214	-
	4 mM PQ	30	13.59±1.21	-	-	0.667	-
	6 mM PQ	30	11.26±0.78	-	-	0.017*	-
<i>klo-2 (ok1862); klo-1 (ok2925)</i>	0 mM PQ	30	14.52±1.09	0.768	0.749	0.354	-
	2 mM PQ	30	17.72±1.49	-	-	-	0.233
	4 mM PQ	30	12.93±1.07	-	-	-	0.961
	6 mM PQ	30	8.46±0.92	-	-	-	0.198

4.3. Discussion: *C. elegans* strains with *klotho* mutant backgrounds exhibit resistance to acute but not chronic stress

4.3.1. *klo-1/ KL* and *klo-2/ KL* mutants have lower overall ROS than wild-type *C. elegans*

Several reports highlight the importance of *klotho* function in oxidative stress responses (Kuro-o, 2008, Yamamoto et al., 2005). Upon investigation into the effects of *klo-1/ KL* and *klo-2/ KL* deletion in oxidative stress responses, it was noted that in control conditions (those that had not been treated with oxidants), wild-type animals show more intensive levels of staining for ROS than those with *klo-1* or *klo-2* genetic backgrounds (see '4.1.5. Staining for Reactive Oxygen Species'). This was surprising given that increased *klotho* activity is demonstrated to decrease oxidative stress in vertebrate models (Yamamoto et al., 2005), and impaired *klotho* signalling is linked to the onset of various conditions characterised by increased oxidative stress (Hu et al., 2011, Lu and Hu, 2017, Zhang and Liu, 2018).

It could be that *KLO-1/ KL* or *KLO-2/ KL* deficiency promotes the activation of oxidative stress response pathways as a compensatory mechanism that results in a greater protective effect in these animals. What is interesting, is that despite demonstrable lower oxidative stress levels in *C. elegans* with *klo-1* or *klo-2* genetic backgrounds, these strains do not have increased longevity, which may suggest an alternate function of *C. elegans* genes compared to mammalian models. As discussed previously (see sub-section "1.2.8. Criticisms of the oxidative damage theory of ageing"), many studies and reviews de-bunk the oxidative damage theory of ageing (Gems and Doonan, 2009, Gladyshev, 2014, Liochev, 2015, Salmon et al., 2010). In line with these criticisms, the data presented in this thesis aligns with the notion that there is not a direct correlation between oxidative stress responses and longevity in *C. elegans*.

Here, something other than oxidative stress may limit lifespan in *C. elegans*. thus explaining why augmented longevity is not evident in *klo-1/ KL* or *klo-2/ KL* mutants despite their resistance to oxidative stress.

4.3.2. Deletion of *klo-1/ KL* and *klo-2/ KL* promotes acute oxidative stress resistance in *C. elegans*

When exposed to acute oxidative stress, *C. elegans* with *klo-1 (ok2925)* or *klo-2 (ok1862)* genetic backgrounds have demonstrated increased survival compared to wild-type

counterparts (see '4.1.1. Survival over 9 hours upon exposure to oxidative stress'). Given the predicted effects of *klo-1* and *klo-2* deletion on KLO-1 and KLO-2 proteins (Polanska et al., 2011), and existing literature documenting the role of *klothos* in oxidative stress responses (Kuro-o, 2019, Yamamoto et al., 2005), these results were unexpected.

Detection of ROS in *C. elegans* strains exposed to acute oxidative stress confirmed this, and actually demonstrated lowered ROS levels following exposure to high concentrations of paraquat in some cases, even in wild-type animals (see '4.1.5. Staining for Reactive Oxygen Species'). Given that paraquat is reported to increase ROS and cause oxidative stress (Lascano et al., 2012), these findings were unexpected.

One explanation for these lowered ROS levels in wild-type *C. elegans* following acute oxidative stress exposure, is that upon paraquat treatment, oxidative stress responses in the nematode are upregulated, so that upon microscopy, these upregulated stress response pathways have "mopped up" many ROS, hence explaining the lowered ROS detection in these animals. For acute oxidative stress exposure, nematodes were incubated in paraquat for between 1-2 hours, then incubated with CellROX stain for 30 minutes, so upregulation of stress response pathways could have resolved the initial increase of ROS levels at the point of microscopy. Several time course analyses of superoxide dismutase activity in response to oxidative stress demonstrate increased activity following the point of exposure (Martins et al., 2020, Moradi et al., 2016, Sindhu et al., 2018). In many cases this upregulation is significant within 15 minutes of initial exposure and can last for several hours offering a plausible theory for the phenomenon demonstrated here (Martins et al., 2020, Moradi et al., 2016, Sindhu et al., 2018).

While staining for oxidative stress in *klo-1* and *klo-2* genetic backgrounds is also lowered in some cases upon acute oxidative stress exposure, this is not to the same degree as that of wild-type animals, further adding to the hypothesis that *klo-1/KL* and *klo-2/KL* deletion could lead to the upregulation of oxidative stress response pathways that could explain these phenomena. This is the case for *rsks-1/S6K* mutants, which have diminished TOR signalling and also display increased resistance to oxidative stress (Seo et al., 2013), likely due to an upregulation in AAK-2/ AMPK pathway known to function antagonistically to TOR signalling (Kim et al., 2011a). Taken together with findings that *rsks-1/S6K* mutants have strikingly similar effects on longevity as *klo-1/KL* or *klo-2/KL* mutants (see '3.6.1.1. Lifespan in *C.*

elegans of *klo-1/ KL* and *klo-2/ KL* genetic backgrounds'), this could indicate diminished TOR signalling or upregulated AAK-2/ AMPK pathways in *C. elegans* with *klo-1/ KL* or *klo-2/ KL* deletion backgrounds.

4.3.3. There is no survival advantage of *klo-1/ KL* or *klo-2/ KL* deletion mutants upon chronic oxidative stress exposure

Due to acute paraquat treatment causing reduced ROS detection in treated *C. elegans*, wild-type animals were exposed to varying concentrations of paraquat to over a prolonged period of time to determine whether paraquat does increase ROS levels, which could translate as increased oxidative stress levels in the nematode.

It was found that lower concentrations of paraquat (20 – 60 mM) did not significantly impact ROS levels after 20 hours, whereas incubation in either 80 mM or 100 mM paraquat significantly increased ROS levels in wild-type animals.

Following the confirmation that paraquat treatment does increase ROS levels, *C. elegans* strains with *klo-1* and *klo-2* genetic backgrounds were also exposed to 100 mM paraquat for a prolonged period of time (20 hours). Here it was found that *C. elegans* strains with *klo-1* or *klo-2* genetic backgrounds do not have increased survival, or oxidative stress levels, compared to wild-type strains upon prolonged paraquat exposure.

Interestingly, while strains with *klo-1* and *klo-2* genetic backgrounds showed an increase for oxidative stress levels upon prolonged paraquat exposure, this was not the case for sodium arsenite (NaAsO₂) exposure. While treatment with 100 μM NaAsO₂ increases ROS levels in wild-type animals, ROS levels in nematodes of *klo-1* or *klo-2* genetic backgrounds remain unaffected by this treatment. So far, the mechanisms governing this phenomenon remain unclear. Many detoxification genes that are upregulated in response to NaAsO₂ are dependent on SKN-1/ Nrf2 pathways in *C. elegans* (Oliveira et al., 2009), so investigation into the relationship between *klo* and SKN-1/ Nrf2 could be a useful avenue to research to elucidate the mechanisms of stress responses governed by KLO-1/ KL and KLO-2/ KL in *C. elegans*.

Chronic paraquat exposure analysis further cemented the idea that the increased survival demonstrated in *klo-1* and/ or *klo-2* strains exposed to acute oxidative stress is only a fleeting occurrence in the course of *C. elegans* life. There was no difference in the survival of *C. elegans* strains containing deletion alleles of *klo-1/ KL* or *klo-2/ KL* compared to their wild-type counterparts regardless of paraquat concentration. Interestingly enough, it was *C. elegans* strains that were exposed to mild oxidative stress (2 mM paraquat) that survived the longest on FUDR-supplemented plates. Not only was this interesting due to the reported effects FUDR typically has on lifespan of *C. elegans* strains with certain genetic backgrounds (as discussed above), but this further plays into the theory of mitohormesis. Mitohormesis is a concept whereby mild exposure to oxidative stress actually has a protective effect and in some cases leads to extended longevity (Bárcena et al., 2018, Ristow, 2014). Coupled with research to suggest that in some cases increased antioxidant activity could have detrimental effects to lifespan (Pérez et al., 2009), this could offer explanations as to why the initial protective effects of *klo-1/ KL* and *klo-2/ KL* deletion in oxidative stress responses are beneficial upon acute oxidant exposure in young adults, this does not necessarily confer to improved healthspan or longevity over time.

4.3.4. Chapter four conclusions

Following investigation into oxidative stress responses and reactive oxygen species in *klo-1/ kl* and *klo-2/ kl* the following conclusions were reached;

- Surprisingly, presumed null mutations for *klo-1/ kl* and *klo-2/ kl* result in increased survival of nematodes upon acute exposure to oxidative agents, contrary to initial hypothesis.
- Additionally, staining for ROS suggests that *klo-1/ kl* and *klo-2/ kl* mutants have lowered ROS levels in comparison to wild-type animals.
- As the oxidative stress resistance phenotype is demonstrated in *klo-1/ kl* and *klo-2/ kl* mutants in acute scenarios only, the current working theory is that deletion of *klotho* could trigger an upregulation in protective pathways that confers short-term oxidative resistance, but that prolonged exposure may override these initially protective

responses resulting in survival that is no greater than that of wild-type strains in chronic oxidative exposure scenarios.

Chapter 5: The effects of *aak-2*/AMPK knockdown in *klo-1* and *klo-2* mutants

5.1. Introduction: overview of AAK-2/ AMPK

5.1.1. Introduction to AMPK

5' Adenosine monophosphate-activated protein kinase (AMPK) is a key regulator of cellular energy homeostasis, activated in low energy states when there is a high AMP/ ADP to ATP ratio. The energy status of the cell may be determined by a variety of factors including nutrient status, oxygen availability or xenobiotic treatments that inhibit the mitochondrial respiratory chain, as detailed in several reviews (Garcia and Shaw, 2017, Hardie, 2011, Hardie et al., 2012, Viollet, 2017, Wu et al., 2018). Upon activation, AMPK promotes upregulation of catabolic processes such as glucose uptake (Abbud et al., 2000, Barnes et al., 2002, O'Neill et al., 2011), fatty acid uptake (Merrill et al., 1997, Wu et al., 2017), and autophagy (Egan et al., 2011, Kim et al., 2011b, Liang et al., 2007), and downregulates anabolic processes including the synthesis of glycogen (Jørgensen et al., 2004), protein (Bolster et al., 2002), cholesterol (Clarke and Hardie, 1990), and fatty acids (Muoio et al., 1999).

5.1.2. AMPK: structure and activation

AMPK is a heterotrimeric enzyme consisting of a catalytic α -subunit, and two regulatory subunits, β - and γ (Steinberg and Kemp, 2009). AMPK can be activated allosterically through the binding of AMP to the γ -subunit, which induces a conformational change in the complex (Cheung et al., 2000), allowing for the phosphorylation of Thr-172 in the AMPK α -subunit (Hawley et al., 1996).

As well as AMP, upstream kinases such as liver kinase B1 (LKB1) and Ca^{2+} / calmodulin-dependent protein kinase β (CaMKK β) are able to activate AMPK through the phosphorylation of Thr-172 in the activation loop of the α -subunit (Hawley et al., 2003, Xie et al., 2009). It has also been shown that ROS may activate AMPK, either directly through the oxidation of glutathione on two conserved cysteine residues in the AMPK- α subunit (Zmijewski et al., 2010), or indirectly secondary to inhibition of ATP synthesis, consequently increasing AMP and ADP levels (Hawley et al., 2010, Hinchy et al., 2018).

5.1.3. Downstream targets of AMPK

Downstream targets activated by AMPK include Forkhead box transcription factors (FoxO) and Nuclear factor erythroid 2-related factor 2 (Nrf2) (Greer et al., 2007, Wang et al., 2017a, Wang et al., 2011, Zhao et al., 2017a). Upon activation, these transcription factors translocate to the nucleus where they promote the transcription of several stress response genes including superoxide dismutase (SOD), catalase (CAT), growth arrest and DNA damage-inducible 45 (GADD45) genes, glutathione-S-transferase (GST) and NADPH quinone oxidoreductase (NQO1) (Fornace et al., 1988, Greer and Brunet, 2005, Kops et al., 2002, Lewis et al., 2015, Tran et al., 2002). Under glucose starvation, AMPK also directly phosphorylates serine/ threonine-protein kinase 1 (ULK1) promoting autophagy (Kim et al., 2011b). The role of AMPK in autophagy is antagonistic to that the mammalian target of rapamycin (mTOR) pathway (Kim et al., 2011b).

AMPK also indirectly inhibits inflammatory responses induced by nuclear factor kappa-light chain enhancer of B cells (NF- κ B), mediated by AMPK downstream targets Sirtuin 1 (SIRT1) and FoxO factors, which may have a significant impact on healthspan and longevity (Salminen and Kaarniranta, 2012).

The role of AMPK in stress responses is further highlighted through the crosstalk with insulin/ IGF-1-like signalling (IIS). Reduced IIS improves stress responses in various organisms (Cui et al., 2006, Honda and Honda, 1999, Partridge et al., 2011), and has been shown to improve longevity in invertebrate model organisms (Kenyon et al., 1993, Tatar et al., 2001), with varying results in mammalian models, with some reports that knockout of an adipose insulin receptor increases lifespan of mice (Blüher et al., 2003), but other reports that mice with increased sensitivity to insulin displaying shortened lifespan (Nelson et al., 2012). Activation of AMPK has been shown to suppress this IIS pathway, through inhibition of insulin receptor substrate 1 (IRS-1) as well as activating FoxO transcription factors known to be suppressed by IIS activity (Greer et al., 2007, Jakobsen et al., 2001, Wang et al., 2011).

5.1.4. AMPK in health and disease

Given the broad roles of AMPK in metabolism, alterations to AMPK activity has vast implications in health and disease. AMPK has been implicated in diseases including cancer

(Faubert et al., 2014, Li et al., 2015, Luo et al., 2010), cardiovascular disease (CVD) (Li et al., 2019, Luo et al., 2010, Shirwany and Zou, 2010), chronic kidney disease (CKD) (Allouch and Munusamy, 2018, Pastor-Soler N. M. et al., 2018), diabetes (Coughlan et al., 2014, Madhavi et al., 2019, Misra and Chakrabarti, 2007), obesity (Kola et al., 2008, Pollard et al., 2019, Yavari et al., 2016), and other inflammatory disorders (Miki et al., 2020, Salt and Palmer, 2012). While the role of AMPK may be somewhat straightforward in some cases, for example in diabetes activation of AMPK using metformin increases insulin sensitivity thus alleviating symptoms of the disease (Rena et al., 2017, Zhou et al., 2001), its role is much more complicated in diseases such as cancer, having protective tumour suppressor effects prior to disease, but with reports of tumour promoting roles following the onset of disease (Vara-Ciruelos et al., 2019).

Overexpression or activation of AMPK in *C. elegans* and *Drosophila melanogaster* has been shown to have lifespan extending effects (Apfeld et al., 2004, Curtis et al., 2006, Funakoshi et al., 2011, Onken and Driscoll, 2010), and knockout of AMPK α 2 in murine models resulted in poor metabolic health and shortened lifespan, emphasising the role of AMPK in ageing (Salminen and Kaarniranta, 2012, Viollet et al., 2003). The role of AMPK in longevity has been attributed to its effects on FoxO and Nrf2 transcription factors (Greer et al., 2009, Onken and Driscoll, 2010), as well as its ability to regulate autophagy (Levine and Kroemer, 2008, Nakamura and Yoshimori, 2018).

5.1.5. AMPK and klotho

Recent studies in mammalian and cell culture models predict a role for AMPK in klotho signalling. It has been reported that the FGF21, which requires β -klotho as a co-factor to bind its respective FGFR, is able to activate AMPK in an LKB1-dependent manner (Chau et al., 2010). In addition to this, FGF21 expression is promoted by pharmacological AMPK activators metformin and 5-aminoimidazole-2-carboxamide ribonucleotide (AICAR) in hepatocytes, offering a link between the AMPK pathway and klotho signalling (Nygaard et al., 2012). FGF21 has been reported to have therapeutic effects in diabetic mice (Kharitonov et al., 2005) and has been reported to increase the expression and activity of glucose transporter 1 (GLUT1) in adipocytes (Ge et al., 2011). AMPK is also reported to increase the activity of GLUT1 in these cells (Abbud et al., 2000), suggesting an overlap in role for FGF21 and AMPK

in glucose metabolism. However, it was found that FGF21 treatment was able to lower glucose and lipid levels in AMPK β 1 β 2 knockout mice, demonstrating there are downstream functions of FGF21 that are not strictly AMPK-dependent (Mottillo et al., 2017).

FGF23 requires α -klotho to bind its cognate FGFR and is involved in the modulation of vitamin D metabolism. Elevated levels of FGF23 in patients with chronic kidney disease (CKD) were found to correlate to biomarkers of oxidative stress including high-sensitivity C-reactive protein (hsCRP), endogenous soluble receptor of advanced glycation end products (esRAGE) and advanced oxidation protein products (AOPP) (Nasrallah et al., 2013). Recent evidence found AMPK to be a regulator of FGF23 (Glosse et al., 2018). AMPK was found to inhibit the expression of FGF23 in UMR106 osteoclast-like cells, and AMPK α -deficient mice were found to have elevated levels of FGF23 in serum (Glosse et al., 2018, Guo et al., 2016).

FGF19 has been found to increase antioxidant response markers including Nrf2 in an AMPK-dependent manner (Guo et al., 2020). FGF19 has also been shown to have protective effects against oxidative stress-induced cardiomyopathy, again via activation of an AMPK-dependent pathway, highlighting the importance of AMPK in mediating FGF19-governed stress responses (Li et al., 2018).

Klotho deficient mice show phenotypes including arterial stiffness and hypertension that can be rescued through an increase in AMPK activity (Gao et al., 2016). AMPK-activation through AICAR treatment augmented the expression of klotho in human lung epithelial cell lines (Cheng et al., 2017), and treatment with thyroid hormone 3,3,5-triiodothyronine (T₃) increases the expression of β -klotho and FGF21 in murine models in an AMPK-dependent manner highlighting a role for AMPK in klotho signalling (Videla et al., 2018).

[5.1.5.1. Cross-talk of AMPK and IIS pathways could offer explanation for how Klotho functions](#)
Several papers link klotho to the IIS pathway, though the mechanisms underlying this remain unclear (Dalton et al., 2017, Lin and Sun, 2012, Rubinek and Modan-Moses, 2016, Yamamoto et al., 2005). It has been proposed that the protective effects of *klotho* could function by inhibiting the phosphorylation of FoxO3a via PI3K/ AKT in mice (Lim et al., 2017) suggesting klotho could have direct effects on this pathway, however a study by Lorenzi et al. (2010) provides evidence opposing a direct role for klotho in IIS. Recent data in *C. elegans* indicates

that *klotho* could function in a pathway parallel to IIS, as deletion of *klo-1* or *klo-2* in combination with the *C. elegans* orthologue for the mammalian insulin receptor, *daf-2*, augments the already prolonged lifespan of *daf-2* single mutants (Buj & Kinnunen, manuscript in preparation). Given the cross talk between AMPK and IIS pathways (see '5.1.3. Downstream targets of AMPK'), and their links to *klotho*, it could be that *klotho* could function via AMPK to exhibit its effects on IIS.

5.1.6. AAK-2 – the *C. elegans* orthologue for mammalian AMPK α

AMPK is an enzyme that is highly conserved throughout eukaryotic organisms from yeast to humans (Hardie and Carling, 1997). In humans, the AMPK α -subunit is encoded for by two genes; PRKAA1 and PRKAA2 (Steinberg and Kemp, 2009). The *C. elegans* genome contains two orthologues for the catalytic subunit of AMPK α , *aak-1* and *aak-2*, which share 52% and 40% homology to human AMPK α 1, respectively (Apfeld et al., 2004). While loss-of-function of either *aak-1* or *aak-2* results in reduced survival in response to stressors, *aak-1* deletion has no impact on the lifespan of *C. elegans*, whereas *aak-2* deletion diminishes the lifespan of nematodes compared to their wild-type counterparts and is required for the longevity effects of reduced IIS mutants (Apfeld et al., 2004).

The role of AAK-2/ AMPK in stress responses is emphasised in dauer larvae. Dauer is a term which roughly translates to “duration” and refers to an alternate development stage of the *C. elegans* designed to halt development and allow the larvae to endure unfavourable conditions for long periods of time (Cassada, 1975). Typically, upon return of favourable conditions, development resumes, and this has been found to be dependent on functional AAK-2/ AMPK (Narbonne and Roy, 2006, Narbonne and Roy, 2009). Functional AAK-2/ AMPK is also required for appropriate and germline proliferation, and oxidative and heat stress responses in *C. elegans* (Fukuyama et al., 2012, Lee et al., 2008).

It has been speculated that *klotho* could function to inhibit IIS, though it remains unclear whether this is direct, or whether the inhibition of IIS is a secondary effect (Yamamoto et al., 2005). Recent data indicates that *klotho* could function in a pathway parallel to IIS in longevity in a DAF-16/ FOXO dependent manner (Buj & Kinnunen, manuscript in preparation).

Given the cross-talk between AMPK and IIS pathways, and their roles in regulating stress responses, paired with evidence gathered from other model organisms and cell lines, whether the stress resistance phenotypes displayed in *klo-1* and *klo-2* mutants (see chapter 3 'Results: the effects of *klo-1* and *klo-2* in stress responses') is dependent on functional AAK-2/ AMPK was determined.

5.1.6. Chapter five: hypotheses to be tested

As discussed above (see '5.1.5. AMPK and *klotho*'), previous links between *klotho* and AMPK function have been identified. *C. elegans* mutants for *klo-1/kl* and *klo-2/kl* in combination with null mutations for *aak-2/AMPK* were subject to health and stress analyses to explore the relationship between AAK-2 and KLO-1/-2 further.

One key research objective to be explored throughout this chapter would be whether knockdown of *aak-2* would impact some of the stress resistance phenotypes demonstrated in previous results (see chapters three and four). If AAK-2/ AMPK was required for these stress resistance phenotypes, it would be expected that stress responses would be diminished to that of wild-type strains in *klotho* strains with *aak-2* null mutant backgrounds.

To explore the genetic pathways further, and to identify whether *aak-2* may function upstream of *klotho*, transgenic strains for *klotho* reporters were exposed to pharmacological AMPK-activators to investigate whether these may impact reporter expression. Should AMPK function upstream of *klotho*, this should result increased expression of *klotho* reporters following pharmacological treatment with forskolin or metformin (reported AMPK-activators).

Pathway relationships are further explored in this chapter using TOR pathway inhibitor rapamycin to assess the impact that reduced TOR signalling may have on *klotho* reporter expression. TOR and AMPK pathways are reported to function antagonistically to one another. Therefore, if it is expected that AMPK-activation would increase expression of *klotho* reporters, it could be expected that TOR inhibition would bring about this same effect.

Finally, if the oxidative resistance phenotype demonstrated in *klotho* mutants is believed to be the result of increased AMPK function in these strains, it would be expected that extracts

for nematodes with *klo-1/kl* or *klo-2/kl* mutant backgrounds would exhibit increased AMPK activity characterised by increased phosphorylated-AMPK. This will be explored in this chapter by means of western blotting.

5.2. Survival advantage of *klo-1/KL* and *klo-2/KL* deletion mutants requires *aak-2/AMPK*

Previous reports indicate that AAK-2/ AMPK is a key mediator of oxidative stress responses in *C. elegans* (Lee et al., 2008). To determine whether the survival advantage of *klo-1* or *klo-2* mutant animals upon exposure to acute oxidative stress (see 'Chapter 4.1. Effects of *klo-1* or *klo-2* deletion in oxidative stress responses') could be mediated by AAK-2/ AMPK, nematodes with defective *aak-2/AMPK*, *klo-1/KL* and *klo-2/KL* genes were exposed to 300 mM paraquat and counted hourly for dead animals up to 9 hours.

Consistent with findings from (Lee et al., 2008), *aak-2* mutants had diminished survival compared to wild-type counterparts ($n = 103$, mean survival of 2.81 ± 0.20), with an mean survival of 1.87 ± 0.30 hours for *aak-2 (ok524)* ($n = 46$) animals and 1.59 ± 0.33 hours for *aak-2 (gt33)* ($n = 30$) mutants, however these findings were not statistically significant (Table 5.1).

In combination with *aak-2* loss of function alleles, the survival advantage of *klo-1/KL* or *klo-2/KL* deletion mutants was completely abolished (figure 5.1; table 5.1). Survival of *klo-1* single mutants ($n = 99$) was diminished from 4.19 ± 0.25 hours to 1.90 ± 0.37 hours and 1.67 ± 0.37 hours for *klo-1; aak-2 (ok524)* ($n = 30$, $P = 0.009$ compared to *klo-1*) and *klo-1; aak-2 (gt33)* ($n = 27$, $P = 0.013$ compared to *klo-1*) double mutants, respectively.

The survival advantage of *klo-2* mutants ($n = 78$, mean survival of 4.61 ± 0.32 hours) was also diminished in combination with defective *aak-2* alleles. *klo-2; aak-2 (ok524)* ($n = 27$) had a mean survival of 1.74 ± 0.32 hours and *klo-2; aak-2 (gt33)* double mutants ($n = 28$) had a mean survival of 1.71 ± 0.30 hours. These reduced survival times were significantly diminished in comparison to *klo-2* single mutants ($P < 0.001$).

Similarly, the survival of *klo-2; klo-1* double mutants ($n = 99$) was also reduced in combination with *aak-2* mutant alleles. Survival was reduced from an average of 4.06 ± 0.27 hours to 2.27 ± 0.46 hours for *klo-2; klo-1; aak-2 (ok524)* ($n = 28$) and *klo-2; klo-1; aak-2 (gt33)* ($n = 30$) triple mutants. Interestingly, triple mutants containing the *aak-2 (gt33)* allele showed a statistically significant reduction in survival compared to *klo-2;klo-1* double mutants ($P < 0.001$), whereas the diminished survival of *klo-2; klo-1; aak-2 (ok524)* mutants was not found to be significantly lower than *klo-2; klo-1* double mutants, statistically. This may be due to

variation within the sample, or possibly due to the severity of dysfunction in AAK-2/ AMPK function caused by the deletions found in *aak-2 (ok524)* and *aak-2 (gt33)* alleles.

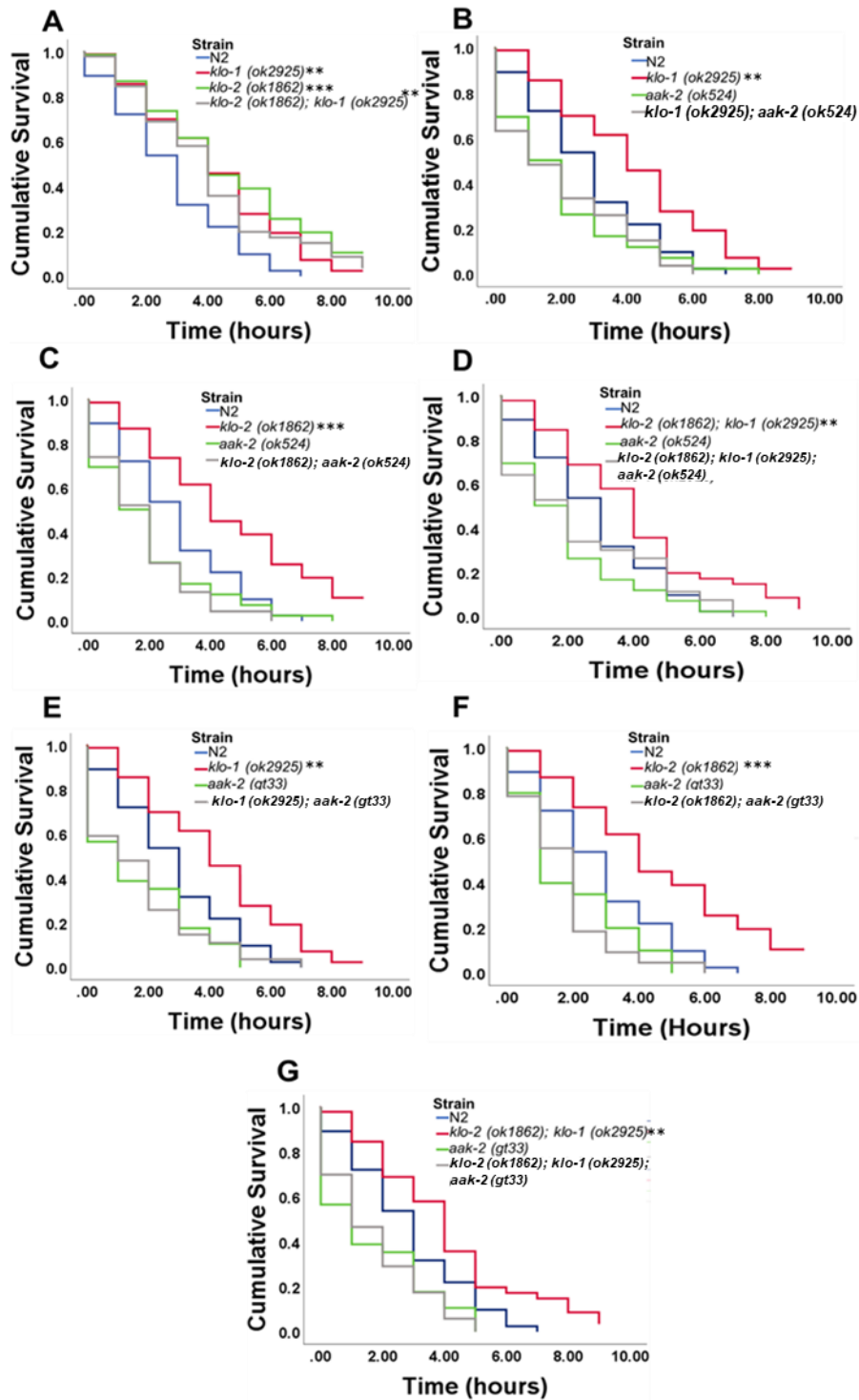


Figure 5.1. Survival of wild-type, *aak-2*, *klo-1* and *klo-2* compound strains over 9 hours when exposed to acute oxidative stress. Nematodes were exposed to 300 mM paraquat to induce

oxidative stress and counted hourly for dead animals for 9 hours. A: wild-type (blue, n = 103); *klo-1* (red, n = 99) ; *klo-2* (green, n = 78), *klo-2; klo-1* (grey, n = 99) B. Wild-type (blue), *klo-1* (red), *aak-2 (ok524)* (green, n = 46) have lower survival compared to wild-type animals. *klo-1; aak-2 (ok524)* (grey, n = 30) mutants have significantly diminished survival compared to *klo-1* single mutants. C. Survival of *klo-2; aak-2 (ok524)* (grey, n = 27) was diminished compared to *klo-2* (red) single mutants. *aak-2 (ok524)* single mutants indicated in green, N2 indicated in blue. D. Wild-type (blue), *klo-2; klo-1* (red), *aak-2 (ok524)* (green) and *klo-2; klo-1; aak-2 (ok524)* (n = 28). E. *aak-2 (gt33)* (green) mutants have reduced survival compared to wild-type (blue) animals. *klo-1; aak-2 (gt33)* double mutants (grey, n = 27) have diminished survival compared to *klo-1* (red) strain. F. Wild-type (blue), *klo-2* (red), *aak-2 (gt33)* (green) and *klo-2; aak-2 (gt33)* (grey, n = 28). G. Wild-type (blue), *klo-2; klo-1* (red), *aak-2 (gt33)* and *klo-2; klo-1; aak-2 (gt33)* (grey, n = 30). *klo-2; klo-1* (red) survival advantage is decreased in combination with *aak-2 (gt33)* mutation. Asterisks indicate significant values compared to wild-type, determined using Tukey's test (*P < 0.05, **P < 0.01, ***P < 0.001).

Table 5.1. Mean survival of wild-type, *klo-1*, *klo-2* and *aak-2* single and compound mutants upon exposure to acute oxidative stress (300 mM paraquat over 9 hours). Statistical significance determined by Tukey's test. Asterisks indicate significant values (*P < 0.05, **P < 0.01, ***P < 0.001).

Strain	n	Censored (%)	Mean Survival ±SEM (hours)	P values					
				N2	<i>aak-2</i> (<i>ok524</i>)	<i>aak-2</i> (<i>gt33</i>)	<i>klo-1</i>	<i>klo-2</i>	<i>klo-2</i> ; <i>klo-1</i>
N2 (wild-type) ^a	103	18.4	2.81±0.20	-	0.967	0.928	0.002**	<0.001*	0.009*
<i>klo-1</i> (<i>ok2925</i>) ^a	99	18.2	4.19±0.25	0.002**	0.001***	0.002**	-	0.977	1.000
<i>klo-2</i> (<i>ok1862</i>) ^a	78	23.1	4.61±0.32	<0.001***	0.000***	0.000***	0.977	-	0.957
<i>klo-2</i> (<i>ok1862</i>); <i>klo-1</i> (<i>ok2925</i>) ^a	99	20.2	4.06±0.27	0.009*	0.003**	0.006**	1.000	0.857	-
<i>aak-2</i> (<i>ok524</i>)	46	6.5	1.87±0.30	0.976	-	1.000	0.001**	<0.000***	0.003**
<i>aak-2</i> (<i>gt33</i>)	30	3.3	1.59±0.33	0.994	1.000	-	0.002**	<0.000***	0.006**
<i>klo-1</i> (<i>ok2925</i>); <i>aak-2</i> (<i>ok524</i>)	30	6.7	1.90±0.37	0.936	1.000	1.000	0.009**	<0.001***	0.026*
<i>klo-1</i> (<i>ok2925</i>); <i>aak-2</i> (<i>gt33</i>)	27	7.2	1.67±0.37	0.993	1.000	1.000	0.013*	0.001**	0.033*
<i>klo-2</i> (<i>ok1862</i>); <i>aak-2</i> (<i>ok524</i>)	27	11.1	1.74±0.32	0.936	1.000	0.996	0.003**	<0.001***	0.009**
<i>klo-2</i> (<i>ok1862</i>); <i>aak-2</i> (<i>gt33</i>)	28	17.9	1.71±0.30	0.760	1.000	1.000	0.001**	<0.001***	0.002**
<i>klo-2</i> (<i>ok1862</i>); <i>klo-1</i> (<i>ok2925</i>); <i>aak-2</i> (<i>ok524</i>)	28	3.6	2.27±0.46	1.000	1.000	1.000	0.193	0.019*	0.349
<i>klo-2</i> (<i>ok1862</i>); <i>klo-1</i> (<i>ok2925</i>); <i>aak-2</i> (<i>gt33</i>)	30	30.0	1.69±0.34	0.247	0.971	0.999	<0.001***	<0.001***	<0.001***

^a Data as shown in Table 4.1 (see '4.1.1. Survival over 9 hours upon exposure to oxidative stress').

5.3. Thermotolerance of *klo-1*/KL and *klo-2*/KL deletion mutants is diminished in combination with *aak-2*/AMPK loss-of-function alleles

Previous data (Chapter 3) indicates that there could be a survival advantage of *klo-1* and *klo-2* single mutants upon exposure to heat stress, at least at the 8-hour time point. To determine whether this survival advantage was dependent on functional AAK-2/ AMPK, animals with deletion alleles for *aak-2*, *klo-1* and *klo-2* were exposed to 37°C heat and counted hourly for dead animals up to 9 hours.

At the 8-hour time point, *klo-1* and *klo-2* single mutants had the largest proportion of living animals, with 82.22% and 80.00% of animals alive, respectively. This was significantly greater than the proportion of living wild-type animals at this time point (61.54% living animals, $n = 91$, $P = 0.009$ compared to *klo-1*, $P = 0.049$ compared to *klo-2*). There was no significant difference between the proportion of living animals of *aak-2* mutants and wild-type strains. *aak-2* (*ok524*) single mutants had 71.11% of animals living at the 8-hour time point ($n = 90$, $P = 0.136$ compared to wild-type), whereas *aak-2* (*gt33*) mutants had 50.00% animals living at the 8-hour time point ($n = 90$, $P = 0.159$ compared to wild-type).

In combination with *aak-2* loss of function alleles, the survival of mutants containing the *klo-1* (*ok2925*) allele diminished from 82.22% at the 8-hour time point, to 50.00% in *klo-1; aak-2* (*ok524*) and *klo-1; aak-2* (*gt33*) double mutants ($P = 0.033$ and $P = 0.033$, respectively, compared to *klo-1*) (Figures 5.2 & 5.3; table 5.2).

Interestingly, in combination with *aak-2* alleles, the survival of *klo-2* mutants was not diminished at the 8-hour time point. Of the *klo-2; aak-2* (*ok524*) mutants 81.67% were alive at the 8-hour time point, and of the *klo-2; aak-2* (*gt33*) double mutants 75.57% were alive, compared to the 80.00% of *klo-2* live animals at the same time point.

While there is a trend for diminished heat stress survival at the 8-hour time point for *klo-2; klo-1* in combination with *aak-2* (*gt33*), these findings were not found to be statistically significant. 46.67% of *klo-2; klo-2; aak-2* (*ok524*) mutants ($n = 90$, $P = 0.080$ compared to *klo-2; klo-1*) and 55.93% *klo-2; klo-1; aak-2* (*gt33*) ($n = 60$, $P = 0.696$ compared to *klo-2; klo-1*) mutants were alive at this time point.

Although there was no difference between the proportion of living animals across strains at the 9 hour time point, there was still a trend for *klo-1* (61.11%), *klo-2* (62.22%) single mutants,

klo-2; klo-1 (60.00%) double mutants, *klo-2; aak-2 (ok524)* (63.33%) and *klo-2; aak-2 (gt33)* (64.44%) double mutants to have increased proportions of living animals at this time point than their counterparts (Figure 5.3; table 5.2). It suggests that while in combination with *aak-2* loss of function alleles *klo-1* mutant survival is diminished, but the survival of *klo-2* mutants is not affected in combination with *aak-2* loss of function alleles.

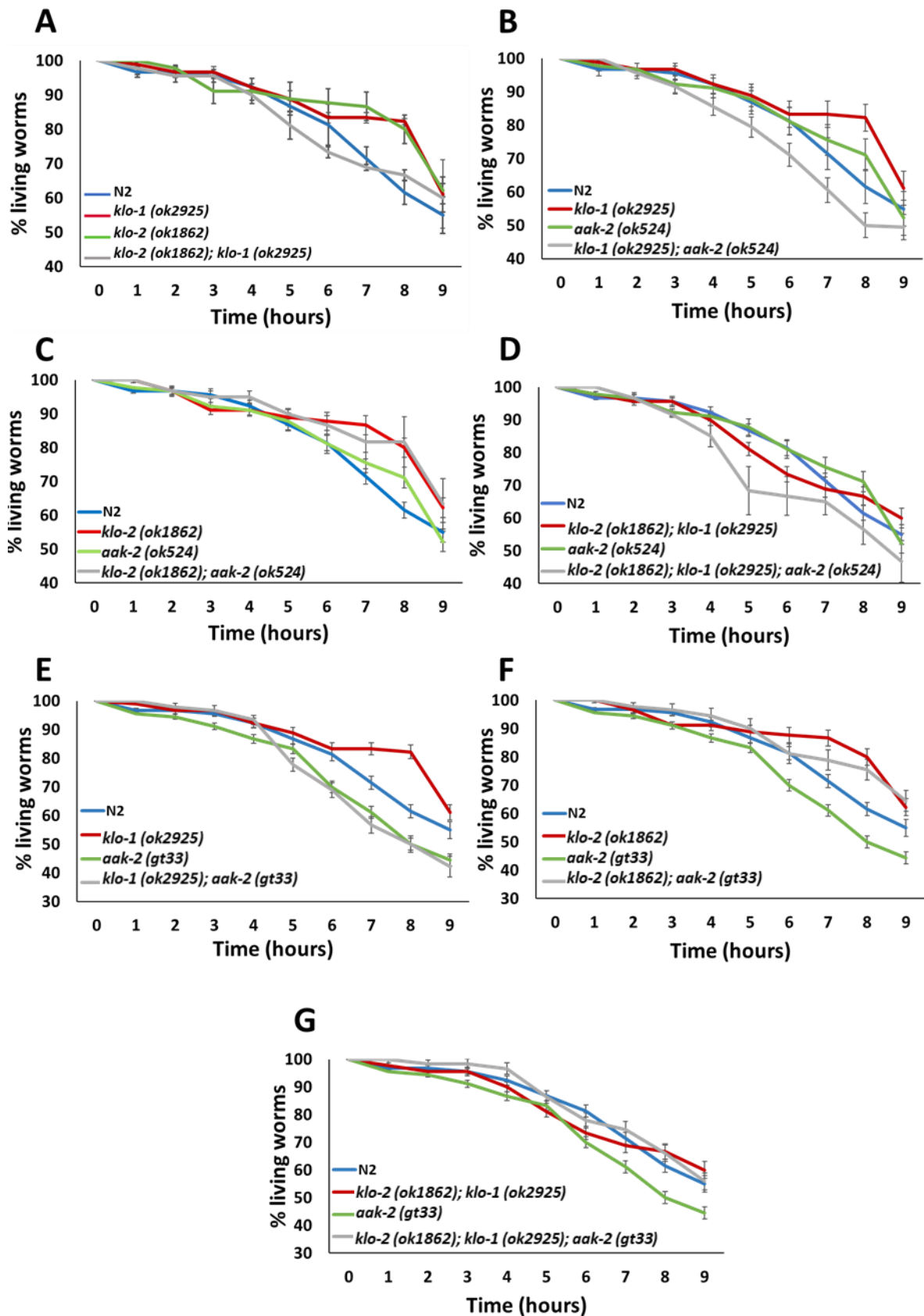


Figure 5.2. Survival of wild-type, *klo-1*; *klo-1*, *aak-2 (gt33)*, *aak-2 (ok524)* and compound mutants upon exposure to 37°C heat stress over 9 hours. A. N2 (blue, n = 91), *klo-1* (red, n =

90), *klo-2* (green, n = 90) and *klo-2; klo-1* (grey, n = 90) survival over 9 hours. B. Strains; N2 (blue), *klo-1* (red), *aak-2 (ok524)* (green, n = 90) and *klo-1; aak-2 (ok524)* (grey, n = 90). C. N2 (blue), *klo-2* (red), *aak-2 (ok524)* (green) and *klo-2; aak-2 (ok524)* (grey, n = 60). D. N2 (blue), *klo-2; klo-1* (red), *aak-2 (ok524)* (green), *klo-2; klo-1; aak-2 (ok524)* (grey, n = 90). E. N2 (blue), *klo-1* (red), *aak-2 (gt33)* (green, n = 90) and *klo-1; aak-2 (gt33)* (grey, n = 90). F. N2 (blue), *klo-2* (red), *aak-2 (gt33)* (green), *klo-2; aak-2 (gt33)* (grey, n = 60). G. N2 (blue), *klo-2; klo-1* (red), *aak-2 (gt33)* (green), *klo-2; klo-1; aak-2 (gt33)* (grey, n = 60). Error bars represent SEM.

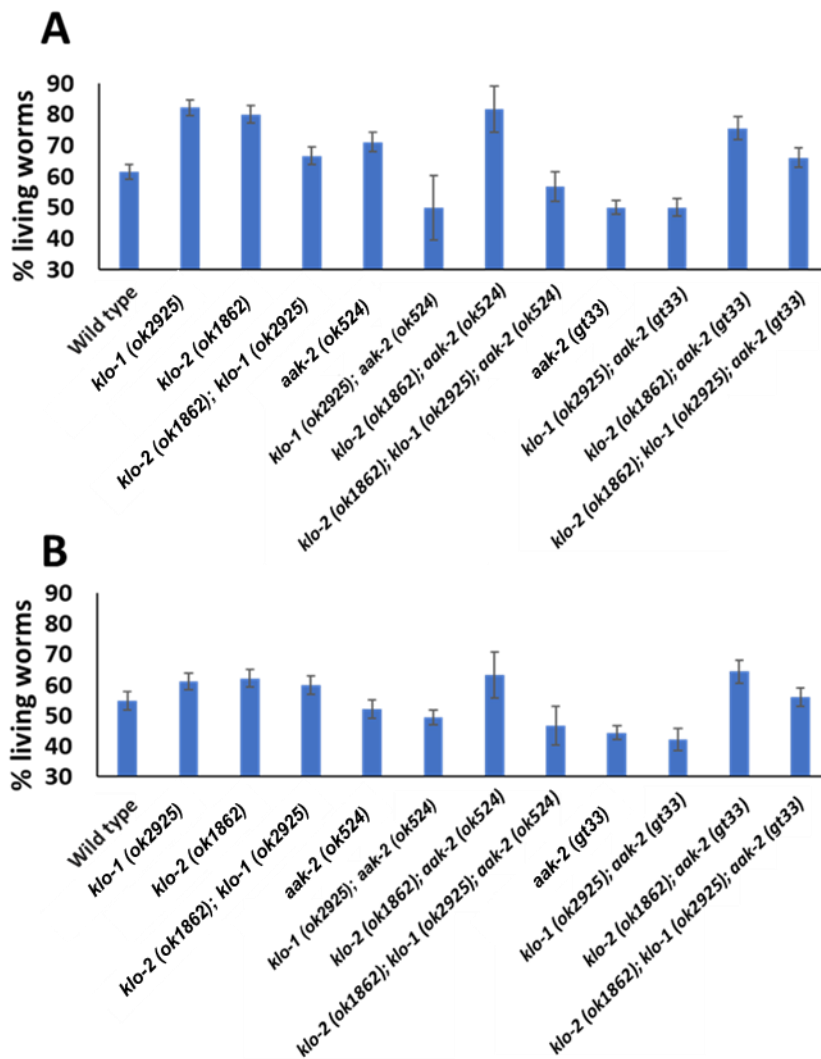


Figure 5.3. Proportion of live animals (%) at 8- and 9-hour time points following exposure to heat stress at 37°C. A. Percentage of live animals at the 8-hour time point. Strains (L-R); wild-type (n = 91, 61.54%), *klo-1* (n = 90, 82.22%), *klo-2* (n = 90, 80.00%), *klo-2; klo-1* (n = 90, 66.67%), *aak-2* (ok524) (n = 90, 71.11%), *klo-1; aak-2* (ok524) (n = 90, 50.00%), *klo-2; aak-2* (ok524) (n = 60, 81.67%), *klo-2; klo-1; aak-2* (ok524) (n = 90, 56.67%), *aak-2* (gt33) (n = 90, 50.00%), *klo-1; aak-2* (gt33) (n = 90, 50.00%), *klo-2; aak-2* (gt33) (n = 60, 75.57%) and *klo-2; klo-1; aak-2* (gt33); (n = 60, 66.10%). **B. Percentage of living animals at the 9-hour time point.** Strains (L-R); wild-type (54.95%), *klo-1* (61.11%), *klo-2* (62.22%), *klo-2; klo-1* (60.00%), *aak-2* (ok524) (52.22%), *klo-1; aak-2* (ok524) (49.44%), *klo-2; aak-2* (ok524) (63.33%), *klo-2; klo-1; aak-2* (ok524) (46.67%), *aak-2* (gt33) (44.44%), *klo-1; aak-2* (gt33) (42.22%), *klo-2; aak-2* (gt33) (64.44%) and *klo-2; klo-1; aak-2* (gt33) (55.93%). Error bars represent SEM. Asterisks indicate statistically significant data compared to wild-type as determined by Tukey's test (*P < 0.05, **P < 0.01, ***P < 0.001).

Table 5.2. Survival of wild-type, *klo-1*, *klo-2* and *aak-2* compound mutants upon exposure to heat stress at 37°C over 9 hours. Percentage of living animals at 7-, 8- and 9-hour time points. Asterisks indicate significance against wild-type animals (*P < 0.05, **P < 0.01, ***P < 0.001).

Strain	n	% Living 7 hours ±SEM	% Living 8 hours ±SEM	% Living 9 hours ±SEM	P value vs N2		
					7 hours	8 hours	9 hours
Wild-type (N2) ^a	91	71.43±3.49	61.54±3.48	54.95±5.34	-	-	-
<i>klo-1</i> (<i>ok2925</i>) ^a	90	83.33±1.57	82.22±0.91	61.11±9.98	0.065	0.009**	0.673
<i>klo-2</i> (<i>ok1862</i>) ^a	90	86.67±4.16	80.00±4.16	62.22±3.95	0.084	0.049*	0.414
<i>klo-2</i> (<i>ok1862</i>); <i>klo-1</i> (<i>ok2925</i>) ^a	90	68.89±0.91	66.67±1.57	60.00±4.15	0.591	0.329	0.565
<i>aak-2</i> (<i>ok524</i>)	90	75.56±3.02	71.11±3.04	52.22±3.00	0.407	0.136	0.717
<i>aak-2</i> (<i>gt33</i>)	90	61.11±2.10	50.00±2.15	44.44±2.15	0.168	0.159	0.452
<i>klo-1</i> (<i>ok2925</i>); <i>aak-2</i> (<i>ok524</i>)	90	60.56±11.86	50.00±10.46	49.44±2.40	0.297	0.206	0.030*
<i>klo-1</i> (<i>ok2925</i>); <i>aak-2</i> (<i>gt33</i>)	90	56.67±2.89	50.00±2.89	42.22±3.59	0.438	0.351	0.380
<i>klo-2</i> (<i>ok1862</i>); <i>aak-2</i> (<i>ok524</i>)	60	81.67±5.05	81.67±7.43	63.33±7.43	0.649	0.810	0.734
<i>klo-2</i> (<i>ok1862</i>); <i>aak-2</i> (<i>gt33</i>)	60	78.89±3.56	75.57±3.69	64.44±3.72	0.572	0.356	0.565
<i>klo-2</i> (<i>ok1862</i>); <i>klo-1</i> (<i>ok2925</i>); <i>aak-2</i> (<i>ok524</i>)	90	65.00±3.95	56.67±4.80	46.67±6.35	0.123	0.272	0.238
<i>klo-2</i> (<i>ok1862</i>); <i>klo-1</i> (<i>ok2925</i>); <i>aak-2</i> (<i>gt33</i>)	60	74.58±2.97	66.10±3.04	55.93±3.02	0.541	0.459	0.722

^a Data as shown in Figure 3.4. (see 3.2. Survival of wild-type vs *klo-1*/KL and *klo-2*/KL deletion mutants upon exposure to acute heat stress at 37°C').

5.4. Functional AAK-2/ AMPK required for longevity in *klo-1/ KL* and *klo-2/ KL* deletion mutant backgrounds

Overexpression of *aak-2/ AMPK* has previously been shown to increase lifespan in *C. elegans* (Curtis et al., 2006), and knockout alleles have a detrimental effect on the health and lifespan of the organisms (Apfeld et al., 2004). The extended lifespan of *daf-2* mutants is also known to be dependent on functional AAK-2 in *C. elegans* (Curtis et al., 2006).

The data presented in this thesis indicates that *klo-1* and *klo-2* deletion mutations do not cause altered lifespans compared to wild-type animals, however it has previously been discovered that in combination with reduced function in *daf-2/ InsR*, the removal of *klo-2* and/or *klo-1* further extends the lifespan of these long-lived *daf-2/ InsR* mutants, indicating there is role for *klo-2* and *klo-1* in lifespan (Buj & Kinnunen, manuscript in preparation).

If *klo-1* and *klo-2* mutants require *aak-2/ AMPK* for longevity, the lifespan of *klo-1* and *klo-2* mutants in combination with *aak-2* loss of function alleles should reflect that of the *aak-2* parent strains. However, if *klo-1* and/ or *klo-2* deletion mutations influence longevity in a pathway independent to, or parallel to the longevity pathways mediated by AAK-2/ AMPK, then these mutants may have altered lifespans to those of the *aak-2/ AMPK* parental strains.

As shown in chapter three (see '3.1.1. Lifespan analysis of *klo-1/ KL* and *klo-2/ KL* mutants'), it was found that *klo-1* ($n = 80$, lifespan of 19.38 ± 1.02 days), *klo-2* ($n = 50$, lifespan of 18.28 ± 1.05 days) and *klo-2; klo-1* ($n = 80$, lifespan of 17.21 ± 0.78 days) mutants do not have altered lifespans to that of wild-type animals ($n = 80$, lifespan of 18.06 ± 0.78 days). Consistent with previous findings (Apfeld et al., 2004), *aak-2 (ok524)* and *aak-2 (gt33)* parent strains have significantly diminished longevity to that of wild-type animals, with a mean lifespan of 11.29 ± 0.69 ($P < 0.001$) and 11.58 ± 0.68 days ($P = 0.005$), respectively (Figures 5.4; table 5.3).

Lifespan was diminished in all mutants containing *aak-2* loss of function alleles, to that similar to *aak-2* parental strains; *klo-1; aak-2 (ok524)* ($n = 55$) had a lifespan of 11.96 ± 0.71 days, *klo-1; aak-2 (gt33)* ($n = 55$) had a lifespan of 11.79 ± 0.67 days, *klo-2; aak-2 (ok524)* ($n = 25$, 12.04 ± 1.25 days), *klo-2; klo-1; aak-2 (ok524)* ($n = 25$, 11.39 ± 0.88 days), and *klo-2; klo-1; aak-2 (okgt33)* ($n = 25$, 12.48 ± 1.31 days). However, compared to wild-type, the lifespan was only statistically significantly shortened for *klo-1; aak-2 (gt33)* animals ($P = 0.001$), presumably due to variation amongst samples (see table 5.3).

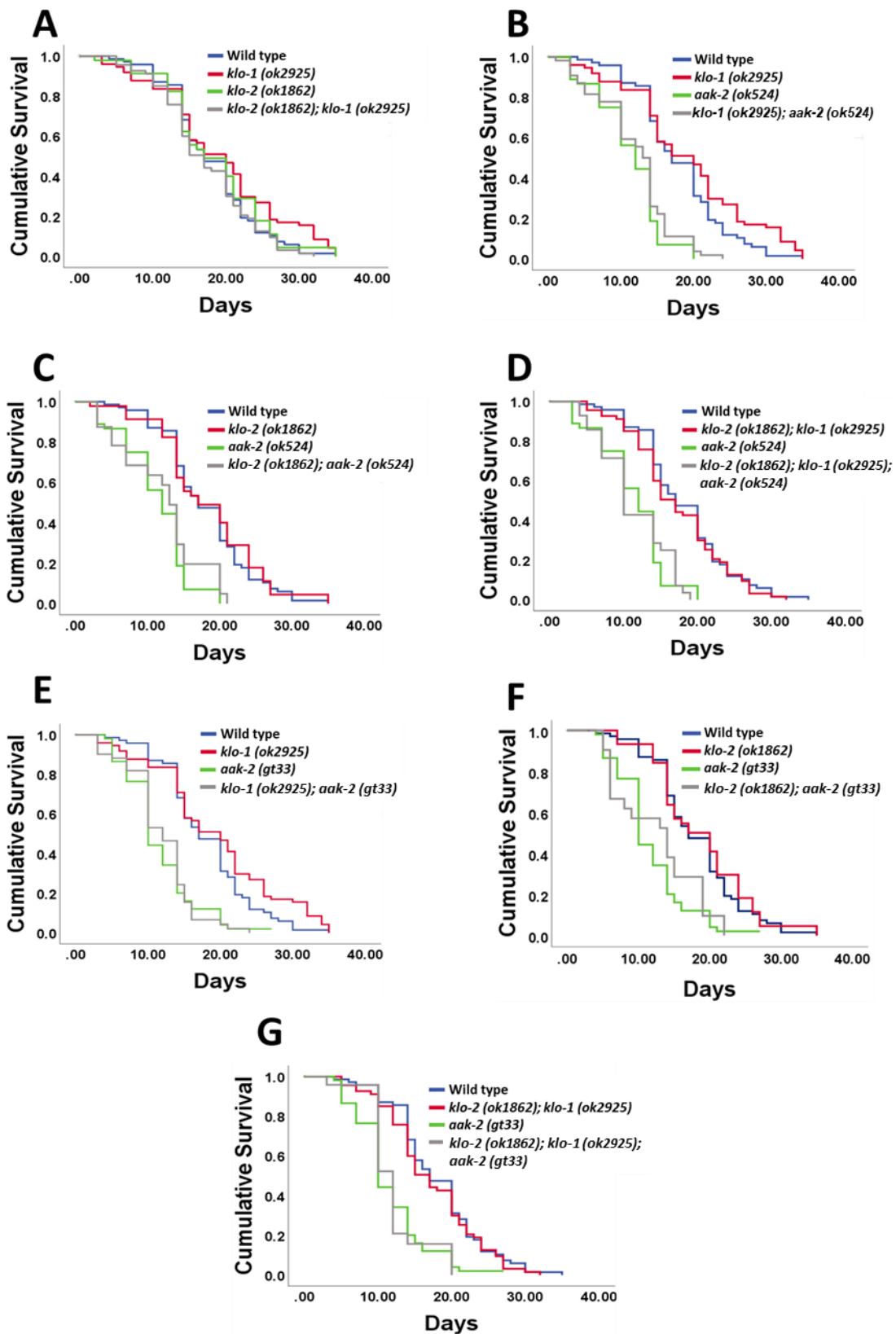


Figure 5.4. Lifespan analysis of wild-type, *klo-1*, *klo-2* and *aak-2* compound mutants. A. Lifespan of wild-type vs *klo-1*, *klo-2* and *klo-2; klo-1* mutants. B. Comparison of lifespan between wild-type (blue, n = 80), *klo-1* (red, n = 80), *aak-2 (ok524)* (green, n = 55), and *klo-1;*

aak-2 (ok524) (grey, n = 55). C. wild-type (blue), *klo-2* (red, n = 50), *aak-2 (ok524)* (green) and *klo-2; aak-2 (ok524)* (grey, n = 25). D. wild-type (blue), *klo-2; klo-1* (red, n = 80), *aak-2 (ok524)* (green) and *klo-2; klo-1; aak-2 (ok524)* (grey, n = 25). E. wild-type (blue), *klo-1* (red), *aak-2 (ok524)* (green) and *klo-1; aak-2 (gt33)* (grey, n = 55). F. wild-type (blue), *klo-2* (red), *aak-2 (gt33)* (green), *klo-2; aak-2 (gt33)* (grey, n = 25 animals). G. wild-type (blue), *klo-2; klo-1* (red) double mutants, *aak-2 (gt33)* (green) and *klo-2; klo-1; aak-2 (gt33)* (grey, n = 30). Asterisks indicate significant difference compared to wild-type lifespan determined by Tukey's test (*P < 0.05, **P < 0.01, ***P < 0.001). See table 5.3 for P values.

Table 5.3. Comparison of mean lifespan of wild-type (N2), *klo-1*, *klo-2* and *aak-2* compound strains. Statistical significance determined using Tukey's test. Asterisks indicate significant values (*P < 0.05, **P < 0.01, ***P < 0.001).

Strain	n	Censored (%)	Mean Lifespan ±SEM (days)	P values			
				Wild-type	<i>klo-1</i>	<i>klo-2</i>	<i>klo-2</i> ; <i>klo-1</i>
N2 (wild-type) ^a	80	15.0	18.06±0.78	-	0.586	0.914	0.683
<i>klo-1</i> (<i>ok2925</i>) ^a	80	11.3	19.38±1.02	0.586	-	0.969	0.084
<i>klo-2</i> (<i>ok1862</i>) ^a	50	10.0	18.38±1.05	0.914	0.969	-	0.364
<i>klo-2</i> (<i>ok1862</i>); <i>klo-1</i> (<i>ok2925</i>) ^a	80	14.5	17.218±0.78	0.683	0.084	0.364	-
<i>aak-2</i> (<i>ok524</i>)	55	21.8	11.29±0.69	<0.001***	<0.001***	<0.001***	0.003**
<i>aak-2</i> (<i>gt33</i>)	55	10.9	11.58±0.68	0.005**	<0.001***	0.001**	0.196
<i>klo-1</i> (<i>ok2925</i>); <i>aak-2</i> (<i>ok524</i>)	55	1.8	11.96±0.71	0.078	0.001**	0.023*	0.732
<i>klo-1</i> (<i>ok2925</i>); <i>aak-2</i> (<i>gt33</i>)	55	16.4	11.79±0.67	0.001**	<0.001***	<0.001***	0.090
<i>klo-2</i> (<i>ok1862</i>); <i>aak-2</i> (<i>ok524</i>)	25	16.0	12.04±1.25	0.062	0.002**	0.019*	0.478
<i>klo-2</i> (<i>ok1862</i>); <i>aak-2</i> (<i>gt33</i>)	25	16.0	12.48±1.31	0.173	0.007**	0.060	0.756
<i>klo-2</i> (<i>ok1862</i>); <i>klo-1</i> (<i>ok2925</i>); <i>aak-2</i> (<i>ok524</i>)	25	6.7	11.39±0.88	0.050	0.001**	0.015*	0.473
<i>klo-2</i> (<i>ok1862</i>); <i>klo-1</i> (<i>ok2925</i>); <i>aak-2</i> (<i>gt33</i>)	30	16.0	12.11±0.87	0.152	0.006**	0.052	0.715

^aData as shown in Table 3.1 (see '3.1.1. Lifespan analysis of *klo-1*/KL and *klo-2*/KL mutants').

5.5. Viable progeny is reduced in *C. elegans* with *aak-2*/AMPK loss-of-function backgrounds

To determine the impact of *aak-2* deletion on reproduction in *klo-1* and *klo-2* deletion mutant strains, viable progeny analysis was conducted on *aak-2*, *klo-1* and *klo-2* compound mutant strains. In combination with *aak-2* (*gt33*) loss of function allele, viable progeny production was reduced in all strains. This was significant in *klo-1*; *aak-2* (*gt33*) (155.6 ± 15.69 , $P = 0.004$ compared to wild-type) and *klo-2*; *aak-2* (*gt33*) (206.2 ± 11.12 , $P = 0.049$) strains, however was not significant in *klo-2*; *klo-1*; *aak-2* (*gt33*) triple mutants (188.0 ± 2.65 , $P = 0.072$).

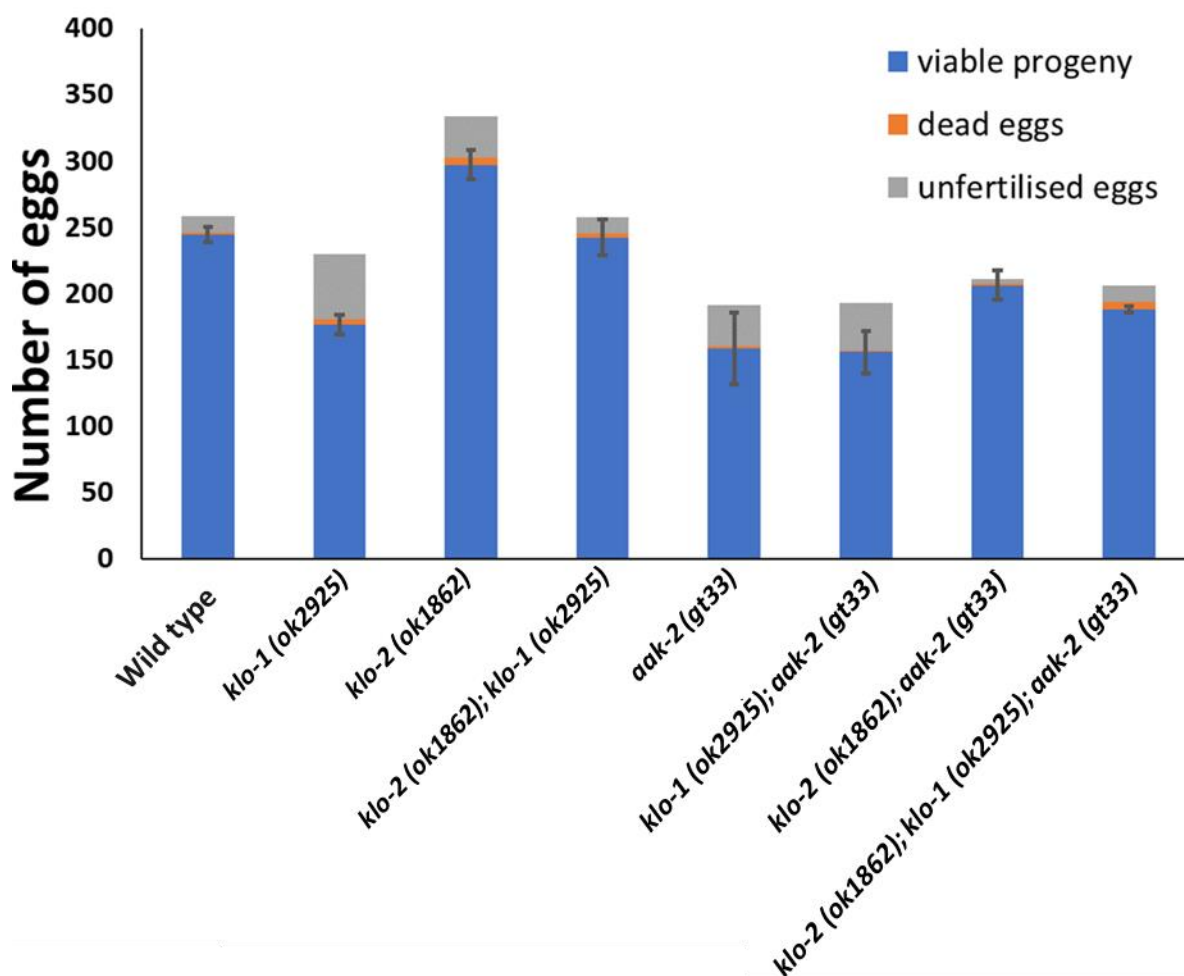


Figure 5.5. Viable progeny analysis for wild-type, *aak-2*, *klo-1* and *klo-2* compound mutants.

Average viable progeny (indicated in blue) per strain is as follows (L-R); Wild-type (N2) 244.2 ± 5.57 , *klo-1* 176.4 ± 7.67 , *klo-2* 296.8 ± 10.95 , *klo-2*; *klo-1* 242.25 ± 13.76 , *aak-2* (*gt33*) 158.4 ± 26.65 , *klo-1*; *aak-2* (*gt33*) 155.6 ± 15.69 , *klo-2*; *aak-2* (*gt33*) 206.2 ± 11.12 and *klo-2*; *klo-1*; *aak-2* (*gt33*) 188.0 ± 2.65 . Unfertilized eggs indicated in grey; values can be found in

appendix 2. Dead eggs indicated in orange. Error bars represent SEM. Asterisks indicate statistical significance compared to wild-type, as determined using Tukey's test (*P < 0.05, **P < 0.01, ***P < 0.001).

Table 5.4. Mean viable progeny values for wild-type, *aak-2*, *klo-1* and *klo-2* compound strains. Progeny of 4-5 nematodes per strain were analysed. Statistical significance determined by Tukey's test, asterisks indicate significant values (*P < 0.05, **P < 0.01, ***P < 0.001). Mean values and statistical analysis for unfertilised and dead eggs can be found in appendix 2.

Strain	n	Mean Viable Progeny ±SEM	P values				
			N2	<i>klo-1</i>	<i>klo-2</i>	<i>klo-2</i> ; <i>klo-1</i>	<i>aak-2</i>
N2 (wild-type) ^a	5	244.2±5.57	-	<0.001***	0.008**	0.905	0.046*
<i>klo-1</i> (<i>ok2925</i>) ^a	5	176.4±7.67	<0.001***	-	<0.001***	<0.001***	0.637
<i>klo-2</i> (<i>ok1862</i>) ^a	5	296.8±10.95	0.008**	<0.001***	-	0.026*	0.007**
<i>klo-2</i> (<i>ok1862</i>); <i>klo-1</i> (<i>ok2925</i>) ^a	4	242.25±13.76	0.905	0.009**	0.026*	-	0.079
<i>aak-2</i> (<i>gt33</i>)	5	158.4±26.65	0.046*	0.637	0.007**	0.079	-
<i>klo-1</i> (<i>ok2925</i>); <i>aak-2</i> (<i>gt33</i>)	5	155.6±15.69	0.004**	0.386	<0.001***	0.012*	0.948
<i>klo-2</i> (<i>ok1862</i>); <i>aak-2</i> (<i>gt33</i>)	5	206.2±11.12	0.049*	0.120	0.002**	0.119	0.252
<i>klo-2</i> (<i>ok1862</i>); <i>klo-1</i> (<i>ok2925</i>); <i>aak-2</i> (<i>gt33</i>);	5	188.0±2.65	0.072	0.685	0.006**	0.117	0.523

^a Data as shown in Table 3.5 (see '3.5. Viable progeny analysis').

5.6. Treatment with AMPK-activators increases expression of *klotho* reporters in *C. elegans*

To assess whether AAK-2/ AMPK activation leads to changes in *klo-1* and *klo-2* gene expression, *C. elegans* carrying *klo-1* and *klo-2* reporter genes were stimulated with Forskolin, a widely known AMPK activator (Alasbahi and Melzig, 2012). In *C. elegans*, Forskolin treatment has been used previously to increase cAMP/ PKA pathway activity which is known to function upstream of AAK-2/ AMPK pathway (Lee et al., 2014b, Mair et al., 2011).

In addition, to assess whether any possible response is dependent on functional KLO-1 and KLO-2, both wild-type and *klo-2; klo-1* double mutants were analysed in parallel. If AAK-2/ AMPK functions upstream of *klo-1/ KL* or *klo-2/ KL*, if these strains have increased AAK-2/ AMPK activity this could manifest in increased baseline expression of these reporters before treatment with an AMPK-activator.

5.6.1. Forskolin treatment increases expression of *pklo-2::GFP* reporter in wild-type and *klo-2; klo-1 C. elegans*

To assess the effects of AAK-2/ AMPK activation on *klo-2* reporter expression, wild-type and *klo-2; klo-1* mutants carrying the *jtEx129* extrachromosomal array, which contains 5' upstream sequences of *klo-2* driving expression of GFP (Polanska et al 2011), were analysed. In untreated wild-type animals and *klo-2; klo-1* double mutants, there is no difference between the expression of the *klo-2* reporter, with *klo-2; klo-1* animals showing a relative expression of 1.01 ± 0.06 compared to wild-type controls (equal to 1) (Figure 5.6; Table 5.5). Upon treatment with Forskolin, there was a trend for increased expression of the *klo-2* reporter in both strains with a mean expression of 1.08 ± 0.05 for wild-type animals, and 1.09 ± 0.05 for *klo-2; klo-1* mutants. This suggests that Forskolin activation of AAK-2 could increase the expression of the *klo-2::GFP* reporter, although these results were not found to be significant (see Table 5.5), and it must be confirmed that the mechanism of forskolin does increase AAK-2/ AMPK activity in *C. elegans*. This research attempts to quantify activated AAK-2/ AMPK in *C. elegans* extracts with little success (see "5.9. Western blotting for AAK-2/ AMPK"). Therefore, more research is required to confirm it is the result of AAK-2/ AMPK

activation, though it is known that Forskolin functions to activate components upstream of AAK-2 in *C. elegans* (Lee et al., 2014b, Mair et al., 2011).

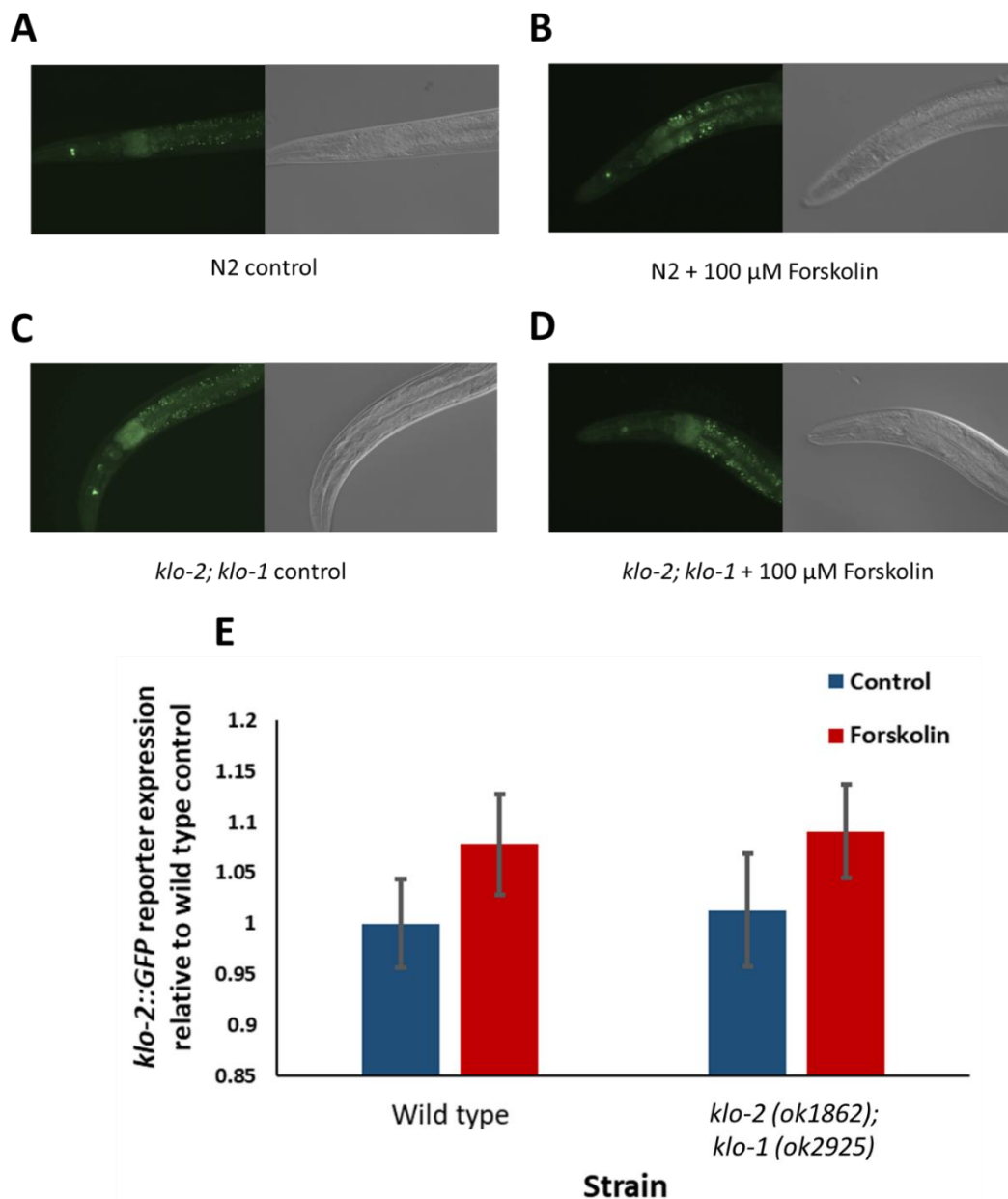


Figure 5.6. *pklo-2* reporter expression in wild-type and *klo-2*; *klo-1* double mutants before and after forskolin treatment. Nematodes were treated with 100 μ M Forskolin for 2 hours. A – D: *pklo-2*::GFP expression (left) and DIC (right) images of wild-type vs *klo-2*; *klo-1* mutants before and after Forskolin treatment. A. wild type control. B. wild-type + Forskolin. C. *klo-2*; *klo-1* double mutant control. D. Forskolin treated *klo-2*; *klo-1* animal. E. Relative *pklo-2*::GFP expression (mean pixel intensity) of wild-type vs *klo-2*; *klo-1* mutants. Where wild-type controls equal 1. Untreated animals indicated in blue, treated animals indicated in red. 20-27

nematodes per strain analysed. Mean pixel intensity was calculated from the first two intestinal cells of the animals with care taken to avoid collection of confounding data caused by gut granule autofluorescence.

Table 5.5. Relative expression (mean pixel intensity) of *pklo-2::GFP* reporter in *klo-2*; *klo-1* double mutants compared to wild-type controls. Where wild-type controls equal 1. 20-27 nematodes per strain analysed. Statistical significance determined using Tukey's test.

Strain	Condition	<i>n</i>	Relative pixel intensity \pm SEM	P values	
				Wild-type	<i>klo-2</i> ; <i>klo-1</i>
N2; <i>jtEx129</i> (wild-type)	Control	27	1.00 \pm 0.04	-	0.853
	+ 100 μ M Forskolin	20	1.08 \pm 0.05	0.243	0.386
<i>klo-2</i> (<i>ok1862</i>); <i>klo-1</i> (<i>ok2925</i>); <i>jtEx129</i>	Control	24	1.01 \pm 0.06	0.853	-
	+ 100 μ M Forskolin	23	1.09 \pm 0.05	0.159	0.287

5.6.2. Forskolin increases *pklo-1::mCherry* expression in wild-type and *klo-2; klo-1 C. elegans*

To determine whether AAK-2/ AMPK activation has an effect on *klo-1* reporter expression, wild-type and *klo-2; klo-1* strains carrying the *jtEx179* extrachromosomal array were examined. This array has 5' upstream sequences of *klo-1* (Polanska et al., 2011) driving mCherry expression. In control (untreated) animals, *klo-2; klo-1* double mutants had significantly increased levels of *pklo-1::mCherry* expression than their wild-type counterparts, with a relative pixel intensity of 1.23 ± 0.06 compared to wild-type animals (where expression is equal to 1) ($P = 0.014$).

Upon forskolin treatment, expression of the *klo-1::mCherry* reporter increased in both strains, to a relative pixel intensity of 1.16 ± 0.08 for wild-type animals, and 1.47 ± 0.06 for *klo-2; klo-1* double mutants (Figure 5.7; Table 5.6). While this increase was not a significant increase in wild-type animals ($P = 0.140$), *klo-2; klo-1* mutants showed a statistically significant increase in *klo-1::mCherry* expression upon forskolin treatment ($P = 0.010$).

The data here shows that under unstimulated conditions *klo-2; klo-1* double mutants have increased expression of the *pklo-1::mCherry* reporter, and that activation of AAK-2/ AMPK through treatment with forskolin further drives the increased expression of this reporter in both wild-type and *klo-2; klo-1* strains. Taken together, this could suggest that AAK-2 may drive *klo-1* expression, and that in wild-type animals, functional KLO-1 and KLO-2 may inhibit transcription of these genes. However, as noted previously (See “5.6.1. Forskolin activation of aak-2/ AMPK increases expression of *pklo-2::GFP* reporter in wild type and *klo-2; klo-1 C. elegans*”), more research is necessary to confirm the effects of Forskolin on AAK-2 function in *C. elegans*.

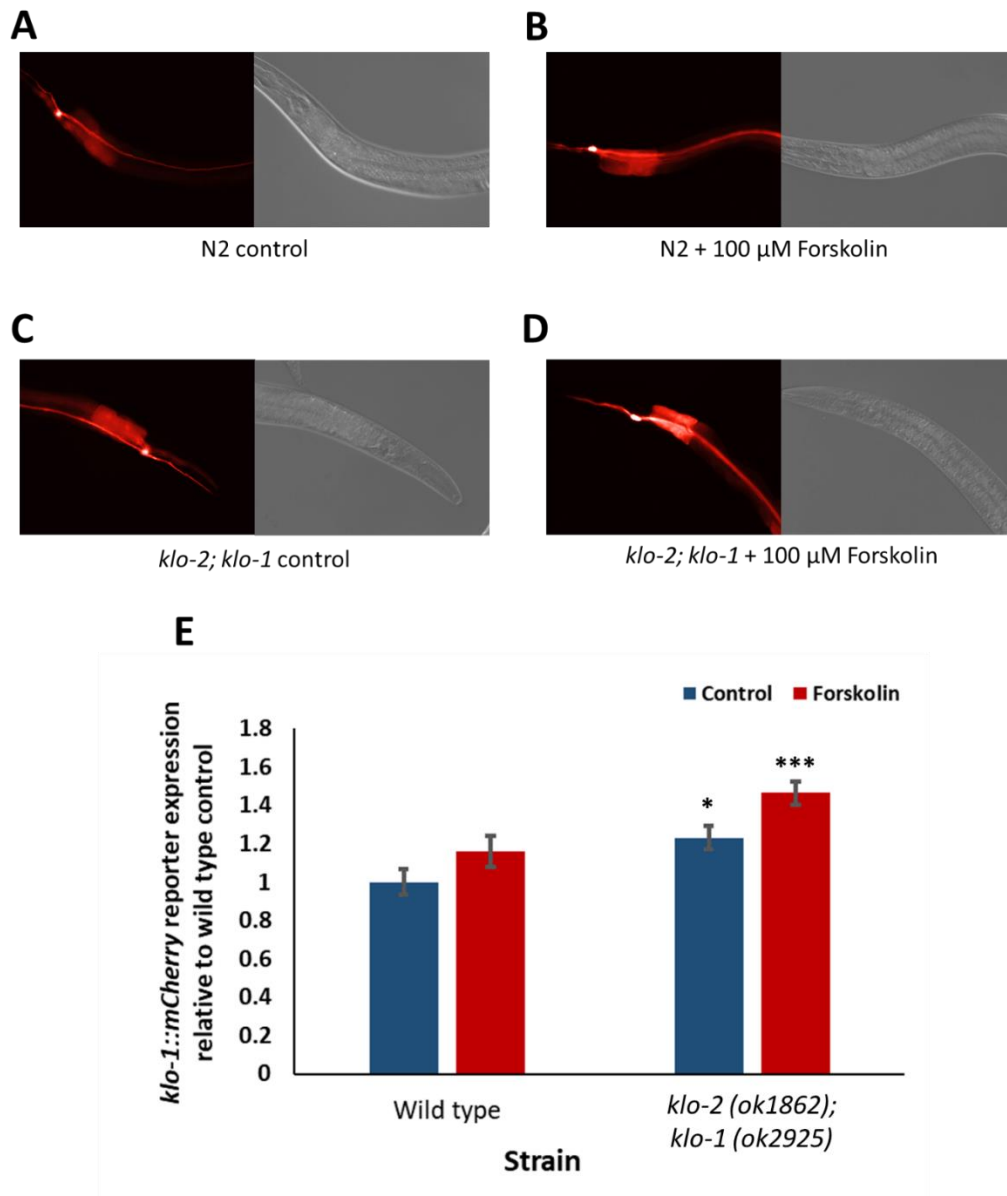


Figure 5.7. *pklo-1* reporter expression in wild-type and *klo-2; klo-1* double mutants, before and after forskolin treatment. Animals were treated with 100 μ M Forskolin for 2 hours. A – D: *pklo-1::mCherry* expression (left) and DIC (right) images of wild-type vs *klo-2; klo-1* mutants before and after Forskolin treatment. A. N2 (wild-type) control. B. Forskolin treated N2 nematode. C. *klo-2; klo-1* double mutant control. D. Forskolin treated *klo-2; klo-1* animal. E. Relative *pklo-1::mCherry* expression (mean pixel intensity) of wild-type vs *klo-2; klo-1* mutants. Untreated controls indicated in blue, treated animals indicated in red. 35-40 animals per strain analysed. Mean pixel intensity was calculated from the first two intestinal cells of the animals. Asterisks indicate significance compared to wild-type controls, determined using Tukey’s test (*P < 0.05, **P < 0.01, ***P < 0.001).

Table 5.6. Mean expression of *pklo-1::mCherry* (relative pixel intensity) in wild-type vs *klo-2*; *klo-1* double mutants. Mean pixel intensity measured using ImageJ software. A total of 35-40 nematodes per strain were analysed. Statistical significance determined using Tukey's test, asterisks indicate significant values (*P < 0.05, **P < 0.01, ***P < 0.001).

Strain	Condition	Relative pixel intensity		P values	
		<i>n</i>	\pm SEM	Wild-type	<i>klo-2</i> ; <i>klo-1</i>
N2; <i>jtEx179</i> (wild-type)	Control	40	1.00 \pm 0.07	-	0.014*
	+ 100 μ M Forskolin	35	1.16 \pm 0.08	0.140	0.500
<i>klo-2</i> (<i>ok1862</i>); <i>klo-1</i> (<i>ok2925</i>); <i>jtEx179</i>	Control	37	1.23 \pm 0.06	0.014*	-
	+ 100 μ M Forskolin	36	1.47 \pm 0.06	<0.001***	0.010*

5.6.3. Forskolin activation of AAK-2/ AMPK could lead to osmotic stress in *C. elegans*

The *C. elegans* excretory canal is formed from a single cell, and is functionally orthologous to the mammalian kidney (Buechner, 2002). The *klo-1* reporter is strongly expressed along the excretory canal of *C. elegans* (Polanska et al., 2011), thus providing a tool to assess the morphology of the excretory canals in nematodes.

Forskolin treatment of nematodes lead to the appearance of periodic swellings resembling “beads” or “pearls” along the excretory canal of some animals (see Figure 5.8). These swellings have been notable in animals under osmotic stress and are suggested to be additions of cytoplasm to the canal (Kolotuev et al., 2013). In wild-type animals under control conditions, this phenotype is infrequent but was found in 5.15% of animals (5 of 97). In untreated *klo-2; klo-1* controls, this phenotype was found more frequently (25.89%, 29 of 112 animals) than in wild-type counterparts, however this was not found to be significant (P = 0.086). Upon activation of AAK-2/ AMPK, the incidence of this phenotype increased in both wild-type and *klo-2; klo-1* mutants, to 42.11% (40 of 95 animals) and 47.67% (41 of 86), respectively.

Given that forskolin treatment increases the incidence of this phenotype, and that under control conditions, *klo-2; klo-1* double mutants display this phenotype more frequently, these findings could suggest that *klo-2; klo-1* mutants are constitutively under low levels of osmotic stress, possibly as a result of increased AAK-2/ AMPK activity in these nematodes.

Given that forskolin has been utilised in this research for its documented effects as an AMPK-activator, it would be useful to determine whether this abnormal canal morphology phenotype is AAK-2-dependent in *C. elegans*. This could be achieved through future work using *aak-2* null mutants that have been crossed to contain the *pklo-1* reporter. This experiment could then be repeated to confirm whether this phenotype would be demonstrated without functional AAK-2.

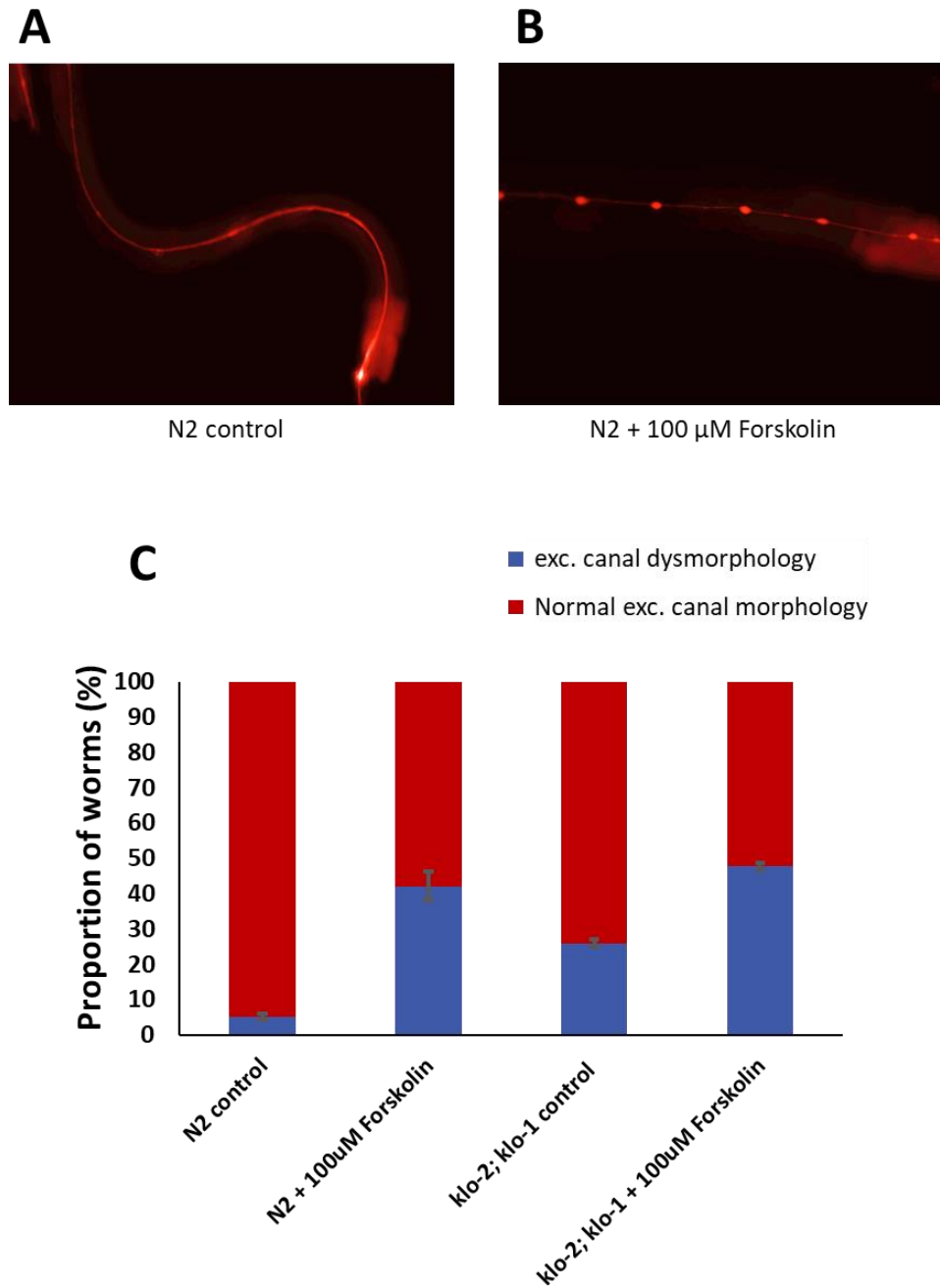


Figure 5.8. Morphology of the excretory canals of wild-type and *klo-2; klo-1* double mutants. A. Morphology of the excretory canal as visualised by *pklo-1* reporter in a wild-type animal. Typically, the canal is smooth. B. Morphology of the excretory canal of a forskolin-treated wild-type animal. C. Proportion (%) of nematodes showing abnormal excretory canal morphology before and after Forskolin treatment. Normal (red) or abnormal (blue; “pearl” morphology) Error bars represent SEM. Asterisks indicate significant values compared to wild-type controls, as determined by Tukey’s test (*P < 0.05, **P < 0.01, *P < 0.001).**

5.7. Effects of metformin on *klo-1/ KL* and *klo-2/ KL* reporter expression

Similar to Forskolin, metformin is a known AMPK activator (Meng et al., 2015). Therefore, wild-type and *klo-2; klo-1* strains positive for *pklo-1::mCherry* and *pklo-2::GFP* reporters were exposed to 50 mM metformin treatment and compared to controls.

5.7.1. Metformin treatment increases the expression of *pklo-1::mCherry* reporter in *C. elegans*

In control conditions, there is a trend for increased *pklo-1::mCherry* expression in *klo-2; klo-1* double mutants compared to wild-type controls ($n = 103$ animals) with a relative *pklo-1::mCherry* reporter expression of 1.09 ± 0.04 ($n = 98$), though this was not found to be statistically significant ($P = 0.053$) (Figure 5.9; Table 5.7).

Upon treatment with metformin, the expression of *pklo-1::mCherry* expression in both wild-type and *klo-2; klo-1* strains increased to 1.27 ± 0.03 and 1.33 ± 0.04 , respectively, relative to wild-type. This increased expression of *pklo-1::mCherry* was statistically significant for both wild-type ($P < 0.001$ compared to wild-type controls) and *klo-2; klo-1* ($P < 0.001$ compared to *klo-2; klo-1* controls) (See Table 5.7).

There was no significant difference between the expression of *pklo-1::mCherry* in wild-type compared to *klo-2; klo-1* under metformin treatment ($P = 0.233$) (Table 5.7).

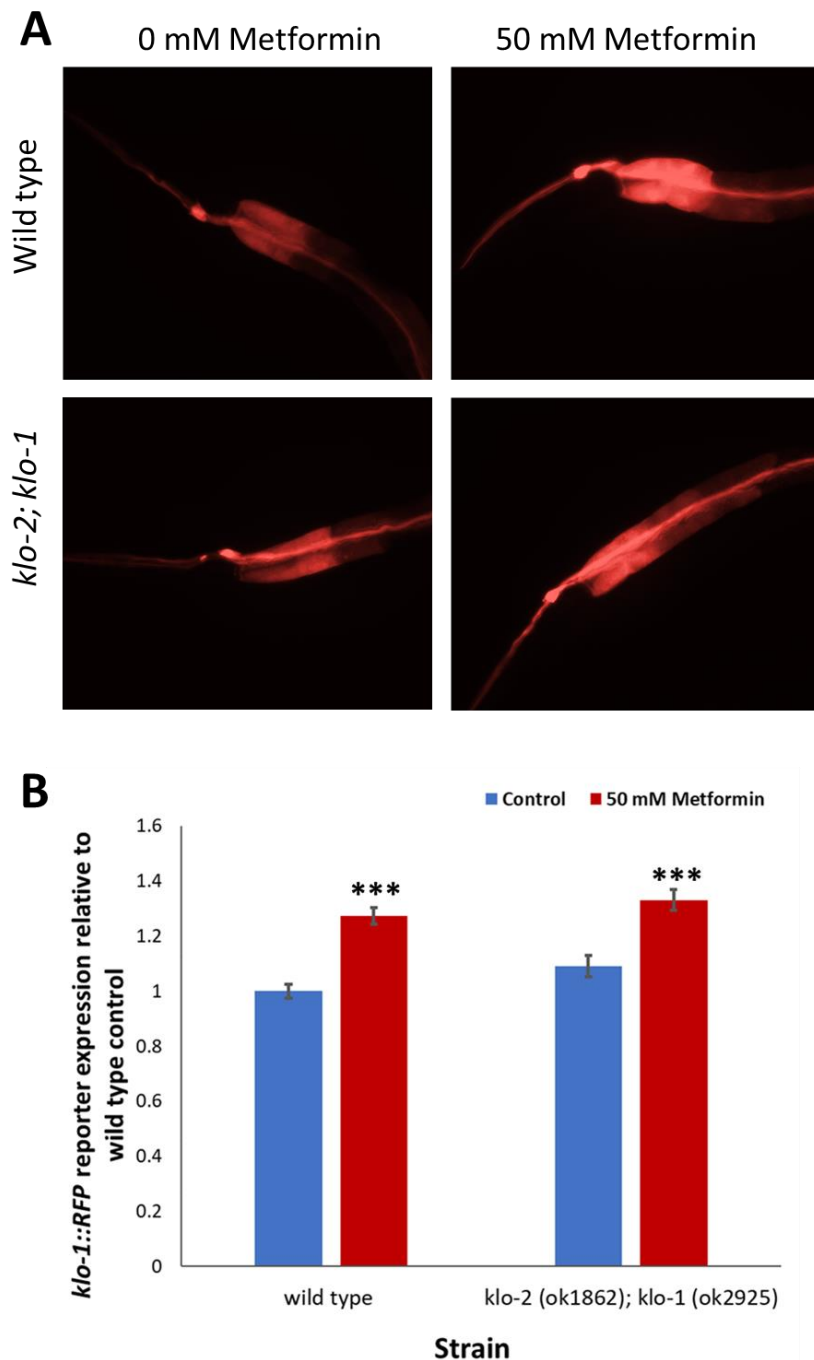


Figure 5.9. Expression of *pklo-1::mCherry* reporter expression in wild-type vs *klo-2; klo-1* strains. A. Expression of *pklo-1::mCherry* reporter in wild-type (top row) vs *klo-2; klo-1* double mutants (bottom row) in control (left column) and 50 mM metformin (right column) conditions. B. Relative expression of *pklo-1::mCherry* reporter expression where wild-type controls. Control condition indicated in blue; 50 mM metformin treatment indicated in red. Error bars represent SEM. 98-103 animals per strain were analysed. Asterisks indicate statistical significance compared to wild-type, as determined using Tukey's test (*P < 0.05, **P < 0.01, ***P < 0.001).

Table 5.7. Relative expression of *pklo::mCherry* reporter in wild-type vs *klo-2*; *klo-1* strains exposed to 50 mM metformin. Values are relative to wild-type controls (equal to 1). 98-103 animals per strain were analysed per assay. Statistical significance determined using Tukey's test, asterisks indicate significant values (*P < 0.05, **P < 0.01, ***P < 0.001).

Strain	Condition	n	Relative expression to wild-type ±SEM	P values			
				Wild-type control	Wild-type treated	<i>klo-2</i> ; <i>klo-1</i> control	<i>klo-2</i> ; <i>klo-1</i> treated
Wild-type	0 mM metformin	103	1.00±0.03	-	<0.001***	0.053	<0.001***
	50 mM metformin	101	1.27±0.03	<0.001***	-	<0.001***	0.233
<i>klo-2</i> (<i>ok1862</i>); <i>klo-1</i> (<i>ok2925</i>)	0 mM metformin	98	1.09±0.04	0.053	<0.001***	-	<0.001***
	50 mM metformin	99	1.33±0.04	<0.001***	0.233	<0.001***	-

5.7.2. Metformin treatment increases *pklo-2::GFP* reporter expression in *C. elegans*

In control conditions, *klo-2; klo-1* animals ($n = 63$, relative expression 0.95 ± 0.02) had slightly decreased expression of *pklo-2::GFP* reporter compared to wild-type controls ($n = 56$), though this was not found to be statistically significant ($P = 0.089$) (see Figure 5.10; Table 5.8).

Treatment with metformin significantly increased the expression of *pklo-2::GFP* to 1.23 ± 0.02 and 1.26 ± 0.04 in wild-type ($n = 65$, $P < 0.001$ compared to wild-type controls) and *klo-2; klo-1* animals ($n = 59$, $P < 0.001$ compared to *klo-2; klo-1* controls), respectively (Figure 5.10; Table 5.8). There was no difference in the expression of *pklo-2::GFP* in wild-type animals treated with Metformin compared to *klo-2; klo-1* metformin-treated animals ($P = 0.707$) (Figure 5.10; Table 5.8).

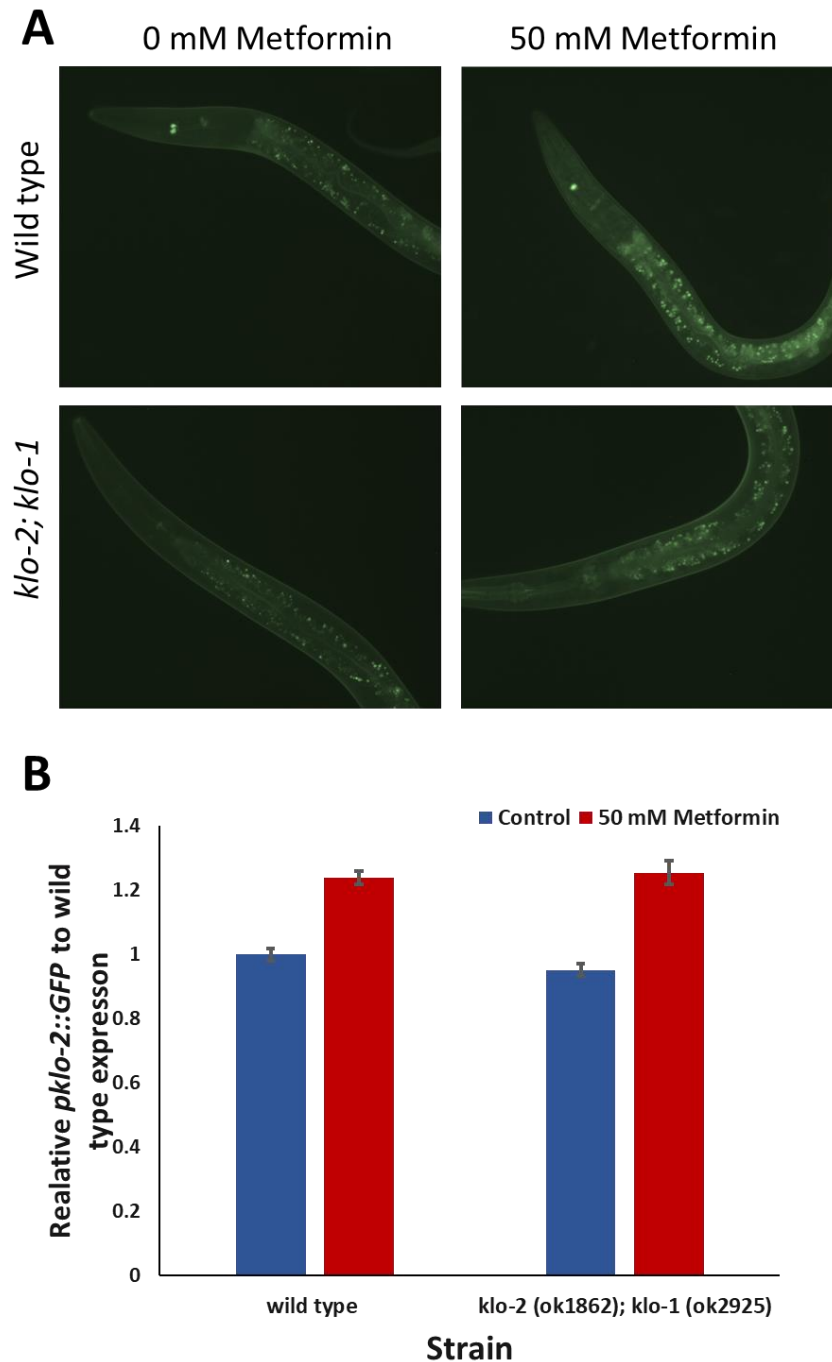


Figure 5.10. Relative expression of *pklo-2::GFP* reporter expression in wild-type and *klo-2; klo-1* strains upon exposure to 50 mM metformin. A. Expression of *pklo-2::GFP* reporter in wild-type (top row) vs *klo-2; klo-1* double mutants (bottom row) in control (left column) vs 50 mM metformin (right column) conditions. B. Relative expression of *pklo-2::GFP* reporter expression. Values comparable to wild-type controls (equal to 1). Untreated controls indicated in blue; metformin treatment indicated in red. Error bars represent SEM. 56-35 animals per strain analysed. Mean pixel intensity was calculated from the first two intestinal cells of the animals with care taken to avoid collection of confounding data caused by gut

granule autofluorescence. Asterisks indicate statistical significance compared to wild-type, as determined using Tukey's test (*P < 0.05, **P < 0.01, ***P < 0.001).

Table 5.8. relative expression of *pklo-2::GFP* reporter in wild-type vs *klo-2*; *klo-1* strains exposed to 50 mM metformin. Values are relative to wild-type controls (equal to 1.000). 15-20 animals per strain were analysed per assay. 56-35 animals per strain analysed. Statistical significance determined using Tukey's test, asterisks indicate significant values (*P < 0.05, **P < 0.01, ***P < 0.001).

Strain	Condition	n	Relative expression to wild-type	P values			
				Wild-type control	Wild-type treated	<i>klo-2</i> ; <i>klo-1</i> control	<i>klo-2</i> ; <i>klo-1</i> treated
Wild-type	0 mM metformin	56	1.000	-	<0.001***	0.089	0.001***
	50 mM metformin	65	1.230	<0.001***	-	<0.001***	0.707
<i>klo-2</i> (<i>ok1862</i>); <i>klo-1</i> (<i>ok2925</i>)	0 mM metformin	63	0.950	0.089	<0.001***	-	<0.001***
	50 mM metformin	59	1.260	<0.001***	0.707	<0.001***	-

5.8. Effects of mTOR signalling manipulation on *klo-1/ KL* and *klo-2/ KL* reporter expression

The data shown suggests that activation of AMPK may promote the expression of *pklo-1::mCherry* and *pklo-2::GFP* reporters in wild-type and *klo-2; klo-1* animals (see '5.7. Effects of AAK-2/ AMPK activation on *klo-1/ KL* and *klo-2/ KL* reporter expression' and '5.8. Effects of metformin on *klo-1/ KL* and *klo-2/ KL* reporter expression'). In addition, *klo-2; klo-1* double mutants display increased *pklo-1::mCherry* reporter expression which could indicate that these mutants have increased AAK-2/ AMPK activity under normal conditions.

To explore this further, the effects of pharmacological manipulation of TOR signalling, a pathway reported to function antagonistically to AMPK (Hindupur et al., 2015, Holczer et al., 2019, Mounier et al., 2011), on the expression of *pklo-1::mCherry* and *pklo-2::GFP* reporters in wild-type and *klo-2; klo-1* double mutants was examined. If *klo-2; klo-1* double mutants have increased AAK-2/ AMPK activity this could be reflected by diminished TOR signalling in this strain.

Rapamycin inhibits TOR signalling through its interaction with FK506-binding protein (FKBP12) which subsequently inhibits mammalian TOR complex 1 (mTORC1) (Li et al., 2014). Wild-type and *klo-2; klo-1* strains positive for either *pklo-1::mCherry* or *pklo-2::GFP* reporters were incubated on NGM agar plates supplemented with rapamycin for 4 hours prior to microscopy to analyse the effects of inhibition of TOR signalling on *klo-1* and *klo-2* reporter expression.

5.8.1. Rapamycin treatment increases expression of *pklo-1::mCherry* reporter in wild-type *C. elegans* but has little effect on *C. elegans* with *klo-2; klo-1* deletion background

The expression of the *pklo-1::mCherry* reporter is naturally higher in *klo-2; klo-1* double mutants in control conditions compared to their wild-type counterparts (Figure 5.11). Where reporter expression of wild-type controls is 1 ($n = 103$), the relative expression of *pklo-1::mCherry* in *klo-2; klo-1* double mutants ($n = 113$) is 1.08, and this was found to be statistically significant ($P = 0.043$, see table 5.9).

Upon treatment with 100 μ M rapamycin, expression of *pklo-1::mCherry* increased in wild-type animals to 1.215 relative to wild-type controls (Figure 5.11; Table 5.9) and this was found to be significant ($P < 0.001$).

In comparison, while there was a slight increase in *pklo-1::mCherry* reporter expression in *klo-1; klo-1* double mutants (1.13 relative to wild-type, $n = 102$) upon rapamycin treatment, this was not found to be statistically significant compared to *klo-2; klo-1* untreated mutants ($P = 0.274$). Interestingly, while *klo-2; klo-1* animals treated with rapamycin showed no significant difference to untreated *klo-2; klo-1* double mutant counterparts, there was no significant difference between these animals and treated wild-type animals ($P = 0.070$), whereas untreated *klo-2; klo-1* double mutants do show significantly lower *pklo-1::mCherry* reporter expression when compared to treated wild-type animals ($P = 0.002$) (see table 5.9).

Taken together, this suggests that inhibition of the TOR pathway promotes the expression of KLO-1/ KL and KLO-2/ KL in *C. elegans*, and suggests that in typical circumstances, TOR activity suppresses the expression of KLO-1/ KL and KLO-2/ KL.

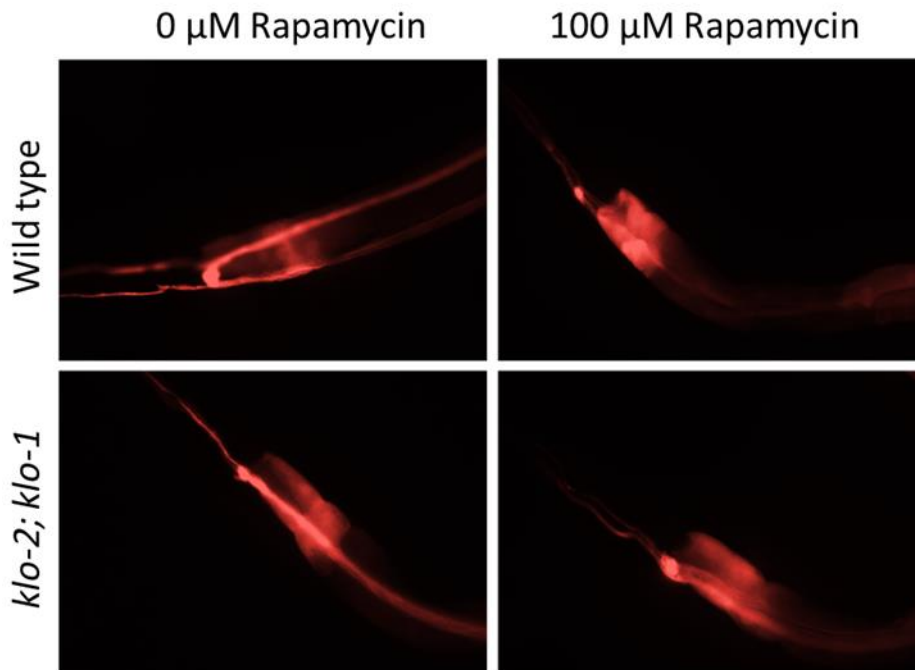
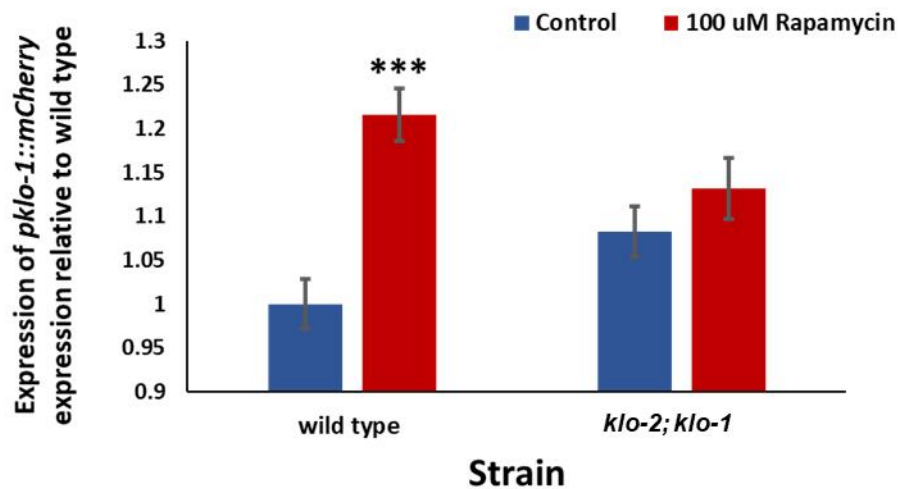
A**B**

Figure 5.11. Expression of *pklo-1::mCherry* reporter expression in wild-type vs *klo-2; klo-1* strains prior to and following treatment with 100 μ M rapamycin. A. Expression of *pklo-1::mCherry* in wild-type (top row) vs *klo-2; klo-1* double mutants (bottom row) in control (left column) vs 100 μ M rapamycin (right column) conditions. B. Relative expression of *pklo-1::mCherry* reporter expression where wild-type controls equal 1. Rapamycin treatment significantly increases *pklo-1::mCherry* reporter expression in wild-type animals but demonstrates no significant increase in expression in *klo-2; klo-1* double mutant strain. Control condition indicated in blue; rapamycin treatment indicated in red. Error bars

represent SEM. Mean pixel intensity was calculated from the first two intestinal cells of the animals. Asterisks indicate where rapamycin has a statistically significant impact on *pklo-1::mCherry* reporter expression versus the control condition, as determined using Tukey's test (*P < 0.05, **P < 0.01, ***P < 0.001).

Table 5.9. Relative expression of *pklo-1::mCherry* expression in wild-type vs *klo-2*; *klo-1* upon treatment with 100 μ M rapamycin. Relative expression of *pklo-1::mCherry* expression where wild-type expression is equal to 1. Assay repeated a minimum of 3 times. Statistical significance determined by Tukey's test, asterisks indicate significant values (*P < 0.05, **P < 0.01, ***P < 0.001).

Strain	Condition	n	Relative expression to wild-type	P values			
				Wild-type control	Wild-type treated	<i>klo-2</i> ; <i>klo-1</i> control	<i>klo-2</i> ; <i>klo-1</i> treated
Wild-type	0 μ M rapamycin	103	1.000	-	<0.001***	0.043*	0.004**
	100 μ M rapamycin	120	1.215	<0.001***	-	0.002**	0.070
<i>klo-2</i> (<i>ok1862</i>); <i>klo-1</i> (<i>ok2925</i>)	0 μ M rapamycin	113	1.08	0.043*	0.002**	-	0.274
	100 μ M rapamycin	102	1.132	0.004**	0.070	0.274	-

5.8.2. Rapamycin treatment shows no effect on *pklo-2::GFP* reporter expression in *C. elegans*
Treatment with rapamycin does not alter the expression levels of the *pklo-2::GFP* reporter in either wild-type or *klo-2; klo-1* double mutant animals. The expression of *klo-2* reporter in wild-type animals is 0.952 ($n = 134$) in rapamycin treated animals relative to wild-type controls where *pklo-2::GFP* expression is equal to 1 (Figure 5.12; Table 5.10).

Upon rapamycin treatment, there is no statistical difference in *pklo-2::GFP* expression in *klo-2; klo-1* which is 0.834 relative to wild-type controls. Similarly, to wild-type strains, *pklo-2::GFP* reporter expression is not altered in *klo-2; klo-1* double mutants upon exposure to rapamycin ($P = 0.512$ compared to *klo-2; klo-1* controls).

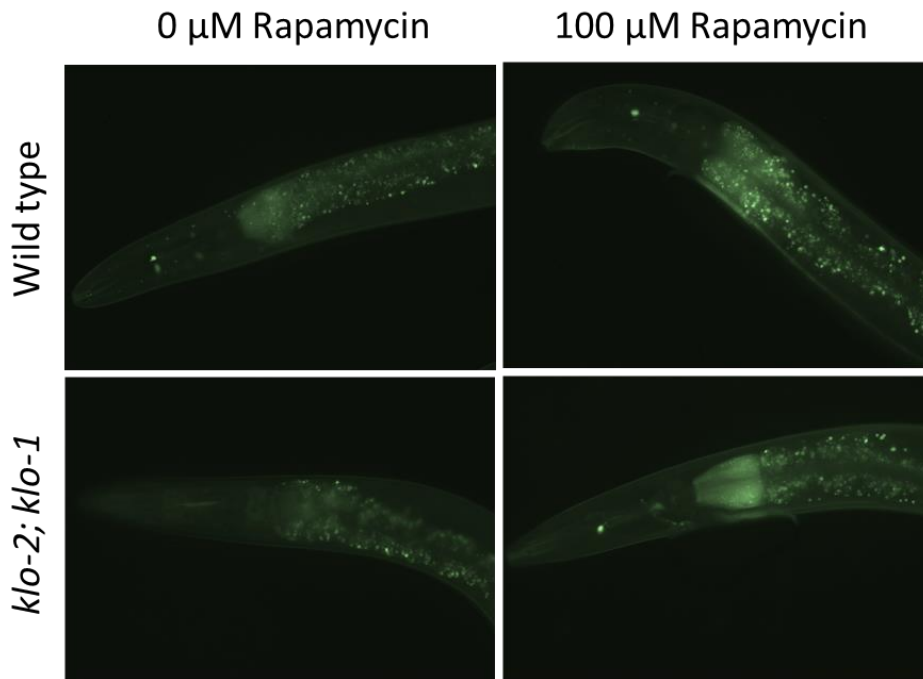
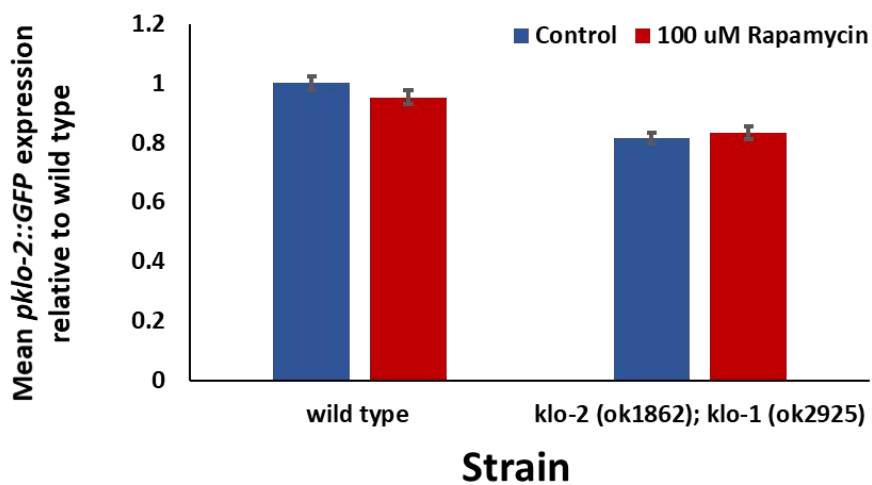
A**B**

Figure 5.12. Expression of *p klo-2::GFP* reporter expression in wild-type vs *klo-2; klo-1* strains. A. Expression of *p klo-2::GFP* reporter in wild-type (top row) vs *klo-2; klo-1* double mutants (bottom row) in control (left column) vs 100 μ M rapamycin (right column) conditions. B. Relative expression of *p klo-2::GFP* reporter expression where wild-type controls equal 1. Control condition indicated in blue; rapamycin treatment indicated in red. Error bars represent SEM. Mean pixel intensity was calculated from the first two intestinal cells of the animals with care taken to avoid collection of confounding data caused by gut granule

autofluorescence. Asterisks indicate statistical significance compared to wild-type, as determined using Tukey's test (*P < 0.05, **P < 0.01, ***P < 0.001).

Table 5.10. Relative expression of *pklo-2::GFP* reporter expression in wild-type vs *klo-2*; *klo-1* upon treatment with 100 μ M rapamycin. Relative expression of *pklo-2::GFP* reporter expression where wild-type expression is equal to 1. Assay repeated a minimum of 3 times. Statistical significance determined by Tukey's test, asterisks indicate significant values (*P < 0.05, **P < 0.01, ***P < 0.001).

Strain	Condition	n	Relative expression to wild-type	P values			
				Wild-type control	Wild-type treated	<i>klo-2</i> ; <i>klo-1</i> control	<i>klo-2</i> ; <i>klo-1</i> treated
Wild-type	0 μ M rapamycin	136	1.000	-	0.135	<0.001***	<0.001***
	100 μ M rapamycin	134	0.952	0.135	-	<0.001***	<0.001***
<i>klo-2</i> (<i>ok1862</i>); <i>klo-1</i> (<i>ok2925</i>)	0 μ M rapamycin	129	0.815	<0.001***	<0.001***	-	0.512
	100 μ M rapamycin	141	0.834	<0.001***	<0.001***	0.512	-

5.9. Western blotting for *aak-2*/AMPK

The increased expression of *klo-1* and *klo-2* reporters upon increased activation of AAK-2/AMPK indicates that AAK-2 could function upstream of KLO-1 and KLO-2, and that it is possible that *klo-2*; *klo-1* double mutants have increased AAK-2/AMPK activity compared to wild-type animals. To determine whether *klo-2*; *klo-1* mutants have altered levels of AMPK, Western blots were performed on wild-type and *klo-2*; *klo-1* double mutants to determine levels of total AAK-2 (total AMPK α), and its phosphorylated (activated) form, as per (Lee et al., 2008). Due to the loss of function of AAK-2/AMPK in *aak-2* (*gt33*) mutants, this strain was used as a negative control.

5.9.1. Western blotting for total AMPK in wild-type vs *klo-1*; *klo-1* double mutants

AAK-2 detection in wild-type, *aak-2* (*gt33*) and *klo-2*; *klo-1* strains used total-AMPK α antibodies (see '2.12. Western blotting of *C. elegans* extracts'). Upon initial blotting (see figure 5.13A), bands were visible in wild-type and *klo-2*; *klo-1* strains however these did not correlate with the predicted band weights for total-AMPK α which is predicted to be 62 kDa. No bands were shown in the *aak-2* (*gt33*) sample. Upon repetition of the blots, no bands were present in wild-type, *aak-2* (*gt33*) or *klo-2*; *klo-1* samples incubated in total-AMPK α antibodies (dilution 1:1000, see Figure 5.13B).

Western blotting was repeated for wild-type, *aak-2* (*gt33*) and *klo-2*; *klo-1* strains before and after treatment with either Forskolin or Paraquat (Figure 5.13C). Forskolin is a reported activator of AMPK (Alasbahi and Melzig, 2012), and paraquat was used to induce oxidative stress in animals prior to freezing, as this has been demonstrated to increase AAK-2/AMPK activity (Lee et al., 2008). For this a secondary antibody dilution of 1:500 was used.

To confirm that there were no issues with the antibody, a blot for total-AMPK α detection in HCT116 lysates was conducted. HCT116 is a human colorectal carcinoma cell line shown to have detectable AMPK α (Allende-Vega et al., 2015). A total-AMPK α antibody dilution of 1:500 was applied, and several bands were present ~60 kDa which is consistent with the predicted weight of total-AMPK α (Figure 5.13D).

Western blotting was repeated in wild-type, *aak-2* (*gt33*) and *klo-2*; *klo-1* *C. elegans* samples using 1:300 dilution of total-AMPK α antibody (Figure 5.13E). HCT116 cell sample was used as

a positive control. Here (Figure 5.13E), bands are shown ~60 kDa for the HCT116 cell line, suggesting the blot was successful in detecting AMPK in this particular sample. However, no bands were shown in any of the *C. elegans* samples.

Taken together, this suggests that total-AMPK α rabbit monoclonal antibodies are not compatible for the detection of AAK-2/ AMPK in *C. elegans* samples.

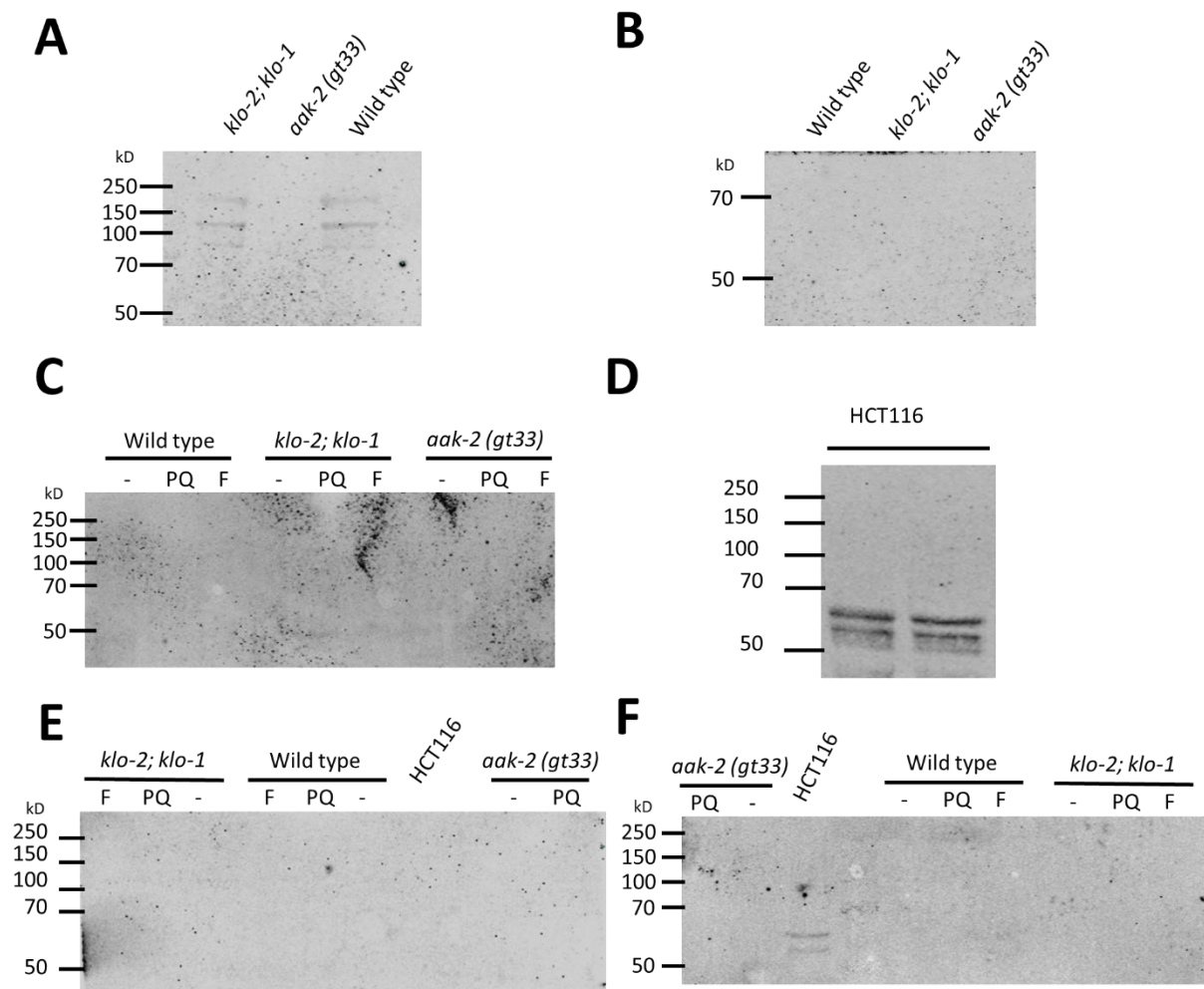


Figure 5.13. Western blotting for AAK-2/ AMPK in *C. elegans*. A and B. Detection of AAK-2 in wild-type, *aak-2(gt33)* and *klo-2; klo-1* animals using antibodies for total-AMPK α at a dilution of 1:1000. C. Detection of AAK-2 in wild-type, *aak-2(gt33)* and *klo-2; klo-1* prior to and following treatment with Forskolin (PQ) or Paraquat (PQ). Membranes were incubated in a 1:500 dilution of total-AMPK α antibody. D. Detection of AMPK in HCT116 cells. E. Detection of AAK-2 in wild-type, *aak-2(gt33)* and *klo-2; klo-1* prior to and following treatment with F

and PQ, using a 1:500 dilution of total-AMPK α antibody. HCT116 cells used as mammalian cell line control. F. Detection of AAK-2 in wild-type, *aak-2 (gt33)* and *klo-2; klo-1 C. elegans* extracts. HCT116 cells were used as a control. Animals were either untreated or incubated in either Forskolin (F) or paraquat (PQ) prior to blotting. Membranes were incubated in a 1:300 dilution of total-AMPK α antibody.

5.9.2. Western blotting for phosphorylated AMPK in wild-type vs *klo-2*; *klo-1* mutants

AMPK is activated through the phosphorylation of its catalytic α -subunit (Cheung et al., 2000, Hawley et al., 2003, Hawley et al., 1996, Xie et al., 2009). To determine whether there was a difference between wild-type and *klo-2*; *klo-1* double mutants for the activated form of AAK-2, membranes were incubated in a blocking solution containing anti-phospho-AMPK anti-rabbit antibody (Cell Signalling Technology).

Initial blotting of wild-type, *aak-2 (gt33)* and *klo-2*; *klo-1* strains was unsuccessful, with no bands present for any strain (Figure 5.14A). Blotting was repeated in wild-type, *aak-2 (gt33)* and *klo-2*; *klo-1* strains before and after treatment with either forskolin or paraquat. Membranes were incubated using a 1:1000 dilution of phospho-AMPK α antibodies, and as with total-AMPK α , phosphorylated AMPK is predicted to show bands at 62 kDa. However, a paper published by Lee et al. (2008) indicated phosphorylated AAK-2/ AMPK was detected in *C. elegans* samples at a weight just under 70 kDa.

Repetition of blotting showed bands slightly below 70 kDa and slightly above 50 kDa for wild-type and *klo-2*; *klo-1* strains untreated and paraquat conditions, however these were faint upon imaging (see Figure 5.14B). Interestingly, no bands were visible for *C. elegans* strains treated with Forskolin prior to freezing. In addition, it is unclear in this blot whether there are bands present in the *aak-2 (gt33)* strain which was selected for the purpose of being a negative control. Therefore, blotting was repeated using an increased dilution of antibody (1:500). Here, the bands displayed below 70 kDa, and above 50 kDa were more prominent in wild-type and *klo-2*; *klo-1* strains (Figure 5.14C). Here, bands were also visible in *C. elegans* samples that were subject to Forskolin treatment prior to freezing. Interestingly, this blot also shows bands of the same weight in the *aak-2 (gt33)* samples (Figure 5.14C). This was unexpected as the purpose of using the *aak-2 (gt33)* strain was as negative controls. Figure 5.14D shows that no phosphorylated AMPK is detected in HCT116 cells, however this is not unexpected for cells that have not been treated with a reagent that augments the activity of AMPK.

Figures 5.14E and 5.14F show repetitions of phosphorylated AAK-2/ AMPK detection using antibody dilutions of 1:500 and 1:300, respectively. Figure 5.14E again shows bands ~70 kDa in all samples, though these faint in the untreated wild-type sample and the *aak-2 (gt33)*

samples (Figure 5.14E). Figure 5.14F showed no bands upon imaging, suggesting an issue with the blotting process for this repetition.

While bands of ~70 kDa in *C. elegans* samples is consistent with previous literature suggesting this could be detection phosphorylated AAK-2, there is concern for the presence of these in *aak-2 (gt33)* samples that were intended as negative controls. Upon closer detection of blots presented in the Lee et al. (2008), these bands in *aak-2 (gt33)* can be expected. This paper goes on to suggest that true phosphorylated AAK-2 is present in *C. elegans* strains that have been treated with paraquat, but this band is present slightly higher than the band shown in these blots. The bands presented in the (Lee et al., 2008) are much fainter than the bands shown at ~70 kDa and are only found in animals exposed to oxidative stress. The blots found in Figure 5.14 do not display a band above those found ~70 kDa in wild-type, *aak-2 (gt33)* and *klo-2; klo-1* suggesting the bands shown are not related to phosphorylated AAK-2, and therefore phosphorylated AAK-2 has not been detected in *C. elegans* here.

It could be that our protein load was much lower, as Lee et al. (2008) used 6 plates worth of nematodes for SDS-PAGE, in comparison to our *C. elegans* collection methods for blotting (see '2.12. Western blotting of *C. elegans* extracts'), which meant phosphorylated AAK-2 was not detected in our samples.

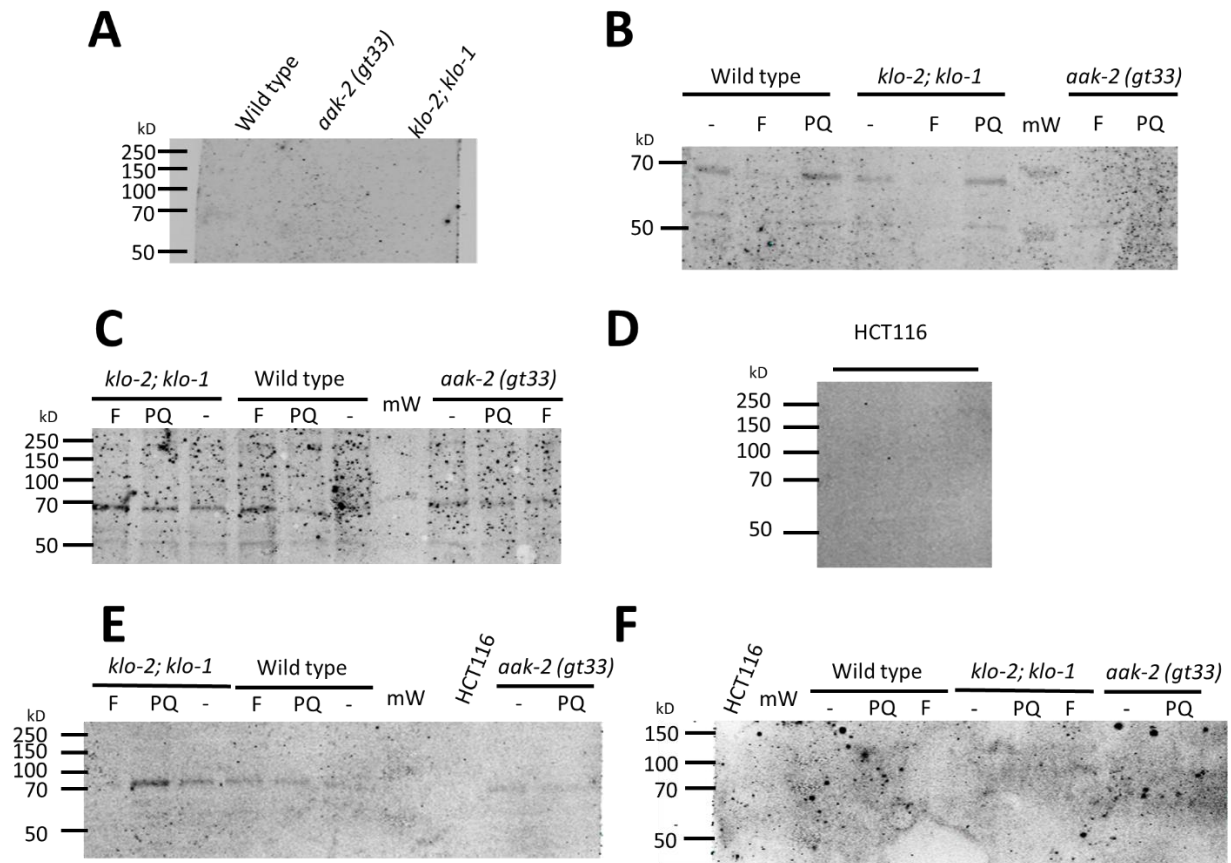


Figure 5.14. Detection of AAK-2 phosphorylation in *C. elegans* strains prior to and following Paraquat (PQ) or Forskolin (F) treatment. A. Detection of phosphorylated AAK-2 in wild-type, *aak-2 (gt33)* and *klo-2; klo-1* strains. Membranes were incubated in antibodies for phospho-AMPK α at a dilution of 1:1000. B and C. Detection of phosphorylated AAK-2 in wild-type, *aak-2 (gt33)* and *klo-2; klo-1* extracts prior to and following treatment with either Forskolin (F) or paraquat (PQ). Detection done using phospho-AMPK α antibodies at a dilution of 1:1000 (Figure 5.14B) and 1:500 (C). D. Detection of phosphorylated AMPK in HCT116 cells using 1:500 dilution of phospho-AMPK α antibodies. E. Detection of phosphorylated AAK-2 in wild-type, *aak-2 (gt33)* and *klo-2; klo-1* prior to and following treatment with F and PQ, using a 1:500 dilution of phospho-AMPK α antibody. HCT116 cells used as mammalian cell line control. F. Detection of AAK-2 in wild-type, *aak-2 (gt33)* and *klo-2; klo-1* extracts. HCT116 cells used as control. Membranes were incubated in a 1:300 dilution of phospho-AMPK α antibody.

5.10. Discussion: survival advantages of *klo-1/ KL* and *klo-2/ KL* deletion mutants is dependent on functional AAK-2/ AMPK

5.10.1. *klo-1* mutants require *aak-2/ AMPK* in heat stress responses

Analysis of acute heat stress responses in *C. elegans* reveals a trend for increased survival for *klo-1* and *klo-2* single mutants, that is diminished to that of wild-type in *klo-2; klo-1* mutant animals. As *klo-1/ KL* and *klo-2/ KL* genes are paralogous, it could be that absence of one promotes the expression of another conferring stress resistance, but removal of both diminishes these survival advantages to that of wild-type.

C. elegans with null *aak-2/ ampk* alleles are reported to display phenotypes of increased hypersensitivity to heat shock so it is unsurprising that these strains are shown to display some diminished survival compared to wild-type counterparts upon exposure to heat (Apfeld et al., 2004). In combination with *klo-1/ KL* and *klo-2/ KL* deletion alleles revealed that AAK-2/ AMPK is required for the survival of *klo-1* mutants upon exposure to acute heat stress. Intriguingly, *aak-2* null mutations in combination with *klo-2* genetic deletion did not cause the same diminished survival upon heat stress exposure. It could be that in the absence of *KLO-2/ KL*, paralogous *klo-1/ KL* expression could be upregulated to counteract this and confer heat stress resistance to these strains in a manner independent of functional AAK-2/ AMPK. It could be worth crossing a *pklo-1::mCherry* reporter into *klo-2; aak-2* mutants and examining them following heat stress exposure to consolidate this theory.

5.10.2. AAK-2/ AMPK is required for oxidative stress resistance in *klo-1/ KL* and *klo-2/ KL* deletion mutants

Data collected from acute paraquat survival assays suggests that *klo-1/ KL* and *klo-2/ KL* deletion mutants require functional AAK-2/ AMPK for survival advantage over wild-type animals. In addition, manipulation of AAK-2/ AMPK activity by pharmacological means, using Forskolin or metformin, suggests *klo-2; klo-1* mutants have increased AAK-2/ AMPK activity compared to wild-type counterparts.

Taken together, if *klo-1/ KL* and *klo-2/ KL* deletion mutants have increased AAK-2/ AMPK activity, this could explain why upon acute oxidative stress exposure, these strains have increased survival compared to wild-type animals, as AMPK activity is linked to a reduction in reactive oxygen species (Zhao et al., 2017b). This theory would also support the observation

that staining for ROS was lowered in *klo-2; klo-1* double mutants, because if AAK-2/ AMPK activity is increased in these strains this may reduce the volume of ROS in these animals.

However, it should be noted that it was not possible to confirm through means of western blotting whether AAK-2/ AMPK activity is increased in *klotho* mutant strains, therefore these deductions require further research to confirm this hypothesis. In addition, this theory does not explain why the phenomenon of increased survival upon oxidative stress exposure in *klo-1/KL* and *klo-2/KL* deletion mutants is temporary. If these mutants did have increased AMPK activity, it could be expected that they should display prolonged longevity compared to wild-type counterparts given reports that overactivation of AAK-2/ AMPK promotes lifespan extension in *C. elegans*, yet while we see there is some longevity promoting effects of *klo-1/KL* mutants, this is not to the same degree as observed in cases of AAK-2/ AMPK overactivation (Curtis et al., 2006)

To determine whether *klo-2; klo-1* strains have increased AAK-2/ AMPK activity compared to wild-type counterparts, western blotting using total-AMPK and phospho-AMPK antibodies was attempted using wild-type, *klo-2; klo-1* and *aak-2 (gt33)* strains with varying success. Total-AMPK detection was unsuccessful on *C. elegans* samples tested here.

Phospho-AMPK α antibodies revealed bands present at the predicted weight in *C. elegans* extracts, however these were present in *aak-2 (gt33)* strain extracts which are presumed null mutants (Apfeld et al., 2004), and should therefore not show activated (phosphorylated) AAK-2/ AMPK in sample. Lee et al. (2008) reported similar findings for this strain and determined that the band present here was non-specific to phospho-AMPK. Lee et al. (2008) determined that phospho-AMPK α was present in wild-type strains following treatment with Paraquat, and that this band was much fainter, and had a slightly higher band weight than the prominent band present ~62 kDa in these nematode extracts. Findings presented here did not show these bands and therefore no conclusions could be drawn.

It could be that the sample size was too low for phospho-AMPK α detection. Nematode extracts were collected as per '2.12.2. Preparation of *C. elegans* extracts', adapted from (Hyman lab, n.d.) collecting 50-100 nematodes per sample. In contrast, Lee et al. (2008) collected six plates per strain for nematode extracts to use for blotting and used an antibody dilution of 1:300 to generate these faint bands upon paraquat treatment. Therefore, it could

be that the quantities of AAK-2/ AMPK in *C. elegans* are too low for detection using these methods and alternative protocols need to be used.

5.10.3. AAK-2/ AMPK could function upstream of KLO-1 and KLO-2

Pharmacological activation of AAK-2/ AMPK via Forskolin and metformin, increased the expression of *klo-1* and *klo-2* reporters in wild-type and *klo-2*; *klo-1* strains indicating an upstream function of AAK-2/ AMPK in KLO-1/ KL and KLO-2/ KL signalling processes in *C. elegans*. These findings support existing literature for a DAF-16/ FOXO-AAK-2/ AMPK feedback loop (Tullet et al., 2014). Findings from Buj have shown *klo-1/ KL* and *klo-2/ KL* deletion strains require *daf-16/ foxo* (Buj & Kinnunen, Manuscript in preparation), however no suggested link to AAK-2 has been made until now. It is known that AAK-2/AMPK activates DAF-16/FOXO, and that there is a feedback mechanism as DAF-16/FOXO promotes the transcription of an AMPK subunit (Tullet et al., 2014). *klo-1/ KL* has also been identified as a Class I responsive gene which is upregulated upon DAF-16/FOXO activation (Tepper et al., 2013), which could explain why there is an increase in *klo-1* reporter expression if these mutants have increased AAK-2/AMPK activity.

5.11. Discussion: a role for TOR signalling in klotho-governed responses

Pharmacological inhibition of TOR signalling using rapamycin increased the expression of *pklo-1::mCherry* and *pklo-2::GFP* reporter expression in wild-type animals, whereas rapamycin had no significant effect on *klo-1* or *klo-2* reporter expression in *C. elegans* strains of *klo-2*; *klo-1* genetic backgrounds. This suggests that TOR signalling pathways could be diminished in *klo-1/ KL* and *klo-2/ KL* mutant strains. Alternatively, TOR activation could require KLO-1/ KL and/ or KLO-2/ KL meaning in nematodes with genetic deletion of either *klo-1/ KL* or *klo-2/ KL* this feedback loop is lacking. This could explain why *klo-1/ KL* and *klo-2/ KL* mutant strains are predicted to have increased AAK-2/ AMPK activity, as TOR and AMPK signalling pathways are reported to function antagonistically to one another (Hindupur et al., 2015, Mounier et al., 2011).

Interestingly, other data has shown that knockdown of *rsk-1/ S6K* (a key component for TOR pathway signalling) in *C. elegans* has little effect on longevity in the nematode until combined

with *daf-2/InsR* hypomorphic alleles where it produces an almost 5-fold extension of lifespan in these strains (Chen et al., 2013a). These findings have striking similarities with previous lab data by Buj that show *klo-1/KL* and *klo-2/KL* deletions have no effects on lifespan in *C. elegans* alone, but in combination with *daf-2* hypomorphic alleles display a similar lifespan to *daf-2; rsk-1* mutants reported by Chen et al. (2013a) (Buj & Kinnunen, Manuscript in preparation). This same paper also showed a trend for increased resistance of *rsk-1* mutants upon exposure to oxidative stress (compared to wild-type), offering more similarities to our *klo-1/KL* and *klo-2/KL* strains.

Taken together, this could suggest that the stress response phenotypes displayed by our *klo-1/KL* and *klo-2/KL* *C. elegans* strains could be attributed to a knockdown of TOR signalling in these mutants, which would also give cause for the predicted increase in AAK-2/ AMPK activity given these pathways function in an antagonistic manner (Hindupur et al., 2015, Mounier et al., 2011).

5.11.1. Chapter five conclusions

To summarise, the main conclusions drawn from the data presented in this chapter are as follows;

- Preliminary data supports the hypothesis that pharmacological activation of AAK-2 leads to increased expression of *klotho* reporters in *C. elegans*.
- Preliminary data suggests that phenotypes displayed by *klotho* mutants could be consistent with diminished TOR signalling, offering plausibility to the hypothesis that *klotho* mutants may exhibit increased AAK-2/ AMPK function.

Chapter 6: Stress responses in *C. elegans* with altered klotho function could be linked to the antagonistic pathways of AMPK and mTOR

6.1. *klo-1/ KL* and *klo-2/ KL* mutants display similar longevity phenotypes to strains with diminished mTOR activity

Given the reported anti-aging properties of klotho (Arking et al., 2005, Chen et al., 2013b, Kuro-o et al., 1997, Kurosu et al., 2005, Majumdar and Christopher, 2011), it is interesting to find that deletion of either *klo-1/ KL* or *klo-2/ KL* has no immediate impact to lifespan of *C. elegans*. What is more intriguing to note is the phenomenon previously reported from our lab that suggests the lifespan of *daf-2/ InsR* mutants (which already demonstrate increased lifespan compared to wild-type counterparts (Kenyon et al., 1993), is further increased in combination of *klo-1/ KL* or *klo-2/ KL* deletion, leading to the conclusion that KLO-1/ KL and KLO-2/ KL do have roles in longevity in *C. elegans* but this is only demonstrable when in combination with diminished IIS (Buj & Kinnunen, manuscript in preparation).

This phenomenon has been demonstrated previously in *C. elegans* strains with hypomorphic *daf-2/ InsR* backgrounds in combination with deletion of *rsks-1/ S6K* (Chen et al., 2013a). Chen et al (2013) noted that *rsks-1/ S6K* mutants, which display diminished TOR signalling, have lifespans similar to that of wild-type counterparts, but in combination with *daf-2/ InsR* hypomorphic alleles, lifespan is extended 5-fold in the nematode (Chen et al., 2013a). As noted previously (see Chapter 3, “3.6.1.1. Lifespan in *C. elegans* of *klo-1/ KL* and *klo-2/ KL* genetic backgrounds”), the lifespan of *daf-2; rsks-1* mutants is dependent on DAF-16/ FoxO activity via AAK-2/ AMPK (Chen et al., 2013a), and is strikingly similar to that of *daf-2; klo-2* mutants (Buj, 2019). The mechanism for lifespan extension in *daf-2* hypomorphic alleles is through suppression of reproductive death which has great impact on longevity in *C. elegans* (Gems et al., 2021). It could be that the suppression of reproductive death in these strains unmask the effect of *rsks-1* mutation and that a similar effect is exhibited in *daf-2; klo-2; klo-1* mutant strains.

This leads to the question of whether the lifespan effects demonstrated by *C. elegans* with *klo-1/ KL* and *klo-2/ KL* deletion backgrounds could be consistent with diminished TOR signalling. If we couple this theory with subsequent findings that the stress resistance phenotypes demonstrated by *klo-1/ KL* and *klo-2/ KL* animals suggests increased activity of

AAK-2/ AMPK (see Chapter 5), which functions antagonistically to the TOR signalling pathway, we can begin to build a plausible picture of the signalling mechanisms altered by *klo-1/ KL* or *klo-2/ KL* deletion.

If longevity in *klo-1/ KL* and *klo-2/ KL* strains is mediated by TOR signalling, this would be consistent with existing literature for other organisms (Bjedov et al., 2010, Harrison et al., 2009, Strong et al., 2020). Lifespan in murine models can be extended as a result of rapamycin treatment (Harrison et al., 2009, Strong et al., 2020). In addition, a study conducted by Bjedov et al (2010) found that in *Drosophila melanogaster*, genetic downregulation of TOR pathways could increase lifespan of reduced IIS pathway mutants, and that inhibition of TOR by rapamycin was linked to increased oxidative stress resistance (Bjedov et al., 2010).

Given that TOR signalling functions antagonistically to AMPK signalling, it is no surprise that increased activation of AMPK has been demonstrated to extend lifespan in several organisms, while reduced activity of this signalling component is associated with diminished lifespan (Apfeld et al., 2004, Curtis et al., 2006, Funakoshi et al., 2011, Salminen and Kaarniranta, 2012, Viollet et al., 2003). What is not clear here is why, if *klo-1/ KL* or *klo-2/ KL* deletion mutants have increased AAK-2/ AMPK activity, that this is not reflected in the lifespan of the organism unless in combination with mutations for diminished IIS activity. It is noted that the majority of lifespan extending effects of AAK-2/ AMPK activity are in relation to dietary restriction as reduced energy levels initiate activity of this enzyme (Greer et al., 2007), therefore it would be useful to explore the use of dietary restriction techniques in *klo-1/ KL* and *klo-2/ KL* strains to determine if this may have an impact on longevity in these animals.

Another interesting route to explore would be to utilise the *rsks-1* hypomorphism in *klo-1* and *klo-2* mutant backgrounds in combination with *daf-2*. The build of triple and quadruple mutant strains for diminished TOR, IIS and functional klotho followed by epistatic analyses as demonstrated throughout this research could serve to elucidate the complex cross-talks between the TOR, IIS and Klotho-FGF pathways underlying longevity and stress responses in *C. elegans*.

6.2. KLO-1/ KL and KLO-2/ KL have demonstrable links to increased AAK-2/ AMPK activity, and decreased mTOR activity in *C. elegans*

This research has demonstrated that activation of AAK-2/ AMPK, or inhibition of TOR signalling in *C. elegans* leads to increased expression of nematode *klothos* (see 'Chapter 5: The effects of *aak-2/ AMPK* knockdown in *klo-1* and *klo-2* mutants'). Rapamycin has previously been demonstrated to increase expression of *klotho* mRNA in murine models both *in vivo* and *in vitro* (Zhao et al., 2015), consistent with our findings here of increased *pklo-1::mCherry* expression upon treatment with the TOR inhibitor. Likewise, several studies have demonstrated that AMPK activation increases the expression of FGF21, *klotho* and β -*klotho* in murine models (Cheng et al., 2017, Nygaard et al., 2012, Videla et al., 2018) indicating that AAK-2/ AMPK functions upstream of KLO-1/ KL and KLO-2/ KL (see Figure 6.1).

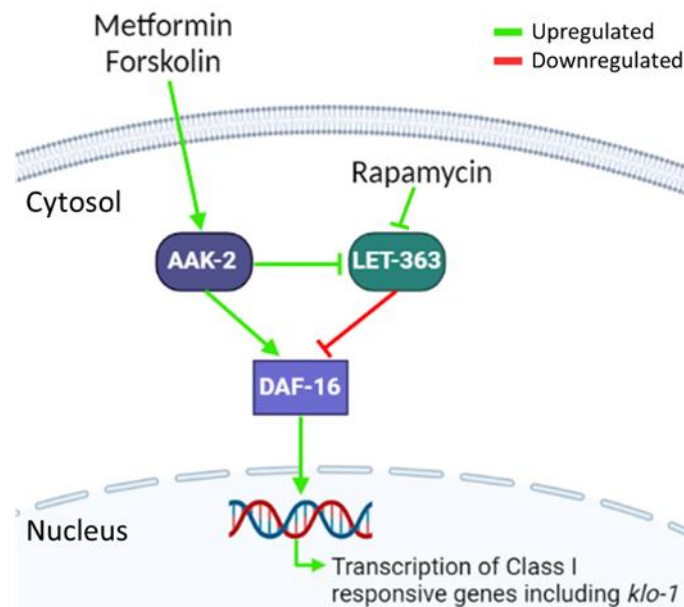


Figure 6.1. Schematic diagram representing effects of AAK-2/ AMPK activators and TOR inhibitors on *klo-1/ KL* expression in *C. elegans*. Upregulated processes indicated in green, downregulated pathways indicated in Red. Metformin or Forskolin is able to increase AAK-2/ AMPK activity leading to activation of downstream transcription factors including DAF-16/ FOXO. Activation of DAF-16/ FOXO promotes the transcription of Class I responsive genes including *klo-1*, offering explanation to why *pklo-1::mCherry* reporter expression is increased following treatment with AMPK activators. Similarly, rapamycin functions to inhibit the TOR signalling pathway. LET-363 is orthologous to mammalian target of rapamycin (mTOR) and functions to suppress DAF-16/ FOXO when active. Rapamycin inhibits pathways governed by

LET-363/ mTOR meaning DAF-16/ FOXO is able to translocate to the nucleus to facilitate transcription of downstream genes, therefore rapamycin promotes the expression of *klo-1* in *C. elegans*. Image created in BioRender.

Findings also revealed that nematodes with deletion alleles of these *klo-1* and *klo-2* genes naturally display higher expression of the *pklo-1::mCherry* reporter. Taken together, this could suggest that the reason *klo-2; klo-1* double mutants display increased expression of this *pklo-1::mCherry* reporter could be the result of increased AAK-2/ AMPK activity, or decreased TOR signalling in this strain. Coupled with the effects of *klo-1/ KL* and *klo-2/ KL* deletion on lifespan (discussed above), and acute oxidative stress responses (see below, '6.3. Oxidative stress responses in *klo-1/ KL* and *klo-2* mutants are characterized by increased AAK-2/ AMPK function') these findings further corroborate this theory.

What is interesting here is if there is increased AAK-2/ AMPK activity in this strain, we do not see the same prolonged protective effects consistent with constitutively active AAK-2/ AMPK activity (Hwang et al., 2014). This could mean that removal of KLO-1/ KL or KLO-2/ KL does not directly lead to activation AAK-2/ AMPK, but rather removal of these proteins could perhaps lead to a low energy state expected to promote increased AAK-2/AMPK activity (Hardie et al., 2012). This AAK-2/ AMPK activation that could lead to a cascade to activate DAF-16/ FOXO, for which *klo-1* has been identified as a Class I responsive gene upregulated upon activation of this transcription factor (Tepper et al., 2013), offering a potential mechanism for why *pklo-1::mCherry* reporter expression is increased upon removal of functional KLO-1/ KL and KLO-2/ KL proteins.

6.3. Oxidative stress responses in *klo-1/ KL* and *klo-2/ KL* mutants are characterized by increased AAK-2/ AMPK function

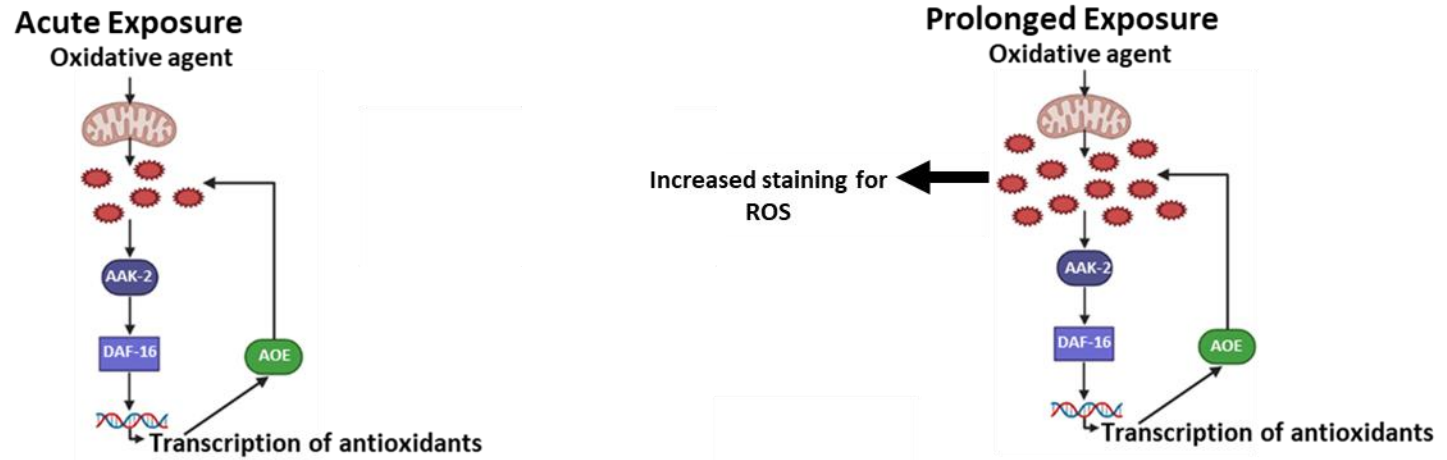
The resistance to acute oxidative stress displayed by *klo-1/ KL* and *klo-2/ KL* mutants suggests this could be attributed to increased AAK-2/ AMPK activity in the nematode (see 'Chapter 5: The effects of *aak-2/ AMPK* knockdown in *klo-1* and *klo-2* mutants'). AAK-2/ AMPK is known to function upstream of DAF-16/ FoxO to promote the transcription of several antioxidant and stress response genes which could confer these stress response phenotypes to *klo-1/ KL* and *klo-2/ KL* strains (Greer et al., 2007, Wang et al., 2017b, Wang et al., 2011, Zhao et al., 2017b). If these strains have upregulated stress responses it could mean that at the point of treatment with an oxidative agent, the antioxidant enzymes are able to "mop up" the ROS

generated, reflecting the lowered CellROX staining of ROS and the increased survival upon paraquat exposure (as discussed in Chapter 5).

Increased AAK-2/AMPK activity in *klotho* deficient nematodes could explain the increased survival of these animals when exposed to acute oxidative stress, and could provide a role for *klotho* in a previously discovered DAF-16/FOXO-AAK-2/AMPK feedback loop. Findings from Buj has shown that *klo-1* and *klo-2* require DAF-16/FOXO for oxidative stress responses (Buj and Kinnunen, manuscript in preparation). Previous findings have not suggested a link to AAK-2, but this research has. It is known that AAK-2/AMPK activates DAF-16/FOXO, and that there is a feedback mechanism as DAF-16/FOXO promotes the transcription of an AMPK subunit (Tullet et al., 2014).

One striking finding was that while deletion of *klo-1/KL* or *klo-2/KL* conferred acute oxidative stress resistance to the organism, this stress resistance diminished over time so that upon chronic exposure to stress, *klo-1* or *klo-2* strains showed little difference to their wild-type counterparts. In this instance, it could be that while these deletion strains have an advantage of increased antioxidant activity at the time of exposure to oxidative stress, over time the generation of ROS (caused by the oxidative agent) overrides these antioxidant responses contributing to detrimental effects on the health and survival of the organism. A schematic depiction of the proposed theory of mechanism can be found in Figure 6.2. However, in instances where AAK-2 is constitutively active, *C. elegans* display increased survival upon chronic exposure to paraquat, which is not demonstrated by *klo-1/KL* or *klo-2/KL* mutants (Hwang et al., 2014).

A



B

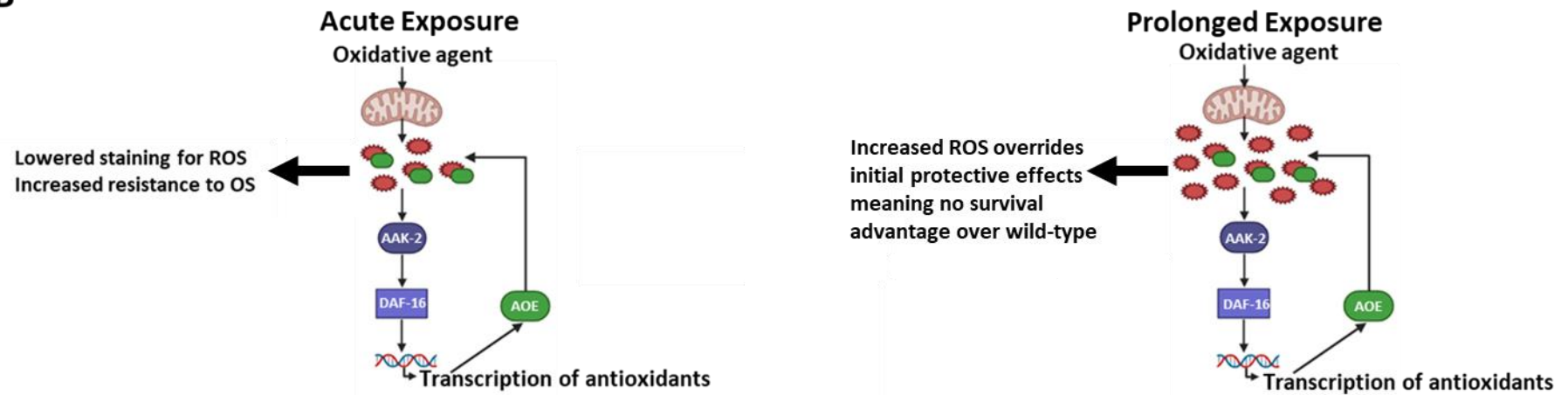


Figure 6.2. Schematic depiction of proposed hypothesis for acute and prolonged oxidative stress responses in wild -type, *klo-1/ KL* and *klo-2/ KL C. elegans*. A. Depiction of oxidative stress responses in wild-type nematodes. Upon exposure to oxidative agent, ROS are increased in

the cells of the organism, contributing to activation of several signalling cascades including pathways governed by AAK-2/ AMPK. AAK-2/ AMPK activates several transcription factors including DAF-16/ FOXO to promote the transcription of antioxidant genes. Antioxidant enzymes (AOE) then function to neutralise potentially harmful ROS. Upon prolonged exposure to oxidative agent, ROS build up in the cells which leads to increased staining for ROS when nematodes are treated with CellROX. **B. Depiction of oxidative stress responses in *C. elegans* mutants with *klo-1/ KL* or *klo-2/ KL* genetic backgrounds.** It is hypothesised that nematodes with deletion of *klo-1/ KL* or *klo-2/ KL* have upregulated stress responses meaning when treated with an oxidative agent, ROS are “mopped up” quicker than in wild-type counterparts leading to increased oxidative stress resistance and reduced staining for ROS in these mutants. Upon prolonged exposure to oxidative agent, it is believed that over time the build-up of ROS overrides the system’s ability to neutralise these potential harmful ROS, leading to increased staining for ROS upon CellROX treatment and could also explain why they display no survival advantage over wild-type counterparts following prolonged exposure to oxidants.

There are some reports that indicate that prolonged overactivation of AMPK may have a detrimental impact on organismal health which could offer some indication as to why these stress resistance phenotypes may only be present in acute scenarios (Kosztelnik et al., 2019). Kosztelnik et al (2019) describe a feedback mechanism whereby under prolonged oxidative stress, increased AAK-2/ AMPK activity can lead to hyperactivation of autophagy. This hyperactivation of autophagy has been demonstrated to have detrimental effects if left uncontrolled (Lewis et al., 2015). It was identified that this hyperactivation of autophagy is negatively regulated by SKN-1/ Nrf2, and that silencing of SKN-1/ Nrf2 resulted in constant activation of AMPK and autophagy overactivation (Kosztelnik et al., 2019). This hypothesis could offer some explanation to why *klo-1/ KL* and *klo-2/ KL* deletion mutants exhibit signs of increased AAK-2/ AMPK activity if SKN-1/ Nrf2 is silenced. This could be an interesting theory to probe into as SKN-1/ Nrf2 activation typically promotes stress resistance consistent with protective effects of klotho in other organisms (Balasubramanian and Longo, 2010, Maltese et al., 2017), but if SKN-1/ Nrf2 is silenced in the absence of functional KLO-1/ KL and KLO-2, this would offer explanation as to why there are protective effects linked to overactivation of AAK-2/ AMPK in acute responses, but not for prolonged time periods. This could also elucidate on the strange phenomena that while *klo-1* and *klo-2* mutations are predicted to be loss-of-function mutations (Polanska et al., 2011), which in other organisms would be consistent with decreased stress resistance (Chen et al., 2013b, Kuro-o et al., 1997, Yamamoto et al., 2005), the data presented here suggests that there could be some acute protective effects of removal of functional KLO-1/ KL and KLO-2/ KL. However, there is currently a lack of data to support this theory, and preliminary data using autophagy reporters (see '3.5. Effects of *klo-1* and *klo-2* deletion on autophagy reporter expression') suggests *klo-1/ KL* and *klo-2/ KL* mutants exhibit lower expression of these markers which would be contradictory to this theory.

6.4. The theory that klotho inhibits IIS pathway in stress responses could be attributed to AMPK-TOR-IIS crosstalk

Several studies have proposed that klotho activity could negatively regulate the IIS pathway, although the mechanisms governing this remain ambiguous (Kurosu et al., 2006, Lim et al., 2017, Utsugi et al., 2000, Wolf et al., 2008, Yamamoto et al., 2005). Given the findings of this research that AAK-2/ AMPK and TOR signalling pathways could be heavily implicated in the expression of *klo-1* and *klo-2* and stress responses governed by KLO-1/ KL and KLO-2/ KL, it should be considered that the effects of klotho on IIS could be governed by the antagonistic relationship between AMPK and TOR.

It has been theorised that klotho could function to indirectly inhibit the IIS pathway through activation of parallel signalling cascades (Buj, unpublished, Château et al., 2010, Lorenzi et al., 2010). Klotho upregulates antioxidants via FoxO-dependent mechanisms to negatively regulate PI3K, an integral component to the IIS pathway (Lim et al., 2017, Yamamoto et al., 2005). Similarly, AMPK suppresses IIS through inhibition of IRS-1 as well as activating FoxO transcription factors (Greer et al., 2007, Jakobsen et al., 2001, Wang et al., 2011).

Given that AMPK is reported to function antagonistically to mTOR (Kim et al., 2011b), and inhibition of mTOR is associated with increased klotho secretion in murine models (Lin et al., 2013), it is no surprise that rapamycin treatment, or pharmacological activation of AMPK leads to increase of *klotho* reporter expression in *C. elegans*.

The above, coupled with reports that FGF19, -21, -23 function in AMPK-dependent pathways (Glosse et al., 2018, Guo et al., 2020, Li et al., 2018, Nygaard et al., 2012), and evidence presented in this research that suggests stress responses in *klo-1/ KL* and *klo-2/ KL* mutants is dependent on functional AAK-2/ AMPK, we can begin to build a picture of how klotho functions to impact AMPK-TOR-IIS crosstalk (see Figure 6.3).

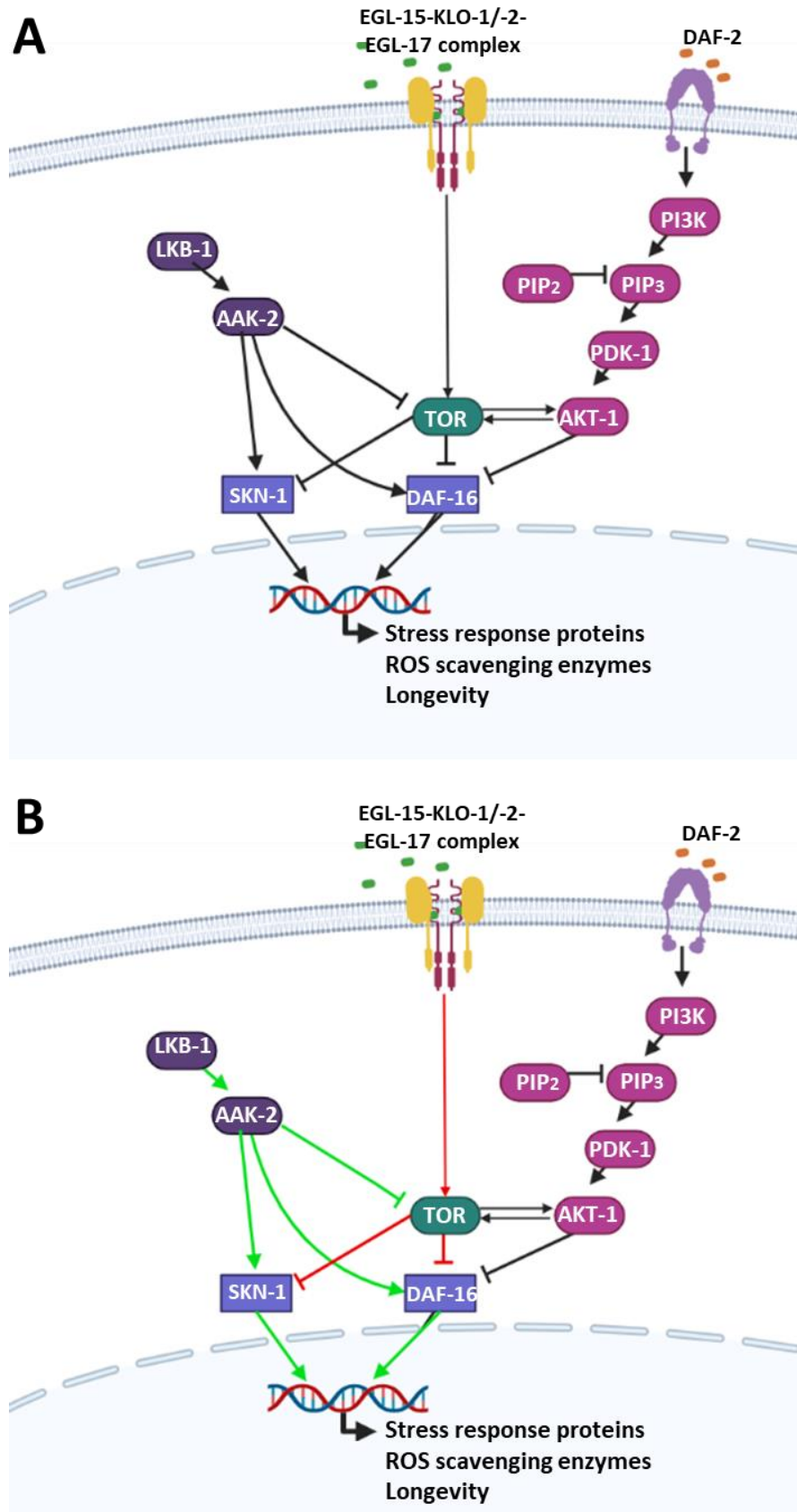


Figure 6.3. Schematic diagram of proposed crosstalk of klotho, AMPK, TOR and IIS signalling in *C. elegans*. A. Klotho signalling in wild type *C. elegans*. Upon typical conditions, klotho

functions upstream of TOR to mediate stress responses and metabolism in *C. elegans*. **B. Klotho signalling in *klo-1/ KL* mutants.** Diminished klotho signalling, accomplished through deletion of *klo-1* or *klo-2* leads to diminished TOR signalling (indicated by red arrows to suggest this pathway is downregulated upon *klo-1/ KL* deletion). This diminished TOR signalling means the antagonistic AAK-2 pathway can promote the transcription of stress responses in *C. elegans* via DAF-16 and SKN-1 (this is indicated by green arrows to suggest the pathway may be upregulated upon *klo-1/ KL* deletion).

Chapter 7: Limitations and future directions

7.1. Limitations: impact of COVID-19 on research output

Following announcement of a nationwide lockdown on 23rd March 2020 as a result of the COVID-19 pandemic, laboratory access was prohibited until August 2020 where lab work was permitted with restrictions in place. Following return to the lab, it was discovered that some *C. elegans* genetic crosses that were carried out prior to lockdown had been lost, due to limitations in generating frozen stocks. In addition, whilst a three-month laboratory extension was granted as a result of the pandemic, the lost lab time during lockdown combined with restricted access and loss of strains following return meant research was impeded.

For example, a cross to generate *klo-1* and *klo-2* strains positive for the *lgg-1::GFP* reporter used to examine autophagy in *C. elegans* was conducted prior to lockdown. Nematodes positive for this reporter are rollers, and as a result the strain is maintained via positive selection of nematodes displaying roller phenotypes. Following lockdown, a *klo-2; klo-1* double mutant strain was lost due to unsuccessful recovery of roller nematodes. This strain had a bacterial contamination prior to lockdown which limited the successful storage of frozen stocks for this strain. Due to time constraints upon return to the lab, this genetic cross could not be repeated therefore data is missing for this strain.

Other impacted assays included hexokinase activity in *C. elegans* homogenate solutions and chronic starvation of wild-type, *klo-1/KL* and *klo-2/KL* strains. Therefore, these assays require improvements and technical repeats, discussed further below.

7.2. Improvements and future work

7.2.1. Investigating the impact of KLO-1 and KLO-2 in autophagic responses

As mentioned above, there were some limitations gathering data for *klo-2; klo-1* strains positive for the *lgg-1::GFP* reporter used to detect autophagy in *C. elegans*. In addition, the data collected here for *LGG-1::GFP* expression in wild-type, *klo-1* and *klo-2* strains is preliminary and requires improvements and technical repeats.

The sample size for this assay was low (~20 animals per strain), and images were taken using a 20 X 100 objective which made quantification of puncta more difficult in these animals. This

assay should be repeated using a greater magnification (63 X 100 objective) and sample size should be increased to be able to reasonably draw conclusions from this data.

The data suggests that *klo-1/ KL* and *klo-2/ KL* deletion leads to impaired signalling of AAK-2/ AMPK and TOR signalling pathways in *C. elegans*, both of which are reported to impact autophagic response (Kim et al., 2011b). In addition, previous lab findings describe a phenotype in *C. elegans* that could be consistent with increased autophagy or necrosis in these animals. Therefore, it would be worthwhile to investigate this further. Another tool that could be implemented to investigate this could be an immunoblot-based assay detailed by (Chapin et al., 2015) where a dual fluorescent protein (dFP) is tagged to LGG-1. When LGG-1 is cleaved by lysosomal proteases, the linker between fluorescent tags on the protein release monomeric fluorescent protein (mFP) that can be probed using an anti-FP antibody to distinguish between full-length dFP and the released mFP offering a means of offering an alternative tool to measure autophagy in *C. elegans* (Chapin et al., 2015).

To further this research, a recent study published by Chang et al. (2017) suggests they have developed an antibody to quantify LGG-1 in *C. elegans*. This could be applied in tandem with the techniques outlined above to consolidate research into autophagy in *klotho* mutant strains.

7.2.2. Further work using *pklo-1::mCherry* and *pklo-2::GFP* reporters

In some cases, it was found that *klo-1/ KL* or *klo-2/ KL* single mutants had slightly greater survival advantages than *klo-2; klo-1* strains, it would be worth repetition of data collected using these *pklo-1::mCherry* and *pklo-2::GFP* reporters to be included with these findings. At the time of experiments, there were no single mutant strains positive for these reporters available. However, crossing of these reporters into single mutants should be relatively straightforward and quick compared to crossing for more complex compound strains.

In addition, it could be worth crossing these reporters into null *aak-2/ AMPK* mutants. If AAK-2/AMPK functions upstream of KLO-1/ KL and KLO-2/ KL, it could be expected that reporters for *klo-1/ KL* and *klo-2/ KL* in these strains would be reduced.

7.2.3. Hexokinase activity of *C. elegans* homogenates

FGF21 and β -klotho have reported roles in glucose metabolism (Ge et al., 2011, Kharitonov et al., 2005, Micanovic et al., 2009, Shi et al., 2018). Therefore, hexokinase assays were performed on *C. elegans* strains as a means to observe whether glucose metabolism may be altered in *klo-1/ KL* and *klo-2/ KL* deletion mutants. Initial readouts for hexokinase assay activity in wild-type, *klo-1*, *klo-2* and *klo-2; klo-1* showed a potential correlation between *klo-1/ KL* deletion with altered hexokinase activity (see appendix 3). However, there was large variation within these results, and technical repetition of this assay was not consistent with original findings.

Initial assays were conducted on mixed stage nematodes that were grown on NGM agar plates or liquid media culture. Preferably, these assays were to be conducted using age synchronised *C. elegans* however due to time limitations following the national lockdown, there was not enough time to collect age synchronised *C. elegans*. Therefore, it would be useful to examine activity in age synchronised nematodes.

7.2.4. Consolidation of the role of AAK-2/ AMPK in *klo-1/ KL* and *klo-2/ KL* deletion mutants

Data from Forskolin and metformin treatment on the expression of *pklo-1::mCherry* and *pklo-2::GFP* reporters suggest that AAK-2/ AMPK functions upstream of *klo-1/ KL* and possibly *klo-2*, and some of this data suggests *klo-2; klo-1* double mutants have increased AAK-2/ AMPK activity.

However, Forskolin functions via adenylyl cyclase having downstream functions on many pathways other than AMPK (Seamon et al., 1981), and it is not known whether the impacts of metformin on AMPK activity are via direct or indirect mechanisms (Hawley et al., 2002). Therefore, additional experiments would be required to confirm the status of AAK-2/ AMPK activity in these mutants.

It could be worth repetition of Western blotting for phosphorylated AAK-2/ AMPK in *C. elegans* extracts using a greater volume of nematodes for these extracts, to see if we can generate the same bands described by Lee et al. (2008). Alternatively, quantification of mRNA transcripts for AAK-2/ AMPK via qPCR could also determine whether the readouts from our Forskolin and metformin assays are consistent with altered AAK-2/ AMPK activity in *klo-1/ KL*

and *klo-2/KL* deletion background strains. It is noted that mRNA quantification may have poor correlation to protein abundances meaning it may be useful to couple this technique with another, such as mass-spectrometry to determine altered metabolism profiles between strains (Maier et al., 2009). Mass spectrometry techniques have previously been applied for *C. elegans* research into AAK-2/ AMPK pathways making this a plausible option for future work (Gao et al., 2017).

7.2.5. Further insights into other pathways mediated by KLO-1/ KL and KLO-2/ KL

A pathway described by Kosztelnik et al. (2019) suggested a delayed feedback mechanism for SKN-1/ Nrf2 deactivating AAK-2/ AMPK. This paper went on to suggest that silencing of SKN-1/ Nrf2 could result in the overactivation of AAK-2/ AMPK that over a prolonged period of time could have detrimental effects to organismal health (Kosztelnik et al., 2019). It would therefore be interesting to examine the role of SKN-1/ Nrf2 in KLO-1/ KL and KLO-2/ KL stress responses. This could be achieved using a reporter for *gst-4::GFP* which is widely used as a downstream reporter for SKN-1/ Nrf2 function (Detienne et al., 2016). Stocks of *C. elegans* positive for this reporter are possessed by our lab, however limitations meant that this was not crossed into *C. elegans* with *klo-1/ KL* and *klo-2/ KL* genetic backgrounds.

An alternative pathway to consider further research into would be TOR signalling. Data from rapamycin treatment on the expression of *klo-1::mCherry* reporter suggests that TOR signalling could be impaired in *klo-2; klo-1* double mutants. To examine this further, stocks for *C. elegans* with a *rsk-1/ S6K* genetic background could be obtained and crossed into strains with *klo-1* and *klo-2* genetic backgrounds prior to health and behavioural analysis to determine whether these pathways function in a linear manner. In addition, this could be further investigated by combination with *daf-2* hypomorphic alleles which would provide further insight into the crosstalk of TOR signalling and klotho function with IIS. Further insights into TOR signalling in *klotho* mutant backgrounds could be achieved through qPCR to quantify mRNA transcripts of RSKS-1 or even LET-363 which encodes the ortholog for human MTOR protein (Vellai et al., 2003).

Chapter 8: Conclusions

Taken together, the data suggests genetic deletion of *klo-1/ KL* and/ or *klo-2/ KL* in *C. elegans* confers acute stress resistance, in particular oxidative stress resistance, but that this survival advantage is a temporary phenomenon.

While some data suggests *klo-1/ KL* and *klo-2/ KL* mutants could have altered AAK-2/ AMPK activity, what remains to be elucidated is the cause for increased AAK-2/ AMPK as a result of genetic deletion of *klo-1/ KL* or *klo-2/ KL* in *C. elegans*. This warrants further investigation, though preliminary evidence suggests this could be linked to impaired TOR signalling, which typically functions antagonistically to AAK-2/ AMPK, and provides plausible hypotheses of klotho function via AMPK-TOR-IIS signalling crosstalk.

These findings are in line with existing literature for the relationship between FGF-klotho-FGFR, IIS, AMPK and mTOR pathways providing evidence that *C. elegans* is a tractable model for the study of these genetic pathways. Paradoxically, some of the findings relating to the role of Klotho in stress responses and longevity are somewhat controversial to existing literature for human and murine models, such as the fact that presumed null mutations of *C. elegans klotho* genes leads to increased stress resistance in this model.

<c-elegans-techniques_protein-biochem.pdf>.

2017. World Population Ageing *United Nations, Department Economical and Social Affairs, Population Division*.
2019. Health state life expectancies, UK 2016 to 2018 *Office for National Statistics*.
- ABBUD, W., HABINOWSKI, S., ZHANG, J. Z., KENDREW, J., ELKAIRI, F. S., KEMP, B. E., WITTERS, L. A. & ISMAIL-BEIGI, F. 2000. Stimulation of AMP-activated protein kinase (AMPK) is associated with enhancement of Glut1-mediated glucose transport. *Arch Biochem Biophys*, 380, 347-52.
- ALASBAHI, R. H. & MELZIG, M. F. 2012. Forskolin and derivatives as tools for studying the role of cAMP. *Pharmazie*, 67, 5-13.
- ALBERT, P. S., BROWN, S. J. & RIDDLE, D. L. 1981. Sensory control of dauer larva formation in *Caenorhabditis elegans*. 198, 435-451.
- ALEXANDER, P. 1967. The role of DNA lesions in the processes leading to aging in mice. *Symp Soc Exp Biol*, 21, 29-50.
- ALLENDE-VEGA, N., KRZYWINSKA, E., ORECCHIONI, S., LOPEZ-ROYUELA, N., REGGIANI, F., TALARICO, G., ROSSI, J. F., ROSSIGNOL, R., HICHERI, Y., CARTRON, G., BERTOLINI, F. & VILLALBA, M. 2015. The presence of wild type p53 in hematological cancers improves the efficacy of combinational therapy targeting metabolism. *Oncotarget*.
- ALLOUCH, S. & MUNUSAMY, S. 2018. AMP-activated Protein Kinase as a Drug Target in Chronic Kidney Disease. *Curr Drug Targets*, 19, 709-720.
- AN, J. H. & BLACKWELL, T. K. 2003. SKN-1 links *C. elegans* mesendodermal specification to a conserved oxidative stress response. *Genes & development*, 17, 1882-1893.
- ANDRUKHOVA, O., BAYER, J., SCHÜLER, C., ZEITZ, U., MURALI, S. K., ADA, S., ALVAREZ-PEZ, J. M., SMORODCHENKO, A. & ERBEN, R. G. 2017. Klotho Lacks an FGF23-Independent Role in Mineral Homeostasis. *Journal of Bone and Mineral Research*, 32, 2049-2061.
- APFELD, J., O'CONNOR, G., MCDONAGH, T., DISTEFANO, P. S. & CURTIS, R. 2004. The AMP-activated protein kinase AAK-2 links energy levels and insulin-like signals to lifespan in *C. elegans*. *Genes Dev*, 18, 3004-9.
- ARKING, D. E., ATZMON G FAU - ARKING, A., ARKING A FAU - BARZILAI, N., BARZILAI N FAU - DIETZ, H. C. & DIETZ, H. C. 2005. Association between a functional variant of the KLOTHO gene and high-density lipoprotein cholesterol, blood pressure, stroke, and longevity.
- ARNLOV, J., CARLSSON, A. C., SUNDSTROM, J., INGELSSON, E., LARSSON, A., LIND, L. & LARSSON, T. E. 2013. Higher fibroblast growth factor-23 increases the risk of all-cause and cardiovascular mortality in the community. *Kidney Int*, 83, 160-6.
- AZZAM, E. I., JAY-GERIN, J.-P. & PAIN, D. 2012a. Ionizing radiation-induced metabolic oxidative stress and prolonged cell injury. *Cancer letters*, 327, 48-60.
- AZZAM, E. I., JAY-GERIN, J. P. & PAIN, D. 2012b. Ionizing radiation-induced metabolic oxidative stress and prolonged cell injury. *Cancer Lett*, 327, 48-60.
- BAI, X., MIAO, D., XIAO, S., QIU, D., ST-ARNAUD, R., PETKOVICH, M., GUPTA, A., GOLTZMAN, D. & KARAPLIS, A. C. 2016. CYP24 inhibition as a therapeutic target in FGF23-mediated renal phosphate wasting disorders. *The Journal of clinical investigation*, 126, 667-680.
- BAI, X. Y., MIAO D FAU - GOLTZMAN, D., GOLTZMAN D FAU - KARAPLIS, A. C. & KARAPLIS, A. C. 2003. The autosomal dominant hypophosphatemic rickets R176Q mutation in fibroblast growth factor 23 resists proteolytic cleavage and enhances in vivo biological potency.
- BALASUBRAMANIAN, B., POGOZELSKI, W. K. & TULLIUS, T. D. 1998. DNA strand breaking by the hydroxyl radical is governed by the accessible surface areas of the hydrogen atoms of the DNA backbone. *Proceedings of the National Academy of Sciences*, 95, 9738-9743.
- BALASUBRAMANIAN, P. & LONGO, V. D. 2010. Linking Klotho, Nrf2, MAP kinases and aging. *Aging*.
- BÁRCENA, C., MAYORAL, P. & QUIRÓS, P. M. 2018. Chapter Two - Mitohormesis, an Antiaging Paradigm. *In: LÓPEZ-OTÍN, C. & GALLUZZI, L. (eds.) International Review of Cell and Molecular Biology*. Academic Press.

- BARNES, K., INGRAM, J. C., PORRAS, O. H., BARROS, L. F., HUDSON, E. R., FRYER, L. G. D., FOUFELLE, F., CARLING, D., HARDIE, D. G. & BALDWIN, S. A. 2002. Activation of GLUT1 by metabolic and osmotic stress: potential involvement of AMP-activated protein kinase (AMPK). *Journal of Cell Science*, 115, 2433.
- BARUTCUOGLU, B., BASOL G FAU - ÇAKIR, Y., ÇAKIR Y FAU - ÇETINKALP, S., ÇETINKALP S FAU - PARILDAR, Z., PARILDAR Z FAU - KABAROGLU, C., KABAROGLU C FAU - ÖZMEN, D., ÖZMEN D FAU - MUTAF, I., MUTAF I FAU - BAYINDIR, O. & BAYINDIR, O. 2011. Fibroblast growth factor-19 levels in type 2 diabetic patients with metabolic syndrome.
- BARZILAI, A. & YAMAMOTO, K. 2004. DNA damage responses to oxidative stress. *DNA Repair (Amst)*, 3, 1109-15.
- BELONGUER-VAREA, Á., TARAZONA-SANTABALBINA, F. J., AVELLANA-ZARAGOZA, J. A., MARTÍNEZ-REIG, M., MAS-BARGUES, C. & INGLÉS, M. 2020. Oxidative stress and exceptional human longevity: Systematic review. *Free Radical Biology and Medicine*, 149, 51-63.
- BERNSTEIN, H., PAYNE, C. M., BERNSTEIN, C., GAREWAL, H. & DVORAK, K. 2008. *Cancer and aging as consequences of un-repaired DNA damage*.
- BEUKERS, R., EKER AP FAU - LOHMAN, P. H. M. & LOHMAN, P. H. 50 years thymine dimer.
- BI, X., YANG, K., ZHANG, B. & ZHAO, J. 2020. The Protective Role of Klotho in CKD-Associated Cardiovascular Disease. *Kidney Diseases*, 6, 395-406.
- BJEDOV, I., TOIVONEN, J. M., KERR, F., SLACK, C., JACOBSON, J., FOLEY, A. & PARTRIDGE, L. 2010. Mechanisms of life span extension by rapamycin in the fruit fly *Drosophila melanogaster*. *Cell metabolism*, 11, 35-46.
- BLÜHER, M., KAHN, B. B. & KAHN, C. R. 2003. Extended Longevity in Mice Lacking the Insulin Receptor in Adipose Tissue. *Science*, 299, 572-574.
- BOLSTER, D. R., CROZIER, S. J., KIMBALL, S. R. & JEFFERSON, L. S. 2002. AMP-activated Protein Kinase Suppresses Protein Synthesis in Rat Skeletal Muscle through Down-regulated Mammalian Target of Rapamycin (mTOR) Signaling. *Journal of Biological Chemistry*, 277, 23977-23980.
- BORA, S., VARDHAN, G. S. H., DEKA, N., KHATANIAR, L., GOGOI, D. & BARUAH, A. 2021. Paraquat exposure over generation affects lifespan and reproduction through mitochondrial disruption in *C. elegans*. *Toxicology*, 447, 152632.
- BORRÁS, C. 2021. The Challenge of Unlocking the Biological Secrets of Aging. *Frontiers in Aging*, 2.
- BRENNER, S. 1974. The genetics of *Caenorhabditis elegans*. *Genetics*, 77, 71-94.
- BUECHNER, M. 2002. Tubes and the single *C. elegans* excretory cell. *Trends in Cell Biology*, 12, 479-484.
- BUJ, D. 2019. KLOTHO PROTEINS KLO-1 AND KLO-2 INTERACT WITH DAF-2/DAF-16 PATHWAY TO REGULATE ENERGY METABOLISM, STRESS RESISTANCE AND AGEING.
- BUJ, D. unpublished. KLOTHO PROTEINS KLO-1 AND KLO-2 INTERACT WITH DAF-2/DAF-16 PATHWAY TO REGULATE ENERGY METABOLISM, STRESS RESISTANCE AND AGEING.
- BURDINE R. D., C. E. B., KWOK, S.F., STERN, M.J. 1996. egl-17 encodes an invertebrate fibroblast growth factor family member required specifically for sex myoblast migration in *Caenorhabditis elegans*. *Proceedings of the National Academy of Sciences of the United States of America*, 94, 2433-2437.
- CABREIRO, F., AU C FAU - LEUNG, K.-Y., LEUNG KY FAU - VERGARA-IRIGARAY, N., VERGARA-IRIGARAY N FAU - COCHEMÉ, H. M., COCHEMÉ HM FAU - NOORI, T., NOORI T FAU - WEINKOVE, D., WEINKOVE D FAU - SCHUSTER, E., SCHUSTER E FAU - GREENE, N. D. E., GREENE ND FAU - GEMS, D. & GEMS, D. 2013. Metformin retards aging in *C. elegans* by altering microbial folate and methionine metabolism. *Cell Press*.
- CARTER, M. E. & BRUNET, A. 2007. FOXO transcription factors. *Curr Biol*, 17, R113-4.
- CASSADA, R. C. R., R.L. 1975. The dauerlarva, a post-embryonic developmental variant of the nematode *Caenorhabditis elegans*. *Developmental Biology*.
- CHANG, J. T., KUMSTA, C., HELLMAN, A. B., ADAMS, L. M. & HANSEN, M. 2017. Spatiotemporal regulation of autophagy during *Caenorhabditis elegans* aging. *eLife*, 6, e18459.

- CHANG, Q., HOEFS, S., VAN DER KEMP, A. W., TOPALA, C. N., BINDELS, R. J. & HOENDEROP, J. G. 2005. The β -Glucuronidase Klotho Hydrolyzes and Activates the TRPV5 Channel. *Science*, 310, 490-493.
- CHAPIN, H. C., OKADA, M., MERZ, A. J. & MILLER, D. L. 2015. Tissue-specific autophagy responses to aging and stress in *C. elegans*. *Aging*, 7, 419-434.
- CHÂTEAU, M. T., ARAIZ C FAU - DESCAMPS, S., DESCAMPS S FAU - GALAS, S. & GALAS, S. 2010. Klotho interferes with a novel FGF-signalling pathway and insulin/Igf-like signalling to improve longevity and stress resistance in *Caenorhabditis elegans*.
- CHAU, M. D., GAO, J., YANG, Q., WU, Z. & GROMADA, J. 2010. Fibroblast growth factor 21 regulates energy metabolism by activating the AMPK-SIRT1-PGC-1 α pathway. *Proc Natl Acad Sci U S A*, 107, 12553-8.
- CHEIKHI, A., BARCHOWSKY, A., SAHU, A., SHINDE, S. N., PIUS, A., CLEMENS, Z. J., LI, H., KENNEDY, C. A., HOECK, J. D., FRANTI, M. & AMBROSIO, F. 2019. Klotho: An Elephant in Aging Research. *J Gerontol A Biol Sci Med Sci*, 74, 1031-1042.
- CHEN, C.-D., PODVIN, S., GILLESPIE, E., LEEMAN, S. E. & ABRAHAM, C. R. 2007. Insulin stimulates the cleavage and release of the extracellular domain of Klotho by ADAM10 and ADAM17. *Proceedings of the National Academy of Sciences*, 104, 19796.
- CHEN, C.-D., TUNG, T. Y., LIANG, J., ZELDICH, E., TUCKER ZHOU, T. B., TURK, B. E. & ABRAHAM, C. R. 2014. Identification of cleavage sites leading to the shed form of the anti-aging protein klotho. *Biochemistry*, 53, 5579-5587.
- CHEN, D., LI, P. W.-L., GOLDSTEIN, B. A., CAI, W., THOMAS, E. L., CHEN, F., HUBBARD, A. E., MELOV, S. & KAPAHI, P. 2013a. Germline signaling mediates the synergistically prolonged longevity produced by double mutations in *daf-2* and *rsks-1* in *C. elegans*. *Cell reports*, 5, 1600-1610.
- CHEN, G., LIU, Y., GOETZ, R., FU, L., JAYARAMAN, S., HU, M.-C., MOE, O. W., LIANG, G., LI, X. & MOHAMMADI, M. 2018. α -Klotho is a non-enzymatic molecular scaffold for FGF23 hormone signalling. *Nature*, 553, 461.
- CHEN, T. H., KURO, O. M., CHEN, C. H., SUE, Y. M., CHEN, Y. C., WU, H. H. & CHENG, C. Y. 2013b. The secreted Klotho protein restores phosphate retention and suppresses accelerated aging in Klotho mutant mice. *Eur J Pharmacol*, 698, 67-73.
- CHEN, Y., SCARCELLI, V. & LEGOUIS, R. 2017. Approaches for Studying Autophagy in *Caenorhabditis elegans*. *Cells*, 6, 27.
- CHENG, X.-Y., LI, Y.-Y., HUANG, C., LI, J. & YAO, H.-W. 2017. AMP-activated protein kinase reduces inflammatory responses and cellular senescence in pulmonary emphysema. *Oncotarget*, 8, 22513-22523.
- CHEUNG, P. C., SALT, I. P., DAVIES, S. P., HARDIE, D. G. & CARLING, D. 2000. Characterization of AMP-activated protein kinase gamma-subunit isoforms and their role in AMP binding. *The Biochemical journal*, 346 Pt 3, 659-669.
- CHIUEH, C. C. 1999. Neuroprotective Properties of Nitric Oxide. *Annals of the New York Academy of Sciences*, 890, 301-311.
- CLARKE, P. R. & HARDIE, D. G. 1990. Regulation of HMG-CoA reductase: identification of the site phosphorylated by the AMP-activated protein kinase in vitro and in intact rat liver. *The EMBO journal*, 9, 2439-2446.
- COIMBRA-COSTA, D., ALVA, N., DURAN, M., CARBONELL, T. & RAMA, R. 2017. Oxidative stress and apoptosis after acute respiratory hypoxia and reoxygenation in rat brain. *Redox Biology*, 12, 216-225.
- CORSI, A. K. 2006. A biochemist's guide to *Caenorhabditis elegans*. *Analytical biochemistry*, 359, 1-17.
- COUGHLAN, K. A., VALENTINE, R. J., RUDERMAN, N. B. & SAHA, A. K. 2014. AMPK activation: a therapeutic target for type 2 diabetes? *Diabetes, metabolic syndrome and obesity : targets and therapy*, 7, 241-253.

- CUI, H., KONG, Y. & ZHANG, H. 2012. Oxidative stress, mitochondrial dysfunction, and aging. *Journal of signal transduction*, 2012, 646354-646354.
- CUI, L., JEONG, H., BOROVECKI, F., PARKHURST, C. N., TANESE, N. & KRAINIC, D. 2006. Transcriptional repression of PGC-1 α by mutant huntingtin leads to mitochondrial dysfunction and neurodegeneration. *Cell*, 127, 59-69.
- CUNNINGHAM, C. & HORN, C. 2003. Energy availability and alcohol-related liver pathology. *Alcohol research & health : the journal of the National Institute on Alcohol Abuse and Alcoholism*, 27, 291-9.
- CURTIS, R., O'CONNOR, G. & DISTEFANO, P. S. 2006. Aging networks in *Caenorhabditis elegans*: AMP-activated protein kinase (aak-2) links multiple aging and metabolism pathways. *Aging Cell*, 5, 119-126.
- CYPHERT, H. A., GE, X., KOHAN, A. B., SALATI, L. M., ZHANG, Y. & HILLGARTNER, F. B. 2012. Activation of the farnesoid X receptor induces hepatic expression and secretion of fibroblast growth factor 21. *The Journal of biological chemistry*, 287, 25123-25138.
- DA COSTA, J. P., VITORINO, R., SILVA, G. M., VOGEL, C., DUARTE, A. C. & ROCHA-SANTOS, T. 2016. A synopsis on aging-Theories, mechanisms and future prospects. *Ageing research reviews*, 29, 90-112.
- DAI, D., WANG, Q., LI, X., LIU, J., MA, X. & XU, W. 2015. Klotho inhibits human follicular thyroid cancer cell growth and promotes apoptosis through regulation of the expression of stanniocalcin-1.
- DALLE-DONNE, I., ROSSI, R., GIUSTARINI, D., MILZANI, A. & COLOMBO, R. 2003. Protein carbonyl groups as biomarkers of oxidative stress. *Clinica Chimica Acta*, 329, 23-38.
- DALTON, G. D., XIE, J., AN, S. W. & HUANG, C. L. 2017. New Insights into the Mechanism of Action of Soluble Klotho. *Front Endocrinol (Lausanne)*, 8, 323.
- DASU, M. R., DEVARAJ, S., ZHAO, L., HWANG, D. H. & JIALAL, I. 2008. High glucose induces toll-like receptor expression in human monocytes: mechanism of activation. *Diabetes*, 57, 3090-8.
- DAVID GEMS, S. P. L. P. 2002. Interpreting interactions between treatments that slow aging. *Ageing Cell*, 1.
- DAVIDSON, A. L. & ARION, W. J. 1987. Factors underlying significant underestimations of glucokinase activity in crude liver extracts: Physiological implications of higher cellular activity. *Archives of Biochemistry and Biophysics*, 253, 156-167.
- DE GREY, A. D. N. J. 2002. HO2 \bullet : The Forgotten Radical. *DNA and Cell Biology*, 21, 251-257.
- DEL RIO, D., STEWART AJ FAU - PELLEGRINI, N. & PELLEGRINI, N. 2005. A review of recent studies on malondialdehyde as toxic molecule and biological marker of oxidative stress.
- DEPAOLI, A. M., ZHOU, M., KAPLAN, D. D., HUNT, S. C., ADAMS, T. D., LEARNED, R. M., TIAN, H. & LING, L. 2019. FGF19 Analog as a Surgical Factor Mimetic That Contributes to Metabolic Effects Beyond Glucose Homeostasis. *Diabetes*, 68, 1315.
- DETIENNE, G., VAN DE WALLE, P., DE HAES, W., SCHOofs, L. & TEMMERMAN, L. 2016. SKN-1-independent transcriptional activation of glutathione S-transferase 4 (GST-4) by EGF signaling. *Worm*, 5, e1230585-e1230585.
- DONATE-CORREA, J., MARTÍN-NÚÑEZ, E., MARTÍNEZ-SANZ, R., MUROS-DE-FUENTES, M., MORA-FERNÁNDEZ, C., PÉREZ-DELGADO, N. & NAVARRO-GONZÁLEZ, J. A.-O. 2015. Influence of Klotho gene polymorphisms on vascular gene expression and its relationship to cardiovascular disease.
- DONG, X., MILHOLLAND, B. & VIJG, J. 2016. Evidence for a limit to human lifespan. *Nature*, 538, 257-259.
- DUTCHAK, P. A., KATAFUCHI T FAU - BOOKOUT, A. L., BOOKOUT AL FAU - CHOI, J. H., CHOI JH FAU - YU, R. T., YU RT FAU - MANGELSDORF, D. J., MANGELSDORF DJ FAU - KLEWER, S. A. & KLEWER, S. A. 2012. Fibroblast growth factor-21 regulates PPAR γ activity and the antidiabetic actions of thiazolidinediones.

- EGAN, D. F., SHACKELFORD, D. B., MIHAYLOVA, M. M., GELINO, S., KOHNZ, R. A., MAIR, W., VASQUEZ, D. S., JOSHI, A., GWINN, D. M., TAYLOR, R., ASARA, J. M., FITZPATRICK, J., DILLIN, A., VIOLLET, B., KUNDU, M., HANSEN, M. & SHAW, R. J. 2011. Phosphorylation of ULK1 (hATG1) by AMP-activated protein kinase connects energy sensing to mitophagy. *Science (New York, N.Y.)*, 331, 456-461.
- FAKHAR, M., NAJUMUDDIN, GUL, M. & RASHID, S. 2018. Antagonistic role of Klotho-derived peptides dynamics in the pancreatic cancer treatment through obstructing WNT-1 and Frizzled binding.
- FAN, M. & CHAMBERS, T. C. 2001. Role of mitogen-activated protein kinases in the response of tumor cells to chemotherapy.
- FARROW, E. G., DAVIS, S. I., SUMMERS, L. J. & WHITE, K. E. 2009. Initial FGF23-mediated signaling occurs in the distal convoluted tubule. *Journal of the American Society of Nephrology : JASN*, 20, 955-960.
- FAUBERT, B., VINCENT, E. E., GRISS, T., SAMBORSKA, B., IZREIG, S., SVENSSON, R. U., MAMER, O. A., AVIZONIS, D., SHACKELFORD, D. B., SHAW, R. J. & JONES, R. G. 2014. Loss of the tumor suppressor LKB1 promotes metabolic reprogramming of cancer cells via HIF-1 α . *Proceedings of the National Academy of Sciences*, 111, 2554-2559.
- FAZELI, P. K., LUN, M., KIM, S. M., BREDELLA, M. A., WRIGHT, S., ZHANG, Y., LEE, H., CATANA, C., KLIBANSKI, A., PATWARI, P. & STEINHAUSER, M. L. 2015. FGF21 and the late adaptive response to starvation in humans. *The Journal of Clinical Investigation*, 125, 4601-4611.
- FÉLÉTOU, M., KÖHLER, R. & VANHOUTTE, P. M. 2012. Nitric oxide: Orchestrator of endothelium-dependent responses. *Annals of Medicine*, 44, 694-716.
- FENTON, H. J. H. 1894. LXXIII.—Oxidation of tartaric acid in presence of iron. *Journal of the Chemical Society, Transactions*, 65, 899-910.
- FORNACE, A. J., JR., ALAMO I JR FAU - HOLLANDER, M. C. & HOLLANDER, M. C. 1988. DNA damage-inducible transcripts in mammalian cells.
- FU, L., JOHN LM FAU - ADAMS, S. H., ADAMS SH FAU - YU, X. X., YU XX FAU - TOMLINSON, E., TOMLINSON E FAU - RENZ, M., RENZ M FAU - WILLIAMS, P. M., WILLIAMS PM FAU - SORIANO, R., SORIANO R FAU - CORPUZ, R., CORPUZ R FAU - MOFFAT, B., MOFFAT B FAU - VANDLEN, R., VANDLEN R FAU - SIMMONS, L., SIMMONS L FAU - FOSTER, J., FOSTER J FAU - STEPHAN, J.-P., STEPHAN JP FAU - TSAI, S. P., TSAI SP FAU - STEWART, T. A. & STEWART, T. A. 2004. Fibroblast growth factor 19 increases metabolic rate and reverses dietary and leptin-deficient diabetes.
- FUKUYAMA, M., SAKUMA, K., PARK, R., KASUGA, H., NAGAYA, R., ATSUMI, Y., SHIMOMURA, Y., TAKAHASHI, S., KAJIHO, H., ROUGVIE, A., KONTANI, K. & KATADA, T. 2012. C. elegans AMPKs promote survival and arrest germline development during nutrient stress. *Biology open*, 1, 929-936.
- FUNAKOSHI, M., TSUDA, M., MURAMATSU, K., HATSUDA, H., MORISHITA, S. & AIGAKI, T. 2011. A gain-of-function screen identifies wdb and lkb1 as lifespan-extending genes in Drosophila. *Biochemical and Biophysical Research Communications*, 405, 667-672.
- GAO, A. W., CHATZISPYROU, I. A., KAMBLE, R., LIU, Y. J., HERZOG, K., SMITH, R. L., VAN LENTHE, H., VERVAART, M. A. T., VAN CRUCHTEN, A., LUYF, A. C., VAN KAMPEN, A., PRAS-RAVES, M. L., VAZ, F. M. & HOUTKOOPE, R. H. 2017. A sensitive mass spectrometry platform identifies metabolic changes of life history traits in C. elegans. *Scientific Reports*, 7, 2408.
- GAO, D., ZUO, Z., TIAN, J., ALI, Q., LIN, Y., LEI, H. & SUN, Z. 2016. Activation of SIRT1 Attenuates Klotho Deficiency-Induced Arterial Stiffness and Hypertension by Enhancing AMP-Activated Protein Kinase Activity. *Hypertension (Dallas, Tex. : 1979)*, 68, 1191-1199.
- GARCIA, D. & SHAW, R. J. 2017. AMPK: Mechanisms of Cellular Energy Sensing and Restoration of Metabolic Balance. *Molecular cell*, 66, 789-800.

- GE, X., CHEN, C., HUI, X., WANG, Y., LAM, K. S. L. & XU, A. 2011. Fibroblast growth factor 21 induces glucose transporter-1 expression through activation of the serum response factor/Ets-like protein-1 in adipocytes. *The Journal of biological chemistry*, 286, 34533-34541.
- GELINO, S., CHANG, J. T., KUMSTA, C., SHE, X., DAVIS, A., NGUYEN, C., PANOWSKI, S. & HANSEN, M. 2016. Intestinal Autophagy Improves Healthspan and Longevity in *C. elegans* during Dietary Restriction. *PLoS genetics*, 12, e1006135-e1006135.
- GEMS, D. & DOONAN, R. 2009. Antioxidant defense and aging in *C. elegans*: is the oxidative damage theory of aging wrong? *Cell Cycle*.
- GEMS, D., KERN, C. C., NOUR, J. & EZCURRA, M. 2021. Reproductive Suicide: Similar Mechanisms of Aging in *C. elegans* and Pacific Salmon. *Frontiers in Cell and Developmental Biology*, 9.
- GIGANTE, M., LUCARELLI G FAU - DIVELLA, C., DIVELLA C FAU - NETTI, G. S., NETTI GS FAU - PONTRELLI, P., PONTRELLI P FAU - CAFIERO, C., CAFIERO C FAU - GRANDALIANO, G., GRANDALIANO G FAU - CASTELLANO, G., CASTELLANO G FAU - RUTIGLIANO, M., RUTIGLIANO M FAU - STALLONE, G., STALLONE G FAU - BETTOCCHI, C., BETTOCCHI C FAU - DITONNO, P., DITONNO P FAU - GESUALDO, L., GESUALDO L FAU - BATTAGLIA, M., BATTAGLIA M FAU - RANIERI, E. & RANIERI, E. 2015. Soluble Serum α Klotho Is a Potential Predictive Marker of Disease Progression in Clear Cell Renal Cell Carcinoma.
- GLADYSHEV, V. N. 2014. The free radical theory of aging is dead. Long live the damage theory! *Antioxidants & redox signaling*, 20, 727-731.
- GLOIRE, G., LEGRAND-POELS S FAU - PIETTE, J. & PIETTE, J. 2006. NF-kappaB activation by reactive oxygen species: fifteen years later.
- GLOSSE, P., FEGER, M., MUTIG, K., CHEN, H., HIRCHE, F., HASAN, A. A., GABALLA, M. M. S., HOCHER, B., LANG, F. & FÖLLER, M. 2018. AMP-activated kinase is a regulator of fibroblast growth factor 23 production. *Kidney International*, 94, 491-501.
- GOETZ, R., OHNISHI, M., DING, X., KUROSU, H., WANG, L., AKIYOSHI, J., MA, J., GAI, W., SIDIS, Y., PITTELOUD, N., KURO-O, M., RAZZAQUE, M. S. & MOHAMMADI, M. 2012. Klotho Coreceptors Inhibit Signaling by Paracrine Fibroblast Growth Factor 8 Subfamily Ligands. *Molecular and Cellular Biology*, 32, 1944-1954.
- GONG, S. G. 2014. Isoforms of receptors of fibroblast growth factors.
- GOODMAN, S. J. 2003. Alternative splicing affecting a novel domain in the *C. elegans* EGL-15 FGF receptor confers functional specificity. *Development*, 130, 3757-3766.
- GREEN, D., FILKIN, G. & WOODS, T. 2021. Our unhealthy nation. *The Lancet Healthy Longevity*, 2, e8-e9.
- GREER, E. L., BANKO, M. R. & BRUNET, A. 2009. AMP-activated protein kinase and FoxO transcription factors in dietary restriction-induced longevity. *Annals of the New York Academy of Sciences*, 1170, 688-692.
- GREER, E. L. & BRUNET, A. 2005. FOXO transcription factors at the interface between longevity and tumor suppression. *Oncogene*, 24, 7410-7425.
- GREER, E. L., DOWLATSHAHI, D., BANKO, M. R., VILLEN, J., HOANG, K., BLANCHARD, D., GYGI, S. P. & BRUNET, A. 2007. An AMPK-FOXO Pathway Mediates Longevity Induced by a Novel Method of Dietary Restriction in *C. elegans*. *Current Biology*, 17, 1646-1656.
- GUARENTE, L. & KENYON, C. 2000. Genetic pathways that regulate ageing in model organisms.
- GUEVARA, E. E., LAWLER, R. R., STAES, N., WHITE, C. M., SHERWOOD, C. C., ELY, J. J., HOPKINS, W. D. & BRADLEY, B. J. 2020. Age-associated epigenetic change in chimpanzees and humans. *Philosophical Transactions of the Royal Society B: Biological Sciences*, 375, 20190616.
- GUO, A., LI, K. & XIAO, Q. 2020. Fibroblast growth factor 19 alleviates palmitic acid-induced mitochondrial dysfunction and oxidative stress via the AMPK/PGC-1 α pathway in skeletal muscle. *Biochemical and Biophysical Research Communications*, 526, 1069-1076.
- GUO, Y., MENG, J., TANG, Y., WANG, T., WEI, B., FENG, R., GONG, B., WANG, H., JI, G. & LU, Z. 2016. AMP-activated kinase α 2 deficiency protects mice from denervation-induced skeletal muscle atrophy. *Archives of Biochemistry and Biophysics*, 600, 56-60.

- HABER, F., WEISS, J. & POPE, W. J. 1934. The catalytic decomposition of hydrogen peroxide by iron salts. *Proceedings of the Royal Society of London. Series A - Mathematical and Physical Sciences*, 147, 332-351.
- HALLIWELL, B. & GUTTERIDGE, J. M. 1995. The definition and measurement of antioxidants in biological systems. *Free Radic Biol Med*, 18, 125-6.
- HAMILTON, R. T., WALSH, M. E. & VAN REMMEN, H. 2012. Mouse Models of Oxidative Stress Indicate a Role for Modulating Healthy Aging. LID - 005 [pii].
- HAN, D., ANTUNES, F., CANALI, R., RETTORI, D. & CADENAS, E. 2003. Voltage-dependent anion channels control the release of the superoxide anion from mitochondria to cytosol. *J Biol Chem*, 278, 5557-63.
- HARDIE, D. G. 2011. AMP-activated protein kinase—an energy sensor that regulates all aspects of cell function. *Genes & Development*, 25, 1895-1908.
- HARDIE, D. G. & CARLING, D. 1997. The AMP-activated protein kinase--fuel gauge of the mammalian cell?
- HARDIE, D. G., ROSS, F. A. & HAWLEY, S. A. 2012. AMPK: a nutrient and energy sensor that maintains energy homeostasis. *Nature reviews. Molecular cell biology*, 13, 251-262.
- HARMAN, D. 2006. Free Radical Theory of Aging: An Update. *Annals of the New York Academy of Sciences*, 1067, 10-21.
- HARRINGTON, A. J., HAMAMICHI S FAU - CALDWELL, G. A., CALDWELL GA FAU - CALDWELL, K. A. & CALDWELL, K. A. 2010. C. elegans as a model organism to investigate molecular pathways involved with Parkinson's disease.
- HARRISON, D. E., STRONG, R., SHARP, Z. D., NELSON, J. F., ASTLE, C. M., FLURKEY, K., NADON, N. L., WILKINSON, J. E., FRENKEL, K., CARTER, C. S., PAHOR, M., JAVORS, M. A., FERNANDEZ, E. & MILLER, R. A. 2009. Rapamycin fed late in life extends lifespan in genetically heterogeneous mice. *Nature*, 460, 392-395.
- HASHMI, S., WANG Y FAU - PARHAR, R. S., PARHAR RS FAU - COLLISON, K. S., COLLISON KS FAU - CONCA, W., CONCA W FAU - AL-MOHANNA, F., AL-MOHANNA F FAU - GAUGLER, R. & GAUGLER, R. 2013. A C. elegans model to study human metabolic regulation.
- HAWLEY, S. A., BOUDEAU, J., REID, J. L., MUSTARD, K. J., UDD, L., MÄKELÄ, T. P., ALESSI, D. R. & HARDIE, D. G. 2003. Complexes between the LKB1 tumor suppressor, STRAD alpha/beta and MO25 alpha/beta are upstream kinases in the AMP-activated protein kinase cascade. *Journal of biology*, 2, 28-28.
- HAWLEY, S. A., DAVISON, M., WOODS, A., DAVIES, S. P., BERI, R. K., CARLING, D. & HARDIE, D. G. 1996. Characterization of the AMP-activated Protein Kinase Kinase from Rat Liver and Identification of Threonine 172 as the Major Site at Which It Phosphorylates AMP-activated Protein Kinase. *Journal of Biological Chemistry*, 271, 27879-27887.
- HAWLEY, S. A., GADALLA, A. E., OLSEN, G. S. & HARDIE, D. G. 2002. The Antidiabetic Drug Metformin Activates the AMP-Activated Protein Kinase Cascade via an Adenine Nucleotide-Independent Mechanism. *Diabetes*, 51, 2420-2425.
- HAWLEY, S. A., ROSS FA FAU - CHEVTZOFF, C., CHEVTZOFF C FAU - GREEN, K. A., GREEN KA FAU - EVANS, A., EVANS A FAU - FOGARTY, S., FOGARTY S FAU - TOWLER, M. C., TOWLER MC FAU - BROWN, L. J., BROWN LJ FAU - OGUNBAYO, O. A., OGUNBAYO OA FAU - EVANS, A. M., EVANS AM FAU - HARDIE, D. G. & HARDIE, D. G. 2010. Use of cells expressing gamma subunit variants to identify diverse mechanisms of AMPK activation.
- HILLIER, L. W., COULSON A FAU - MURRAY, J. I., MURRAY JI FAU - BAO, Z., BAO Z FAU - SULSTON, J. E., SULSTON JE FAU - WATERSTON, R. H. & WATERSTON, R. H. 2004. Genomics in C. elegans: so many genes, such a little worm.
- HINCHY, E. C., GRUSZCZYK, A. V., WILLOWS, R., NAVARATNAM, N., HALL, A. R., BATES, G., BRIGHT, T. P., KRIEG, T., CARLING, D. & MURPHY, M. P. 2018. Mitochondria-derived ROS activate AMP-activated protein kinase (AMPK) indirectly. *The Journal of biological chemistry*, 293, 17208-17217.

- HINDUPUR, S. K., GONZÁLEZ, A. & HALL, M. N. 2015. The opposing actions of target of rapamycin and AMP-activated protein kinase in cell growth control. *Cold Spring Harbor perspectives in biology*, 7, a019141-a019141.
- HO, B. B. & BERGWITZ, C. 2020. FGF23 signalling and physiology. LID - JME-20-0178.R1 [pii] LID - 10.1530/JME-20-0178 [doi].
- HOAC, T., DAUN, C., TRAFIKOWSKA, U., ZACKRISSON, J. & ÅKESSON, B. 2006. Influence of heat treatment on lipid oxidation and glutathione peroxidase activity in chicken and duck meat. *Innovative Food Science & Emerging Technologies*, 7, 88-93.
- HODGKIN, J. & BARNES, T. M. 1991. More is Not Better: Brood Size and Population Growth in a Self-Fertilizing Nematode. *Proceedings: Biological Sciences*, 246, 19-24.
- HOLCZER, M., HAJDÚ, B., LŐRINCZ, T., SZARKA, A., BÁNHEGYI, G. & KAPUY, O. 2019. A Double Negative Feedback Loop between mTORC1 and AMPK Kinases Guarantees Precise Autophagy Induction upon Cellular Stress. *International journal of molecular sciences*, 20, 5543.
- HONDA, Y. & HONDA, S. 1999. The daf-2 gene network for longevity regulates oxidative stress resistance and Mn-superoxide dismutase gene expression in *Caenorhabditis elegans*. *Faseb j*, 13, 1385-93.
- HONDARES, E., IGLESIAS R FAU - GIRALT, A., GIRALT A FAU - GONZALEZ, F. J., GONZALEZ FJ FAU - GIRALT, M., GIRALT M FAU - MAMPEL, T., MAMPEL T FAU - VILLARROYA, F. & VILLARROYA, F. 2011. Thermogenic activation induces FGF21 expression and release in brown adipose tissue.
- HOSAMANI, R. & MURALIDHARA 2013. ACUTE EXPOSURE OF *Drosophila melanogaster* TO PARAQUAT CAUSES OXIDATIVE STRESS AND MITOCHONDRIAL DYSFUNCTION. *Archives of Insect Biochemistry and Physiology*, 83, 25-40.
- HRUBÁ, M. 2007. dCAPS method: Advantages, troubles and solution. *Plant, Soil and Environment*, 53, 417-420.
- HRYCAY, E. G. & BANDIERA, S. M. 2012. The monooxygenase, peroxidase, and peroxygenase properties of cytochrome P450. *Archives of Biochemistry and Biophysics*, 522, 71-89.
- HSU, A.-L., MURPHY, C. T. & KENYON, C. 2003. Regulation of Aging and Age-Related Disease by DAF-16 and Heat-Shock Factor. *Science*, 300, 1142-1145.
- HSUCHOU, H., PAN, W. & KASTIN, A. J. 2007. The fasting polypeptide FGF21 can enter brain from blood. *Peptides*, 28, 2382-2386.
- HU, M. C., SHI, M., ZHANG, J., QUIÑONES, H., GRIFFITH, C., KURO-O, M. & MOE, O. W. 2011. Klotho deficiency causes vascular calcification in chronic kidney disease. *Journal of the American Society of Nephrology*, 22, 124-136.
- HWANG, A., RYU, E.-A., ARTAN, M., CHANG, H.-W., KABIR, M., NAM, H.-J., LEE, D., YANG, J.-S., KIM, S., MAIR, W., LEE, C., LEE, S. & LEE, S.-J. 2014. Feedback regulation via AMPK and HIF-1 mediates ROS-dependent longevity in *Caenorhabditis elegans*. *Proceedings of the National Academy of Sciences of the United States of America*, 111.
- IMAI, M., ISHIKAWA, K., MATSUKAWA, N., KIDA, I., OHTA, J., IKUSHIMA, M., CHIHARA, Y., RUI, X., RAKUGI, H. & OGIHARA, T. 2004. Klotho protein activates the PKC pathway in the kidney and testis and suppresses 25-hydroxyvitamin D3 1alpha-hydroxylase gene expression. *Endocrine*, 25, 229-34.
- INAGAKI, T., CHOI, M., MOSCHETTA, A., PENG, L., CUMMINS, C. L., MCDONALD, J. G., LUO, G., JONES, S. A., GOODWIN, B., RICHARDSON, J. A., GERARD, R. D., REPA, J. J., MANGELSDORF, D. J. & KLIEWER, S. A. 2005. Fibroblast growth factor 15 functions as an enterohepatic signal to regulate bile acid homeostasis. *Cell Metabolism*, 2, 217-225.
- INAGAKI, T., DUTCHAK, P., ZHAO, G., DING, X., GAUTRON, L., PARAMESWARA, V., LI, Y., GOETZ, R., MOHAMMADI, M., ESSER, V., ELMQUIST, J. K., GERARD, R. D., BURGESS, S. C., HAMMER, R. E., MANGELSDORF, D. J. & KLIEWER, S. A. 2007. Endocrine Regulation of the Fasting

- Response by PPAR β -Mediated Induction of Fibroblast Growth Factor 21. *Cell Metabolism*, 5, 415-425.
- ITO, S., KINOSHITA, S., SHIRAISHI, N., NAKAGAWA, S., SEKINE, S., FUJIMORI, T. & NABESHIMA, Y.-I. 2000. Molecular cloning and expression analyses of mouse β klotho, which encodes a novel Klotho family protein. *Mechanisms of Development*, 98, 115-119.
- ITO, N., OHTA, H. & KONISHI, M. 2015. Endocrine FGFs: Evolution, Physiology, Pathophysiology, and Pharmacotherapy. *Frontiers in Endocrinology*, 6, 154.
- IZUMIYA, Y., BINA, H. A., OUCHI, N., AKASAKI, Y., KHARITONENKOV, A. & WALSH, K. 2008. FGF21 is an Akt-regulated myokine. *FEBS Letters*, 582, 3805-3810.
- JADAVJI, N. M., MURRAY, L. K., EMMERSON, J. T., RUDYK, C. A., HAYLEY, S. & SMITH, P. D. 2019. Paraquat Exposure Increases Oxidative Stress Within the Dorsal Striatum of Male Mice With a Genetic Deficiency in One-carbon Metabolism. *Toxicological Sciences*, 169, 25-33.
- JAKOBSEN, S. N., HARDIE, D. G., MORRICE, N. & TORNQVIST, H. E. 2001. 5'-AMP-activated Protein Kinase Phosphorylates IRS-1 on Ser-789 in Mouse C2C12 Myotubes in Response to 5-Aminoimidazole-4-carboxamide Riboside. *Journal of Biological Chemistry*, 276, 46912-46916.
- JASTROCH, M., DIVAKARUNI, A. S., MOOKERJEE, S., TREBERG, J. R. & BRAND, M. D. 2010. Mitochondrial proton and electron leaks. *Essays Biochem*, 47, 53-67.
- JENSEN, P. K. 1966. Antimycin-insensitive oxidation of succinate and reduced nicotinamide-adenine dinucleotide in electron-transport particles. II. Steroid effects. *Biochim Biophys Acta*, 122, 167-74.
- JIA, Q. Q., WANG, J. C., LONG, J., ZHAO, Y., CHEN, S. J., ZHAI, J. D., WEI, L. B., ZHANG, Q., CHEN, Y. & LONG, H. B. 2013. Sesquiterpene lactones and their derivatives inhibit high glucose-induced NF-kappaB activation and MCP-1 and TGF-beta1 expression in rat mesangial cells. *Molecules*, 18, 13061-77.
- JIN, K. 2010. Modern Biological Theories of Aging.
- JOHNSON, C. L., WESTON, J. Y., CHADI, S. A., FAZIO, E. N., HUFF, M. W., KHARITONENKOV, A., KÖESTER, A. & PIN, C. L. 2009. Fibroblast Growth Factor 21 Reduces the Severity of Cerulein-Induced Pancreatitis in Mice. *Gastroenterology*, 137, 1795-1804.
- JOHNSON, D. B. F. A. T. E. 1988. A Mutation in the age-1 Gene in *Caenorhabditis elegans* Lengthens Life and Reduces Hermaphrodite Fertility. *Genetics*, 118, 75-86.
- JOHNSON, T. E. 1990. Increased life-span of age-1 mutants in *Caenorhabditis elegans* and lower Gompertz rate of aging. *Science*, 249, 908-12.
- JØRGENSEN, S. B., NIELSEN, J. N., BIRK, J. B., OLSEN, G. S., VIOLLET, B., ANDREELLI, F., SCHJERLING, P., VAULONT, S., HARDIE, D. G., HANSEN, B. F., RICHTER, E. A. & WOJTASZEWSKI, J. F. P. 2004. The α 2-5'AMP-Activated Protein Kinase Is a Site 2 Glycogen Synthase Kinase in Skeletal Muscle and Is Responsive to Glucose Loading. *Diabetes*, 53, 3074.
- JUNG, C. H., RO, S.-H., CAO, J., OTTO, N. M. & KIM, D.-H. 2010. mTOR regulation of autophagy. *FEBS letters*, 584, 1287-1295.
- KANG, C., YOU, Y.-J. & AVERY, L. 2007. Dual roles of autophagy in the survival of *Caenorhabditis elegans* during starvation. *Genes & development*, 21, 2161-2171.
- KATO, Y., MIYAJI, M. & ZHANG-AKIYAMA, Q. M. 2017. FUDR extends the lifespan of the short-lived AP endonuclease mutant in *Caenorhabditis elegans* in a fertility-dependent manner. *Genes Genet Syst*, 91, 201-207.
- KEANEY, M., MATTHIJSSENS, F., SHARPE, M., VANFLETEREN, J. & GEMS, D. 2004. Superoxide dismutase mimetics elevate superoxide dismutase activity in vivo but do not retard aging in the nematode *Caenorhabditis elegans*. *Free Radic Biol Med*, 37, 239-50.
- KENYON, C., CHANG, J., GENSCH, E., RUDNER, A. & TABTIANG, R. 1993. A *C. elegans* mutant that lives twice as long as wild type. *Nature*, 366, 461-464.
- KHARITONENKOV, A., SHIYANOVA, T. L., KÖESTER, A., FORD, A. M., MICANOVIC, R., GALBREATH, E. J., SANDUSKY, G. E., HAMMOND, L. J., MOYERS, J. S., OWENS, R. A., GROMADA, J.,

- BROZINICK, J. T., HAWKINS, E. D., WROBLEWSKI, V. J., LI, D. S., MEHRBOD, F., JASKUNAS, S. R. & SHANAFELT, A. B. 2005. FGF-21 as a novel metabolic regulator. *J Clin Invest*, 115, 1627-35.
- KIM, H. J., LEE, J., CHAE, D.-W., LEE, K.-B., SUNG, S. A., YOO, T.-H., HAN, S. H., AHN, C. & OH, K.-H. 2019. Serum klotho is inversely associated with metabolic syndrome in chronic kidney disease: results from the KNOW-CKD study. *BMC Nephrology*, 20, 119.
- KIM, J.-H., CHOI, T. G., PARK, S., YUN, H. R., NGUYEN, N. N. Y., JO, Y. H., JANG, M., KIM, J., KIM, J., KANG, I., HA, J., MURPHY, M. P., TANG, D. G. & KIM, S. S. 2018. Mitochondrial ROS-derived PTEN oxidation activates PI3K pathway for mTOR-induced myogenic autophagy. *Cell Death & Differentiation*, 25, 1921-1937.
- KIM, J.-H., HWANG, K.-H., PARK, K.-S., KONG, I. D. & CHA, S.-K. 2015. Biological Role of Anti-aging Protein Klotho. *Journal of lifestyle medicine*, 5, 1-6.
- KIM, J., KUNDU M FAU - VIOLLET, B., VIOLLET B FAU - GUAN, K.-L. & GUAN, K. L. 2011a. AMPK and mTOR regulate autophagy through direct phosphorylation of Ulk1. *Nature Cell Biology*.
- KIM, J., KUNDU, M., VIOLLET, B. & GUAN, K.-L. 2011b. AMPK and mTOR regulate autophagy through direct phosphorylation of Ulk1. *Nature cell biology*, 13, 132-141.
- KIM, K. H., JEONG YT FAU - OH, H., OH H FAU - KIM, S. H., KIM SH FAU - CHO, J. M., CHO JM FAU - KIM, Y.-N., KIM YN FAU - KIM, S. S., KIM SS FAU - KIM, D. H., KIM DH FAU - HUR, K. Y., HUR KY FAU - KIM, H. K., KIM HK FAU - KO, T., KO T FAU - HAN, J., HAN J FAU - KIM, H. L., KIM HL FAU - KIM, J., KIM J FAU - BACK, S. H., BACK SH FAU - KOMATSU, M., KOMATSU M FAU - CHEN, H., CHEN H FAU - CHAN, D. C., CHAN DC FAU - KONISHI, M., KONISHI M FAU - ITOH, N., ITOH N FAU - CHOI, C. S., CHOI CS FAU - LEE, M.-S. & LEE, M. S. 2013. Autophagy deficiency leads to protection from obesity and insulin resistance by inducing Fgf21 as a mitokine.
- KIMURA, K. D., TISSENBAUM, H. A., LIU, Y. & RUVKUN, G. 1997. daf-2, an Insulin Receptor-Like Gene That Regulates Longevity and Diapause in *Caenorhabditis elegans*. *Science*, 277, 942-946.
- KINNUNEN, T., HUANG, Z., TOWNSEND, J., GATDULA, M. M., BROWN, J. R., ESKO, J. D. & TURNBULL, J. E. 2005. Heparan 2-O-sulfotransferase, hst-2, is essential for normal cell migration in *Caenorhabditis elegans*. *Proceedings of the National Academy of Sciences of the United States of America*, 102, 1507-1512.
- KINNUNEN, T. K. 2019. Fibroblast Growth Factors in Development. *eLS*.
- KIR, S., BEDDOW SA FAU - SAMUEL, V. T., SAMUEL VT FAU - MILLER, P., MILLER P FAU - PREVIS, S. F., PREVIS SF FAU - SUINO-POWELL, K., SUINO-POWELL K FAU - XU, H. E., XU HE FAU - SHULMAN, G. I., SHULMAN GI FAU - KLIEWER, S. A., KLIEWER SA FAU - MANGELSDORF, D. J. & MANGELSDORF, D. J. 2011. FGF19 as a postprandial, insulin-independent activator of hepatic protein and glycogen synthesis.
- KLEBANOFF, S. J. 2005. Myeloperoxidase: friend and foe. *Journal of Leukocyte Biology*, 77, 598-625.
- KOHLI, L. & ROTH, K. A. 2010. Autophagy: cerebral home cooking. *The American journal of pathology*, 176, 1065-1071.
- KOKEL, M., BORLAND, C. Z., DELONG, L., HORVITZ, H. R. & STERN, M. J. 1998. clr-1 encodes a receptor tyrosine phosphatase that negatively regulates an FGF receptor signaling pathway in *Caenorhabditis elegans*. *Genes & development*, 12, 1425-1437.
- KOLA, B., GROSSMAN, A. B. & KORBONITS, M. 2008. The role of AMP-activated protein kinase in obesity. *Front Horm Res*, 36, 198-211.
- KOLOTUEV, I., HYENNE, V., SCHWAB, Y., RODRIGUEZ, D. & LABOUESSE, M. 2013. A pathway for unicellular tube extension depending on the lymphatic vessel determinant Prox1 and on osmoregulation. *Nature Cell Biology*, 15, 157.
- KOPP, W. 2019. How Western Diet And Lifestyle Drive The Pandemic Of Obesity And Civilization Diseases. *Diabetes, metabolic syndrome and obesity : targets and therapy*, 12, 2221-2236.
- KOPS, G. J., DANSEN TB FAU - POLDERMAN, P. E., POLDERMAN PE FAU - SAARLOOS, I., SAARLOOS I FAU - WIRTZ, K. W. A., WIRTZ KW FAU - COFFER, P. J., COFFER PJ FAU - HUANG, T.-T., HUANG TT FAU - BOS, J. L., BOS JL FAU - MEDEMA, R. H., MEDEMA RH FAU - BURGERING, B. M. T. &

- BURGERING, B. M. 2002. Forkhead transcription factor FOXO3a protects quiescent cells from oxidative stress.
- KOSZTELNIK, M., KURUCZ, A., PAPP, D., JONES, E., SIGMOND, T., BARNA, J., TRAKA, M. H., LORINCZ, T., SZARKA, A., BANHEGYI, G., VELLAI, T., KORCSMAROS, T. & KAPUY, O. 2019. Suppression of AMPK/aak-2 by NRF2/SKN-1 down-regulates autophagy during prolonged oxidative stress. *FASEB J*, 33, 2372-2387.
- KRAEN, M., FRANTZ, S., NIHLÉN, U., ENGSTRÖM, G., LÖFDAHL, C. G., WOLLMER, P. & DENCKER, M. 2021. Fibroblast growth factor 23 is an independent marker of COPD and is associated with impairment of pulmonary function and diffusing capacity. *Respir Med*, 182, 106404.
- KRISKO, A. & RADMAN, M. 2019. Protein damage, ageing and age-related diseases.
- KURO-O, M. 2008. Klotho as a regulator of oxidative stress and senescence. *Biol Chem*, 389, 233-41.
- KURO-O, M. 2019. The Klotho proteins in health and disease. *Nature Reviews Nephrology*, 15, 27-44.
- KURO-O, M., MATSUMURA, Y., AIZAWA, H., KAWAGUCHI, H., SUGA, T., UTSUGI, T., OHYAMA, Y., KURABAYASHI, M., KANAME, T., KUME, E., IWASAKI, H., IIDA, A., SHIRAKI-IIDA, T., NISHIKAWA, S., NAGAI, R. & NABESHIMA, Y.-I. 1997. Mutation of the mouse klotho gene leads to a syndrome resembling ageing. *Nature*, 390, 45.
- KUROSU, H., OGAWA, Y., MIYOSHI, M., YAMAMOTO, M., NANDI, A., ROSENBLATT, K. P., BAUM, M. G., SCHIAVI, S., HU, M.-C., MOE, O. W. & KURO-O, M. 2006. Regulation of Fibroblast Growth Factor-23 Signaling by Klotho. *Journal of Biological Chemistry*, 281, 6120-6123.
- KUROSU, H., YAMAMOTO, M., CLARK, J. D., PASTOR, J. V., NANDI, A., GURNANI, P., MCGUINNESS, O. P., CHIKUDA, H., YAMAGUCHI, M., KAWAGUCHI, H., SHIMOMURA, I., TAKAYAMA, Y., HERZ, J., KAHN, C. R., ROSENBLATT, K. P. & KURO-O, M. 2005. Suppression of aging in mice by the hormone Klotho. *Science*, 309, 1829-33.
- KUWABARA, P. E. & O'NEIL, N. 2001. The use of functional genomics in *C. elegans* for studying human development and disease.
- LAKEY, P. S. J., BERKEMEIER, T., TONG, H., ARANGIO, A. M., LUCAS, K., POSCHL, U., SHIRAIWA, M. 2016. Chemical exposure-response relationship between air pollutants and reactive oxygen species in the human respiratory tract. *Scientific Reports* 6.
- LANZANI, C., CITTERIO, L. & VEZZOLI, G. 2020. Klotho: a link between cardiovascular and non-cardiovascular mortality. *Clinical Kidney Journal*, 13, 926-932.
- LASCANO, H., MUNOZ, N., ROBERT, G., RODRÍGUEZ, M., MELCHIORRE, M., TRIPPI, V. & QUERO, G. N. 2012. Paraquat: An Oxidative Stress Inducer.
- LEE, C. H., WOO, Y. C., CHOW, W. S., CHEUNG, C. Y. Y., FONG, C. H. Y., YUEN, M. M. A., XU, A., TSE, H. F. & LAM, K. S. L. 2017. Role of Circulating Fibroblast Growth Factor 21 Measurement in Primary Prevention of Coronary Heart Disease Among Chinese Patients With Type 2 Diabetes Mellitus. *Journal of the American Heart Association*, 6, e005344.
- LEE, E. Y., KIM, S. S., LEE, J.-S., KIM, I. J., SONG, S. H., CHA, S.-K., PARK, K.-S., KANG, J. S. & CHUNG, C. H. 2014a. Soluble α -Klotho as a Novel Biomarker in the Early Stage of Nephropathy in Patients with Type 2 Diabetes. *PLOS ONE*, 9, e102984.
- LEE, H., CHO, J. S., LAMBACHER, N., LEE, J., LEE, S.-J., LEE, T. H., GARTNER, A. & KOO, H.-S. 2008. The *Caenorhabditis elegans* AMP-activated protein kinase AAK-2 is phosphorylated by LKB1 and is required for resistance to oxidative stress and for normal motility and foraging behavior. *The Journal of biological chemistry*, 283, 14988-14993.
- LEE, J., JEONG, D.-J., KIM, J., LEE, S., PARK, J.-H., CHANG, B., JUNG, S.-I., YI, L., HAN, Y., YANG, Y., KIM, K. I., LIM, J.-S., YANG, I., JEON, S., BAE, D. H., KIM, C.-J. & LEE, M.-S. 2010. The anti-aging gene KLOTHO is a novel target for epigenetic silencing in human cervical carcinoma. *Molecular Cancer*, 9, 109.
- LEE, J. H., KONG, J., JANG, J. Y., HAN, J. S., JI, Y., LEE, J. & KIM, J. B. 2014b. Lipid droplet protein LID-1 mediates ATGL-1-dependent lipolysis during fasting in *Caenorhabditis elegans*. *Molecular and cellular biology*, 34, 4165-4176.

- LEE, K. J., JANG, Y. O., CHA, S. K., KIM, M. Y., PARK, K. S., EOM, Y. W. & BAIK, S. K. 2018a. Expression of Fibroblast Growth Factor 21 and β -Klotho Regulates Hepatic Fibrosis through the Nuclear Factor- κ B and c-Jun N-Terminal Kinase Pathways.
- LEE, S., CHOI, J., MOHANTY, J., SOUSA, L. P., TOME, F., PARDON, E., STEYAERT, J., LEMMON, M. A., LAX, I. & SCHLESSINGER, J. 2018b. Structures of β -klotho reveal a 'zip code'-like mechanism for endocrine FGF signalling. *Nature*, 553, 501-505.
- LEHTINEN, M. K., YUAN Z FAU - BOAG, P. R., BOAG PR FAU - YANG, Y., YANG Y FAU - VILLÉN, J., VILLÉN J FAU - BECKER, E. B. E., BECKER EB FAU - DIBACCO, S., DIBACCO S FAU - DE LA IGLESIA, N., DE LA IGLESIA N FAU - GYGI, S., GYGI S FAU - BLACKWELL, T. K., BLACKWELL TK FAU - BONNI, A. & BONNI, A. 2006. A conserved MST-FOXO signaling pathway mediates oxidative-stress responses and extends life span.
- LEVINE, B. & KROEMER, G. 2008. Autophagy in the pathogenesis of disease. *Cell*, 132, 27-42.
- LEWIS, K. N., WASON, E., EDREY, Y. H., KRISTAN, D. M., NEVO, E. & BUFFENSTEIN, R. 2015. Regulation of Nrf2 signaling and longevity in naturally long-lived rodents.
- LI, J., KIM, S. G. & BLENIS, J. 2014. Rapamycin: one drug, many effects. *Cell Metab*, 19, 373-9.
- LI, W., SAUD, S. M., YOUNG, M. R., CHEN, G. & HUA, B. 2015. Targeting AMPK for cancer prevention and treatment. *Oncotarget*, 6, 7365-7378.
- LI, X., LIU, J., LU, Q., REN, D., SUN, X., ROUSSELLE, T., TAN, Y. & LI, J. 2019. AMPK: a therapeutic target of heart failure-not only metabolism regulation. *Bioscience reports*, 39, BSR20181767.
- LI, X., WU, D. & TIAN, Y. 2018. Fibroblast growth factor 19 protects the heart from oxidative stress-induced diabetic cardiomyopathy via activation of AMPK/Nrf2/HO-1 pathway. *Biochemical and Biophysical Research Communications*, 502, 62-68.
- LIANG, J., SHAO, S. H., XU, Z.-X., HENNESSY, B., DING, Z., LARREA, M., KONDO, S., DUMONT, D. J., GUTTERMAN, J. U., WALKER, C. L., SLINGERLAND, J. M. & MILLS, G. B. 2007. The energy sensing LKB1-AMPK pathway regulates p27kip1 phosphorylation mediating the decision to enter autophagy or apoptosis. *Nature Cell Biology*, 9, 218-224.
- LIM, K., GROEN, A., MOLOSTVOV, G., LU, T., LILLEY, K. S., SNEAD, D., JAMES, S., WILKINSON, I. B., TING, S., HSIAO, L.-L., HIEMSTRA, T. F. & ZEHNDER, D. 2015. α -Klotho Expression in Human Tissues. *The Journal of Clinical Endocrinology and Metabolism*, 100, E1308-E1318.
- LIM, S. W., JIN, L., LUO, K., JIN, J., SHIN, Y. J., HONG, S. Y. & YANG, C. W. 2017. Klotho enhances FoxO3-mediated manganese superoxide dismutase expression by negatively regulating PI3K/AKT pathway during tacrolimus-induced oxidative stress. *Cell Death & Disease*, 8, e2972.
- LIN, K., DORMAN, J. B., RODAN, A. & KENYON, C. 1997. daf-16: An HNF-3/forkhead Family Member That Can Function to Double the Life-Span of *Caenorhabditis elegans*. *Science*, 278, 1319-1322.
- LIN, X. 2004. Functions of heparan sulfate proteoglycans in cell signaling during development. *Development*, 131, 6009-6021.
- LIN, Y., KURO-O M FAU - SUN, Z. & SUN, Z. 2013. Genetic deficiency of anti-aging gene klotho exacerbates early nephropathy in STZ-induced diabetes in male mice.
- LIN, Y. & SUN, Z. 2012. Antiaging gene Klotho enhances glucose-induced insulin secretion by up-regulating plasma membrane levels of TRPV2 in MIN6 β -cells. *Endocrinology*, 153, 3029-3039.
- LIN, Z., ZHOU, Z., LIU, Y., GONG, Q., YAN, X., XIAO, J., WANG, X., LIN, S., FENG, W. & LI, X. 2011. Circulating FGF21 Levels Are Progressively Increased from the Early to End Stages of Chronic Kidney Diseases and Are Associated with Renal Function in Chinese. *PLOS ONE*, 6, e18398.
- LIOCHEV, S. I. 2015. Which Is the Most Significant Cause of Aging? *Antioxidants (Basel, Switzerland)*, 4, 793-810.
- LIU, H., FERGUSSON, M. M., CASTILHO, R. M., LIU, J., CAO, L., CHEN, J., MALIDE, D., ROVIRA, II, SCHIMEL, D., KUO, C. J., GUTKIND, J. S., HWANG, P. M. & FINKEL, T. 2007. Augmented Wnt signaling in a mammalian model of accelerated aging. *Science*, 317, 803-6.

- LIU, Y. N., ZHOU, J., LI, T., WU, J., XIE, S. H., LIU, H.-F., LIU, Z., PARK, T. S., WANG, Y. & LIU, W. J. 2017. Sulodexide Protects Renal Tubular Epithelial Cells from Oxidative Stress-Induced Injury via Upregulating Klotho Expression at an Early Stage of Diabetic Kidney Disease. *Journal of Diabetes Research*, 2017, 10.
- LORENZI, O., VEYRAT-DUREBEX, C., WOLLHEIM, C. B., VILLEMEN, P., ROHNER-JEANRENAUD, F., ZANCHI, A. & VISCHER, U. M. 2010. Evidence against a direct role of klotho in insulin resistance. *Pflugers Arch*, 459, 465-73.
- LOSCHEN, G., AZZI, A., RICHTER, C. & FLOHE, L. 1974. Superoxide radicals as precursors of mitochondrial hydrogen peroxide. *FEBS Lett*, 42, 68-72.
- LU, X. & HU, M. C. 2017. Klotho/FGF23 Axis in Chronic Kidney Disease and Cardiovascular Disease. *Kidney Diseases*, 3, 15-23.
- LUO, Z., ZANG, M. & GUO, W. 2010. AMPK as a metabolic tumor suppressor: control of metabolism and cell growth. *Future oncology (London, England)*, 6, 457-470.
- MACNEIL, L. T., WATSON, E., ARDA, H. E., ZHU, L. J. & WALHOUT, A. J. M. 2013. Diet-induced developmental acceleration independent of TOR and insulin in *C. elegans*. *Cell*, 153, 240-252.
- MADHAVI, Y. V., GAIKWAD, N., YERRA, V. G., KALVALA, A. K., NANDURI, S. & KUMAR, A. 2019. Targeting AMPK in Diabetes and Diabetic Complications: Energy Homeostasis, Autophagy and Mitochondrial Health.
- MAIER, T., GÜELL, M. & SERRANO, L. 2009. Correlation of mRNA and protein in complex biological samples. *FEBS Letters*, 583, 3966-3973.
- MAIR, W., MORANTTE, I., RODRIGUES, A. P. C., MANNING, G., MONTMINY, M., SHAW, R. J. & DILLIN, A. 2011. Lifespan extension induced by AMPK and calcineurin is mediated by CRTC-1 and CREB. *Nature*, 470, 404-408.
- MAJUMDAR, V. & CHRISTOPHER, R. 2011. Association of exonic variants of Klotho with metabolic syndrome in Asian Indians.
- MALIK, Y. 2019. DAP-1 regulates starvation survival and Ingeivity in *Caenorhabditis elegans*. *University of Dundee*.
- MALTESE, G., PSEFTALI, P.-M., RIZZO, B., SRIVASTAVA, S., GNUDI, L., MANN, G. E. & SIOW, R. C. M. 2017. The anti-ageing hormone klotho induces Nrf2-mediated antioxidant defences in human aortic smooth muscle cells. *Journal of cellular and molecular medicine*, 21, 621-627.
- MAROIS, G., MUTTARAK, R. & SCHERBOV, S. 2020. Assessing the potential impact of COVID-19 on life expectancy. *PLOS ONE*, 15, e0238678.
- MARTINEZ DE LA ESCALERA, L., KYROU, I., VRBIKOVA, J., HAINER, V., SRAMKOVA, P., FRIED, M., PIYA, M. K., KUMAR, S., TRIPATHI, G. & MCTERNAN, P. G. 2017. Impact of gut hormone FGF-19 on type-2 diabetes and mitochondrial recovery in a prospective study of obese diabetic women undergoing bariatric surgery. *BMC medicine*, 15, 34-34.
- MARTINS, D., MCKAY, G. A., ENGLISH, A. M. & NGUYEN, D. 2020. Sublethal Paraquat Confers Multidrug Tolerance in *Pseudomonas aeruginosa* by Inducing Superoxide Dismutase Activity and Lowering Envelope Permeability. *Frontiers in Microbiology*, 11, 2337.
- MATSUMURA, Y., AIZAWA, H., SHIRAKI-IIDA, T., NAGAI, R., KURO-O, M. & NABESHIMA, Y.-I. 1998. Identification of the Human Klotho Gene and Its Two Transcripts Encoding Membrane and Secreted Klotho Protein. *Biochemical and Biophysical Research Communications*, 242, 626-630.
- MAYNARD, S., FANG, E. F., SCHEIBYE-KNUDSEN, M., CROTEAU, D. L. & BOHR, V. A. 2015. DNA Damage, DNA Repair, Aging, and Neurodegeneration. *Cold Spring Harbor perspectives in medicine*, 5, a025130.
- MCMULLEN, P. D., APRISON, E. Z., WINTER, P. B., AMARAL, L. A. N., MORIMOTO, R. I. & RUVINSKY, I. 2012. Macro-level modeling of the response of *C. elegans* reproduction to chronic heat stress. *PLoS computational biology*, 8, e1002338-e1002338.
- MEGALOU, E. V. & TAVERNARAKIS, N. 2009. Autophagy in *Caenorhabditis elegans*. *Biochimica et Biophysica Acta (BBA) - Molecular Cell Research*, 1793, 1444-1451.

- MEITZLER, J. L., ANTONY, S., WU, Y., JUHASZ, A., LIU, H., JIANG, G., LU, J., ROY, K. & DOROSHOW, J. H. 2014. NADPH oxidases: a perspective on reactive oxygen species production in tumor biology. *Antioxidants & redox signaling*, 20, 2873-2889.
- MENEELY, P. M., DAHLBERG, C. L. & ROSE, J. K. 2019. Working with Worms: *Caenorhabditis elegans* as a Model Organism. *Current Protocols Essential Laboratory Techniques*, 19, e35.
- MENG, S., CAO, J., HE, Q., XIONG, L., CHANG, E., RADOVICK, S., WONDISFORD, F. E. & HE, L. 2015. Metformin activates AMP-activated protein kinase by promoting formation of the $\alpha\beta$ heterotrimeric complex. *The Journal of biological chemistry*, 290, 3793-3802.
- MERRILL, KURTH, HARDIE & WINDER 1997. AICA riboside increases AMP-activated protein kinase, fatty acid oxidation, and glucose uptake in rat muscle. *American Journal of Physiology-Endocrinology and Metabolism*, 273, E1107-E1112.
- MICANOVIC, R., RACHES, D. W., DUNBAR, J. D., DRIVER, D. A., BINA, H. A., DICKINSON, C. D. & KHARITONENKOV, A. 2009. Different roles of N- and C- termini in the functional activity of FGF21. *J Cell Physiol*, 219, 227-34.
- MICHELIS, C. 2004. Physiological and Pathological Responses to Hypoxia. *The American Journal of Pathology*, 164, 1875-1882.
- MIKI, S., SUZUKI, J.-I., KUNIMURA, K. & MORIHARA, N. 2020. Mechanisms underlying the attenuation of chronic inflammatory diseases by aged garlic extract: Involvement of the activation of AMP-activated protein kinase. *Experimental and therapeutic medicine*, 19, 1462-1467.
- MISRA, P. & CHAKRABARTI, R. 2007. The role of AMP kinase in diabetes. *Indian J Med Res*, 125, 389-98.
- MIZUSHIMA, N., YAMAMOTO, A., MATSUI, M., YOSHIMORI, T. & OHSUMI, Y. 2004. In vivo analysis of autophagy in response to nutrient starvation using transgenic mice expressing a fluorescent autophagosome marker. *Molecular biology of the cell*, 15, 1101-1111.
- MORADI, N., DEHESTANI, A., RAHIMIAN, H. & BABAEIZAD, V. 2016. Cucumber Response to *Sphaerotheca fuliginea*: Differences in Antioxidant Enzymes Activity and Pathogenesis-Related Gene Expression in Susceptible and Resistant Genotypes. *Journal of Plant Molecular Breeding*, 4, 33-40.
- MOROVAT, A., WEERASINGHE, G., NESBITT, V., HOFER, M., AGNEW, T., QUAGHEBEUR, G., SERGEANT, K., FRATTER, C., GUHA, N., MIRZAZADEH, M. & POULTON, J. 2017. Use of FGF-21 as a Biomarker of Mitochondrial Disease in Clinical Practice. *Journal of clinical medicine*, 6, 80.
- MOTTILLO, E. P., DESJARDINS, E. M., FRITZEN, A. M., ZOU, V. Z., CRANE, J. D., YABUT, J. M., KIENS, B., ERION, D. M., LANBA, A., GRANNEMAN, J. G., TALUKDAR, S. & STEINBERG, G. R. 2017. FGF21 does not require adipocyte AMP-activated protein kinase (AMPK) or the phosphorylation of acetyl-CoA carboxylase (ACC) to mediate improvements in whole-body glucose homeostasis. *Molecular metabolism*, 6, 471-481.
- MOUNIER, R., LANTIER L FAU - LECLERC, J., LECLERC J FAU - SOTIROPOULOS, A., SOTIROPOULOS A FAU - FORETZ, M., FORETZ M FAU - VIOLLET, B. & VIOLLET, B. 2011. Antagonistic control of muscle cell size by AMPK and mTORC1. *Cell cycle*.
- MOYERS, J. S., SHYANOVA, T. L., MEHRBOD, F., DUNBAR, J. D., NOBLITT, T. W., OTTO, K. A., REIFEL-MILLER, A. & KHARITONENKOV, A. 2007. Molecular determinants of FGF-21 activity—synergy and cross-talk with PPAR γ signaling. *Journal of Cellular Physiology*, 210, 1-6.
- MUISE, E. S., SOUZA S FAU - CHI, A., CHI A FAU - TAN, Y., TAN Y FAU - ZHAO, X., ZHAO X FAU - LIU, F., LIU F FAU - DALLAS-YANG, Q., DALLAS-YANG Q FAU - WU, M., WU M FAU - SARR, T., SARR T FAU - ZHU, L., ZHU L FAU - GUO, H., GUO H FAU - LI, Z., LI Z FAU - LI, W., LI W FAU - HU, W., HU W FAU - JIANG, G., JIANG G FAU - PAWELETZ, C. P., PAWELETZ CP FAU - HENDRICKSON, R. C., HENDRICKSON RC FAU - THOMPSON, J. R., THOMPSON JR FAU - MU, J., MU J FAU - BERGER, J. P., BERGER JP FAU - MEHMET, H. & MEHMET, H. 2013. Downstream signaling pathways in mouse adipose tissues following acute in vivo administration of fibroblast growth factor 21.

- MUOIO, D. M., SEEFELD, K., WITTERS, L. A. & COLEMAN, R. A. 1999. AMP-activated kinase reciprocally regulates triacylglycerol synthesis and fatty acid oxidation in liver and muscle: evidence that sn-glycerol-3-phosphate acyltransferase is a novel target. *The Biochemical journal*, 338 (Pt 3), 783-791.
- MURPHY, C. T. & HU, P. J. 2013. Insulin/insulin-like growth factor signaling in *C. elegans*. *WormBook : the online review of C. elegans biology*, 1-43.
- NAKAMURA, S. & YOSHIMORI, T. 2018. Autophagy and Longevity. *Molecules and cells*, 41, 65-72.
- NARBONNE, P. & ROY, R. 2006. Inhibition of germline proliferation during *C. elegans* dauer development requires PTEN, LKB1 and AMPK signalling. *Development*, 133, 611-9.
- NARBONNE, P. & ROY, R. 2009. Caenorhabditis elegans dauers need LKB1/AMPK to ration lipid reserves and ensure long-term survival. *Nature*, 457, 210-4.
- NASRALLAH, M. M., EL-SHEHABY, A. R., OSMAN, N. A., FAYAD, T., NASSEF, A., SALEM, M. M. & SHARAF EL DIN, U. A. 2013. The Association between Fibroblast Growth Factor-23 and Vascular Calcification Is Mitigated by Inflammation Markers. *Nephron Extra*, 3, 106-112.
- NELSON, J. F., STRONG, R., BOKOV, A., DIAZ, V. & WARD, W. 2012. Probing the relationship between insulin sensitivity and longevity using genetically modified mice. *The journals of gerontology. Series A, Biological sciences and medical sciences*, 67, 1332-1338.
- NIE, F., WU, D., DU, H., YANG, X., YANG, M., PANG, X. & XU, Y. 2017. Serum klotho protein levels and their correlations with the progression of type 2 diabetes mellitus. *Journal of Diabetes and its Complications*, 31, 594-598.
- NISHIMURA, T., NAKATAKE Y FAU - KONISHI, M., KONISHI M FAU - ITOH, N. & ITOH, N. 2000. Identification of a novel FGF, FGF-21, preferentially expressed in the liver.
- NYGAARD, E. B., VIENBERG, S. G., ØRSKOV, C., HANSEN, H. S. & ANDERSEN, B. 2012. Metformin stimulates FGF21 expression in primary hepatocytes. *Experimental diabetes research*, 2012, 465282-465282.
- O'NEILL, H. M., MAARBJERG, S. J., CRANE, J. D., JEPPESEN, J., JØRGENSEN, S. B., SCHERTZER, J. D., SHYROKA, O., KIENS, B., VAN DENDEREN, B. J., TARNOPOLSKY, M. A., KEMP, B. E., RICHTER, E. A. & STEINBERG, G. R. 2011. AMP-activated protein kinase (AMPK) beta1beta2 muscle null mice reveal an essential role for AMPK in maintaining mitochondrial content and glucose uptake during exercise. *Proceedings of the National Academy of Sciences of the United States of America*, 108, 16092-16097.
- OLEJNIK, A., FRANCAZAK, A., KRZYWONOS-ZAWADZKA, A., KAŁUŻNA-OLEKSY, M. & BIL-LULA, I. 2018. The Biological Role of Klotho Protein in the Development of Cardiovascular Diseases. *BioMed Research International*, 2018, 5171945.
- OLIVEIRA, R. P., PORTER ABATE, J., DILKS, K., LANDIS, J., ASHRAF, J., MURPHY, C. T. & BLACKWELL, T. K. 2009. Condition-adapted stress and longevity gene regulation by *Caenorhabditis elegans* SKN-1/Nrf. *Aging Cell*, 8, 524-41.
- ONKEN, B. & DRISCOLL, M. 2010. Metformin induces a dietary restriction-like state and the oxidative stress response to extend *C. elegans* Healthspan via AMPK, LKB1, and SKN-1. *PLoS One*, 5, e8758.
- ORNITZ, D. M. & ITOH, N. 2015. The Fibroblast Growth Factor signaling pathway. *Wiley Interdisciplinary Reviews. Developmental Biology*, 4, 215-266.
- PACHER, P., BECKMAN, J. S. & LIAUDET, L. 2007. Nitric Oxide and Peroxynitrite in Health and Disease. *Physiological Reviews*, 87, 315-424.
- PALMISANO, N. J. & MELÉNDEZ, A. 2016. Detection of Autophagy in *Caenorhabditis elegans* Using GFP::LGG-1 as an Autophagy Marker. *Cold Spring Harbor protocols*, 2016, pdb.prot086496-pdb.prot086496.
- PALRASU, M. & SIDDAVARAM, N. 2018. Cytochrome P450 Structure, Function and Clinical Significance: A Review. *Current Drug Targets*, 19, 38-54.
- PAN, J., ZHONG J FAU - GAN, L. H., GAN LH FAU - CHEN, S. J., CHEN SJ FAU - JIN, H. C., JIN HC FAU - WANG, X., WANG X FAU - WANG, L. J. & WANG, L. J. 2011. Klotho, an anti-senescence

related gene, is frequently inactivated through promoter hypermethylation in colorectal cancer.

- PARKER, H. & WINTERBOURN, C. C. 2013. Reactive oxidants and myeloperoxidase and their involvement in neutrophil extracellular traps. *Frontiers in immunology*, 3, 424-424.
- PARTRIDGE, L., ALIC, N., BJEDOV, I. & PIPER, M. D. W. 2011. Ageing in *Drosophila*: the role of the insulin/Igf and TOR signalling network. *Experimental gerontology*, 46, 376-381.
- PASTOR-SOLER N. M., RAJANI R., MANCINO V., OMI K. & R., H. K. 2018. Metabolic acidosis inhibits AMPK function in kidney cells. *The FASEB Journal*, 32, 851.13-851.13.
- PATEL, R., BOOKOUT, A. L., MAGOMEDOVA, L., OWEN, B. M., CONSIGLIO, G. P., SHIMIZU, M., ZHANG, Y., MANGELSDORF, D. J., KLEWER, S. A. & CUMMINS, C. L. 2015. Glucocorticoids Regulate the Metabolic Hormone FGF21 in a Feed-Forward Loop. *Molecular Endocrinology*, 29, 213-223.
- PÉREZ, V. I., VAN REMMEN, H., BOKOV, A., EPSTEIN, C. J., VIJG, J. & RICHARDSON, A. 2009. The overexpression of major antioxidant enzymes does not extend the lifespan of mice. *Aging cell*, 8, 73-75.
- PHANIENDRA, A., JESTADI, D. B. & PERIYASAMY, L. 2015. Free radicals: properties, sources, targets, and their implication in various diseases. *Indian journal of clinical biochemistry : IJCB*, 30, 11-26.
- PILLAI, S., ORESAJO C FAU - HAYWARD, J. & HAYWARD, J. Ultraviolet radiation and skin aging: roles of reactive oxygen species, inflammation and protease activation, and strategies for prevention of inflammation-induced matrix degradation - a review.
- PIZZINO, G., IRRERA, N., CUCINOTTA, M., PALLIO, G., MANNINO, F., ARCORACI, V., SQUADRITO, F., ALTAVILLA, D. & BITTO, A. 2017. Oxidative Stress: Harms and Benefits for Human Health. *Oxid Med Cell Longev*, 2017, 8416763.
- PLANAVILA, A., REDONDO-ANGULO, I., RIBAS, F., GARRABOU, G., CASADEMONT, J., GIRALT, M. & VILLARROYA, F. 2015. Fibroblast growth factor 21 protects the heart from oxidative stress. *Cardiovasc Res*, 106, 19-31.
- POLANSKA, U. M., EDWARDS, E., FERNIG, D. G. & KINNUNEN, T. K. 2011. The Cooperation of FGF Receptor and Klotho Is Involved in Excretory Canal Development and Regulation of Metabolic Homeostasis in *Caenorhabditis elegans*. *Journal of Biological Chemistry*, 286, 5657-5666.
- POLANSKA, U. M., FERNIG DAVID, G. & KINNUNEN, T. 2009. Extracellular interactome of the FGF receptor–ligand system: Complexities and the relative simplicity of the worm. *Developmental Dynamics*, 238, 277-293.
- POLLARD, A. E., MARTINS, L., MUCKETT, P. J., KHADAYATE, S., BORNOT, A., CLAUSEN, M., ADMYRE, T., BJURSELL, M., FIADAIRO, R., WILSON, L., WHILDING, C., KOTIADIS, V. N., DUCHEN, M. R., SUTTON, D., PENFOLD, L., SARDINI, A., BOHLOOLY-Y, M., SMITH, D. M., READ, J. A., SNOWDEN, M. A., WOODS, A. & CARLING, D. 2019. AMPK activation protects against diet-induced obesity through Ucp1-independent thermogenesis in subcutaneous white adipose tissue. *Nature Metabolism*, 1, 340-349.
- PYRKOV, T. V., AVCHACIOV, K., TARKHOV, A. E., MENSHIKOV, L. I., GUDKOV, A. V. & FEDICHEV, P. O. 2021. Longitudinal analysis of blood markers reveals progressive loss of resilience and predicts human lifespan limit. *Nature Communications*, 12, 2765.
- QUARLES, L. D. 2012. Role of FGF23 in vitamin D and phosphate metabolism: Implications in chronic kidney disease. *Experimental Cell Research*, 318, 1040-1048.
- RAHMAN, T., HOSEN, I., ISLAM, M. M. T. & SHEKHAR, H. U. 2012. Oxidative stress and human health. *Advances in Bioscience and Biotechnology*, 03, 997-1019.
- RAKUGI, H., MATSUKAWA, N., ISHIKAWA, K., YANG, J., IMAI, M., IKUSHIMA, M., MAEKAWA, Y., KIDA, I., MIYAZAKI, J.-I. & OGIHARA, T. 2007. Anti-oxidative effect of Klotho on endothelial cells through cAMP activation. *Endocrine*, 31, 82-87.

- RAZZAQUE, M. S. 2009. The FGF23-Klotho axis: endocrine regulation of phosphate homeostasis. *Nat Rev Endocrinol*, 5, 611-9.
- RENA, G., HARDIE, D. G. & PEARSON, E. R. 2017. The mechanisms of action of metformin. *Diabetologia*, 60, 1577-1585.
- RISTOW, M. 2014. Unraveling the Truth About Antioxidants: Mitohormesis explains ROS-induced health benefits. *Nature Medicine*, 20, 709-711.
- ROBIDA-STUBBS, S., GLOVER-CUTTER, K., LAMMING, D. W., MIZUNUMA, M., NARASIMHAN, S. D., NEUMANN-HAEFELIN, E., SABATINI, D. M. & BLACKWELL, T. K. 2012. TOR signaling and rapamycin influence longevity by regulating SKN-1/Nrf and DAF-16/FoxO. *Cell Metabolism*, 15, 713-724.
- ROCHLANI, Y., POTHINENI, N. V., KOVELAMUDI, S. & MEHTA, J. L. 2017. Metabolic syndrome: pathophysiology, management, and modulation by natural compounds. *Therapeutic advances in cardiovascular disease*, 11, 215-225.
- ROLLINS, J. A., HOWARD, A. C., DOBBINS, S. K., WASHBURN, E. H. & ROGERS, A. N. 2017. Assessing Health Span in *Caenorhabditis elegans*: Lessons From Short-Lived Mutants. *The journals of gerontology. Series A, Biological sciences and medical sciences*, 72, 473-480.
- ROUBIN, R. G., NAERT, K., POPOVICI, C., VATCHER, G., COULIER, F. O., THIERRY-MIEG, J., PONTAROTTI, P., BIRNBAUM, D., BAILLIE, D. & THIERRY-MIEG, D. 1999. let-756, a *C. elegans* fgf essential for worm development. *Oncogene*, 18, 6741-6747.
- RUBINEK, T. & MODAN-MOSES, D. 2016. Chapter Four - Klotho and the Growth Hormone/Insulin-Like Growth Factor 1 Axis: Novel Insights into Complex Interactions. In: LITWACK, G. (ed.) *Vitamins & Hormones*. Academic Press.
- SACHDEVA, A., GOUGE, J., KONTOVOUNISIOS, C., NIKOLAOU, S., ASHWORTH, A., LIM, K. & CHONG, I. 2020. Klotho and the Treatment of Human Malignancies. *Cancers*, 12, 1665.
- SALMINEN, A. & KAARNIRANTA, K. 2012. AMP-activated protein kinase (AMPK) controls the aging process via an integrated signaling network. *Ageing Research Reviews*, 11, 230-241.
- SALMINEN, A., KAUPPINEN, A. & KAARNIRANTA, K. 2016. FGF21 activates AMPK signaling: impact on metabolic regulation and the aging process.
- SALMON, A. B., RICHARDSON, A. & PÉREZ, V. I. 2010. Update on the oxidative stress theory of aging: does oxidative stress play a role in aging or healthy aging? *Free radical biology & medicine*, 48, 642-655.
- SALT, I. P. & PALMER, T. M. 2012. Exploiting the anti-inflammatory effects of AMP-activated protein kinase activation. *Expert Opin Investig Drugs*, 21, 1155-67.
- SCHAAP, F. G., KREMER, A. E., LAMERS, W. H., JANSEN, P. L. & GAEMERS, I. C. 2013. Fibroblast growth factor 21 is induced by endoplasmic reticulum stress. *Biochimie*, 95, 692-9.
- SCHMEISSER, S., SCHMEISSER, K., WEIMER, S., GROTH, M., PRIEBE, S., FAZIUS, E., KUHLLOW, D., PICK, D., EINAX, J. W., GUTHKE, R., PLATZER, M., ZARSE, K. & RISTOW, M. 2013. Mitochondrial hormesis links low-dose arsenite exposure to lifespan extension. *Aging Cell*, 12, 508-17.
- SCOTT, B. A., AVIDAN, M. S. & CROWDER, C. M. 2002. Regulation of Hypoxic Death in *C. elegans* by the Insulin/IGF Receptor Homolog DAF-2. *Science*, 296, 2388-2391.
- SEAMON, K. B., PADGETT, W. & DALY, J. W. 1981. Forskolin: unique diterpene activator of adenylate cyclase in membranes and in intact cells. *Proceedings of the National Academy of Sciences of the United States of America*, 78, 3363-3367.
- SELMAN, C., MCLAREN, J. S., COLLINS, A. R., DUTHIE, G. G. & SPEAKMAN, J. R. 2013. Deleterious consequences of antioxidant supplementation on lifespan in a wild-derived mammal. *Biology Letters*, 9, 20130432.
- SENCHEK, M. M., DUES, D. J. & VAN RAAMSDONK, J. M. 2017. Measuring Oxidative Stress in *Caenorhabditis elegans*: Paraquat and Juglone Sensitivity Assays. *Bio Protoc*, 7.
- SENONER, T. & DICHTL, W. 2019. Oxidative Stress in Cardiovascular Diseases: Still a Therapeutic Target? *Nutrients*, 11, 2090.

- SEO, K., CHOI, E., LEE, D., JEONG, D.-E., JANG, S. K. & LEE, S.-J. 2013. Heat shock factor 1 mediates the longevity conferred by inhibition of TOR and insulin/IGF-1 signaling pathways in *C. elegans*. *Aging Cell*, 12, 1073-1081.
- SERPEN, A., GÖKMEN, V. & FOGLIANO, V. 2012. Total antioxidant capacities of raw and cooked meats. *Meat Science*, 90, 60-65.
- SHI, S. Y., LU, Y.-W., RICHARDSON, J., MIN, X., WEISZMANN, J., RICHARDS, W. G., WANG, Z., ZHANG, Z., ZHANG, J. & LI, Y. 2018. A systematic dissection of sequence elements determining β -Klotho and FGF interaction and signaling. *Scientific Reports*, 8, 11045.
- SHIELS, P. G., MCGUINNESS, D., ERIKSSON, M., KOOMAN, J. P. & STENVINKEL, P. 2017. The role of epigenetics in renal ageing. *Nat Rev Nephrol*, 13, 471-482.
- SHIMADA, T., KAKITANI, M., YAMAZAKI, Y., HASEGAWA, H., TAKEUCHI, Y., FUJITA, T., FUKUMOTO, S., TOMIZUKA, K. & YAMASHITA, T. 2004. Targeted ablation of Fgf23 demonstrates an essential physiological role of FGF23 in phosphate and vitamin D metabolism. *The Journal of clinical investigation*, 113, 561-568.
- SHIRAKI-IIDA, T., AIZAWA, H., MATSUMURA, Y., SEKINE, S., IIDA, A., ANAZAWA, H., NAGAI, R., KURO-O, M. & NABESHIMA, Y. 1998. Structure of the mouse klotho gene and its two transcripts encoding membrane and secreted protein. *FEBS Lett*, 424, 6-10.
- SHIRWANY, N. A. & ZOU, M.-H. 2010. AMPK in cardiovascular health and disease. *Acta pharmacologica Sinica*, 31, 1075-1084.
- SIMIONI, C., ZAULI, G., MARTELLI, A. M., VITALE, M., SACCHETTI, G., GONELLI, A. & NERI, L. M. 2018. Oxidative stress: role of physical exercise and antioxidant nutraceuticals in adulthood and aging. *Oncotarget*, 9, 17181-17198.
- SINDHU, S., AKHTER, N., KOCHUMON, S., THOMAS, R., WILSON, A., SHENOUDA, S., TUOMILEHTO, J. & AHMAD, R. 2018. Increased Expression of the Innate Immune Receptor TLR10 in Obesity and Type-2 Diabetes: Association with ROS-Mediated Oxidative Stress. *Cellular Physiology and Biochemistry*, 45, 572-590.
- SMITH, P. K., R. I., KROHN RI FAU - HERMANSON, G. T., HERMANSON GT FAU - MALLIA, A. K., MALLIA AK FAU - GARTNER, F. H., GARTNER FH FAU - PROVENZANO, M. D., PROVENZANO MD FAU - FUJIMOTO, E. K., FUJIMOTO EK FAU - GOEKE, N. M., GOEKE NM FAU - OLSON, B. J., OLSON BJ FAU - KLENK, D. C. & KLENK, D. C. 1985. Measurement of protein using bicinchoninic acid. *Analytical Biochemistry*.
- SOMM, E. & JORNAYVAZ, F. R. 2018. Fibroblast Growth Factor 15/19: From Basic Functions to Therapeutic Perspectives.
- SON, Y., KIM S FAU - CHUNG, H.-T., CHUNG HT FAU - PAE, H.-O. & PAE, H. O. 2013. Reactive oxygen species in the activation of MAP kinases.
- STADTMAN, B. S. B. A. E. R. 1997. Protein Oxidation in Aging, Disease, and Oxidative Stress. *The Journal of biological chemistry*, 272, 20313-20316.
- STEINBERG, G. R. & KEMP, B. E. 2009. AMPK in Health and Disease. *Physiological Reviews*, 89, 1025-1078.
- STENVINKEL, P. 2010. Chronic kidney disease: a public health priority and harbinger of premature cardiovascular disease.
- STIERNAGLE, T. 2006. Maintenance of *C. elegans*. *WormBook*, 1-11.
- STRONG, R., MILLER, R. A., BOGUE, M., FERNANDEZ, E., JAVORS, M. A., LIBERT, S., MARINEZ, P. A., MURPHY, M. P., MUSI, N., NELSON, J. F., PETRASCHECK, M., REIFSNYDER, P., RICHARDSON, A., SALMON, A. B., MACCHIARINI, F. & HARRISON, D. E. 2020. Rapamycin-mediated mouse lifespan extension: Late-life dosage regimes with sex-specific effects. *Aging Cell*, 19, e13269.
- SUNAGA, H., KOITABASHI, N., ISO, T., MATSUI, H., OBOKATA, M., KAWAKAMI, R., MURAKAMI, M., YOKOYAMA, T. & KURABAYASHI, M. 2019. Activation of cardiac AMPK-FGF21 feed-forward loop in acute myocardial infarction: Role of adrenergic overdrive and lipolysis byproducts. *Scientific Reports*, 9, 11841.

- SZEWCZYK, N. J. & JACOBSON, L. A. 2003. Activated EGL-15 FGF receptor promotes protein degradation in muscles of *Caenorhabditis elegans*. *The EMBO journal*, 22, 5058-5067.
- TAGUCHI, K., MOTOHASHI H FAU - YAMAMOTO, M. & YAMAMOTO, M. 2011. Molecular mechanisms of the Keap1-Nrf2 pathway in stress response and cancer evolution.
- TAN, B. L., NORHAIZAN, M. E. & LIEW, W. P. 2018. Nutrients and Oxidative Stress: Friend or Foe? *Oxid Med Cell Longev*, 2018, 9719584.
- TANG, X., FAN, Z., WANG, Y., JI, G., WANG, M., LIN, J. & HUANG, S. 2016. Expression of klotho and β -catenin in esophageal squamous cell carcinoma, and their clinicopathological and prognostic significance.
- TATAR, M., KOPELMAN, A., EPSTEIN, D., TU, M.-P., YIN, C.-M. & GAROFALO, R. S. 2001. A Mutant *Drosophila* Insulin Receptor Homolog That Extends Life-Span and Impairs Neuroendocrine Function. *Science*, 292, 107-110.
- TEODORO, J. S., DUARTE, F. V., GOMES, A. P., VARELA, A. T., PEIXOTO, F. M., ROLO, A. P. & PALMEIRA, C. M. 2013. Berberine reverts hepatic mitochondrial dysfunction in high-fat fed rats: A possible role for Sirt3 activation. *Mitochondrion*, 13, 637-646.
- TEPPER, R. G., ASHRAF, J., KALETSKY, R., KLEEMANN, G., MURPHY, C. T. & BUSSEMAKER, H. J. 2013. PQM-1 complements DAF-16 as a key transcriptional regulator of DAF-2-mediated development and longevity. *Cell*, 154, 676-690.
- TEZZE, C., ROMANELLO, V. & SANDRI, M. 2019. FGF21 as Modulator of Metabolism in Health and Disease. *Front Physiol*, 10, 419.
- THORNER, K., COLOMBA A FAU - CECCATO, L., CECCATO L FAU - DELSOL, G., DELSOL G FAU - PAYRASTRE, B., PAYRASTRE B FAU - GAITS-IACOVONI, F. & GAITS-IACOVONI, F. 2009. Reactive oxygen species and lipoxygenases regulate the oncogenicity of NPM-ALK-positive anaplastic large cell lymphomas.
- TOMIYAMA, K.-I., MAEDA, R., URAKAWA, I., YAMAZAKI, Y., TANAKA, T., ITO, S., NABESHIMA, Y., TOMITA, T., ODORI, S., HOSODA, K., NAKAO, K., IMURA, A. & NABESHIMA, Y.-I. 2010. Relevant use of Klotho in FGF19 subfamily signaling system in vivo. *Proceedings of the National Academy of Sciences*, 107, 1666.
- TOMLINSON, E., FU, L., JOHN, L., HULTGREN, B., HUANG, X., RENZ, M., STEPHAN, J. P., TSAI, S. P., POWELL-BRAXTON, L., FRENCH, D. & STEWART, T. A. 2002. Transgenic Mice Expressing Human Fibroblast Growth Factor-19 Display Increased Metabolic Rate and Decreased Adiposity. *Endocrinology*, 143, 1741-1747.
- TRAN, H., BRUNET, A., GRENIER, J. M., DATTA, S. R., FORNACE, A. J., DISTEFANO, P. S., CHIANG, L. W. & GREENBERG, M. E. 2002. DNA Repair Pathway Stimulated by the Forkhead Transcription Factor FOXO3a Through the Gadd45 Protein. *Science*, 296, 530.
- TRIPATHI, P. 2007. Nitric oxide and immune response. *Indian J Biochem Biophys*, 44, 310-9.
- TROŠT, N., PEÑA-LLOPIS, S., KOIRALA, S., STOJAN, J., POTTS, P. R., FON TACER, K. & MARTINEZ, E. D. 2016. γ Klotho is a novel marker and cell survival factor in a subset of triple negative breast cancers. *Oncotarget*, 7, 2611-2628.
- TRUONG, T., KARLINSKI, Z. A., O'HARA, C., CABE, M., KIM, H. & BAKOWSKA, J. C. 2015. Oxidative Stress in *Caenorhabditis elegans*: Protective Effects of Spartin. *PLOS ONE*, 10, e0130455.
- TULLET, J. M. A., ARAIZ, C., SANDERS, M. J., AU, C., BENEDETTO, A., PAPTAEODOROU, I., CLARK, E., SCHMEISSER, K., JONES, D., SCHUSTER, E. F., THORNTON, J. M. & GEMS, D. 2014. DAF-16/FoxO Directly Regulates an Atypical AMP-Activated Protein Kinase Gamma Isoform to Mediate the Effects of Insulin/IGF-1 Signaling on Aging in *Caenorhabditis elegans*. *PLOS Genetics*, 10, e1004109.
- UI-TEI, K. 2013. Optimal choice of functional and off-target effect-reduced siRNAs for RNAi therapeutics. *Frontiers in genetics*, 4, 107-107.
- ULFIG, A. & LEICHERT, L. I. 2020. The effects of neutrophil-generated hypochlorous acid and other hypohalous acids on host and pathogens. *Cellular and Molecular Life Sciences*.

- UNO, M. & NISHIDA, E. 2016. Lifespan-regulating genes in *C. elegans*. *npj Aging and Mechanisms of Disease*, 2, 16010.
- UTSUGI, T., OHNO T FAU - OHYAMA, Y., OHYAMA Y FAU - UCHIYAMA, T., UCHIYAMA T FAU - SAITO, Y., SAITO Y FAU - MATSUMURA, Y., MATSUMURA Y FAU - AIZAWA, H., AIZAWA H FAU - ITOH, H., ITOH H FAU - KURABAYASHI, M., KURABAYASHI M FAU - KAWAZU, S., KAWAZU S FAU - TOMONO, S., TOMONO S FAU - OKA, Y., OKA Y FAU - SUGA, T., SUGA T FAU - KURO-O, M., KURO-O M FAU - NABESHIMA, Y., NABESHIMA Y FAU - NAGAI, R. & NAGAI, R. 2000. Decreased insulin production and increased insulin sensitivity in the *klotho* mutant mouse, a novel animal model for human aging.
- VAN HECKE, T., VOSSEN, E., HEMERYCK, L. Y., VANDEN BUSSCHE, J., VANHAECKE, L. & DE SMET, S. 2015. Increased oxidative and nitrosative reactions during digestion could contribute to the association between well-done red meat consumption and colorectal cancer. *Food Chemistry*, 187, 29-36.
- VAN HJELMBORG, B. J., IACHINE I FAU - SKYTTHE, A., SKYTTHE A FAU - VAUPEL, J. W., VAUPEL JW FAU - MCGUE, M., MCGUE M FAU - KOSKENVUO, M., KOSKENVUO M FAU - KAPRIO, J., KAPRIO J FAU - PEDERSEN, N. L., PEDERSEN NL FAU - CHRISTENSEN, K. & CHRISTENSEN, K. 2006. Genetic influence on human lifespan and longevity.
- VAN LOON, E. P. M., PULSKENS, W. P., VAN DER HAGEN, E. A. E., LAVRIJSEN, M., VERVLOET, M. G., VAN GOOR, H., BINDELS, R. J. M. & HOENDEROP, J. G. J. 2015. Shedding of *klotho* by ADAMs in the kidney. *American Journal of Physiology-Renal Physiology*, 309, F359-F368.
- VAN RAAMSDONK, J. M. & HEKIMI, S. 2011. FUDR causes a twofold increase in the lifespan of the mitochondrial mutant *gas-1*. *Mechanisms of ageing and development*, 132, 519-521.
- VAN RAAMSDONK, J. M. & HEKIMI, S. 2012. Superoxide dismutase is dispensable for normal animal lifespan.
- VANFLETEREN, J. R. 1993. Oxidative stress and ageing in *Caenorhabditis elegans*. *The Biochemical journal*, 292 (Pt 2), 605-608.
- VARA-CIRUELOS, D., RUSSELL F. M. & G., H. D. 2019. The strange case of AMPK and cancer: Dr Jekyll or Mr Hyde? *Open Biology*, 9, 190099.
- VELLAI, T., TAKACS-VELLAI, K., ZHANG, Y., KOVACS, A. L., OROSZ, L. & MÜLLER, F. 2003. Influence of TOR kinase on lifespan in *C. elegans*. *Nature*, 426, 620-620.
- VENUGOPAL, R. & JAISWAL, A. K. 1996. Nrf1 and Nrf2 positively and c-Fos and Fra1 negatively regulate the human antioxidant response element-mediated expression of NAD(P)H:quinone oxidoreductase₁ gene. *Proceedings of the National Academy of Sciences*, 93, 14960.
- VIDELA, L. A., VARGAS, R., RIQUELME, B., FERNÁNDEZ, J. & FERNÁNDEZ, V. 2018. Thyroid Hormone-Induced Expression of the Hepatic Scaffold Proteins Sestrin2, β -Klotho, and FRS2 α in Relation to FGF21-AMPK Signaling. *Exp Clin Endocrinol Diabetes*, 126, 182-186.
- VIOLLET, B. 2017. The Energy Sensor AMPK: Adaptations to Exercise, Nutritional and Hormonal Signals. In: SPIEGELMAN, B. (ed.) *Hormones, Metabolism and the Benefits of Exercise*. Cham (CH).
- VIOLLET, B., ANDREELLI, F., JØRGENSEN, S. B., PERRIN, C., FLAMEZ, D., MU, J., WOJTASZEWSKI, J. F. P., SCHUIT, F. C., BIRNBAUM, M., RICHTER, E., BURCELIN, R. & VAULONT, S. 2003. Physiological role of AMP-activated protein kinase (AMPK): insights from knockout mouse models. *Biochemical Society Transactions*, 31, 216-219.
- WALTERS, J. R., TASLEEM AM FAU - OMER, O. S., OMER OS FAU - BRYDON, W. G., BRYDON WG FAU - DEW, T., DEW T FAU - LE ROUX, C. W. & LE ROUX, C. W. 2009. A new mechanism for bile acid diarrhea: defective feedback inhibition of bile acid biosynthesis.
- WALTON, M., WOODGATE, A.-M., SIRIMANNE, E., PETER, G. & DRAGUNOW, M. 1998. ATF-2 phosphorylation in apoptotic neuronal death. *Molecular Brain Research*, 63, 198-204.
- WANG, H., QIANG, L. & FARMER, S. R. 2008. Identification of a Domain within Peroxisome Proliferator-Activated Receptor γ Regulating Expression of a Group of Genes Containing

- Fibroblast Growth Factor 21 That Are Selectively Repressed by SIRT1 in Adipocytes. *Molecular and Cellular Biology*, 28, 188-200.
- WANG, L., HAN, J., SHAN, P., YOU, S., CHEN, X., JIN, Y., WANG, J., HUANG, W., WANG, Y. & LIANG, G. 2017a. MD2 Blockage Protects Obesity-Induced Vascular Remodeling via Activating AMPK/Nrf2. *Obesity*, 25, 1532-1539.
- WANG, S., GENG, Z., YU, Y. & GUO, J. 2012. Arsenite Exposure Induces Oxidative Stresses in the Nematode *Caenorhabditis Elegans*. In: ZHU, E. & SAMBATH, S. (eds.) *Information Technology and Agricultural Engineering*. Berlin, Heidelberg: Springer Berlin Heidelberg.
- WANG, Y., DANG, N., SUN, P., XIA, J., ZHANG, C. & PANG, S. 2017b. The effects of metformin on fibroblast growth factor 19, 21 and fibroblast growth factor receptor 1 in high-fat diet and streptozotocin induced diabetic rats. *Endocrine Journal*, 64, 543-552.
- WANG, Y., WU, Z., LI, D., WANG, D., WANG, X., FENG, X. & XIA, M. 2011. Involvement of oxygen-regulated protein 150 in AMP-activated protein kinase-mediated alleviation of lipid-induced endoplasmic reticulum stress. *The Journal of biological chemistry*, 286, 11119-11131.
- WEBSTER, A. C., NAGLER, E. V., MORTON, R. L. & MASSON, P. 2017. Chronic Kidney Disease.
- WEN, C., WANG, H., WU, X., HE, L., ZHOU, Q., WANG, F., CHEN, S., HUANG, L., CHEN, J., WANG, H., YE, W., LI, W., YANG, X., LIU, H. & PENG, J. 2019. ROS-mediated inactivation of the PI3K/AKT pathway is involved in the antitumor effects of thioredoxin reductase-1 inhibitor chaetocin. *Cell Death & Disease*, 10, 809.
- WENTWORTH, P., MCDUNN, J.E., WENTWORTH, A.D., TAKEUCHI, C., NIEVA, J., JONES, T., BAUTISTA, C., RUEDI, J.M., GUTIERREZ, A., JANDA, K.D., BABIOR, B.M., ESCHENMOSER, A., LERNER, R.A. 2002. Evidence for Antibody-Catalyzed Ozone Formation in Bacterial Killing and Inflammation. *Science*, 298, 2195-2199.
- WHITE, K. E., EVANS, W. E., O'RIORDAN, J. L. H., SPEER, M. C., ECONS, M. J., LORENZ-DEPIEREUX, B., GRABOWSKI, M., MEITINGER, T. & STROM, T. M. 2000. Autosomal dominant hypophosphataemic rickets is associated with mutations in FGF23. *Nature Genetics*, 26, 345.
- WOLF, I., LEVANON-COHEN, S., BOSE, S., LIGUMSKY, H., SREDNI, B., KANETY, H., KURO-O, M., KARLAN, B., KAUFMAN, B., KOEFFLER, H. P. & RUBINEK, T. 2008. Klotho: a tumor suppressor and a modulator of the IGF-1 and FGF pathways in human breast cancer. *Oncogene*, 27, 7094-105.
- WU, A.-L., COULTER, S., LIDDLE, C., WONG, A., EASTHAM-ANDERSON, J., FRENCH, D. M., PETERSON, A. S. & SONODA, J. 2011. FGF19 Regulates Cell Proliferation, Glucose and Bile Acid Metabolism via FGFR4-Dependent and Independent Pathways. *PLOS ONE*, 6, e17868.
- WU, D. & CEDERBAUM, A. I. 2003. Alcohol, oxidative stress, and free radical damage. *Alcohol research & health : the journal of the National Institute on Alcohol Abuse and Alcoholism*, 27, 277-284.
- WU, L., ZHANG, L., LI, B., JIANG, H., DUAN, Y., XIE, Z., SHUAI, L., LI, J. & LI, J. 2018. AMP-Activated Protein Kinase (AMPK) Regulates Energy Metabolism through Modulating Thermogenesis in Adipose Tissue. *Frontiers in Physiology*, 9, 122.
- WU, W., FENG, J., JIANG, D., ZHOU, X., JIANG, Q., CAI, M., WANG, X., SHAN, T. & WANG, Y. 2017. AMPK regulates lipid accumulation in skeletal muscle cells through FTO-dependent demethylation of N6-methyladenosine. *Scientific Reports*, 7, 41606.
- WU, X., GE, H., GUPTE, J., WEISZMANN, J., SHIMAMOTO, G., STEVENS, J., HAWKINS, N., LEMON, B., SHEN, W., XU, J., VENIANT, M. M., LI, Y. S., LINDBERG, R., CHEN, J. L., TIAN, H. & LI, Y. 2007. Co-receptor requirements for fibroblast growth factor-19 signaling. *J Biol Chem*, 282, 29069-72.
- XIE, Z., DONG, Y., ZHANG, J., SCHOLZ, R., NEUMANN, D. & ZOU, M.-H. 2009. Identification of the serine 307 of LKB1 as a novel phosphorylation site essential for its nucleocytoplasmic transport and endothelial cell angiogenesis. *Molecular and cellular biology*, 29, 3582-3596.
- YAMAMOTO, M., CLARK, J. D., PASTOR, J. V., GURNANI, P., NANDI, A., KUROSU, H., MIYOSHI, M., OGAWA, Y., CASTRILLON, D. H., ROSENBLATT, K. P. & KURO-O, M. 2005. Regulation of

- Oxidative Stress by the Anti-aging Hormone Klotho. *Journal of Biological Chemistry*, 280, 38029-38034.
- YAN, Y., WANG, Y., XIONG, Y., LIN, X., ZHOU, P. & CHEN, Z. 2017. Reduced Klotho expression contributes to poor survival rates in human patients with ovarian cancer, and overexpression of Klotho inhibits the progression of ovarian cancer partly via the inhibition of systemic inflammation in nude mice.
- YANG, W. & HEKIMI, S. 2010. A mitochondrial superoxide signal triggers increased longevity in *Caenorhabditis elegans*. *PLoS Biol*, 8, e1000556.
- YAVARI, A., STOCKER, C. J., GHAFARI, S., WARGENT, E. T., STEEPLES, V., CZIBIK, G., PINTER, K., BELLAHCENE, M., WOODS, A., MARTÍNEZ DE MORENTIN, P. B., CANSELL, C., LAM, B. Y. H., CHUSTER, A., PETKEVICIUS, K., NGUYEN-TU, M.-S., MARTINEZ-SANCHEZ, A., PULLEN, T. J., OLIVER, P. L., STOCKENHUBER, A., NGUYEN, C., LAZDAM, M., O'DOWD, J. F., HARIKUMAR, P., TÓTH, M., BEALL, C., KYRIAKOU, T., PARNIS, J., SARMA, D., KATRITSIS, G., WORTMANN, D. D. J., HARPER, A. R., BROWN, L. A., WILLOWS, R., GANDRA, S., PONCIO, V., DE OLIVEIRA FIGUEIREDO, M. J., QI, N. R., PEIRSON, S. N., MCCRIMMON, R. J., GEREKEN, B., TRETTER, L., FEKETE, C., REDWOOD, C., YEO, G. S. H., HEISLER, L. K., RUTTER, G. A., SMITH, M. A., WITHERS, D. J., CARLING, D., STERNICK, E. B., ARCH, J. R. S., CAWTHORNE, M. A., WATKINS, H. & ASHRAFIAN, H. 2016. Chronic Activation of γ 2 AMPK Induces Obesity and Reduces β Cell Function. *Cell metabolism*, 23, 821-836.
- YIE, J., HECHT, R., PATEL, J., STEVENS, J., WANG, W., HAWKINS, N., STEAVENSON, S., SMITH, S., WINTERS, D., FISHER, S., CAI, L., BELOUSKI, E., CHEN, C., MICHAELS, M. L., LI, Y. S., LINDBERG, R., WANG, M., VENIANT, M. & XU, J. 2009. FGF21 N- and C-termini play different roles in receptor interaction and activation. *FEBS Lett*, 583, 19-24.
- YOUNUS, H. 2018. Therapeutic potentials of superoxide dismutase. *International journal of health sciences*, 12, 88-93.
- YU, C. W. & LIAO, V. H. 2014. Arsenite induces neurotoxic effects on AFD neurons via oxidative stress in *Caenorhabditis elegans*. *Metallomics*, 6, 1824-31.
- ZHANG, B., XIAO, R., RONAN, E. A., HE, Y., HSU, A.-L., LIU, J. & XU, X. Z. S. 2015. Environmental Temperature Differentially Modulates *C. elegans* Longevity through a Thermosensitive TRP Channel. *Cell reports*, 11, 1414-1424.
- ZHANG, L. & LIU, T. 2018. Clinical implication of alterations in serum Klotho levels in patients with type 2 diabetes mellitus and its associated complications.
- ZHANG, X., YEUNG, D. C. Y., KARPISEK, M., STEJSKAL, D., ZHOU, Z.-G., LIU, F., WONG, R. L. C., CHOW, W.-S., TSO, A. W. K., LAM, K. S. L. & XU, A. 2008. Serum FGF21 Levels Are Increased in Obesity and Are Independently Associated With the Metabolic Syndrome in Humans. *Diabetes*, 57, 1246-1253.
- ZHANG, Y., XIE, Y., BERGLUND, E. D., COATE, K. C., HE, T. T., KATAFUCHI, T., XIAO, G., POTTHOFF, M. J., WEI, W., WAN, Y., YU, R. T., EVANS, R. M., KLIOWER, S. A. & MANGELSDORF, D. J. 2012. The starvation hormone, fibroblast growth factor-21, extends lifespan in mice. *Elife*, 1, e00065.
- ZHAO, C., ZHANG, Y., LIU, H., LI, P., ZHANG, H. & CHENG, G. 2017a. Fortunellin protects against high fructose-induced diabetic heart injury in mice by suppressing inflammation and oxidative stress via AMPK/Nrf-2 pathway regulation. *Biochemical and Biophysical Research Communications*, 490, 552-559.
- ZHAO, Y., HU, X., LIU, Y., DONG, S., WEN, Z., HE, W., ZHANG, S., HUANG, Q. & SHI, M. 2017b. ROS signaling under metabolic stress: cross-talk between AMPK and AKT pathway. *Molecular Cancer*, 16, 79.
- ZHAO, Y., ZHAO, M. M., CAI, Y., ZHENG, M. F., SUN, W. L., ZHANG, S. Y., KONG, W., GU, J., WANG, X. & XU, M. J. 2015. Mammalian target of rapamycin signaling inhibition ameliorates vascular calcification via Klotho upregulation. *Kidney International*.

- ZHOU, G., MYERS, R., LI, Y., CHEN, Y., SHEN, X., FENYK-MELODY, J., WU, M., VENTRE, J., DOEBBER, T., FUJII, N., MUSI, N., HIRSHMAN, M. F., GOODYEAR, L. J. & MOLLER, D. E. 2001. Role of AMP-activated protein kinase in mechanism of metformin action. *The Journal of clinical investigation*, 108, 1167-1174.
- ZMIJEWSKI, J. W., BANERJEE S FAU - BAE, H., BAE H FAU - FRIGGERI, A., FRIGGERI A FAU - LAZAROWSKI, E. R., LAZAROWSKI ER FAU - ABRAHAM, E. & ABRAHAM, E. 2010. Exposure to hydrogen peroxide induces oxidation and activation of AMP-activated protein kinase.
- ZOROV, D. B., JUHASZOVA, M. & SOLLITT, S. J. 2014. Mitochondrial reactive oxygen species (ROS) and ROS-induced ROS release. *Physiological reviews*, 94, 909-950.
- ZOU, D., WU, W., HE, Y., MA, S. & GAO, J. 2018. The role of klotho in chronic kidney disease. *BMC Nephrology*, 19, 285.

Appendix 1

Table 1. Proportion of living animals per day for chronic starvation of N2 (wild-type), *klo-1* (*ok2925*), *klo-2* (*ok1862*) and *klo-2* (*ok1862*); *klo-1* (*ok2925*) animals. Per assay, 3 aliquots of *C. elegans* were analysed per strain. Statistical significance compared to wild-type strain was determined using Tukey's test. Asterisks indicate significant values (*P < 0.05, **P < 0.01, ***P < 0.001).

Strain	Day 1			Day 2			Day 3		
	<i>n</i>	Proportion living ±SEM	P value vs N2	<i>n</i>	Proportion living ±SEM	P value vs N2	<i>n</i>	Proportion living ±SEM	P value vs N2
N2 (wild-type)	516	0.912±0.01	-	302	0.847±0.01	-	310	0.801±0.02	-
<i>klo-1</i> (<i>ok2925</i>)	252	0.898±0.01	0.313	283	0.863±0.01	0.411	293	0.825±0.01	0.472
<i>klo-2</i> (<i>ok1862</i>)	754	0.718±0.01	<0.001***	615	0.711±0.01	0.001**	399	0.710±0.02	0.056
<i>klo-2</i> (<i>ok1862</i>); <i>klo-1</i> (<i>ok2925</i>)	310	0.823±0.01	0.125	335	0.731±0.02	0.108	352	0.719±0.02	0.146
	Day 4			Day 5			Day 6		
	<i>n</i>	Proportion living ±SEM	P value vs N2	<i>n</i>	Proportion living ±SEM	P value vs N2	<i>n</i>	Proportion living ±SEM	P value vs N2
N2 (wild-type)	-	N.A.	-	253	0.790±0.03	-	192	0.812±0.01	-
<i>klo-1</i> (<i>ok2925</i>)	253	0.797±0.02	-	229	0.781±0.01	0.862	-	N.A.	-

<i>klo-2</i> (<i>ok1862</i>)	-	N.A.	-	110	0.685±0.04	0.175	407	0.681±0.01	<0.001***
<i>klo-2</i> (<i>ok1862</i>); <i>klo-1</i> (<i>ok2925</i>)	368	0.719±0.02	-	427	0.654±0.02	0.039*	-	N.A.	-
	Day 7			Day 8			Day 9		
	<i>n</i>	Proportion living ±SEM	P value vs N2	<i>n</i>	Proportion living ±SEM	P value vs N2	<i>n</i>	Proportion living ±SEM	P value vs N2
N2 (wild-type)	187	0.733±0.03	-	167	0.710±0.03	-	-	N.A.	-
<i>klo-1</i> (<i>ok2925</i>)	-	N.A.	-	180	0.691±0.01	0.628	228	0.685±0.02	-
<i>klo-2</i> (<i>ok1862</i>)	321	0.698±0.02	0.433	201	0.538±0.04	0.043*	-	N.A.	-
<i>klo-2</i> (<i>ok1862</i>); <i>klo-1</i> (<i>ok2925</i>)	-	N.A.	-	290	0.613±0.01	0.051	314	0.577±0.02	-
	Day 10			Day 11			Day 12		
	<i>n</i>	Proportion living ±SEM	P value vs N2	<i>n</i>	Proportion living ±SEM	P value vs N2	<i>n</i>	Proportion living ±SEM	P value vs N2
N2 (wild-type)	129	0.675±0.01	-	134	0.707±0.02	-	-	N.A.	-

<i>klo-1</i> (<i>ok2925</i>)	196	0.599±0.01	0.034*	222	0.540±0.01	0.005**	321	0.520±0.03	-
<i>klo-2</i> (<i>ok1862</i>)	191	0.562±0.03	0.063	207	0.474±0.02	0.002**	-	N.A.	-
<i>klo-2</i> (<i>ok1862</i>); <i>klo-1</i> (<i>ok2925</i>)	312	0.523±0.01	0.001**	314	0.461±0.01	<0.001***	309	0.460±0.01	-
	Day 14			Day 15			Day 16		
	<i>n</i>	Proportion living ±SEM	P value vs N2	<i>n</i>	Proportion living ±SEM	P value vs N2	<i>n</i>	Proportion living ±SEM	P value vs N2
N2 (wild-type)	70	0.321±0.02	-	206	0.283±0.01	-	-	N.A.	-
<i>klo-1</i> (<i>ok2925</i>)	-	N.A.	-	243	0.477±0.02	0.002**	255	0.392±0.01	-
<i>klo-2</i> (<i>ok1862</i>)	115	0.188±0.01	0.013*	263	0.150±0.03	0.019*	-	N.A.	-
<i>klo-2</i> (<i>ok1862</i>); <i>klo-1</i> (<i>ok2925</i>)	-	N.A.	-	293	0.348±0.02	0.041*	335	0.329±0.03	-
	Day 17			Day 18			Day 19		
	<i>n</i>	Proportion living ±SEM	P value vs N2	<i>n</i>	Proportion living ±SEM	P value vs N2	<i>n</i>	Proportion living ±SEM	P value vs N2

N2 (wild-type)	-	N.A.	-	155	0.243±0.02	-	-	N.A.	-
<i>klo-1</i> (ok2925)	224	0.364±0.01	-	234	0.312±0.03	0.205	228	0.238±0.04	-
<i>klo-2</i> (ok1862)	-	N.A.	-	178	0.199±0.03	0.394	-	N.A.	-
<i>klo-2</i> (ok1862); <i>klo-1</i> (ok2925)	389	0.276±0.02	-	415	0.264±0.01	0.500	399	0.234±0.04	-
	Day 20			Day 21			Day 22		
	<i>n</i>	Proportion living ±SEM	P value vs N2	<i>n</i>	Proportion living ±SEM	P value vs N2	<i>n</i>	Proportion living ±SEM	P value vs N2
N2 (wild-type)	77	0.064±0.01	-	147	0.039±0.01	-	-	N.A.	-
<i>klo-1</i> (ok2925)	-	N.A.	-	-	N.A.	-	212	0.113±0.02	-
<i>klo-2</i> (ok1862)	112	0.098±0.02	0.268	112	0.054±0.03	0.742	-	N.A.	-
<i>klo-2</i> (ok1862); <i>klo-1</i> (ok2925)	-	N.A.	-	-	N.A.	-	237	0.115±0.02	-
	Day 23			Day 24					

	<i>n</i>	Proportion living ±SEM	P value vs N2	<i>n</i>	Proportion living ±SEM	P value vs N2
N2 (wild-type)	105	0.000±0.00	-	127	0.000±0.00	-
<i>klo-1</i> (<i>ok2925</i>)	216	0.079±0.02	0.051	205	0.000±0.00	-
<i>klo-2</i> (<i>ok1862</i>)	118	0.021±0.01	0.122	135	0.069±0.01	0.374
<i>klo-2</i> (<i>ok1862</i>); <i>klo-1</i> (<i>ok2925</i>)	218	0.050±0.02	0.080	199	0.000±0.00	-

Appendix 2

P values for Viable Progeny analysis of *klo-1*, *klo-1* and *aak-2* compound mutants

Table 2. Viable progeny analysis for *aak-2* vs *klotho* mutant strains. Mean viable progeny, unfertilized eggs and dead eggs counted for N2 (wild-type), *klo-1* (*ok2925*), *klo-2* (*ok1862*), *klo-2* (*ok1862*); *klo-1* (*ok2925*), *aak-2* (*gt33*), *aak-2* (*gt33*); *klo-1* (*ok2925*), *aak-2* (*gt33*); *klo-2* (*ok1862*) and *aak-2* (*gt33*); *klo-2* (*ok1862*); *klo-1* (*ok2925*) strains. 5 animals per strain analysed. Statistical significance determined using Tukey's test, asterisks indicate significant values (*P < 0.05, **P < 0.01, *P < 0.001).**

Strain	Mean viable progeny ±SEM	P values for mean viable progeny			Mean unfertilized eggs ±SEM	P values for mean unfertilized eggs				Mean dead eggs ±SEM
		<i>klo-1</i>	<i>klo-2</i>	<i>klo-2</i> ; <i>klo-1</i>		N2	<i>klo-1</i>	<i>klo-2</i>	<i>klo-2</i> ; <i>klo-1</i>	
N2 (wild-type)	244.2±5.57	<0.000***	0.008**	0.905	12.8±1.70	-	0.021*	0.021*	0.972	1.4±0.61
<i>klo-1</i> (<i>ok2925</i>)	176.4±7.67	-	<0.000***	0.009**	49±11.43	0.021*	-	0.237	0.045*	4.0±1.32
<i>klo-2</i> (<i>ok1862</i>)	296.8±10.95	<0.000***	-	0.026*	31.2±4.98	0.021*	0.237	-	0.106	5.4±1.41
<i>klo-2</i> (<i>ok1862</i>); <i>klo-1</i> (<i>ok2925</i>)	242.3±13.76	0.009**	0.026*	-	12.5±7.77	0.972	0.045*	0.106	-	2.5±1.32
<i>aak-2</i> (<i>gt33</i>)	158.4±26.65	0.637	0.007**	0.079	45.4±12.62	0.092	0.868	0.453	0.132	1.6±0.38
<i>klo-1</i> (<i>ok2925</i>); <i>aak-2</i> (<i>gt33</i>)	155.6±15.69	0.386	<0.000***	0.012*	67.2±14.68	0.025*	0.458	0.119	0.052	1.8±0.44
<i>klo-2</i> (<i>ok1862</i>); <i>aak-2</i> (<i>gt33</i>)	206.2±11.12	0.120	0.002**	0.119	2.6±1.41	0.007**	0.006**	0.002**	0.209	1.6±0.45
<i>klo-2</i> (<i>ok1862</i>); <i>klo-1</i> (<i>ok2925</i>); <i>aak-2</i> (<i>gt33</i>)	188.0±2.65	0.685	0.006**	0.118	12.2±2.65	0.890	0.022*	0.028*	0.974	6.0±0.17

Appendix 3

Hexokinase activity in *C. elegans* homogenates

Initial readouts for hexokinase activity in *C. elegans* homogenates showed similar activity for *klo-1 (ok2925)* single mutants compared to *daf-2 (e1370)* indicating these could function in a linear pathway, however upon repetition of the assay these results were not found to be replicable.

There are several reasons that could provide explanation for discrepancies in the data. First, the *C. elegans* stocks for homogenate were harvested at mixed stage, so it could be that the age of the animals used could have caused discrepancies in the data. Alternatively, the reasons for the polar data collected could be due to the state of health of the populations used. As animals were gathered on NGM plates when they were densely populated, it could be that on a given day/ assay, some of the strains could have been starved, explaining the reason for dramatically altered hexokinase activity.

To correct for this, animals were to be collected in liquid media and age synchronised to ensure no age discrepancies. It was ensured that animals would be well-fed (*ad libitum*) before freezing to ensure nutritional status would not affect assay results.

However, limitations brought about by the COVID-19 pandemic impacted collection of nematodes of the same age. Therefore, it would be worth repetition of this assay with age synchronised *C. elegans* to determine whether hexokinase activity is impacted by genetic background.

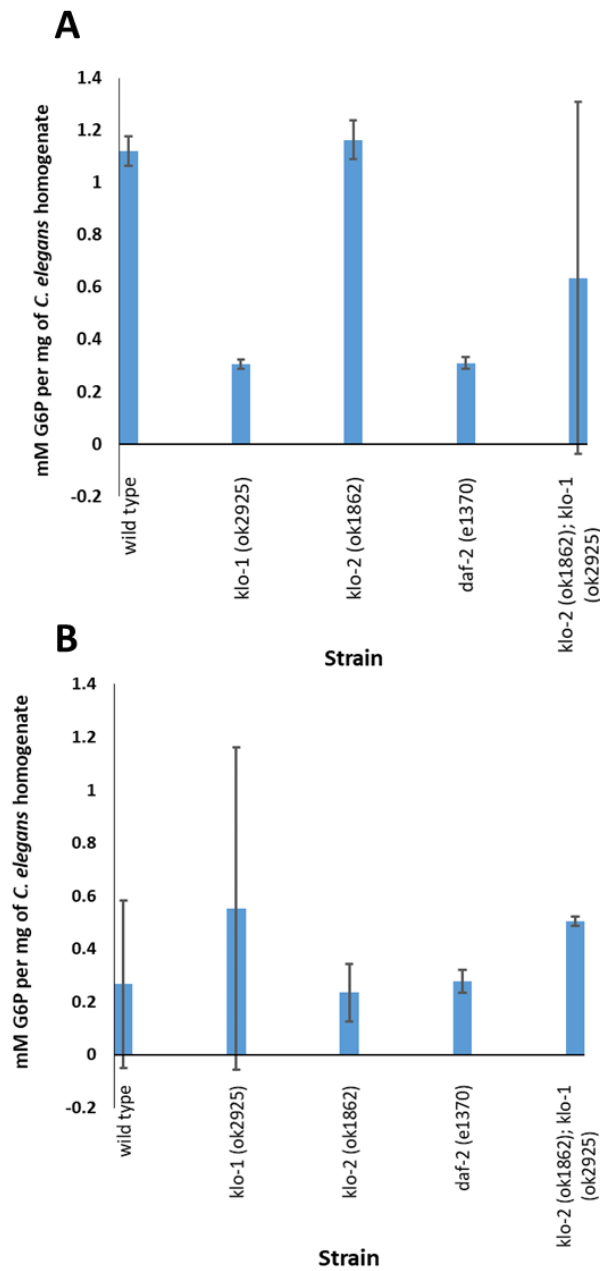


Figure 1. Hexokinase activity in *C. elegans* homogenates. Hexokinase activity determined based on micromoles of glucose-6-phosphate (G6P) detected per mg of *C. elegans* homogenate. *NADH production detected at 340 nm*. **A.** Hexokinase activity read outs from first assay. **B.** Hexokinase activity recordings from technical repeat.

Appendix 4

P values gathered from staining for Reactive Oxygen Species

Table 1. P values for CellROX staining to determine ROS levels of wild-type, *klo-1* (*ok2925*), *klo-2* (*ok1862*) and *klo-2* (*ok1862*); *klo-1* (*ok2925*) double mutants before and after treatment with 300 mM paraquat (PQ) for 1 hour. Statistical significance was determined using Tukey's test. Asterisks indicate statistical differences (*P < 0.05, **P < 0.01, *P < 0.001).**

Strain	Condition	n	P values							
			Wild type control	<i>klo-1</i> control	<i>klo-2</i> control	<i>klo-2;klo-1</i> control	Wild type + 300 mM PQ	<i>klo-1</i> + 300 mM PQ	<i>klo-2</i> + 300 mM PQ	<i>klo-2; klo-1</i> + 300 mM PQ
Wild-type	Control	54	-	<0.001***	<0.001***	<0.001***	<0.001***	<0.001***	<0.001***	<0.001***
	+ 300 mM PQ	46	<0.001***	<0.001***	<0.001***	0.001**	-	<0.001***	0.757	0.074
<i>klo-1</i> (<i>ok2925</i>)	Control	27	<0.001***	-	0.991	0.684	<0.001***	0.445	<0.001***	<0.001***
	+ 300 mM PQ	42	<0.001***	0.445	0.369	0.766	<0.001***	-	<0.001***	<0.001***
<i>klo-2</i> (<i>ok1862</i>)	Control	44	<0.001***	0.991	-	0.653	<0.001***	0.369	<0.001***	<0.001***
	+ 300 mM PQ	31	<0.001***	<0.001***	<0.001***	<0.001***	0.757	<0.001***	-	0.008**
<i>klo-2</i> (<i>ok1862</i>); <i>klo-1</i> (<i>ok2925</i>)	Control	41	<0.001***	0.684	0.653	-	0.001**	0.766	<0.001***	<0.001***
	+ 300 mM PQ	39	<0.001***	<0.001***	<0.001***	<0.001***	0.074	<0.001***	0.008**	-

Table 2. P values for CellROX staining to determine ROS levels of wild-type, *klo-1* (*ok2925*), *klo-2* (*ok1862*) and *klo-2* (*ok1862*); *klo-1* (*ok2925*) double mutants before and after treatment with 200 mM paraquat (PQ) for 1 hour. Statistical significance was determined using Tukey's test. Asterisks indicate statistical differences (*P < 0.05, **P < 0.01, *P < 0.001).**

Strain	Condition	n	P values					
			Wild-type control	<i>klo-2</i> control	<i>klo-2;klo-1</i> control	Wild-type + 200 mM PQ	<i>klo-2</i> + 200 mM PQ	<i>klo-2; klo-1</i> + 200 mM PQ
Wild-type	Control	34	-	0.029*	0.028*	0.139	0.013*	0.077
	+ 200 mM PQ	20	0.139	0.480	0.551	-	0.363	0.838
<i>klo-2</i> (<i>ok1862</i>)	Control	22	0.029*	-	0.860	0.480	0.874	0.582
	+ 200 mM PQ	24	0.013*	0.874	0.711	0.363	-	0.443
<i>klo-2</i> (<i>ok1862</i>); <i>klo-1</i> (<i>ok2925</i>)	Control	37	0.028*	0.860	-	0.551	0.711	0.675
	+ 200 mM PQ	25	0.077	0.582	0.675	0.838	0.443	-

Table 3. P values for CellROX staining to determine ROS levels of wild-type, *klo-1* (ok2925), *klo-2* (ok1862) and *klo-2* (ok1862); *klo-1* (ok2925) double mutants before and after treatment with 100 mM paraquat (PQ) for 2 hours. Statistical significance was determined using Tukey's test. Asterisks indicate statistical differences (*P < 0.05, **P < 0.01, *P < 0.001).**

Strain	Condition	n	P values							
			Wild-type control	<i>klo-1</i> control	<i>klo-2</i> control	<i>klo-2;klo-1</i> control	Wild-type + 100 mM PQ	<i>klo-1</i> + 100 mM PQ	<i>klo-2</i> + 100 mM PQ	<i>klo-2; klo-1</i> + 100 mM PQ
Wild-type	Control	53	-	<0.001***	<0.001***	<0.001***	0.008**	0.063	<0.001***	0.207
	+ 100 mM PQ	60	0.008**	0.096	<0.001***	0.194	-	0.434	0.001**	0.586
<i>klo-1</i> (ok2925)	Control	62	<0.001***	-	0.049*	0.961	0.096	0.017*	0.148	0.104
	+ 100 mM PQ	64	0.063	0.017*	<0.001***	0.056	0.434	-	<0.001***	0.987
<i>klo-2</i> (ok1862)	Control	60	<0.001***	0.049*	-	0.118	<0.001***	<0.001***	0.607	0.005**
	+ 100 mM PQ	60	<0.001***	0.148	0.607	0.237	0.001**	<0.001***	-	0.011*
<i>klo-2</i> (ok1862); <i>klo-1</i> (ok2925)	Control	59	<0.001***	0.961	0.118	-	0.194	0.056	0.237	0.150
	+ 100 mM PQ	57	0.207	0.104	0.005**	0.150	0.586	0.987	0.011*	-

Table 4. P values for CellROX staining to determine ROS levels of wild-type, *klo-1* (*ok2925*), *klo-2* (*ok1862*) and *klo-2* (*ok1862*); *klo-1* (*ok2925*) double mutants before and after treatment with 100 mM paraquat (PQ) for 20 hours. Statistical significance was determined using Tukey's test. Asterisks indicate statistical differences (*P < 0.05, **P < 0.01, *P < 0.001).**

Strain	Condition	n	P values							
			Wild-type control	<i>klo-1</i> control	<i>klo-2</i> control	<i>klo-2;klo-1</i> control	Wild-type + 100 mM PQ	<i>klo-1</i> + 100 mM PQ	<i>klo-2</i> + 100 mM PQ	<i>klo-2; klo-1</i> + 100 mM PQ
Wild-type	Control	39	-	0.002**	0.020*	0.006**	<0.001***	0.009**	0.003**	<0.001***
	+ 100 mM PQ	34	<0.001***	<0.001***	<0.001***	<0.001***	-	0.237	0.035*	0.195
<i>klo-1</i> (<i>ok2925</i>)	Control	52	0.002**	-	0.328	0.533	<0.001***	<0.001***	<0.001***	<0.001***
	+ 100 mM PQ	34	0.009**	<0.001***	<0.001***	<0.001***	0.237	-	0.559	0.877
<i>klo-2</i> (<i>ok1862</i>)	Control	39	0.020*	0.328	-	0.685	<0.001***	<0.001***	<0.001***	<0.001***
	+ 100 mM PQ	41	0.003**	<0.001***	<0.001***	<0.001***	0.035*	0.559	-	0.314
<i>klo-2</i> (<i>ok1862</i>); <i>klo-1</i> (<i>ok2925</i>)	Control	45	0.006**	0.533	0.685	-	<0.001***	<0.001***	<0.001***	<0.001***
	+ 100 mM PQ	45	<0.001***	<0.001***	<0.001***	<0.001***	0.195	0.877	0.314	-

Table 5. P values for CellROX staining to determine ROS levels of wild-type, *klo-1* (*ok2925*), *klo-2* (*ok1862*) and *klo-2* (*ok1862*); *klo-1* (*ok2925*) double mutants before and after treatment with 100 μ M sodium arsenite (NaAsO₂) for 24 hours. Statistical significance was determined using Tukey's test. Asterisks indicate statistical differences (*P < 0.05, **P < 0.01, *P < 0.001).**

Strain	Condition	n	P values							
			Wild-type control	<i>klo-1</i> control	<i>klo-2</i> control	<i>klo-2;klo-1</i> control	Wild-type + NaAsO ₂	<i>klo-1</i> + NaAsO ₂	<i>klo-2</i> + NaAsO ₂	<i>klo-2; klo-1</i> + NaAsO ₂
Wild-type	Control	73	-	0.152	0.251	0.915	<0.001***	0.716	0.020*	0.244
	+ 100 μ M NaAsO ₂	74	<0.001***	<0.001***	<0.001***	<0.001***	-	<0.001***	<0.001***	<0.001***
<i>klo-1</i> (<i>ok2925</i>)	Control	67	0.152	-	0.695	0.141	<0.001***	0.096	0.533	0.022*
	+ 100 μ M NaAsO ₂	68	0.716	0.096	0.158	0.801	<0.001***	-	0.013*	0.070
<i>klo-2</i> (<i>ok1862</i>)	Control	77	0.251	0.695	-	0.230	<0.001***	0.158	0.251	0.035*
	+ 100 μ M NaAsO ₂	68	0.020*	0.533	0.251	0.020*	<0.001***	0.013*	-	0.002**
<i>klo-2</i> (<i>ok1862</i>); <i>klo-1</i> (<i>ok2925</i>)	Control	72	0.915	0.141	0.230	-	<0.001***	0.801	0.020*	0.299
	+ 100 μ M NaAsO ₂	68	0.244	0.022*	0.035*	0.299	<0.001***	0.430	0.002**	-

Appendix 5

P values for heat stress analysis of *klo-1*, *klo-2* and *aak-2* compound mutants

Table 1. Tukey's test data for heat stress data; *aak-2* vs *klo* strains. Asterisks indicate significant values (* $p < 0.05$, ** $P < 0.01$, * $P < 0.001$).**

Strain	P values vs <i>klo-1</i>			P values vs <i>klo-2</i>			P values vs <i>klo-2</i> ; <i>klo-1</i>		
	7 hours	8 hours	9 hours	7 hours	8 hours	9 hours	7 hours	8 hours	9 hours
N2 (wild-type)	0.065	0.009**	0.673	0.084	0.049*	0.414	0.591	0.329	0.565
<i>klo-1</i> (<i>ok2925</i>)	-	-	-	0.573	0.692	0.937	0.003**	0.002**	0.937
<i>klo-2</i> (<i>ok1862</i>)	0.573	0.692	0.936	-	-	-	0.027*	0.070	0.768
<i>klo-2</i> (<i>ok1862</i>); <i>klo-1</i> (<i>ok2925</i>)	0.003**	0.002**	0.937	0.027*	0.070	0.768	-	-	-
<i>aak-2</i> (<i>ok524</i>)	0.025*	0.024*	0.509	0.100	0.205	0.114	0.013*	0.275	0.210
<i>aak-2</i> (<i>gt33</i>)	0.010*	0.003**	0.361	0.019*	0.014*	0.202	0.165	0.038*	0.256
<i>klo-1</i> (<i>ok2925</i>); <i>aak-2</i> (<i>ok524</i>)	0.110	0.033*	0.075	0.096	0.048*	0.005**	0.346	0.120	0.008**
<i>klo-1</i> (<i>ok2925</i>); <i>aak-2</i> (<i>gt33</i>)	0.187	0.033*	0.314	0.160	0.056	0.170	0.505	0.177	0.215
<i>klo-2</i> (<i>ok1862</i>); <i>aak-2</i> (<i>ok524</i>)	0.074	0.064	0.891	0.078	0.113	0.763	0.868	0.450	0.920
<i>klo-2</i> (<i>ok1862</i>); <i>aak-2</i> (<i>gt33</i>)	0.717	0.631	0.866	0.563	0.763	0.887	0.427	0.530	0.779
<i>klo-2</i> (<i>ok1862</i>); <i>klo-1</i> (<i>ok2925</i>); <i>aak-2</i> (<i>ok524</i>)	0.009**	0.007**	0.262	0.017*	0.023*	0.094	0.114	0.080	0.128
<i>klo-2</i> (<i>ok1862</i>); <i>klo-1</i> (<i>ok2925</i>); <i>aak-2</i> (<i>gt33</i>)	0.494	0.419	0.969	0.370	0.548	0.902	0.338	0.696	0.980